CRANFIELD UNIVERSITY

DEFENCE COLLEGE OF MANAGEMENT AND TECHNOLOGY

ENGINEERING SYSTEMS DEPARTMENT

PHD THESIS

Academic Year 2005-2006

Sriram Krishnamurthy

PRESTRESSED ADVANCED FIBRE REINFORCED COMPOSITES: FABRICATION AND MECHANICAL PERFORMANCE

***Supervisors*: Dr RA Badcock and Professor JG Hetherington**

February 2006

To my Parents and Gurus

ABSTRACT

ADVANCED COMPOSITE MATERIALS have high strength-to-weight ratios, corrosion resistance and durability and are extensively used in aerospace, energy and defence industries. This research concentrates on minimising the process-induced residual stresses, and improving the fibre alignment of composites by employing a fibre prestress methodology. A novel flat-bed fibre prestress methodology for autoclave processing of composites was developed. This research investigates the effect of fibre prestress on 1) residual stresses, 2) fibre alignment, 3) static tensile and compression properties and 4) fatigue behaviour of composites.

Experimental results show that this prestress methodology, on a 16-ply unidirectional E-glass/913 epoxy composite, reduces the residual strain of the composite from –600 με to approximately zero for a prestress of 108 MPa. The strains measured from optical fibre sensors were in close agreement with those obtained using strain gauge. The results from fibre alignment studies showed that fibre prestressing improved the fibre alignment from 20% of fibres aligned to 0° degree in non-prestressed composites to 75% of fibres aligned to 0° degree in 108 MPa prestressed composites.

Findings have shown that prestressing is beneficial to the static compressive and tensile performance of composites. The results show that fibre prestressing improves the fatigue life and resistance to stiffness degradation in the low stress level fatigue region. Also a change in static and fatigue damage mechanism was observed. The improvement in the static and fatigue properties is due to the reduction in residual stresses and fibre waviness. Overall the fibre prestressing methodology enhances the performance of composites by increasing the resistance to static and fatigue loading. The thesis also suggests that there is an existence of prestress limits to retain optimal material performance.

Keywords: fibre prestressing, polymer composites, residual strain monitoring, optical fibre sensors, static tension, static compression, fatigue and composite damage mechanisms.

ACKNOWLEDGEMENTS

I would like to thank Professor Gerard Franklyn Fernando, for providing me with the opportunity to pursue my research in the field of composites and for his invaluable guidance and support. I would also like to thank Dr Rodney Badcock for his encouragement and constructive criticism throughout my study.

I would like to thank Professor Brian Ralph for his valuable advice, prompt response and suggestions relating to this thesis.

I would like to thank Professor John G Hetherington and Dr Mike Iremonger for their valuable guidance and inspiration in theoretical modelling and also their pastoral care.

I would like to thank Dr Amer Hameed and Mr Mike Teagle for providing technical assistance in design and development of prestress rig and for their unfailing encouragement and support.

I would like to thank Dr Paul Robinson and Dr J Hodgkinson at the Department of Aerospace Engineering, Imperial College, London for giving me permission to use their facilities in order to undertake compression test of composites.

I would like to acknowledge Cranfield University [DCMT] for sponsoring this project.

Thanks are also due to Mr Brian Duguid, Mr Tony Fallon at the mechanical workshop, DCMT for manufacturing the prestress rig.

I am grateful to the late Mr John Tetlow, Dr Thomas Butler, Dr G Kister and Dr Balakrishnan Degamber for providing help in optical fibre sensors.

Thank you to Dr John Rock, Mr Rajanikanth Machavaram, Dr James Talbot and Mr Samual Proctor for their help and encouragement throughout my period of study.

Thank you to Mr Joseph Meggyesi, Mr Gary Senior and Mr Russell Stracey at the Department of Aerospace Engineering, Imperial College, London for assisting in specimen preparation and compression testing.

I would like to thank Ms Maggie Keats, Mrs Ros Gibson, Mrs Alison McFee and Mrs Paula Bentley for their administrative support and entertainment.

I also thank the DCMT library staff especially Miss Raichel Daniels, Mr Mike Groves and Ms Louise Tucker for their assistance in processing the many interlibrary loan requests and quickly responding to my stack requests.

I am eternally grateful to my father Sri MS Krishnamurthy, my mother Srimathi Sundhari and my sister Srimathi Yamini, for their endless support, encouragement and prayers.

To my friends Dr Vidyashankar Buravalla, Mr Suresh Jeyaraman, and Miss Darina Fišerová from whom I drew much inspiration and encouragement; to them I express my deepest gratitude.

I thank Ms Anna Ward for providing me with a homely environment.

TABLE OF CONTENTS

LIST OF FIGURES

LIST OF TABLES

ABBREVIATONS

ASTM	American society for testing materials
CARALL	Carbon fibre reinforced aluminium alloy laminate
CCD	Charged coupling device
CDS	Characteristic damage state
CFRP	Carbon fibre reinforce plastics
CRAG	Composite research advisory group
DSC	Differential scanning calorimetry
EB	Electron beam
EFPI	Extrinsic Fabry-Pérot interferometric
ERSG	Electrical resistance strain gauges
ETJCET	End-tab jig cured end-tabs
FBG	Fibre Bragg grating
FBPM	Flat-bed prestress methodology
GFRP	Glass fibre reinforced plastics
HPCET	Hot-press cured end-tabs
ICSTM	Imperial college of science, technology and medicine
IFSS	Interfacial shear stress
ILSS	Interlaminar shear stress
ISO	International organisation for standardisation
PEEK	Poly (etheretherketone)
PEI	Poly (etherimide)

PP	Poly (propylene)
PPS	Poly (phenylene sulphide)
PTFE	Poly (tetrafluroethylene)
RT	Room temperature
SEM	Scanning electron microscope
SLD	Super-luminescence diode
SMA	Shape memory alloy
S-N	Peak stress verses the logarithmic of number of cycles to failure
T-C	Tension – compression
T-T	Tension- tension
T_g	Glass transition temperature
UCS	Ultimate compressive strength
UTS	Ultimate tensile strength
VIRALL	Vinylon fibre/epoxy-aluminium laminates

CHAPTER 1

Introduction

OVERVIEW

- Research motivation and rationale is stated.
- The research aims are presented.
- The contributions of this research to knowledge are given.
- Scientific publications generated in the course of PhD are presented.
- Organisation of the thesis.

THIS PHD THESIS investigates the effect of fibre prestress on, (i) residual stress, (ii) fibre alignment and (iii) static and fatigue performance of composites. Fibre prestressing is utilised to minimise the process-induced residual stress and fibre waviness in composites. This method also improves the static mechanical and fatigue properties of composites.

The motivation and rationale for this research is outlined in this chapter and the problem statement is presented as a set of aims and objectives. The contributions from this thesis are presented, and finally, the organisation of the thesis is explained.

1.1 Research motivation and rationale

During processing of advanced composite materials, residual stresses and fibre waviness are induced. The residual stresses are developed in composites because of the mismatch in thermal expansion between fibre and matrix, on the micro-mechanical scale, and between adjacent plies of different orientation on the macro-mechanical scale[1]. Fibre waviness is induced due to fibre movement during processing. These process-induced issues can

degrade the structural performance of composites. The presence of residual stresses in a composite can reduce the strain to micro-cracking and this could expose the fibres to environmental degradation. The effect of fibre waviness has a detrimental effect on the overall composite structural integrity by adversely affecting the compressive strength, fatigue life and tensile strength.

The next generation aircraft structures for civil aviation industry are manufactured using advanced composite materials. In particular, the primary structures such as wings of the A380 (AIRBUS Ltd) and fuselage and wings of 787 "Dreamliner" (Boeing Ltd) were manufactured using composite materials that were processed in an autoclave. These primary aircraft structures will be subjected to various types of mechanical loading including fatigue during service. The presence of residual stresses and fibre waviness could have a detrimental effect on the mechanical properties of composite structures and this could reduce the service life of aircraft. Therefore, it is of paramount importance to reduce the process-induced residual stresses and fibre waviness. These process-induced issues play a vital role in motivating our research.

In recent years fibre prestressing has been proposed as a way to minimise the residual stresses and to improve mechanical properties of composites[2, 3].

Prestressed composites are prepared by applying pre-tension to the fibres and subsequently curing the composite. Once the composite is cured and cooled down to room temperature, the pre-tension is released. Now the pre-tensioned fibres will tend to contract, inducing compressive stresses to the matrix, which will minimise the residual stresses resulting from the cure cycle. In literature fibre prestressing methodology has been theoretically shown as a method for reducing residual stresses and experimentally demonstrated to enhance mechanical properties of polymer composite laminates. In addition, as the fibres are subjected to a constant load throughout the curing process, fibre misalignment or fibre waviness in composites can be minimised.

In this research, fibre prestressing is chosen as a method to provide immunity against the development of process-induced issues in composites.

1.2 Aims and objectives

The aims and objectives of this research are as follows:

- To design and evaluate a bespoke fibre prestressing methodology for autoclave processing of composites.
- To measure and quantify the residual stress reduction in composites with fibre prestress.
- To investigate the fibre alignment in composites with fibre prestress.

- To model theoretically, the effect of fibre prestressing on residual stresses and compare the same with experimental results.
- To investigate the effect of fibre prestress on static tensile and compressive properties.
- To investigate the fatigue behaviour of prestressed composites in both tension-tension and tension-compression modes and compare with non-prestressed composites.
- To understand the influence of fibre prestressing on damage of composites subjected to both static and fatigue loading.

Initially, it was planned to use a prestressing methodology designed by a previous researcher in this group. However, after initial trials it was found that this system was not suitable for the current requirements. Hence this research embarked on designing a prestress rig that satisfies the current requirements.

1.3 Contributions

The contributions of this research are as follows

- Novel design and development of a bespoke prestressing methodology for fibre reinforced composites. This methodology is successfully used to manufacture composites in an autoclave using conventional vacuum bagging techniques. The pre-load applied to the composites is monitored online throughout the curing cycle.
- *In-situ* monitoring of residual strain development during autoclave processing and prestress release is demonstrated using optical fibre sensors in real-time. The strain release recorded using optical fibre sensors and surface-mounted electrical resistance strain gauge sensors are in good agreement.
- Experimentally, fibre prestress methodology is shown as a method to minimise and control residual stresses in fibre reinforced composites. The residual strain in composites with different prestress levels is quantified.
- A theoretical model was developed to predict the strain released to the composite for a given applied prestress. The experimental results from optical fibre sensors and strain gauges are in good agreement with the theoretical model. The model was further developed to predict the Poisson's effect on the strain variation through the width of the composite panel.
- Fibre alignment of the composites improved with increasing fibre prestress up to an optimum limit of 108 MPa prestress. No improvement was observed beyond this limit.
- From the static tensile results it was found that with fibre prestress, strain at deviation from linearity increases. This suggests that prestressing enhanced the

resistance to initial damage like matrix cracking, weak fibre failure during tensile loading. However, the tensile strength and modulus are independent of applied prestress.

- Compressive strength and modulus properties increased with fibre prestress. This suggests that the improvement in fibre alignment with prestress have enhanced the compressive properties. The non-prestressed composites fractured by typical fibre kink-band failure, whereas the prestressed composites fractured by extensive longitudinal splitting and matrix cracking, resulting in a crushing mode of failure. This also suggests that the improvement in fibre alignment could have changed the compression damage mode of composites.
- Improvement in fatigue life and resistance to stiffness degradation was observed in matrix-dominated fatigue region. This suggests that minimising the matrix tensile residual stresses by fibre prestressing has enhanced the fatigue properties in the matrix-dominated fatigue region. The improvement in fatigue life and resistance to stiffness degradation observed in tension-compression fatigue was greater than in tension-tension fatigue. This is because of a reduction in matrix residual stress, improvement in fibre alignment and also the presence of tensile residual stress in fibre.
- The degree of longitudinal splitting in prestressed composites was lower than the non-prestressed composites in the low stress fatigue region in both tension-tension and tension-compression fatigue modes. Also in tension-compression fatigue the extent of compression damage of fibres was lower in prestressed composites. This change in the damage mechanism is due to the reduction in matrix tensile residual stresses and improvement in fibre alignment in composites with fibre prestress.

1.4 Work disseminations

The research findings were presented in the following publications:

- S Krishnamurthy, RA Badcock, GF Fernando and A Hameed, "Novel prestress methodology for autoclave processing of composites: fabrication and mechanical performance", Proceedings of the SAMPE 2005 conference, Long Beach, USA, May 2005.
- S Krishnamurthy, RA Badcock, GF Fernando and A Hameed, "Design and evaluation of novel prestress methodology for fibre reinforced composites: fabrication and *in-situ* monitoring", *Composite Science and Technology Journal.* under review.

The following publications are generated in collaboration with other researchers during the course of PhD:

- R.Badcock, S.Krishnamurthy, G.F.Fernando, T,Butler, R.Chen and J.Tetlow, "Health monitoring of composite structures using a novel fibre optic acoustic emission sensors", *The 11th European Conference on Composite Materials*, 31 May - 3 June 2004 Rhodes , Greece.
- T.Butler, R.Chen, S.Krishnamurthy, R.Badcock and G.F.Fernando, " A low-cost fibre optic acoustic emission sensor for damage detection in engineering composite materials and structures", *The 4th International Workshop on Structural Health Monitoring*, Stanford University, USA, September 15-17, 2003.

1.5 Organisation of thesis

This thesis is structured into nine chapters.

CHAPTER 2

This chapter is intended to set the scene, there are three parts in this chapter. The first part surveys the current literature covering process-induced residual stress development, techniques for measuring and predicting residual stresses, factors instigating fibre waviness during manufacturing process and its effect on mechanical properties of composites. This is followed by various techniques reported in the literature to minimise process-induced issues. The second part presents a comprehensive review of the fibre prestress literature. This includes a critical review of the various prestress methods reported in the literature and the effect of prestress on mechanical properties of composites. The final part discusses issues relating to fatigue behaviour and failure modes of unidirectional glass fibre/epoxy composites.

CHAPTER 3

This chapter presents design criteria for fibre prestress methodology proposed in this current research. This is followed by a design using flat-bed prestress methodology, which satisfies all the design criteria. Design calculations are included in this chapter.

CHAPTER 4

The experimental procedures for composite manufacturing, residual strain monitoring, fibre alignment, quality control, static and fatigue test conditions are presented.

The experimental results are described and discussed in chapters five to nine.

CHAPTER 5

The results from the evaluation of prestress methodology and sensors are presented and discussed.

CHAPTER 6

This chapter is structured into two parts: 1) residual strain development and 2) fibre alignment. The residual strain development in non-prestressed composites during autoclave processing is presented. This is followed by the residual strain development and strain release results of prestressed composites. The reduction in residual stress with fibre prestress was quantified. The measured fibre alignment in non-prestressed and prestressed composites are presented and discussed.

CHAPTER 7

In this chapter, a theoretical model is developed to predict the strain released to the composite for a given applied fibre prestress based on micromechanical theory. This model is further developed to predict the Poisson's effect on the strain variation through the width of the panel during strain release. The experimental results from embedded optical fibre sensors and surface-mounted strain gauges are compared with theoretical predictions.

CHAPTER 8

The results from static tensile and compression tests, and post-failure analysis of non-prestressed and prestressed composites are presented and discussed.

CHAPTER 9

This chapter present the tension-tension and tension-compression fatigue test results and discusses the influence of prestress on fatigue life, stiffness degradation, surface temperature rise and fracture mechanisms of composites.

CHAPTER 10

The overall conclusions of this study and directions for future research are presented.

CHAPTER 2

Literature review

OVERVIEW

- The development of process-induced residual stresses and fibre waviness during composite processing is described;
- The methods to mitigate process-induced issues are reviewed;
- A critical literature survey on prestressed composites, methodology for fibre prestressing and the effect of fibre prestress on static mechanical properties is presented;
- A review of composite fatigue behaviour and damage mechanisms, relevant to this study is presented.

2.1 Introduction

A COMPOSITE MATERIAL IS a combination of two or more materials, whose properties are superior to those of the constituent materials acting independently. Fibre-reinforced polymer composites are usually manufactured by embedding stiff and strong fibres into a relatively less stiff and compliant, polymeric matrix. The primary role of the fibres is to provide strength and stiffness to the composite. Typical reinforcing fibres used are glass, carbon and aramid, with fibre diameters in the range of 6-14 μm.

The role of the matrix resin is to hold the fibres in their position, protect the fibres from abrasion and the external environment (such as chemicals or moisture) and transfer load between fibres. Matrices for polymeric composites can be either thermosets or thermoplastics. Thermoset resins usually consist of a low-molecular weight resin and a

compatible curing agent (also called a hardener). When the resin and hardener are mixed they form a low viscosity liquid that undergoes a chemical reaction to form three-dimensional cross-linked structures, resulting in an insoluble solid phase that cannot be reprocessed on reheating. Thermoset polymeric matrices include epoxies, polyesters, vinyl esters, bismaleimides, cynate esters, polyimides and phenolics. On the other hand, thermoplastics are fully reacted high-molecular weight polymers that do not cross-link on heating. On heating to their softening or melting temperature they can be reprocessed a number of times. Typical thermoplastics used in composites are poly(etheretherketone) (PEEK), poly(phenylene sulfide) (PPS), Poly(etherimide) (PEI) and Poly(propylene) (PP).

The attainment of good mechanical properties in a composite material depends crucially upon the efficiency of stress transfer from the matrix to the fibre, which requires optimisation of the adhesion of the fibre to the matrix. To promote the fibre-matrix adhesion, different surface treatments/coupling agents are applied to the fibre surfaces to provide chemical bonding with the polymeric matrix. Silane type coupling agents are normally applied to glass fibre surfaces during manufacture while carbon fibres are surface treated by oxidation[4] and aramid fibres are usually treated with an epoxy finish[5]. The adhesion between fibre and matrix occurs during the processing of composites. The processing parameters control the properties and therefore the quality of the composites. This will be discussed in the following section.

2.2 Processing of composites

Composite manufacturing can be mainly categorised into two phases: a) pre-forming and b) processing. This is schematically represented as a flowchart in Figure 2-1. The two main raw materials for processing composites are fibres and matrix. In the pre-forming phase the reinforcing fibres and the accompanying matrix material are placed or shaped into a structural form. The fibre and matrix may be in a pre-impregnated form or the fibre and matrix material may be combined for the first time during this step of developing the structural form. The next step is processing wherein the temperature and pressure are used to consolidate the structure. For thermoset plastics the chemical cross-linking reaction solidifies the structure, whereas thermoplastic matrixes become hard after cooling from their melting temperature.

The end properties of the composite part are determined not only by the function of the individual properties of the resin matrix and fibre, but also as a function of the arrangement of the materials themselves into the part, the ratio of the constituent materials and also the way in which they are processed.

This thesis investigates composites using thermoset matrices. From hereon only theromset composites are considered. Composites can be manufactured using a wide variety of processing techniques such as hand lay-up, hot-pressing, vacuum bagging, pressure bagging, resin transfer moulding, filament winding, pultrusion and autoclave moulding

techniques. Autoclave-based processing is a widely used method of producing high-quality composites in the aerospace industry[6], and will be utilised in this study.

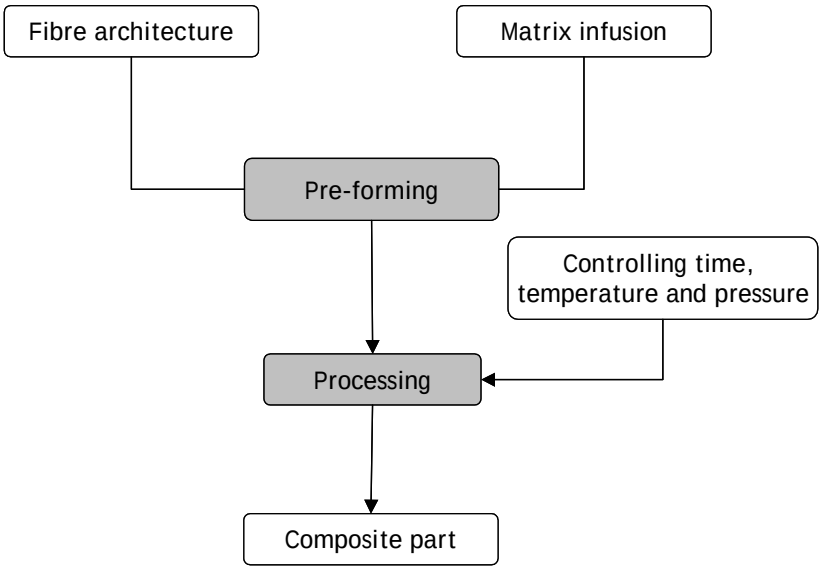

Figure 2-1: Schematic representation of the principle of composite processing.

An autoclave process is a technique that can generate a controlled pressure and temperature environment. A typical autoclave system consists of a pressure vessel, a gas compressor, a heater system, a vacuum pump and a control system. Prepreg is widely used, as a starting material in an autoclave. A prepreg system is a pre-impregnated sheet of a combination of the reinforcing fibres and the resin matrix (with hardener). In a prepreg, the resin is advanced to a B-stage condition in which it is a semi-solid (represents a partially cured state) at room temperature, which melts and flows during the cure cycle. The B-staged resin normally contains some tack or stickiness to allow it to adhere during the lay-up operation. With reference to the manufacturing of prepreg-based composites, the unidirectional prepreg laminas are stacked-up or laminated with the fibres in the required orientation. This is carried out either manually or by a lay-up machine which places the individual plies of the prepreg in the required orientation directly onto the tool surface. The laminated prepreg is then vacuum bagged with release film and breather cloths. The vacuum bagged prepreg laminate is placed inside the autoclave where a combination of heat, pressure and vacuum consolidates and cures the laminate.

Figure 2-2 shows a typical autoclave cure cycle for prepreg-based composites. With reference to the figure, the vacuum is applied before the heating stage of the cure cycle and maintained throughout the cure cycle. During the heating cycle, initially the viscosity of the resin decreases, and this allows the entrapped air between the laminas to be removed by the application of the vacuum. The pressure applied on the prepreg stack will consolidate the

laminate. During the isothermal stage of the cure cycle, the temperature and pressure are kept constant. In this dwell period, the polymerisation of the resin takes place by an exothermic reaction; this increases the viscosity of the resin rapidly.

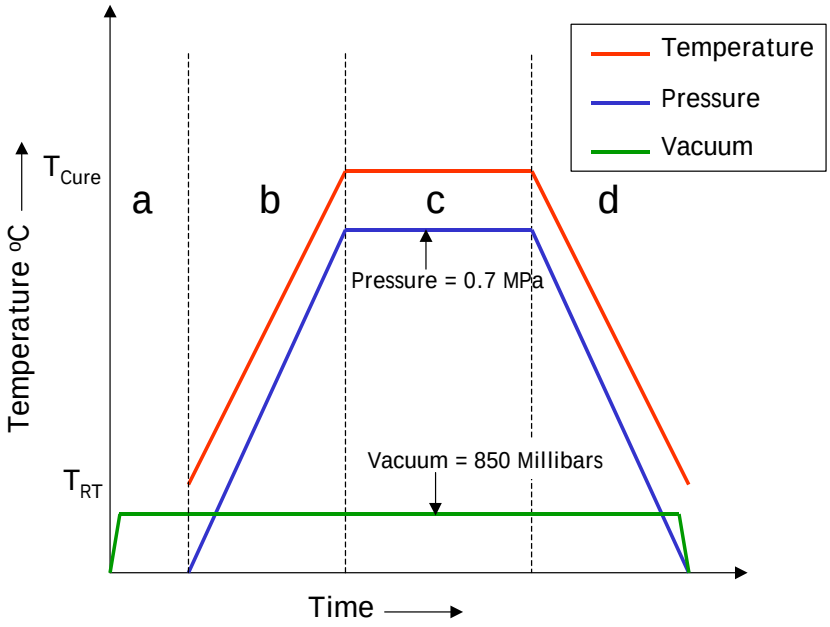

Figure 2-2: Typical autoclave cure cycle for prepreg-based composites. a) vacuum application, b) heating cycle, c) isothermal cure and d) cooling cycle.

As the reaction proceeds, the molecular weight of the resin increases by linking several chains to form a three-dimensional cross-linked network. This transformation from viscous liquid to elastic gel is known as the gel point. The degree of cure determines the amount of cross-linking in the resin. This degree of cure of the resin determines the composite's performance[7]. After the dwell period, the cool-down stage of the cure cycle commences by gradually reducing the temperature and pressure. At the end of the cure cycle, the part is left to cool down to room temperature. The above steps of converting low molecular weight viscous resin to a high molecular weight solid by a polymerisation process is also called curing hence the name cure cycle.

2.3 Process-related issues

Advanced fibre reinforced composites are generally processed at elevated temperatures. The quality and performance of the composite part is determined by various processing parameters such as heating rate, dwell time, cooling rate, pressure and tool plate material[8, 9, 10]. These processing parameters influence the development of process-induced residual stresses and fibre waviness, which have been shown to affect the performance of

composite parts.[10,11] The development of process-induced residual stresses and fibre waviness is discussed in the following sections.

2.4 Residual stresses

Residual stresses are developed in composites during processing and in-service due to the anisotropic thermal expansion and elastic properties of their constituents. During processing of composites at elevated temperatures residual stresses develop due to 1) cure-induced shrinkage of the polymer matrix and 2) constituents thermal expansion mismatch-induced volume changes. The cure-induced residual stresses are developed due to the shrinkage of the resin during the polymerisation reaction, which forms cross-linked networks.[12,13] Thermally-induced stresses are developed because of the mismatch in thermal expansion between the fibre and matrix, on the micro-mechanical scale, and between adjacent plies of different orientation on the macro-mechanical scale.

Unlike homogeneous materials, residual stresses in composites cannot be removed by annealing because the expansion mismatch is between two different materials, not within the same material. However, some relaxation of residual stresses in time is possible as a result of the viscoelasticity inherent in most resins.[14] The presence of residual stresses may result in dimensional instability of composite parts. In fact residual stresses can be high enough to cause cracking within the matrix even before the mechanical loading is applied. In addition, micro-failures such as matrix cracking, delamination and fibre buckling may be developed in the composites, which can adversely affect the resistance to crack initiation and propagation, strength of the material, service limits, and exposes the fibres to chemical degradation. [10,15]

2.4.1. Techniques for measuring residual stresses

In general, residual stress measurement can be divided into two categories, namely destructive and non-destructive testing methods. The basic drawback of destructive methods (hole drilling[16] and a first ply failure test[17]) is the obvious disadvantage of damaging the part to obtain the measurements. The second category, non-destructive testing methods includes a cure-referencing method[18], X-ray diffraction[19], photoelasticity[20], optical fluorescence[21], Raman spectroscopy[22], embedded strain gauge[23], and embedded optical fibre sensors.[24,25,26]

Table 2-1 shows the advantages and disadvantages of these residual stress measurement techniques. In this study, extrinsic Fabry-Pérot interferometric (EFPI) and fibre Bragg grating (FBG) embedded optical fibre sensors are used to monitor the process-induced residual strain development. In the following sections, a brief introduction and working principles of EFPI and FBG sensors are given. This is followed by a literature review on residual strain monitoring of composites using optical-fibre sensors.

Table 2-1: Advantages and disadvantages of the various residual stress measurement techniques.

Technique	Advantages	Disadvantages
Hole drilling	○ Widely available ○ Quick and simple ○ Wide range of materials	○ Destructive ○ Interpretation of data
X-ray diffraction	○ Simple method ○ Non-contact	○ Foreign particle inclusions leads to stress concentration ○ Lab-based systems
Curvature and layer removal	○ Simple method ○ Wide range of materials	○ Limited to simple shapes ○ Destructive
Photoelasticity	○ Simple method ○ Non-contact	○ Only transparent materials ○ Lab-based measurement
Raman spectroscopy	○ High resolution ○ In-situ measurement	○ Surface measurements ○ Limited range of materials
Cure referencing method	○ Simple method ○ Non-contact	○ Surface measurements ○ Lab-based measurement ○ Restricted to flat-surfaces
Embedded strain gauges	○ In-situ measurement ○ Small in size ○ Simple method	○ Difficult to control the alignment during cure ○ Susceptible to electrical and magnetic interference (EMI) ○ Formation of matrix pocket leading to stress concentration
Embedded optical fibre sensors	○ In-situ measurement ○ Mimicking the shape of the reinforcing fibre ○ Immune to EMI ○ Multiplexing capability ○ Temperature compensated	○ Fragile to use before embedding ○ Matrix pocket formation

Embedded optical fibre sensors

Researchers have demonstrated that optical fibre sensors can be used to monitor a wide range of parameters including strain, temperature, pressure, humidity, vibration, acoustic-emission and fracture[27,28,29]. Recently embedded optical fibre sensors are increasingly used in advanced composites for process monitoring[26,30] and structural health monitoring[31,32]. The two main types of embedded optical fibre sensors used are extrinsic Fabry-Pérot interferometric (EFPI) and fibre Bragg grating (FBG) sensors.

(i) *Optical-fibre EFPI sensors*

Figure 2-3 shows a schematic of an EFPI sensor. EFPI sensors are fabricated by glueing or fusion-welding two optical fibres into a glass capillary tube and are separated by an air gap[33]. The distance between the two optical fibre ends is called the Fabry-Pérot cavity length. The gauge length is defined as the distance between the two fusion points in the capillary tube.

When light from a broadband source is launched into the lead-in fibre, a portion of the light is reflected from the end of the lead-in fibre (R_1). The transmitted light travels through the air-gap, and is partially reflected at the reflector fibre end-face (R_2). The light reflected from the two surfaces is transmitted back through the lead-in fibre. The reflections at glass/air and air/glass interfaces are called Fresnel reflections. These Fresnel reflections undergo interference to produce fringes of superposition as shown in Figure 2-4.

This interference fringe is used to calculate the Fabry-Pérot cavity length d using the following formula:

$$d = \frac{n\lambda_1\lambda_2}{2000(\lambda_2 - \lambda_1)}\mu m \qquad (2.1)$$

where *n* is the number of fringes between λ_1 and λ_2 wavelengths in nm as shown in Figure 2-4.

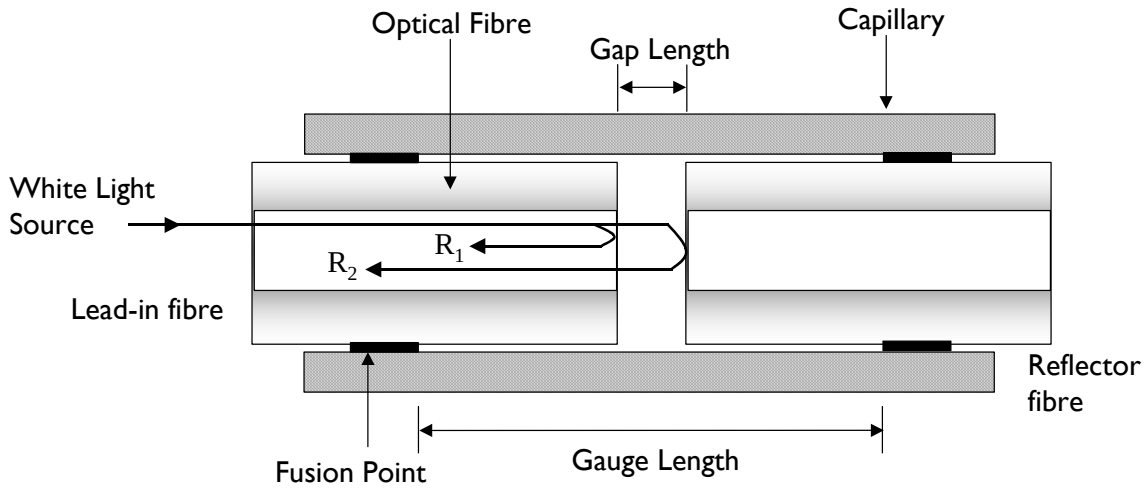

Figure 2-3: Schematic illustration of the extrinsic Fabry-Pérot interferometric sensor design.

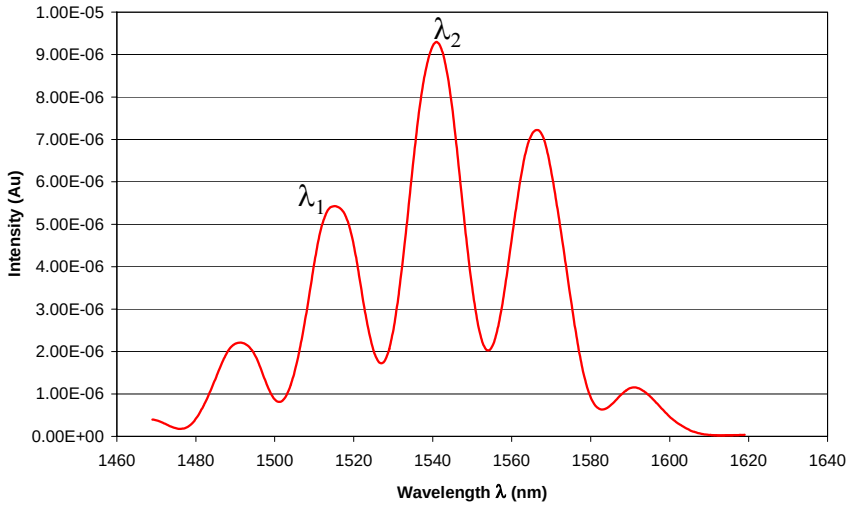

Figure 2-4: Interference fringe from an EFPI sensor.

When the sensor is subjected to an axial displacement, there will be a change in cavity length, which will result in a change in the path length of the Fresnel reflections. The resulting phase changes produce an interference pattern, which is different from the initial interference. The change in the cavity length can be calculated from the new interference pattern. If the gauge length (L) is known, then the strain can be calculated by:

$$\varepsilon = \left(\frac{\Delta d}{L} \right) \tag{2.2}$$

where Δd is the change in Fabry-Pérot cavity length from the strain-free condition.

(ii) *Optical-fibre Bragg grating sensors*

Fibre Bragg gratings are fabricated by irradiating optical fibres to the interference of ultra-violet laser beams. This irradiation produces periodic refractive index moduluation on the core of the optical fibre. When light is coupled into the fibre Bragg grating, the superposition of Fresnel reflections produces a stronger narrow band reflection. This is also known as the Bragg peak wavelength. The basic working principle of a fibre Bragg grating (FBG)-based sensor system is the measurand-induced shift in Bragg peak reflection. This shift is due to the change in the effective refractive index and the period of the grating. These sensors are used to measure strain and temperature[27, 33]. A schematic representation of the mode of operation of a fibre Bragg grating sensor is illustrated in Figure 2-5.

The Bragg wavelength λ_B, is related to the effective core index of refraction, n, and the grating pitch, Λ, by the relation:

$$\lambda_B = 2n\Lambda \tag{2.3}$$

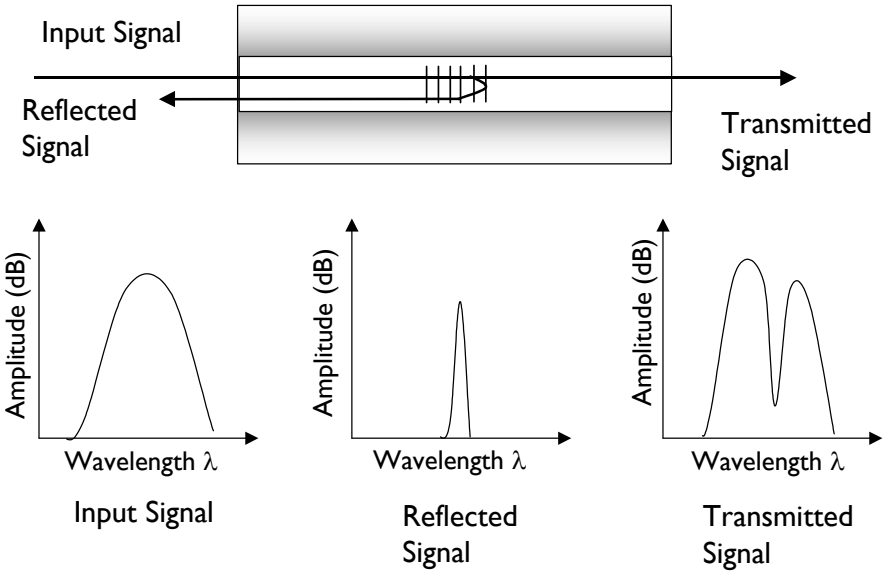

Figure 2-5: Principle of operation of an optical-fibre Bragg grating.

Since this Bragg wavelength will shift with changes in either n or Λ, monitoring the wavelength of this narrow band spectrum will serve to determine the strain or temperature environment to which the optical fibre is subjected[34]. Comprehensive reviews of the fundamentals of Bragg gratings are given elsewhere in the literature.

For a temperature change ΔT, the corresponding wavelength shift $\Delta\lambda_B$ is given by:

$$\Delta\lambda_B = \lambda_B(\alpha + \xi)\Delta T \tag{2.4}$$

where $\alpha = (1/\Lambda)(\partial\Lambda/\partial T)$ is the thermal expansion coefficient for the fibre (approximately 0.55 x 10^{-6} °C^{-1} for silica). The quantity $\xi = (1/n)(\partial n/\partial T)$ is called the thermo-optic coefficient and represents the change in refractive index (optical density) with temperature. For a germanium-doped silica core fibre, ξ = 8.6 x 10^{-6} °C^{-1}.

Fibre Bragg gratings are also sensitive to axial, lateral and radial strains. Therefore, for temperature measurement, the grating has to be isolated from strain and this is achieved by housing the Bragg grating sealed inside a capillary tube[35].

Residual strain monitoring using optical fibre sensors

The reported residual strain monitoring using embedded optical fibre sensors in the literature is discussed herein.

Many researchers have used optical fibre strain sensors to monitor cure-induced[26,36,37] and thermally-induced[24,26] residual strain development during composite processing.

The feasibility of measuring the residual strain using optical fibre EFPI sensors was first demonstrated by Liu *et al.* in cross-ply carbon/epoxy composite. In their experiments, they embedded two temperature-compensated EFPI strain sensors between plies number 2 and 3 (sensor 1), and 8 and 9 (sensor 2) in a cross-ply $(0, 90_2, 0_2, 90, 0, 90)_S$ carbon/epoxy laminate. They measured the cavity length of EFPI sensors before and after curing of the composite. From the EFPI cavity length measurements they calculated the residual strain to be 90 με and 550 με in sensor 1 and sensor 2 respectively. The uncertainty in their residual strain measurements is apparent. The authors explained that the actual orientation of the sensor in relation to the reinforcing fibre directions was not established, which resulted in the uncertainty in their measurements. However, the authors suggested that these results demonstrate that the residual strain in composites can be measured using EFPI sensors.

Lawrence *et al.*[26] have taken one step forward and showed that EFPI sensors can be used for *in situ* monitoring of residual strain development in 20 ply unidirectional and $[0_5/90_5]_S$ cross-ply carbon/epoxy laminate during the hot press curing process. In the unidirectional 20 ply laminate two sensors are embedded between plies number 10 and 11 in both 0°and 90° directions. In cross-ply laminates two EFPI sensors are embedded between plies number 3 and 4, and 10 and 11, in parallel to the reinforcing fibres. From their experimental results they reported a gradual shrinkage of the laminate during the two isothermal dwell periods of the cure cycle, which they attributed to cure-induced residual stresses. The cure-induced shrinkage of unidirectional and cross-ply laminates was 20 με and 40 με respectively. Also during the cool-down cycle they measured a compressive residual strain, which they attributed to mismatch in thermal expansion properties between the fibre and matrix. The magnitude of the thermally-induced residual strain was higher than the cure-induced residual strain. Their experimental results are shown in Table 2-2.

Table 2-2: The compressive residual strain results of unidirectional and cross-ply carbon/epoxy laminates reported by Lawrence *et al.*.

Laminate sequence	Compressive residual strain measurement	
	0° direction	90° direction
Unidirectional 20 ply	65 με	4600 με
Cross-ply $[0_5/90_5]_S$	450 με	580 με

It can be observed from Table 2-2 that there is a significant difference between the residual strain measurements from sensors embedded in the 0°and 90° directions of a 20 ply unidirectional laminate. The authors explained that was because of the presence of reinforcing fibres, the matrix is restrained to shrinking in the 0° direction. This results in a very small compressive residual strain. On the other hand, in the 90° direction, there are no

restrictions for the matrix to shrink, which resulted in a high compressive residual strain. The magnitude of residual strain measured in the 0° direction is less than the 90° direction of the cross-ply laminate. They suggested that possible reasons for the difference in the measurement could be due to 1) misalignment of the EFPI sensor, 2) variation in adhesion between sensor and composite, 3) error in sensor calibration and 4) strain and temperature gradients in the panel.

Jinno *et al.* have also shown that EFPI strain sensors can be used for *in-situ* monitoring of residual strain similar to Lawrence *et al.* but in autoclave processed composites. In addition, Jinno *et al.* have shown that EFPI sensors can also be used to measure the resin cure shrinkage termination point by correlating the EFPI strain to the specific volume change of the matrix caused by cure shrinkage. This resin cure shrinkage termination point corresponds to a certain degree of cure of the resin. Thus, by monitoring the EFPI strain they showed that the degree of cure of the resin could be measured.

However, Jinno *et al.* also reported that at the start of the isothermal period an exotherm was observed. This exotherm reaches a peak temperature, which was 20°C higher than the isothermal temperature. After 20 minutes the exotherm temperature cooled down to the isothermal temperature. This suggests that measurement of cure-induced residual strain in Jinno *et al.* results also include thermal shrinkage of the resin due to cool-down from the exotherm peak temperature to the isothermal temperature. Also, it is difficult to de-couple the cure-induced and thermally-induced shrinkage during the curing of the composite. This suggests that the correlation of cure-induced strain to degree of cure of the resin would result in error.

From the review of the literature, it was shown that embedded optical fibre sensors can be used to measure residual strain development during composite processing. It was shown that the magnitude of thermally-induced residual strain is higher than the cure-induced residual strain. It also indicated that it is difficult to separate the cure-induced and thermally-induced residual strains during the curing of the composite. Also, in all the above reported residual strain measurements using embedded optical fibre sensors, the effect of strain measured from sensors on the cure cycle parameters such as temperature and pressure (independently and combined) are not considered. These cure cycle parameters may have an effect on the measured residual strain.

2.4.2. Prediction of residual stresses

In the literature, numerous micro-mechanical models have been reported in both mathematical[38,39,40] and computational[41,42] analysis. Wagner has excellently reviewed the micro-mechanical models that are relevant for polymer composites. He showed that the residual stress prediction from one-dimensional model of Tsai and Hahn and three-dimensional model of Wagner's are in close agreement for macro composites. These two models are used in this study to predict the residual stresses in composites.

The assumptions of Tsai and Hahn's model are:

- Both fibre and matrix are isotropic materials;
- The system is a unidirectional composite in a state of plane stress corresponding to thin laminates, under a thermal strain;
- No mechanical stress is applied;
- There is perfect bonding between fibre and matrix;
- Modulus and thermal expansion coefficients of fibre and matrix are independent of temperature.

The residual stress components present in the fibres and the matrix in the longitudinal direction are given by:

$$\sigma^f = (\alpha_m - \alpha_f)(T - T_{ref}) \frac{E_f}{1 + \left(\frac{\phi_f}{\phi_m}\right)\left(\frac{E_f}{E_m}\right)} \tag{2.5}$$

$$\sigma^m = -\sigma^f \left(\frac{\phi_f}{\phi_m}\right) \tag{2.6}$$

where α and E are the coefficient of thermal expansion and Young's modulus, respectively, ϕ is the volume fraction, with the f and m for the fibre and matrix respectively, and where T is the test temperature and T_{ref} is the stress-free reference temperature.

Most of the Tsai and Hahn assumptions were considered in the Wagner model except that Wagner considers a concentric cylindrical model of fibre and matrix having transverse isotropic properties. Transverse isotropic materials are a special class of orthotropic materials that have the same properties in one plane (e.g. the x-y plane) and different properties in the direction normal to this plane (e.g. the z-axis fibre direction). However, both of these models only predict the thermally-induced residual stresses and not cure-induced residual stresses.

2.5 Fibre waviness

Fibre waviness or misalignment commonly arises during processing of continuous fibre reinforced composites. Fibre waviness in composites can be categorised as in-plane and out-of-plane waviness[43]. In-plane waviness involves the co-operative movement of fibres within the plane of the lamina. Out-of-plane waviness, also known as layer waviness or ply waviness, involves the co-operative motion of multiple plies through the thickness of the laminate and is prevalent in thick composites. Figure 2-6 shows a cross-section of a cross-ply $[0/90/0/90/90/0/90/0]_S$ laminate. With reference to Figure 2-6 the presence of both in-plane and out-of-plane fibre waviness in this cross-ply composite can be observed.

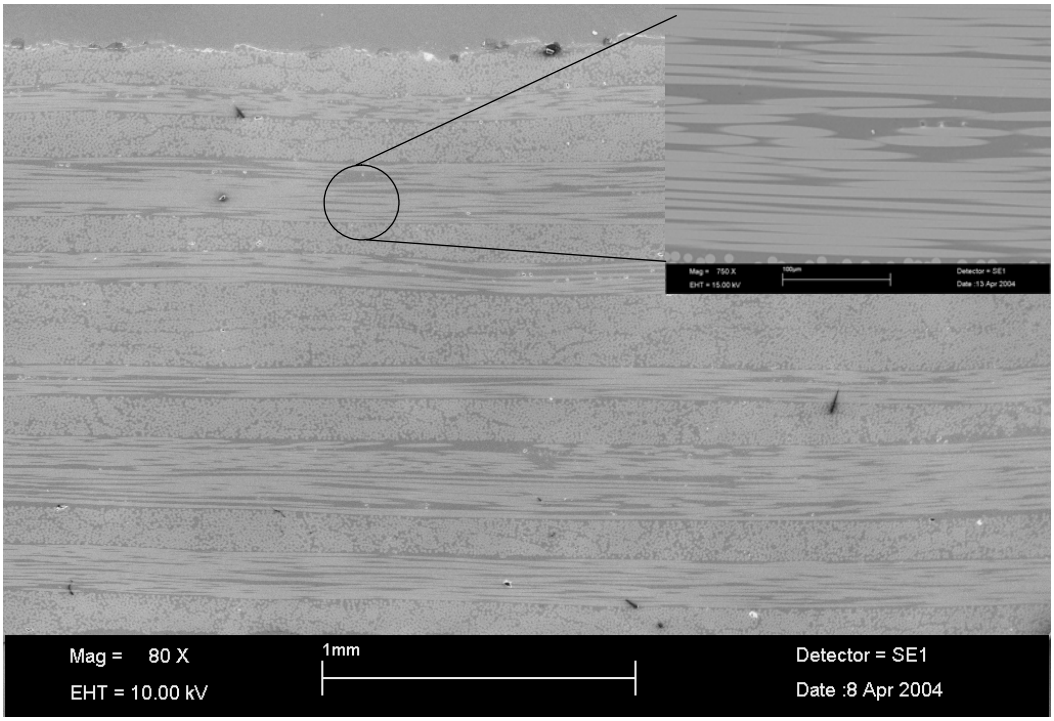

Figure 2-6: Fibre waviness in cross-ply laminate.

With specific reference to prepreg-based autoclave cured composites, there are a number of possible reasons that can cause fibre waviness, for example:

- fibre movement during pressurisation and/or during the minimum viscosity phase of the resin matrix;
- mismatch in thermal expansion between tool plate material and composite;
- excessive resin-bleeding inducing fibre movement;
- over-pressurisation during processing;
- misalignment induced during the prepreg lay-up process;
- entrapped air and foreign body inclusions.

Many researchers have shown that fibre misalignment has a significant influence on composite properties such as static longitudinal tensile modulus[44], static longitudinal compressive strength[45] and modulus[46], compression fatigue[47] and delamination fracture toughness. Piggott has comprehensively reviewed the effect of fibre waviness on the static and fatigue properties of composites. Mrse and Piggott have observed that for a fibre misalignment angle varying from 1° to 6°, the compression strength reduces from 1.9 to 1.5 GPa. Adams and Hyer have shown that in compression-compression fatigue artificially induced fibre waviness in composites reduced the fatigue life when compared to a controlled composite.

Chun *et al.*[48] investigated theoretically and experimentally, the effect of fibre waviness on the nonlinear behaviour of unidirectional composites under tensile and compressive loadings. They studied the properties in thick composites with fibre waviness in the sinusoidal form of ratios (amplitude/wavelength (a/λ)) 0.011, 0.034, 0.059. They found that the fibre waviness significantly affected the tensile and compressive elastic properties and nonlinear behaviour in composite materials. They showed that composites with fibre waviness under tensile loading tend to stretch the waved fibres so that they stiffen during the deformation. However, coupons under compressive loading tend to undulate further more the waved fibres so that they soften during the deformation.

2.5.1. Techniques for measuring fibre alignment

The method commonly used to measure fibre alignment or misalignment in continuous fibre composites is the simple sectioning procedure demonstrated by Yurgartis[49]. This method is based on the simple observation that a cylinder cut by a plane at an angle θ to its diameter presents an elliptical shape (see Figure 2-7). The smaller the angle θ between the cylinder axis (B) and the cutting plane (A), the more elongated the ellipse. The major axis of the ellipse l, is related to the angle between the sectioning plane and the cylinder axis, θ by:

$$\sin\theta = \frac{d}{l} \tag{2.7}$$

where d is the diameter of the cylinder. Therefore, the angle θ can be rewritten as

$$\theta = \sin^{-1}\left(\frac{d}{l}\right) \tag{2.8}$$

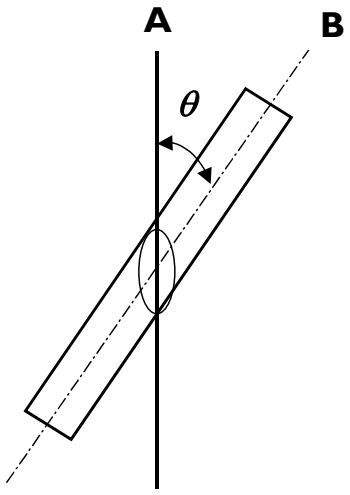

Figure 2-7: Ellipse resulting from the plane section of a right circular cylinder.

If an array of cylinders were cut by the same plane, then measuring the distribution of l_i will give the distribution of θ_i where the subscript indicates the ith cylinder.

To apply these observations to the determination of the fibre angle distribution in a composite, it must be assumed that all the fibres are cylindrical and have the same diameter.

It is also possible, by noting the angle between a reference direction and the major axis of the ellipse, to obtain information about the three-dimensional orientation distribution. However, this method is extremely cumbersome and can only give information about the orientation of a relatively small number of fibres at a few locations within the material. The use of confocal scanning laser microscopy to image material below the surface, can give some 3D alignment information without the need for serial sectioning was shown by Clarke *et al.*[50] in glass fibre reinforced composites. However, the maximum useable depth will depend upon the transparency of the matrix, volume fraction of the fibres and the distribution of fluorescence in the matrix. For example a maximum depth of about 150 μm is possible with a fibre volume fraction of less than 30%. For a fibre volume fraction of 50% the maximum possible depth is only 30-40 μm.

2.6 Techniques to minimise process-induced residual stresses and fibre waviness

The techniques reported in the literature to minimise process-induced residual stresses and fibre waviness are: 1) optimisation of the cure cycle, 2) using a low temperature cure prepreg, 3) electron beam curing, 4) modify the interphase properties, 5) use expandable monomers, 6) use shape memory alloys, 7) use fibre prestressing.

2.6.1. Optimisation of the cure cycle

As discussed in section 2.4 residual stresses develop during both polymer crosslinking and cool down of a curing cycle. Hahn investigated the effect of residual stresses on the cure cycle, and has shown that a longer hold at the gel temperature decreases the centre deflection of an unsymmetrical laminate due to the lower residual stresses in the composite. The reduction in residual stress could be due to the relaxation of the cure-induced shrinkage of the matrix. Chen *et al.* have also studied the development of residual stresses in composites using a viscoelastic micromechanical model. They have shown that a higher cooling rate results in higher residual stresses than a lower cooling rate.

White and Hahn[51] studied the effect of dwell temperature, dwell time and cool-down rate on residual stresses using unsymmetrical cross-ply laminates. They showed that by curing at lower temperatures for longer time or utilising an intermediate low-temperature dwell between two dwell cure cycles, the curvature of the laminate could be reduced by 25-30%.

Also by reducing the cool-down rate of the composite the laminate curvature could be reduced by 25%.

Madhukar *et al.* [12] have shown that changing the cure cycle parameters such as dwell temperature, number of dwells, duration of dwells and heating rate between dwells influences directly the development of cure-induced residual stresses. In a micro-composite, using a trial and error method they showed that an optimum cure cycle with minimum cure-induced residual stresses could be obtained by controlling the cure parameters. The same authors in subsequent publications showed that using results of a feedback control system the optimum cure cycle for a composite system that reduces residual stresses could be obtained.[52,53] The feedback control system is based on maximising the cancellation of stresses due to cross-linking shrinkage with a combination of stress relaxation and thermal expansion while completing the cure in a short time. They also showed that slow heating rates allow more time for the polymers to relax and relieve stresses caused by cure shrinkage of the polymer. Similarly, many other researchers have shown that optimisation of the cure cycle can be used to minimise process-induced residual stresses.[54]

From the above discussion it can be seen that optimisation of cure cycle parameters could be used as a method to minimise the process-induced residual stresses in composites. However, this method of controlling the cure cycle parameters varies with different resin systems and dimensions of the composite parts. In addition, it will be difficult to control the temperature in thick (>4mm) composites due to greater exothermic temperatures.

2.6.2. Low temperature cure systems

Low temperature cure systems are resins that can be cured at ambient temperatures. The duration of the cure cycle depends on the type of the resin, type of the hardener and their mixing ratio. In low temperature resin systems, the residual stresses will develop due to the cure-induced shrinkage of the resin. However, the thermally-induced stresses will be less compared to an elevated temperature resin cure system because the temperature difference between the cure temperature and room temperature will be small.

However, in low temperature cure systems, the glass transition temperature of the resin will be lower than for elevated resin cure systems; this will reduce the mechanical properties of the resin[55].

2.6.3. Electron beam curing

Electron beam (EB) curing uses high-energy electrons from an accelerator to generate free-radicals to initiate polymerisation and cross-linking reactions at ambient cure temperatures.[56] Because the temperature changes in the composite during EB cure can be kept less than for thermal curing systems, the residual stress development in EB cured

composites will be lower than for thermally-cured composites. To enable EB curing of epoxy resins, cationic initiators of required concentrations (generally 1-3%) need to be added to the polymers[57]. These cationic initiators react when subjected to irradiation of a beam of high-energy electrons. EB curing of composites enables fast curing and therefore a high production rate, resin curing at ambient temperature and therefore less thermal residual stresses. However, Goodman and Palmese[58] showed that the compressive and interlaminar shear strength (ILSS) of EB-cured composites are lower than those of thermally-cured composites. The authors suggested that this could be the result of the brittle nature of EB-cured cationic epoxy systems and also the existence of poor interfacial shear strength (IFSS) of EB composites. The adhesion between the fibre and matrix has been optimised for the thermal cure of epoxy-amine systems.

EB curing of composites is propitious in minimising residual stress development, increasing production rate and offers the possibility of on-site repair of composite structures. However, the adhesion between the fibre and matrix need to be optimised in order to improve the mechanical properties such as compression and ILSS of composites.

2.6.4. Tailoring interphase properties

During the manufacturing of reinforcing fibres, sizing or coupling agents are coated on the surface of the fibres to provide chemical interactions with the polymer matrix and to protect the fibres during handling and impregnation. For example silane coupling agents are commercially used on glass fibres to give good adhesion to epoxy matrixes. The net result of this is the nature of the differing interactions; the physical mixing of matrix and coupling agents and the nature of chemisorption at the fibre surface gives rise to an *interphase* region as opposed to a distinct interface between fibre and matrix[59].

Asp *et al.*[60] have shown from a numerical model that the modulus of the interphase region has a significant effect on the local interfacial thermal residual stresses and transverse failure stress and strain. If the elastic modulus of the interphase region is lower than the value of the resin, the local thermal residual stresses are minimised and vice-versa. However, they also showed that increasing the thickness of the interphase region to greater than 10% of the fibre radius would reduce the mechanical properties of the composites.

From both computational and experimental results, Hiemstra and Sottos[61] have demonstrated that for a low modulus interphase region, microcracks in the matrix were minimised as a result of lower thermal residual stresses. Later Sottos *et al.*[62] have also shown that the glass transition temperature (T_g) of the interphase region influences the thermal residual stresses and microcracking of the composite. From experimental results they showed that the presence of a low T_g interphase region increases the resistance to microcracking. On the other hand, the performance of the composite would be affected at high temperatures (that is above the T_g of the interphase region).

The method of tailoring the interphase properties was shown by researchers to reduce the residual stress development[60,62]. By using a low modulus interphase region, the T_g of the interphase region is reduced, which minimises the temperature difference during the cooling cycle. Therefore, the thermally-induced residual stresses are minimised. However, it is not possible to change the interphase region (or coupling agents) in a commercially-available prepreg laminate. Indeed, the modification has to be done during the fibre manufacturing process. Also the type and properties of the coupling agents have to be optimised for different fibre/matrix systems.

2.6.5. Shape memory alloys

Shape memory alloys (SMAs) are materials that change their crystalline structure in response to a change of temperature or mechanical deformation[63]. SMAs are available in the form of wires, strips, and films. In particular, binary Ni-Ti or tertiary Ni-Ti-X (where X could be copper (Cu), Cobalt (Co) or Ferrous (Fe)) SMA wires are now commercially available with diameters in the range of 50-200 μm[64]. The shape memory effect that these wires exhibit is associated with the reverse transformation from austenite to martensite during cooling or mechanical deformation.

Psarras *et al.* have embedded thin SMA wires into aramid/epoxy composites and the stress distributions in the aramid fibres were obtained by means of laser Raman spectroscopy. They have shown that by the addition of SMA wires to the composite thermal residual stresses reduced from –25 MPa to –6 MPa in aramid fibres.

The major drawbacks of using SMA in composite materials are 1) they induce fibre misalignment[65], 2) they create a variation in stress distribution in the composite between two SMA wires and 3) give stress concentration areas.

2.6.6. Expanding monomers

This technique involves the addition of an expanding monomer to the polymer matrix resin. An expanding monomer usually consists of a double ring that opens as the monomer copolymerises with the polymer matrix resin (see Figure 2-8).[66] The opening of the double ring tends to reduce the T_g of the cured resin system, which results in a decrease in the shrinkage occurring in the cool-down cycle from T_g to room temperature[67].

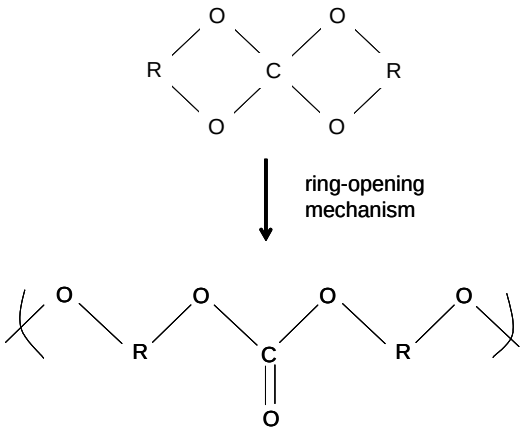

Figure 2-8: Ring opening mechanism of expanding monomers.

This mechanism reduces the residual stresses in the cured resin. However, it also reduces the modulus and glass transition temperature of the matrix. Orso and Vizzini[68] showed that by the addition of expanding monomers, the strain to initiate the transverse cracking in cross-ply composites could be delayed. However, the transverse crack growth rate was increased. The authors suggested that this could be due to the increase in the brittleness of the fibre-matrix interface. They also showed that the longitudinal modulus of the composite was not affected by the addition of the expanding monomers. However, the longitudinal strength was reduced by up to 15%.

2.6.7. Fibre prestressing

In the past decade, researchers have demonstrated theoretically that fibre prestressing can be used as a method to reduce residual stresses in composites. Prestressed composites are prepared by applying pre-tension to the fibres and subsequently curing the composite. Once the composite is cured and cooled down to room temperature, the pretension is released. Now the pretensioned fibres will tend to contract, inducing compressive stresses to the matrix, which will minimise both the cure-induced and thermally-induced residual stresses resulting from the cure cycle. Also, it was suggested by Dvorak and Suvorov[69] that as the fibres were prestressed and this was maintained throughout the curing process it was also possible to minimise the fibre misalignment in composites. However, in order to apply prestress to the fibres, a suitable prestress methodology is required, which can apply a uniform fibre prestress and maintain it throughout the curing process.

In the above section various solutions available in the literature to minimise process-induced issues such as residual stresses and fibre misalignment were discussed. From the discussion it can be observed that fibre prestressing is the only possible technique, which can counteract both process-induced residual stresses and fibre waviness. The following section will explain fibre prestressing in detail.

2.7 Fibre prestressed composites

The basic principle of prestressing in composites is adapted from the principle of production of prestressed concrete. In the Oxford dictionary of English[70] the word prestressed means "*previously subjected to stressing; into which stress has been deliberately introduced during manufacture*". In the literature, the prestressing concept is addressed by different terminologies like "pre-strained composite" and "pre-tensioned composites".

Prestressed composites are prepared by applying a pre-load to an n-ply laminate prior to cure. Since the uncured polymeric matrix possesses negligible stiffness, essentially all the pre-load applied would be carried by the fibres. The laminate would then be cured normally, causing the polymeric matrix to gel and solidify. Following cure and cool down the fibre pre-load is released, and the resulting elastic contraction of fibres relieves the tensile residual stress in the matrix resulting from the curing cycle by inducing compressive stresses. This process of prestressing is illustrated in the Figure 2-9.

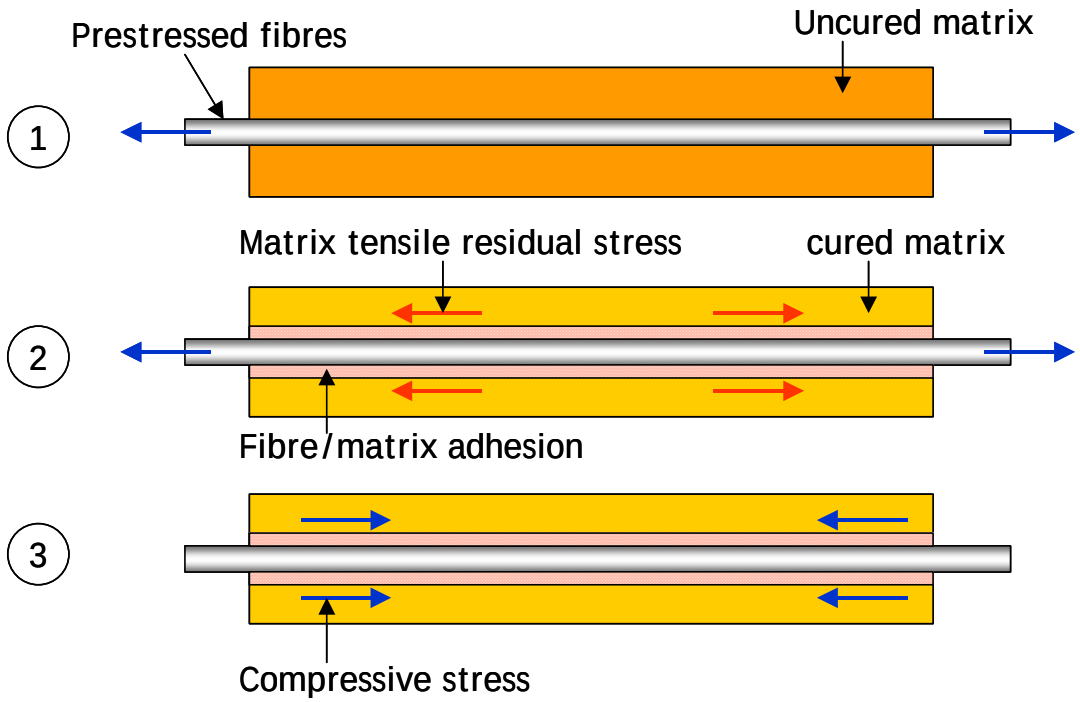

Figure 2-9: Schematic illustration of the fibre prestressing principle. 1) prestressing the fibres in the uncured matrix, 2) matrix curing and formation of fibre/matrix bonding and development of tensile residual stress in the matrix and 3) release of fibre prestress at ambient temperature, which induces compressive stress to the matrix.

The creation of compressive stresses in the matrix would impede crack propagation through the matrix, thereby delaying or preventing the formation of matrix cracks in the composite. This could enhance the matrix-dominated properties of composites. Table 2-3 briefly presents the papers published in the literature on prestressed composites in chronological order. These papers are critically reviewed in the subsequent sections.

2.8 Theoretical analysis of fibre prestressing

In literature, the effect of fibre prestress on residual stresses and the onset of failure in continuous fibre composites were mathematically predicted using micro- and macro-mechanics theory. The prestress theories reported in the literature are discussed herein.

Tuttle proposed a simple micro-mechanics theory based on a rule-of-mixtures to predict the effect of fibre prestress on the matrix residual stresses in composites. The assumptions used in his theory were 1) perfect fibre/matrix bonding, 2) both fibre and matrix are isotropic linear elastic materials and 3) fibre and matrix properties are independent of temperature. From the theory, Tuttle predicted that the final residual strain in the matrix (ε_m) is given by:

$$\varepsilon_m = \frac{-\sigma_f^p V_f}{E_{11}} + \Delta T.\alpha_{11} \tag{2.9}$$

where σ_f^p is the applied fibre prestress, V_f is the fibre volume fraction, E_{11} is the composite Young's modulus in the fibre direction, α_{11} is the composite thermal expansion coefficient in the fibre direction and ΔT is the change in temperature.

From the model, Tuttle predicted that in a non-prestressed (σ_f^p=0 MPa) carbon/epoxy composite with 60% V_f, the matrix is subjected to a tensile residual stress of about 24 MPa in the fibre direction, which is 60% of the ultimate strength of the epoxy resin. By applying a fibre prestress of 1.4 GPa, he showed that the matrix tensile residual stresses could be reduced to 0.98 MPa, which is 2.5% of the epoxy ultimate strength. Similar models were also proposed by other researchers.

Hadi and Ashton have further developed Tuttle's model to predict the tensile strength of prestressed composites. From a rule-of-mixtures the tensile strength of the unidirectional composite (σ_C) is given by:

$$\sigma_C = \sigma_f V_f + \sigma_m V_m \tag{2.10}$$

where σ_f and σ_m are the fibre and matrix tensile strength respectively and V_m is the volume fraction of the matrix.

Table 2-3: Literature review of prestressed composites

Reference	Material	Research area	Prestress method	Findings
Tuttle (1988)	Carbon fibre/ epoxy unidirectional composite.	Micromechanical modelling of the effect of prestress on residual stresses in composites.	not applicable	He predicted that in non-prestressed composite (V_f = 60%), tensile residual stresses in matrix is 24 MPa for a temperature difference of 150°C. Applying 1.4 GPa prestress, reduces matrix residual stress to 0.98 MPa.
Jorge *et al.*[71] (1990)	E-glass fibre/ polyester unidirectional composite. *Fibre volume fraction*: 56 ± 4 %	Tensile properties in fibre direction	Dead weight	Tensile strength and modulus initially increases with prestress, above a prestress limit it shows a tendency to stabilise. *Fractographic analysis*: No difference between prestressed and non-prestressed composites.
Schulte and Marrisen (1992)	Aramid fibre (0°)/ Carbon fibre (90°) / epoxy hybrid cross-ply composite with (0/90/90/0) laminate sequence.	Tensile properties in fibre direction and transverse cracking	V-slot Mechanical fastening	Prestressing increased the average fracture stress and fracture strain by 2.8% and 3.3% respectively. Increases the strain to transverse crack initiation by 0.2% strain for a 341 MPa prestress.
Rose and Whitney[72] (1993)	Carbon fibre/ epoxy cross-ply composite with (0/90/90/0) laminate sequence. *Fibre volume fraction*: 70 %	Mathematical modelling and experimental measurement of first ply failure.	Filament winding	Prestressing enhanced first ply failure strength in composites. For a prestress of 690 MPa, first ply failure stress increased by 29%. However, their model does not correlate with the experimental results.
Sui *et al.*[73] (1995)	Vinylon (poly(vinyl alcohol)) fibre /epoxy-aluminium laminate (VIRALL). *Fibre volume fraction*: 32± 1 % *Aluminium volume fraction*: 56.5 ± 1.5 %	Tensile properties in fibre direction	not specified	Prestressing increases initial modulus, elastic limit strain, yield strength and failure strength, together with a decrease in failure strain.
Tuttle *et al.*[74] (1996)	Carbon fibre/ epoxy unsymmetrical cross-ply composite. *Fibre volume fraction*: 70 %	Tensile properties and transverse cracking	Hydraulic cylinder rig	Curvature of unsymmetrical laminates decreases by increasing fibre prestress. Transverse cracks reduced with prestress. No difference in ultimate tensile strength of the composite with prestress.

…. continued

Table 2-3: Literature review of prestressed composites ... continued

Reference	Material	Research area	Prestress method	Findings
Motahhari and Cameron[75] (1997)	E-glass fibre/ epoxy unidirectional composite. *Fibre volume fraction*: 62 ± 2 %	Measurement of applied pre-load and mathematical modelling of residual stress	Horizontal tensile testing machine	Prestressing reduced the residual stresses in the matrix and the fibre/matrix interface.
Motahhari and Cameron[76] (1998)	E-glass fibre/ epoxy unidirectional composite. *Fibre volume fraction*: 62 ± 2 %	Impact properties	Horizontal tensile testing machine	33% increase in impact strength was reported for a 60 MPa prestressed composite when compared to non-prestressed composites. Above this prestress level a reduction in impact strength was reported. *Fractographic analysis*: Prestressed composites resulted in more splitting and delamination compared to non-prestressed composites.
Zhao and Cameron[77] (1998)	Co-mingled E-glass fibre/ poly(propylene) (PP) unidirectional composite. *Fibre volume fraction*: 34.2 %	Tensile, flexural and Interlaminar shear strength (ILSS)	Fibre alignment rig	Fibre prestressing enhances tensile strength, flexural strength and ILSS of composites by 20%, 21% and 10% respectively. Above an optimum prestress level the properties stabilises.
Hadi and Ashton[78] (1998)	E-glass fibre/ epoxy unidirectional composite. *Fibre volume fraction*: 30%, 45% and 60 %	Tensile properties in fibre direction	Filament winding	Improvement in tensile strength and modulus with prestress.
Motahhari and Cameron[79] (1999)	E-glass fibre/ epoxy unidirectional composite. *Fibre volume fraction*: 60 ± 2%	Flexural properties	Horizontal tensile testing machine	Flexural strength and modulus increases by 33% with prestress. Above an optimum prestress level the flexural properties decreases.
Dvorak and Suvorov[69] (2000)	S-glass fibre/ epoxy cross-ply and quasi-isotropic laminates. *Fibre volume fraction*: 50 %	Mathematical modelling of the effect of residual stresses on prestress and failure envelopes.	not applicable	From the model it was shown that the fibre prestress reduces the residual stress in matrix and could increase the resistance to matrix damage.
Jevons *et al.*[80] (2002)	E-glass fibre/ epoxy cross-ply laminates with $[0/90_2/0_2/90/\ 0/90]s$ laminate sequence. *Fibre volume fraction*: 56%	Low velocity impact.	Biaxial loading frame	They reported a small improvement in low velocity impact properties of composites with prestress.

Hadi and Ashton predicted that the tensile strength of a prestressed unidirectional composite (σ_C^p) is given by:

$$\sigma_C^p = \sigma_f V_f + \sigma_m V_m + V_f \sigma_f^p \tag{2.11}$$

Results from Hadi and Ashton's model shows that the unidirectional composite tensile strength increases with an increase in fibre prestress. However, Motahhari and Cameron have shown that not all the fibre prestress (applied prior to matrix cure) is released to the cured matrix, some part of the prestress remains in the fibre as tensile residual stresses. They also showed that this residual tensile stress in the fibre increases with fibre prestress.

It is well known that in the fibre direction of the composite, the main load-bearing member is the fibre. If the fibres are initially subjected to a tensile residual stress due to the prestress curing process then subsequent mechanical loading of the composite will result in a reduction in the tensile strength.

Dvorak and Suvorov have predicted the effect of fibre prestressing on symmetrical elastic laminates using laminate plate theory. From the stress analysis calculations they have shown that the overall contribution of fibre prestress to the symmetrical elastic laminate is equivalent to applying compressive mechanical stresses to each ply, when removing the prestress forces originally applied to the respective plies. This reduces the matrix residual stresses in the composite. From their prediction of ply failure using a maximum stress criterion, they showed that fibre prestressing could increase the resistance to first ply failure (90° laminates) by reducing the tensile residual stresses in the matrix. Also they suggested that fibre prestressing could minimise the fibre waviness in composites, because the fibres are subjected to prestress during the curing process, which will minimise the movement of the fibres. This could result in an improvement of the compressive strength of composites. From their stress analysis calculations they have shown that fibre prestress can be optimised to control the overall deformation in symmetric laminates.

When a compressive load is applied to the prestressed composite, at first the tensile residual stress in the fibres has to go to zero and is then subjected to compression. This could also results in improvement in compressive strength of the composites.

From the Tuttle and the Dvorak and Suvorov models for prestressed composites, it was shown that fibre prestressing minimises the residual stresses in the matrix. By reducing the residual stresses Dvorak and Suvorov showed that the first ply failure strength of the composites could be improved. This also suggests that the matrix-dominated properties such as impact, flexural and low stress level fatigue of prestressed composites could be improved.

2.9 Evaluation of existing fibre prestress methodologies

The manufacture of a prestressed composite entails the need for a rig to impart a predetermined prestress during the cure cycle. To this effect, designing the right rig for this purpose is critical for this research. Before implementing a design, a study was carried out to ascertain whether existing approaches to solving this problem could be used for this study. The following section briefly discusses the fibre prestress methodologies reported in the literature to verify their suitability for the current design criteria.

2.9.1. Dead-weight method

Jorge *et al.* showed that prestressed composites can be prepared by applying a suitable load to the fibre ends by attaching and tightening the fibres to steel pins with a spacing of 2 mm to provide a uniform distribution of prestress, as shown in Figure 2-10. They prepared E-glass/polyester resin composites using a wet lay-up process. The E-glass fibre rovings were applied through two combs like sets of steel pins (see Figure 2-10), on parallel sides of the lower glass plate, producing a separation of approximately 2 mm between the rovings. The pre-load was applied to the ends of the fibres by tying it to a dead-weight. The resin was applied to the fibres. The fibres were impregnated with polyester resin manually. The composite was cured at room temperature for 24 hours, followed by a 3 hours post-cure at 80°C. The applied pre-load was in the range of 0-100 N.

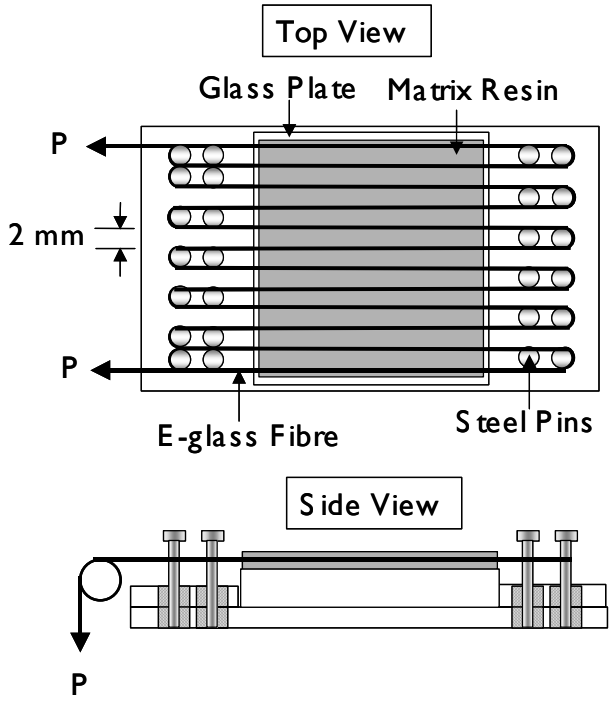

Figure 2-10: Dead-weight method. [71]

Using this methodology it is difficult to obtain a uniform fibre distribution through the width of the composite. The bending of the fibres in the steel pin region may cause fibre fracture. Conventional prepreg tape material cannot be used and is difficult to process in autoclave.

2.9.2. V-slot mechanical fastening method

Using aluminium plates with two V-shaped slots machined at the ends, Schulte and Marissen have shown a method of prestressing composites. They prepared hybrid (0°-Kevlar/90°-Carbon epoxy) cross-ply composites with a [0/90/90/0] laminate sequence. The prepreg laminates were laid-up between two aluminium plates. At both ends of the lower plate the 0° plies were mechanically fastened with a V-shaped bar into these slots as shown in Figure 2-11. The total pre-strain achieved was 1.1%. The composite was cured in a hot-press at 125°C. As the composite was cured at 125°C, pre-strain will also be applied by the thermal expansion of the aluminium plate. I was unable to gather from Schulte and Marissen article whether the thermally-induced pre-strain was included in the total-pre-strain calculation.

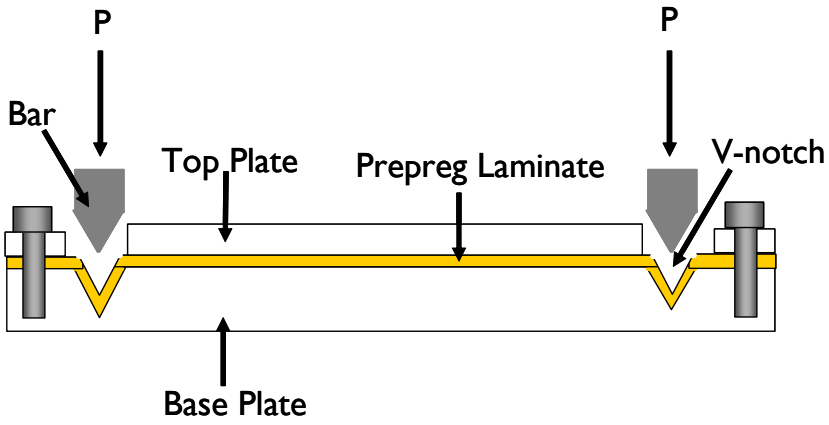

Figure 2-11: V-slot mechanical fastening method.

This method can be used to apply only one prestress level. Brittle fibres like glass and carbon cannot be prestressed using this technique because the kinking of fibres in the V-slots will result in numerous fibre fractures leading to an uneven stress distribution. In addition, as the thickness of the composite increases, there is a possibility of variation in applied prestress through the thickness. In other words, the top ply of the prepreg will experience more pre-strain than the bottom ply of the laminate, which is due to the V-slot clamp design.

2.9.3. Filament winding

In filament winding, a continuous band or tape of resin-impregnated fibres is laid onto a revolving mandrel to produce a composite structure. As shown in Figure 2-12, a large number of fibre rovings are pulled with a known pre-load, collimated into a band through the use of textile thread board or a stainless steel comb, passed into a liquid resin bath and a doctor blade, and then warped over the mandrel. Hadi and Ashton showed that by applying different pre-load levels, composites with various prestress levels could be prepared.

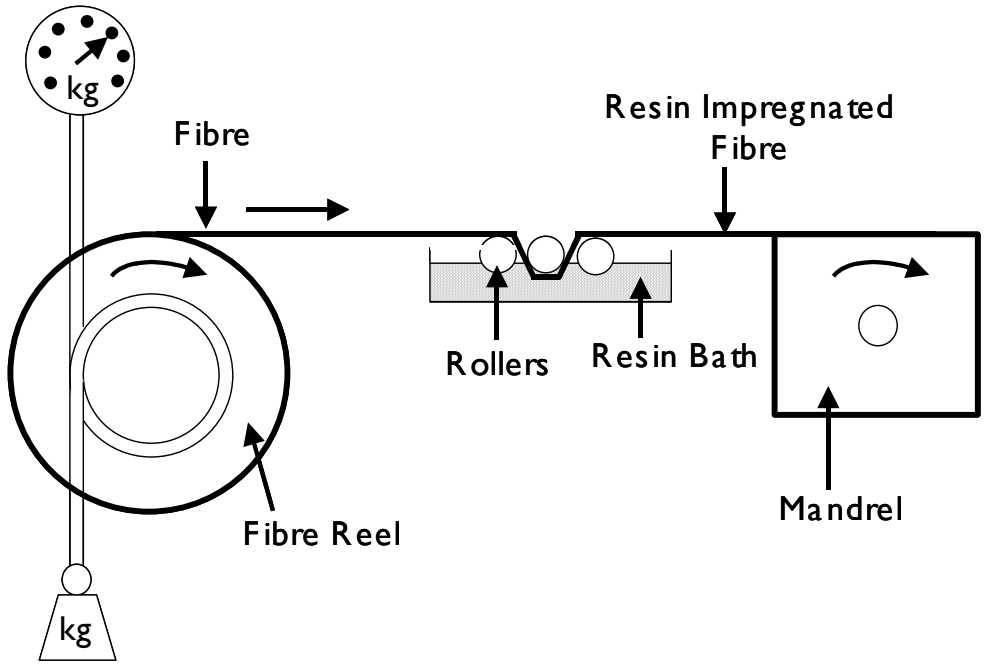

Figure 2-12: Filament winding.

Hadi and Ashton prepared uni-directional prestressed composites using this method in a square flat sided mandrel. Rose and Whitney prepared cross-ply laminates by constructing a square mandrel, which could be rotated appropriately during the winding process. After prestressing, the composites were cured in an autoclave.

The inherent drawback of using this method is that it is very difficult to monitor the pre-load during the curing process and before releasing. Therefore it will be difficult to determine the prestress released to the composite. In addition, with fibre prestress, the fibre volume fraction of the composite will increase because of the increase in compaction of fibres laid onto the mandrel (see Section 2.10.1). Therefore it will be difficult to manufacture composites with various levels of prestress and with uniform fibre volume fractions. Care should be taken in selecting the mandrel material because if the composite is processed at elevated temperatures the mandrel thermal expansion-induced prestress should also be included.

2.9.4. Hydraulic cylinder prestress rig

Tuttle *et al.* have shown that by using a hydraulic cylinder and a hot press, composites with different levels of prestress can be manufactured (see Figure 2-13). The cylinder was mounted on a horizontal frame, such that the prestressed plies remain parallel to the heated platens of the hot press. This technique enables prepreg laminates to be manufactured. The prepreg plies to be prestressed are wrapped around both the movable loading rod and a fixed loading rod mounted on the far side of the hot-press. They reported that in the initial experiments, slippage occurred between the ply and loading rod surface at high fibre prestress levels, which was latter eliminated by knurling the surface of the loading rods.

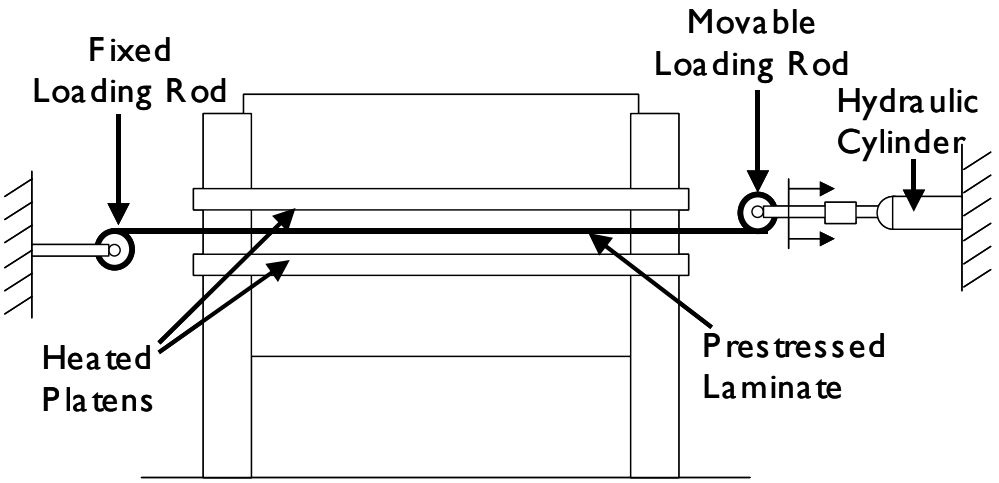

Figure 2-13: Hydraulic cylinder prestress rig.

The load applied to the fibres was monitored from the pressure gauge fixed in the cylinder. Nevertheless, this technique is limited to a hot-press manufacturing process.

2.9.5. Horizontal tensile testing machine

Motahhari and Cameron showed that by using a horizontal tensile testing machine, fibre prestress could be achieved (as shown in Figure 2-14). The electric motor provides the mechanical energy and rotates the drum, which pulls the fibres in one direction. The load applied was monitored by a load cell. A U-shaped mould was used to prepare composites. A similar method was also used by Lee[81] and Ali[82] to prestress prepreg-based composites.

This prestress methodology is very simple and can measure the pre-load applied during the curing process. However, this method restricts itself to room temperature and hot-press cure composite systems.

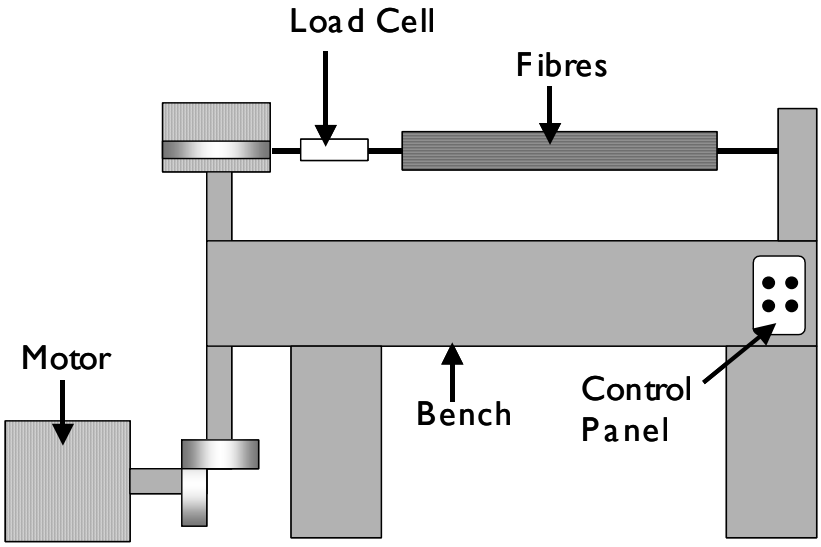

Figure 2-14: Horizontal tensometer prestress rig.

2.9.6. Fibre alignment rig

Zhao and Cameron have designed a fibre alignment device as shown in Figure 2-15 for manufacturing composites with different levels of prestress.

The fibres were first wound onto a steel frame, which was then transferred to the fibre loading device. The frame was attached to a tensile testing machine to be stretched to the required level, the lock nut of the locking system was then turned down to lock the bars at the required position. The composite was cured by a compression moulding process.

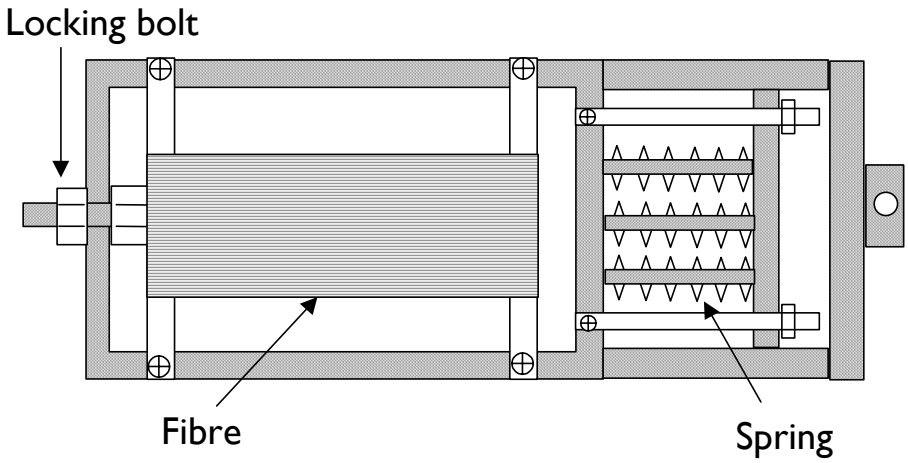

Figure 2-15: Fibre alignment rig.

Using this prestressing technique, it will be difficult to monitor the fibre prestress during cure and prestress release and therefore difficult to determine the prestress applied. Also the load applied by the tensile testing machine may reduce after locking the load due to bending of the frame. In Zhao and Cameron's work they use co-mingled fibres, which consist of E-glass fibres and poly (propylene) (PP) fibres in 34.2:65.8 ratio. During prestressing, initially both E-glass and PP fibres will be carrying the applied pre-load, but during processing as the PP fibres melt and wet the E-glass fibres, the pre-load carried by the PP fibres will be transferred to the E-glass fibres. Therefore, the prestress applied to the E-glass fibres increases, which has to be recalculated to find the actual prestress in the fibres. This was not discussed in their paper. Also it is difficult to manually align the fibre to 0° while winding onto a steel frame.

2.9.7. Biaxial loading frame method

Jevons *et al.* [80] have shown a method for prestressing cross-ply laminates and processing in an autoclave. Their design consisted of C-channel section frame with four clamps linked to the frame by bolts as shown in the Figure 2-16. Prestressed composites were manufactured by laying up cross-ply prepreg laminate, and curing the prepreg ends with aluminium end tabs. After curing the end tabs and cooling down to room temperature, seven holes of 10 mm diameter were drilled. These end tabs were secured into the clamps by tightening the bolts. Prestress was applied by tensioning the locking bolts between the clamps and the frame, by a pre-determined amount. The frame was vacuum bagged and processed in an autoclave.

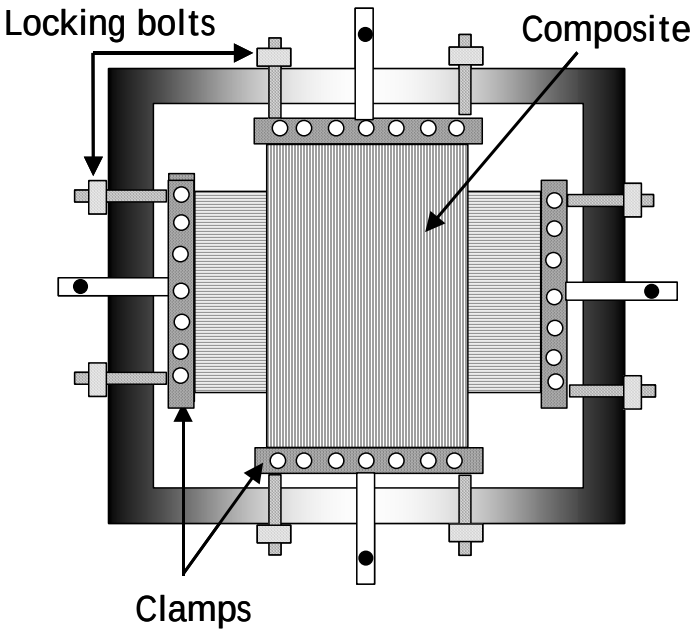

Figure 2-16: Biaxial loading frame method.

This is the first method published in the literature to enable prestressing in two directions and curing in autoclave. However, in this method, the tension applied to the fibres may reduce because of the bending of the channel frame (39.4 nm per unit force), which was calculated as shown in Appendix A. Consequently, determining the applied pre-load to the composite panel is cumbersome. It will be difficult to control the alignment of the clamps, which are crucial in order to apply uniform prestress in both directions. In addition to that, as the rig has may sharp corners and complicated shapes, conventional vacuum bagging is difficult. This raises a need for a special vacuum bagging system to prepare composites in autoclave.

Table 2-4 shows a comparison of all the prestress methods discussed above.

Table 2-4: Comparison of existing prestressing methods.

Prestress methodology	Processing technique	Measurement of prestress during composite processing	Measurement of composite residual stress
Dead-weight	Room Temperature (RT)	Yes	No
V-slot mechanical fastening	Hot-press	No	No
Filament winding[72, 78]	Oven and Autoclave	No	No
Hydraulic cylinder	Hot-press	Yes	No
Tensile testing machine[75, 81, 82]	RT and Hot-plate	Yes	No
Fibre alignment rig	Compression moulding	No	No
Biaxial loading frame	Autoclave	No	No

2.10 Static mechanical properties

Researchers have investigated the effect of fibre prestress on tensile, impact and flexural properties of composites. In this section, the above mentioned static mechanical properties are reviewed.

2.10.1. Tensile properties

The tensile properties in unidirectional prestressed composites are studied by Jorge *et al.*, Zhao and Cameron, Hadi and Ashton, and Huang *et al.*[83].

Jorge *et al.* studied the effect of prestress on tensile properties in unidirectional glass/polyester composites. They used a dead-weight prestressing method to prepare composites with different prestress levels. Figure 2-17 shows the tensile strength and modulus results reported from their study. They interpreted that there is an improvement in tensile strength and modulus with fibre prestress. However, from the statistical analysis

using 95% confidence level it was found that their tensile strength results for all the prestressed composites are within the standard deviation of the measurements.

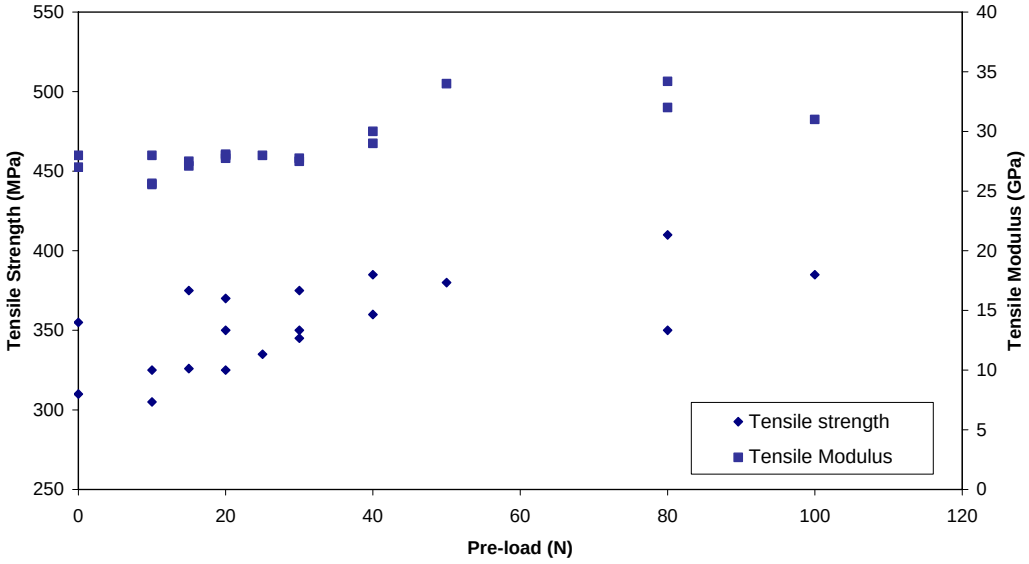

Figure 2-17: Influence of pre-load on the tensile strength and modulus of glass/polyester composites.

Zhao and Cameron have studied the effect of fibre prestress on co-mingled poly(propylene) (PP)/glass fibre. They reported that as the fibre prestress increased, the tensile strength and modulus increased up to a critical limit of applied prestress (85 MPa) and above this limit the properties decreased. Figure 2-18 shows a trend of improvement in tensile strength and modulus with fibre prestressing. From their results, it can be observed that there is no significant difference between the tensile strength and modulus of all the prestressed composites except 0 MPa prestress level. This raises a question about the quality of the 0 MPa prestressed composite. They have not reported the method of manufacturing 0 MPa prestressed composites and the extent of fibre waviness in the 0 MPa composite. Therefore, their interpretation of "improvement in tensile strength and modulus" is questionable.

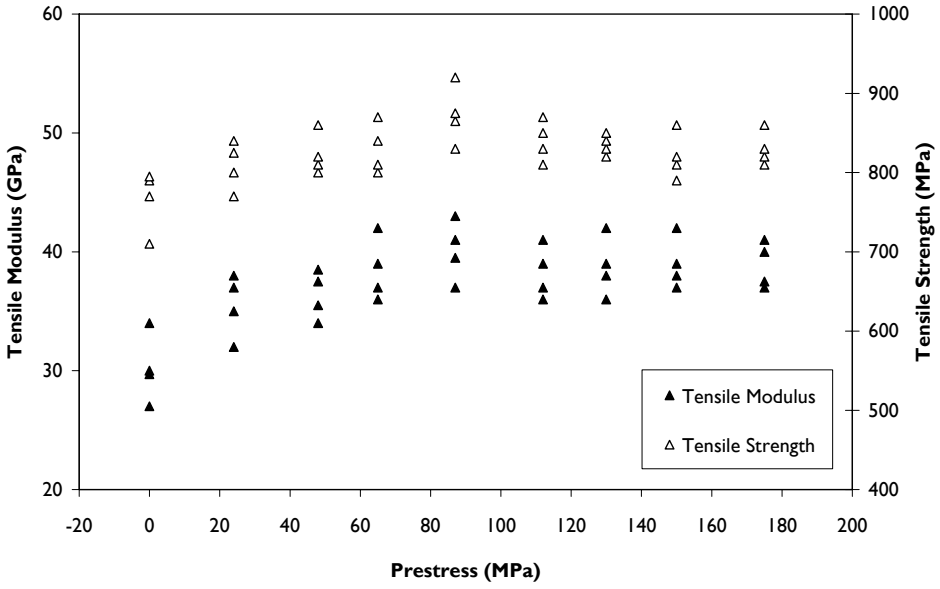

Figure 2-18: Tensile strength and modulus as a function of prestress (Zhao and Cameron).

Huang *et al.* [83] and Hadi and Ashton studied the tensile properties of composites prestressed using a filament winding technique. Huang *et al.* have reported that prestressing increased the fibre volume fraction of the composites by increasing the compaction of fibre bundles. Optical micrographs of various levels of prestressed composites are shown in Figure 2-19. At low levels of prestress, there is a gap between the Zylon fibre bundles. As the prestress increases, the fibre volume fraction of Zylon fibres increased. As a result, the ultimate tensile strength (UTS) and modulus of the composites also increased (see Table 2-5). Also Hadi and Ashton found that fibre prestressing enhanced the tensile strength and modulus of the composites. However, Hadi and Ashton did not report the effect of prestress on fibre volume fraction in their composite systems.

Table 2-5: Summary of tensile properties reported by Huang *et al.* [83].

Prestress (MPa)	UTS (GPa)	Modulus (GPa)	Fibre Volume fraction V_f (%)
0	2.9	170	67.3
700	3.3	205	77.5

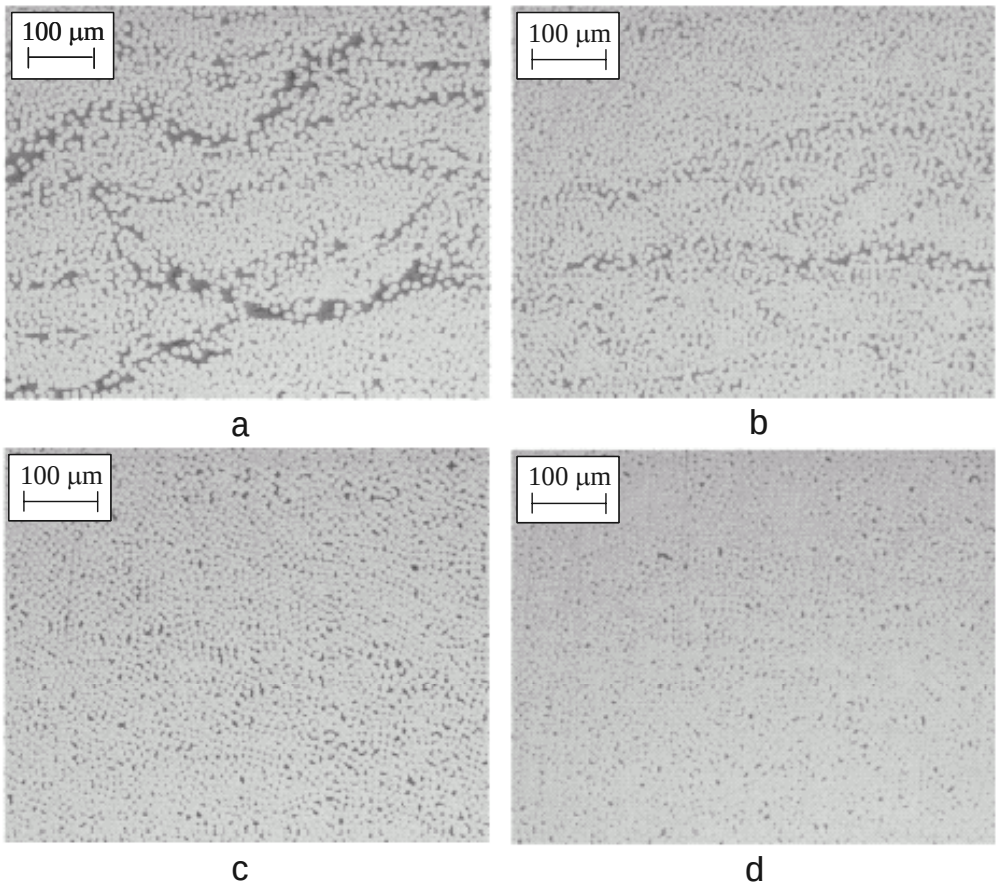

Figure 2-19: Cross-sections of Zylon/epoxy composite samples show the effect of fibre prestress on the distribution of fibre in epoxy matrix. (a) <70 MPa prestress, (b) 280 MPa prestress, (c) 700 MPa prestress, and (d) 1000 MPa prestress (Huang *et al.*[83]).

Schulte and Marissen and Tuttle *et al.* have studied the tensile behaviour of 0° direction prestressed cross-ply composites. Schulte and Marissen studied the effect of prestress on tensile properties and transverse cracking of hybrid fibre (Kevlar fibre in 0° and carbon fibre 90°) epoxy cross-ply composite with a [0/90/90/0] laminate sequence. They showed that prestressing the 0° Kevlar fibres increased the strain to initiate the transverse ply cracking and the resistance to transverse crack propagation during tensile loading of composites (see Figure 2-20). They suggested that the delaying of transverse cracks could be due to the reduction in tensile residual stress in the 90° plies as a result of 0° prestressing. They also showed that there was an improvement in the average tensile strength and fracture strain of the composites. From Table 2-6 reproduced from their paper, it can be observed that the average tensile strength and fracture strain shows an improvement. However, the standard deviation of their measurements shows that the properties of prestressed composites are within the limits of non-prestressed composites.

Table 2-6: Mechanical properties of the prestressed and non-prestressed laminate reported by Schulte and Marissen. Results are an average of seven tests.

Tensile Properties	Hybrid Kevlar/Carbon fibre epoxy cross-ply composite	
	Non-prestressed	Prestressed
Fracture strain ε (%)	1.75 (±0.15)	1.81 (±0.1)
Tensile Strength σ (MPa)	555 (±24)	571 (±40)
Modulus E (GPa)	31 (±1)	31 (±1.1)

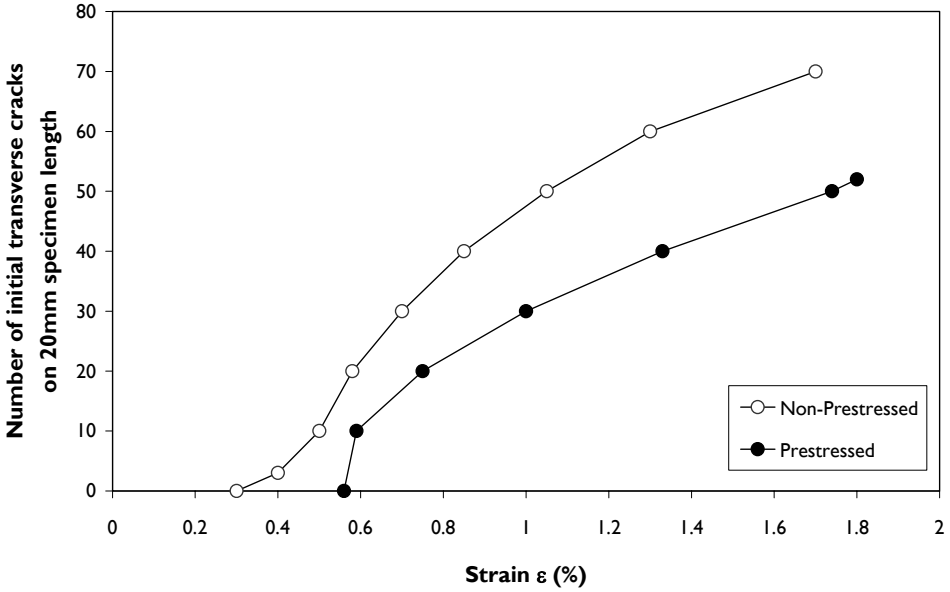

Figure 2-20: Number of initial transverse cracks versus strain, which was obtained by light microscopy. The mean values of four tests are given here and the data was taken from the specimen edge (Schulte and Marissen).

Tuttle *et al.* have shown a method to fabricate unsymmetrical laminates with a range of prestress applied to 0° plies. They reported that fibre prestressing significantly reduced the number of matrix cracks induced within the 90° ply of a $[0^p/90]_T$ specimen (the superscript 'p' represents prestress) as shown in Figure 2-21. This was also observed by Schulte and Marissen. They also suggested that this could be due to the reduction in tensile residual stresses within the 90° ply as a result of 0° prestressing. However, unlike Schulte and Marissen, they have shown that there is no correlation between ultimate tensile strength and fibre prestress.

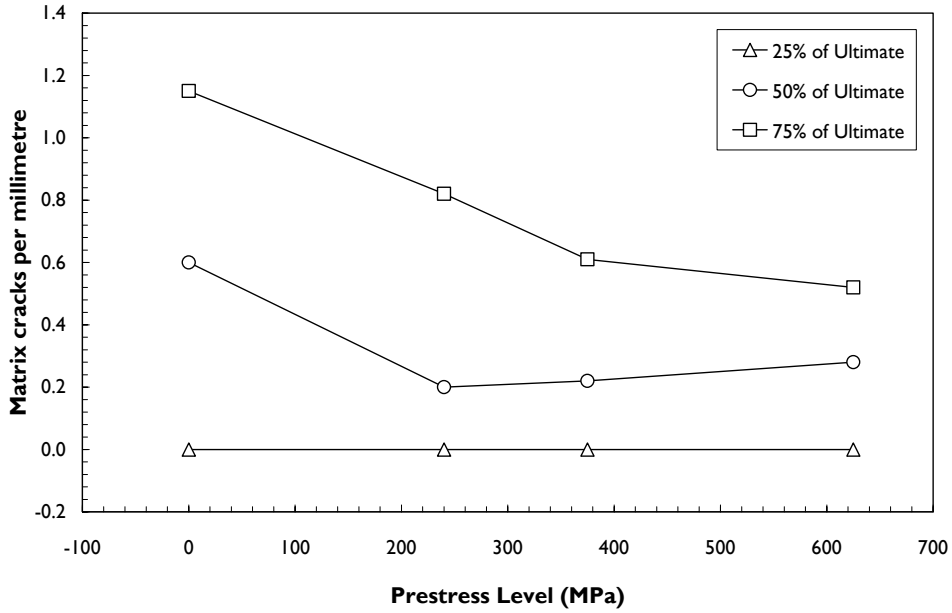

Figure 2-21: Matrix cracks induced in $[0^P/90]_T$ specimens as a function of prestress level (Tuttle *et al*.).

2.10.2. Impact properties

Motahhari and Cameron reported that fibre prestressing increased the impact strength of composites up to an optimum prestress level of 60 MPa prestress and above this level, it decreased (see Figure 2-22). The authors' explanation was that as the fibre prestress increased the debonding fracture overcame the transverse fracture, resulting in the formation of new large surface areas, which absorbed more energy. Above a critical limit of prestress (60 MPa), the impact properties declined as the ability of the interface to resist shear debonding decreased.

The author's suggested that the increase in the resistance to transverse fracture of the matrix could be due to the reduction in matrix residual stresses. As a result, the fracture mode changes from transverse to interfacial debonding, leading to more energy absorption.

Fancey[84] studied the effect of viscoelastically-induced prestress on impact properties of composites. In his work, Nylon 6,6 fibres were stretched under a load, which was released prior to matrix impregnation. On solidification of the matrix, the viscoelastically-strained fibres impart compressive stresses. From their results of charpy impact test they have shown that prestressed composites absorb 25% more impact energy than non-prestressed composites.

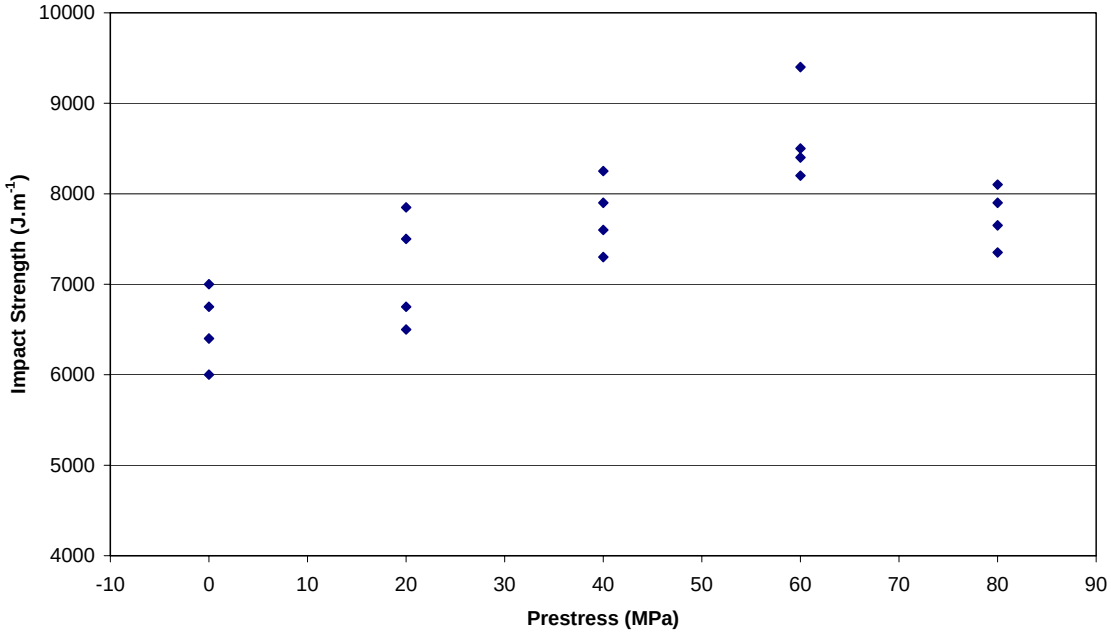

Figure 2-22: Influence of prestress on impact strength of composites.

2.10.3. Flexural properties

Motahhari and Cameron investigated the effect of fibre prestressing on the flexural properties of glass fibre/epoxy composites, and showed that prestressing increases the flexural strength and modulus of composites (see Figure 2-23). Zhao and Cameron also observed this effect in PP/glass fibre composites.

Motahhari and Cameron presented two reasons for the improvement in flexural properties 1) a tensile residual stress in the fibres and 2) a reduction in matrix and interface residual stresses. The same authors in another publication showed that as the fibre prestress increases the tensile residual stresses in fibres increase. The tensile residual stress in fibres produces a component normal to the direction of the fibres. This force component acts against the bending force during the flexural test. As a result, compared to the non-prestressed composite, more bending force is required to cause a certain amount of deflection. Therefore, the flexural properties increase.

Also, as the applied fibre prestress increases, the compressive residual stress in the matrix increase and consequently more resistance against crack initiation and propagation. Therefore, more bending force was required to provide the crack with enough energy to grow. Above an optimum level of prestressing there was a drop in strength, which they attributed to the fibre-matrix debonding. At higher prestress levels, the residual shear stress at the interface increases. This, upon raising the applied load, progressively results in debonding of the fibres and matrix and reduces the overall strength of the composite.

Thus, they have shown that there exists an optimum fibre prestress limit to obtain the maximum possible flexural strength and modulus, and therefore resistance to crack initiation and opening. Above this optimum prestress limit the flexural properties are reduced by the rapid fibre-matrix debonding damage.[79]

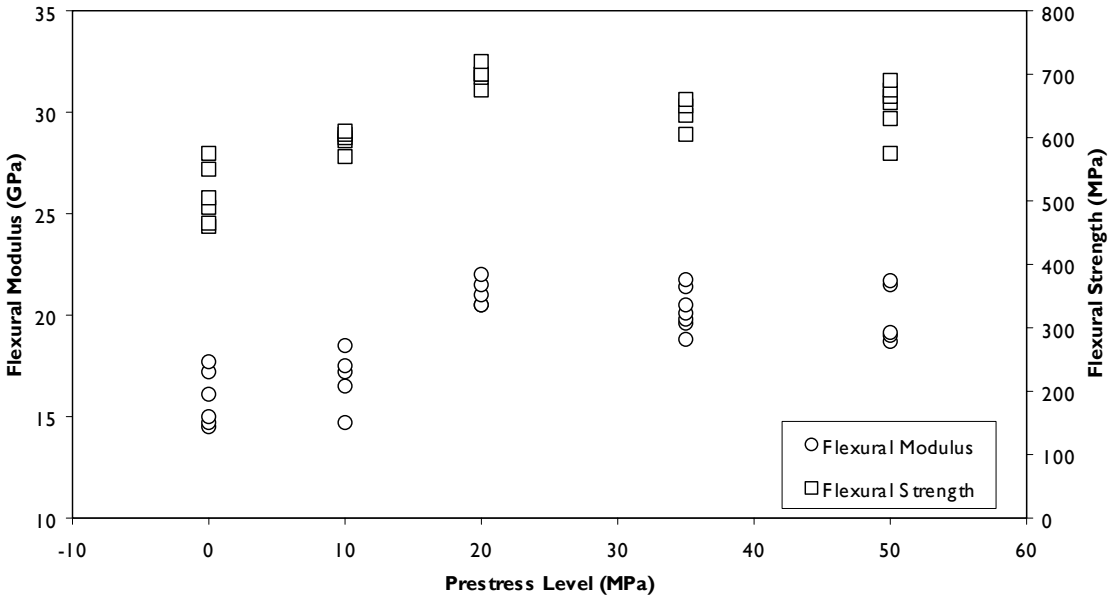

Figure 2-23: Flexural strength and modulus as a function of fibre prestress (Motahhari and Cameron).

2.11 Fatigue of composites

Almost all engineering components are subjected to varying loads throughout their working life, and fatigue is easily the most common failure in service. Fatigue in materials is their response to cyclic loading or, in other words, fatigue is a process whereby mechanical damage caused by repetitive or fluctuating stresses results in a material failure at lower stress levels than would be required under static loading. The purpose of this review is to understand the fatigue life diagrams, damage mechanisms and various factors, which influence the fatigue properties of Glass Fibre Reinforced Plastics (GFRP). This is followed by review of literature on the effect of fibre prestress on the fatigue performance of composites.

2.11.1. Fatigue life diagrams

Traditionally the fatigue data is represented by an *S-N* curve (peak stress verses the logarithm of the number of cycles to failure). A typical tension-tension fatigue (R = +0.1) *S-N* curve of a unidirectional glass/epoxy composite[85] is presented in Figure 2-24. With reference to this figure, it can be observed that the fatigue behaviour of the composite appears to show a linear relationship. Many researchers previously observed this linear behaviour.[85,86]

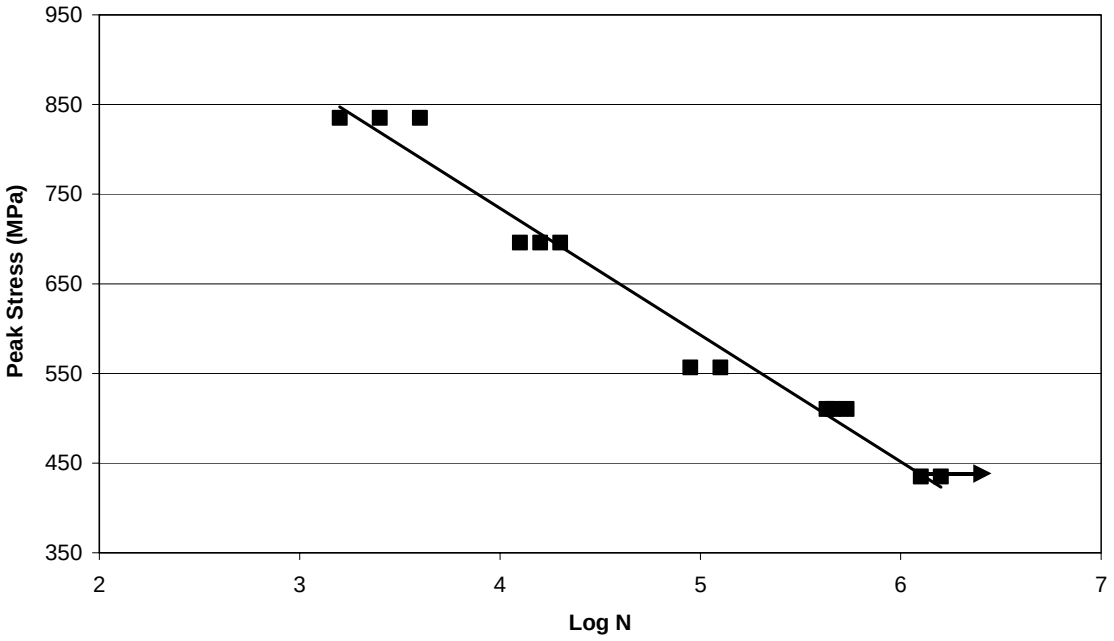

Figure 2-24: Tension-tension fatigue life diagrams of glass/epoxy composites.

Mandell conducted a series of experiments on different types of glass-fibre reinforced plastics (GFRP). He showed that when the number of cycles to failure lay between 10^2 and 10^6, the *S-N* curve could be approximated by a straight line of the form:

$$\sigma_{\max} = \sigma_{UTS} + b \log N \tag{2.12}$$

where σ_{max} is the maximum applied stress, σ_{UTS} is the ultimate tensile strength, N is the number of cycles to failure and b is a constant. The ratio of b/σ_{UTS} was defined by Mandell as the fractional loss in tensile strength per decade of cycles.

Daniel and Charewicz[87] showed that the fatigue data of unidirectional and cross-ply graphite/epoxy composites could also be fitted by a second-order polynomial curve:

$$\sigma_{\max} = \sigma_{equ} + x \log N + y(\log N)^2 \tag{2.13}$$

where σ_{max} is the maximum applied stress, σ_{equ} is the equivalent UTS, N is the number of cycles to failure and x and y are constants. Using this equation Daniel and Charewicz showed that the fatigue life of a composite could also be predicted.

The arrow mark in Figure 2-24 shows the run-out of the glass/epoxy composite that is the composite has reached its matrix fatigue limit. Fatigue damage mechanisms are discussed in Section 2.12.3.

2.11.2. Factors affecting the fatigue life of GFRP

Fatigue life can be influenced by frequency, stress concentration, stress levels, temperature and environment.

(i) *Frequency and temperature*

The monotonic strengths of GFRP are markedly loading-rate dependent, by virtue of the viscoelastic character of the matrix and because the strength of the glass fibres is rate dependent, the fatigue response will vary with test frequency.[88,89] Unlike CFRP, GFRP composites cannot readily dissipate heat and they gradually heat up during cycling. The structure and properties of glass reinforcement will not be influenced by this temperature difference, but the matrix properties can be substantially altered. Mainly the residual stress state will be altered due to the superposition of thermally-induced stresses, which in turn will reduce the strength properties of the matrix.[90] The matrix strength decrease will adversely affect the transverse strength of unidirectional plies so that the cross-ply will begin to fail. Thus, fatigue failure is hastened. Generally laminates dominated by mainly continuous fibres in the test direction show lower strains and little hysteresis heating at test frequencies around 10 Hz.

(ii) *Stress Levels*

The mean tensile stress has been shown to have an important effect on the fatigue properties of fibre reinforced composites. For 0° and ±15° E-glass/epoxy laminates, the stress amplitude at a constant life tends to decrease with increasing tensile mean stress. In GFRP there is a significant rate effect; the greater the rate of testing the greater the strength. Therefore, in GFRP static and fatigue tests are carried out at the same rate.

(iii) *Environment*

In GFRP, the moisture content has a detrimental effect mainly due to the stress corrosion of fibres[91]. In matrix resins, the moisture may act as a plasticiser and will lead to higher failure strains. This may tend to increase fatigue resistance by inhibiting local crack growth. However, water also weakens the reinforcing glass fibres so that the net result is more likely

to be a reduction in fatigue resistance.[92] The water ingress may be stopped by efficient fibre matrix adhesion and by minimising debonding.

2.11.3. Fatigue of prestressed composites

Harris[93] comprehensively reviewed the fatigue and accumulation of damage in fibre reinforced composites. He said, "*there is clear evidence from fatigue tests on many reinforced plastics that the matrix and interface are the weak links as far as fatigue resistance is concerned. In consequence, any materials treatment or processing that can improve resistance to crack propagation of the matrix or strengthen the adhesion at the fibre/matrix interface is likely to improve the fatigue properties*".

Tuttle from his mathematical model showed that tensile residual stresses in the matrix could be minimised or even subjected to compressive stress by applying a controlled prestress level to the laminates. The reduction of residual stresses in the matrix could increase the resistance to matrix crack propagation. Many researchers[3,76,77] have also shown that fibre prestressing enhances the static mechanical properties of composites as a result of a reduction in residual stresses (see Section 2.10). Tuttle suggested that *"the fatigue life and/or the ultimate strength of a properly prestressed laminate will be improved to that of an otherwise identical but non-prestressed laminate"*. In the following, the effect of prestress on fatigue properties of composites is reviewed.

Sui *et al.*[94] investigated the fatigue properties of prestressed VIRALL (Vinylon (poly(vinyl alcohol)) fibre/epoxy-aluminium laminates). VIRALL are produced by laminating vinylon/epoxy composite layers and aluminium alloy layers alternately. During the manufacturing process because of the thermal mismatch, a tensile stress was induced in the aluminium layers and compressive stresses were induced in the vinylon/epoxy layers. This residual stress development might reduce the fatigue properties of VIRALL laminates. Sui *et al.* have prestressed the vinylon fibre prior to cure and bonded this to aluminium laminates using epoxy adhesive. The prestress was held throughout the curing process at about 120°C and released after cooling to ambient temperatures. They have shown that the fatigue life of the prestressed VIRALL laminates increased by eight times at a low peak stress level of 100 MPa. On the other hand at high peak stress levels there is no significant difference between the non-prestressed and prestressed composites.

Sui *et al.* have reasoned that with increasing prestress, the compressive stress induced to the aluminium layers increases and this results in increasingly lower stress in the aluminium layer under subsequent fatigue loading of the VIRALL. However, they suggested that there was a prestress limit, beyond which the interlaminar shear strength will not be able to sustain the stresses developed and the laminate will debond.

Lin *et al.*[95] have studied the effect of thermal residual stresses on the fatigue properties of CARALL (Carbon fibre reinforced aluminium alloy laminate). From their prediction of thermal residual stresses, there exists a tensile residual stress in the aluminium layer and compressive stresses in the carbon/epoxy layer. From their study, they have predicted that

thermal mismatch between the aluminium alloy sheet and the carbon/epoxy layer can be reduced by placing a glass/epoxy layer between the aluminium alloy sheet and carbon/epoxy layer. They have also shown that post-cure stretching of the carbon/epoxy plies in the CARALL laminate after curing or prior to mechanical testing can further reduce the tensile residual stress in the aluminium alloy sheet. This induces a compressive stress in the aluminium layer.

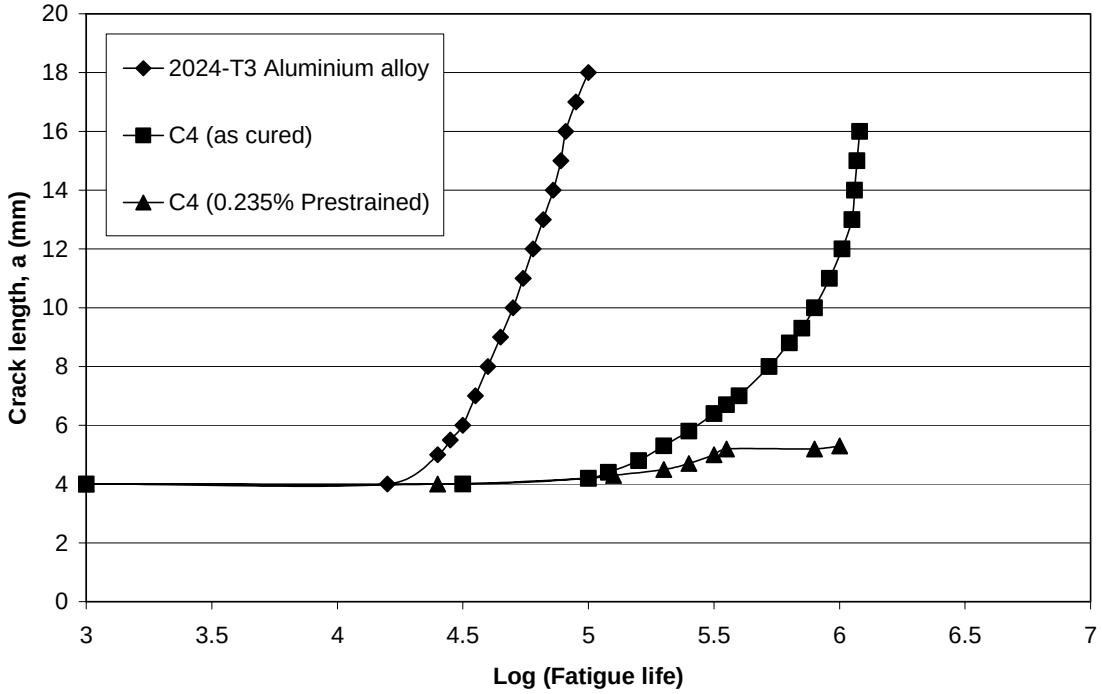

Figure 2-25: Fatigue crack propagation of aluminium alloy, CARALL laminates as cured and prestrained (Lin *et al.*)

From Figure 2-25 it can be observed that the composite with 0.235% prestrain showed greater resistance to fatigue crack growth. They suggested that the increase in resistance to fatigue crack growth could be due to the reduction in the residual stresses in aluminium layers of the CARALL laminate.

The experimental studies on the effect of fibre prestress on fatigue properties are so far carried out on metal-composite laminates. As polymer composites are widely used in aerospace structures, the demand for materials with higher resistance to fatigue increases. To the best of the author's knowledge so far the effect of prestress on fatigue of fibre reinforced polymer composites has not been studied. From the above review, it can be observed that the prestress effect on metal-composite laminates was shown to improve the resistance to crack propagation. From the above reviewed literature, it can be observed that prestressing the laminates could enhance the fatigue performance of the composites.

2.12 Damage mechanisms

This section presents a brief literature review of damage mechanisms in unidirectional composites tested in quasi-static tension, compression and fatigue.

2.12.1. Static tension failure mechanisms

Researchers have shown that the tensile failure process in polymer composites begins with fracture of weak fibres at an early stage of tensile load application along with matrix cracks[96,97]. The fibre fracture will occur at its weakest point determined by internal or surface flaws. The subsequent fracture will depend upon the fibre/matrix interface adhesive strength. A schematic illustration of the tensile failure of composites with weak and strong interfaces is shown in Figure 2-26.

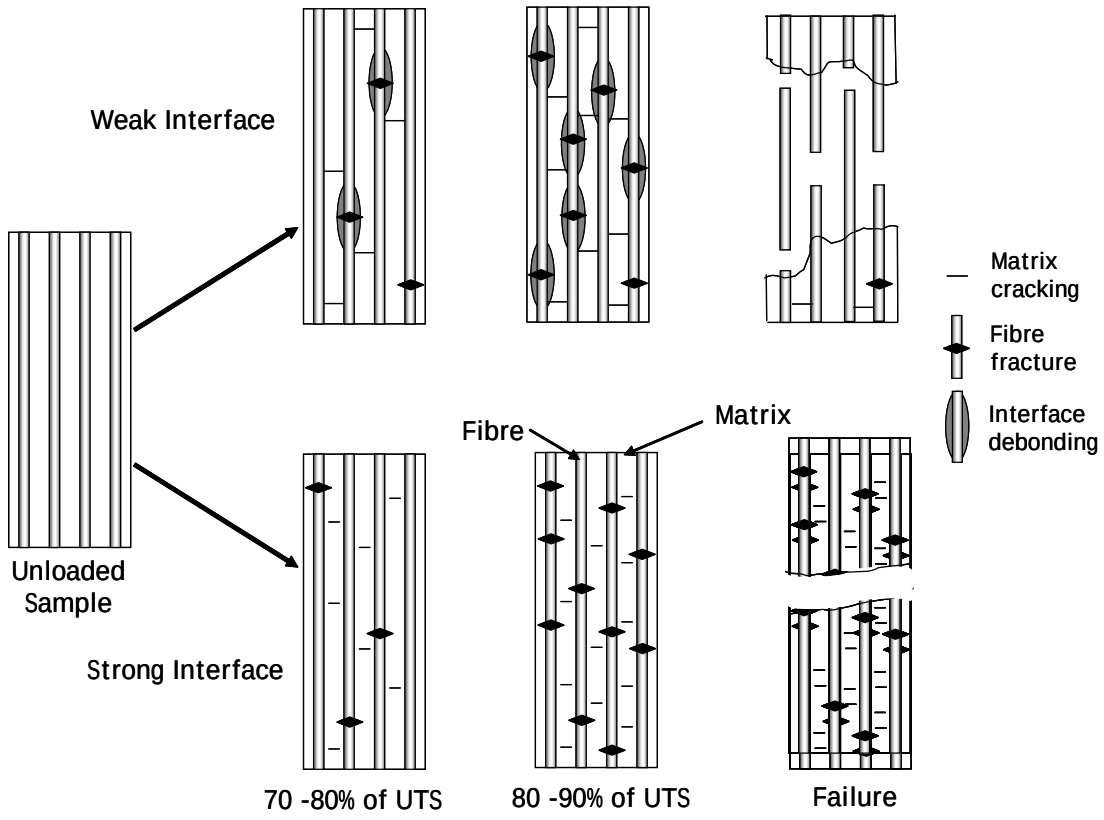

Figure 2-26: Schematic Illustration of tensile failure of composites with weak and strong interfaces.

If the fibre/matrix interface is weak, the failure is expected to occur along the interface (see Figure 2-26). This will lead to extensive longitudinal splitting combined with fibre fracture giving rise to the classical "brush-like" failure. This type of failure is typically observed in glass fibre/epoxy composites[85,86]. On the other hand, if the adhesion between the fibre and

matrix is strong, the failure may occur in the form of matrix cracks away from the interface region with greater fibre fracture density (see Figure 2-26). This will lead to separation of the sample into two or more pieces. This type of failure is typically observed in carbon fibre/epoxy composites.

2.12.2. Static compression failure mechanisms

The compressive strength of unidirectional fibre reinforced composites is typically 60 – 80 % of their tensile strength as a consequence of 0° fibre microbuckling,[98,99] which is of major concern since there are many applications in which such materials are subjected to high compressive stress. An understanding of the phenomena involved in compressive failure is crucial to the development of improved composite materials.

Modes of failure

Jelf and Fleck[100] identified elastic microbuckling, fibre crushing, matrix failure and plastic microbuckling as failure from experiments on model composite systems designed to exhibit one particular mode. A schematic illustration of the compression failure modes is presented in Figure 2-27.

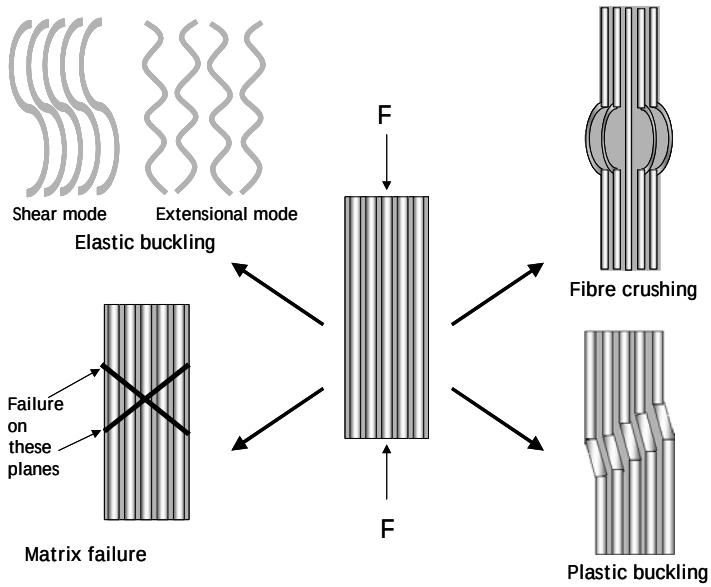

Figure 2-27: Compression failure modes of composites.

Generally, three macroscopic failure modes are observed in unidirectional composites. The first mode of failure is associated with poor fibre-matrix adhesion, which will lead to interfacial failure and longitudinal splitting. As most of the engineering composite systems involve fairly strong interfaces, this usually is not the dominant mode of failure. The

second mode of failure is associated with fibre microbuckling and kink-band formation. A significant number of previous experimental results have revealed that fibre microbuckling and kink-band failure along the fibre direction of a unidirectional composite are the initiating mechanisms of compressive failure that lead to global instability. The third mode of failure is fibre "crushing" which is associated with pure compressive failure of the fibres themselves. This occurs when the axial strain within the composite attains a value equal to the critical crushing strain of the fibres. This higher compressive strength failure mode is usually prevented by the occurrence of fibre microbuckling at lower stress levels due to fibre misalignment.

Kink-band formation

Previous researchers[100,101,102] have shown that fibre microbuckling or kink-band formation are the usual compressive failure mechanisms of unidirectional fibre reinforced composites. A schematic representation of kink-band formation is shown in Figure 2-28.

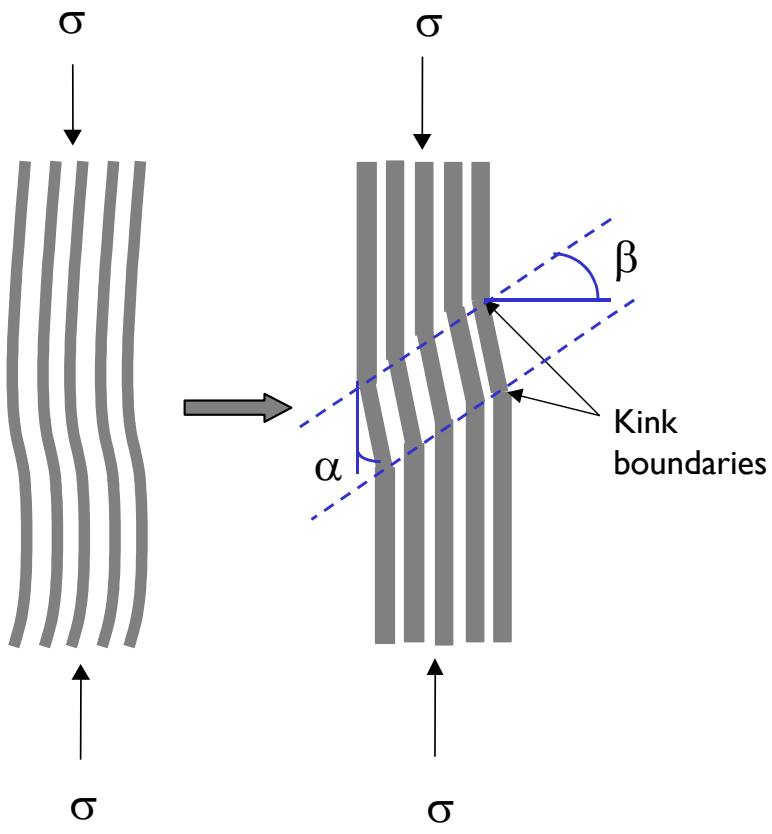

Figure 2-28: Schematic of a kink-band formation from initial fibre misalignment. Kink orientation, α, and the boundary orientation, β, are also indicated.

Published experimental evidence suggests that kink bands in unidirectional composites loaded in compression form in three steps: elastic kinking and plastic kinking followed by final collapse as a result of fibre fracture at the kink boundaries.[99,103,104] The elastic kinking is initiated by defects such as fibre misalignment, residual stresses[105], voids and poor bonding[106]. In the plastic kinking stage, the matrix within the kink band deforms plastically in shear under the applied compressive load. Berbinau *et al.* analysed the shear strain developed in the matrix due to fibre microbuckling failure and showed that the criterion of fibre failure is initiated on the compression side at points of maximum fibre curvature and not on the tensile stress on the convex side of the fibre curvature. This leads to the final collapse as a result of fibre fracture.

2.12.3. Fatigue damage mechanics

Fatigue damage can be defined as the cyclic-dependent degradation of internal integrity. The degree of influence of these changes in integrity on the mechanical response of materials may vary greatly. This suggests that one will only be concerned with those damages, which are directly related to strength, stiffness, or service life of the component.

Composite materials exhibit very complex failure mechanisms under static and fatigue loading due to the anisotropic characteristics of their strength and stiffness. They accumulate damage in a random rather than a localised fashion, and failure does not always occur by propagation of a single macroscopic crack. The basic microstructural mechanisms of damage accumulation in composites are fibre-matrix debonding, matrix cracking, delamination and fibre breakage. Any combination of these could cause fatigue damage that will result in reduced strength and stiffness. Both the type and degree of damage vary widely, depending on material properties, laminations and type of fatigue loading.

For any composite, in the early stages of fatigue life, the weak fibres will begin to break in a random fashion throughout the loading region as shown in Figure 2-29. Locally, the matrix will transfer the loads shed by the broken fibres into neighbouring fibres. At reasonable working strains, an unbroken fibre reinforcement network carries the majority of the load in the composite.

When the stress amplitude is above the elastic levels of the matrix, viscoelastic flow occurs preferentially between closely spaced fibres, because of the high strain magnification in these regions. This flow will not be fully reversible when the stress is reduced and during cyclic loading additional stress and strain concentrations develop which lead to the initiation of debonding at applied stresses below those observed in monotonic loading. The debonding cracks grow during cyclic loading because some flow occurs at the crack tip during the loading half of the cycle, which is not fully reversed on unloading. As in uni-axial tensile tests the cracks nucleate and propagate in regions of closely spaced fibres by the growth and coalescence of individual fibre debonds. When the fibres are widely spaced, the growth of the crack from one fibre to the next depends on the fatigue crack growth

resistance of the matrix. As the laminate is further stressed, matrix cracking will subsequently occur from the weakest (transverse ply) to the strongest layers (unidirectional ply). The majority of the fatigue life of a laminate is spent in the crack multiplication stage where the density of cracks increases.

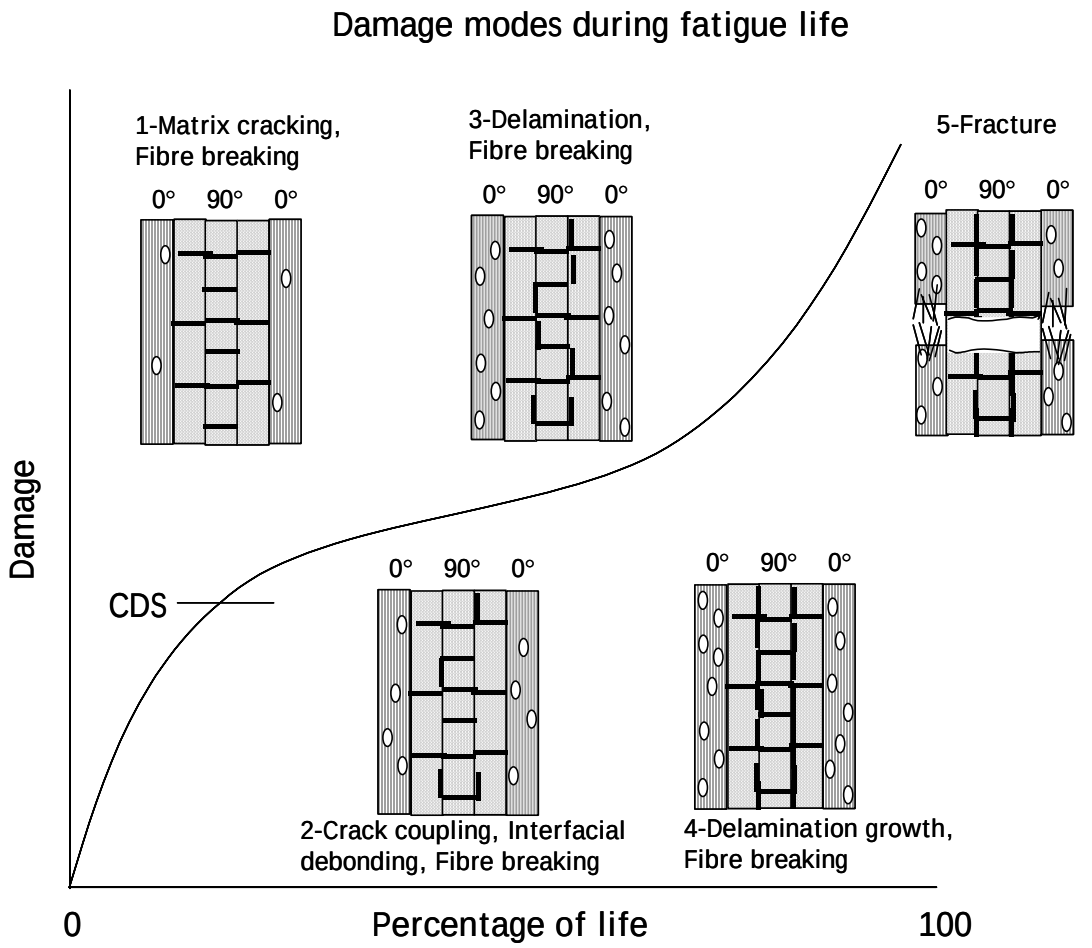

Figure 2-29: Schematic representation of the development of damage in cross-ply laminates during the fatigue life.[88]

As the crack density increases, cracks begin to grow into each other, forming larger cracks. When the laminate is still further loaded, the crack density will be increased to a limiting value where stress redistribution would limit the initiation of new cracks. This state of damage is known as the Characteristic Damage State (CDS) and is a laminate property, which is achieved near the first stage as shown in Figure 2-29. At this point, matrix cracking becomes a macroscopic form of damage that could dictate the initiation of other damage mechanisms. The subsequent damage is usually delamination and then fibre breakage as shown in Figure 2-29.

The overall deterioration process is manifested as a general loss of both stiffness and residual strength as cycling proceeds. These changes are often monitored as indicators of fatigue damage. The point at which the residual strength of the composite has fallen to the level of the peak cyclic stress determines the effective life of the material. In practice, GFRP composites have a great deal of variability in the strength, and this again is provoked by the stochastic nature of damage accumulation during fatigue. Thus, the residual strength curve always exhibits scatter and, as fatigue regimens in service are usually variable, it becomes a statistical problem to define the effective life of glass fibre reinforced composites.

Damage mechanics in unidirectional composites

Talreja[107] suggested that the damage mechanisms in unidirectional composites depend strongly on the relationship between the static failure strain of composites, which reflects the stiffness and failure strain of fibre, and matrix fatigue strain limits. The damage mechanisms in unidirectional composites under tensile fatigue can be divided into three regions namely fibre breakage, matrix cracking, and interfacial shear failure.

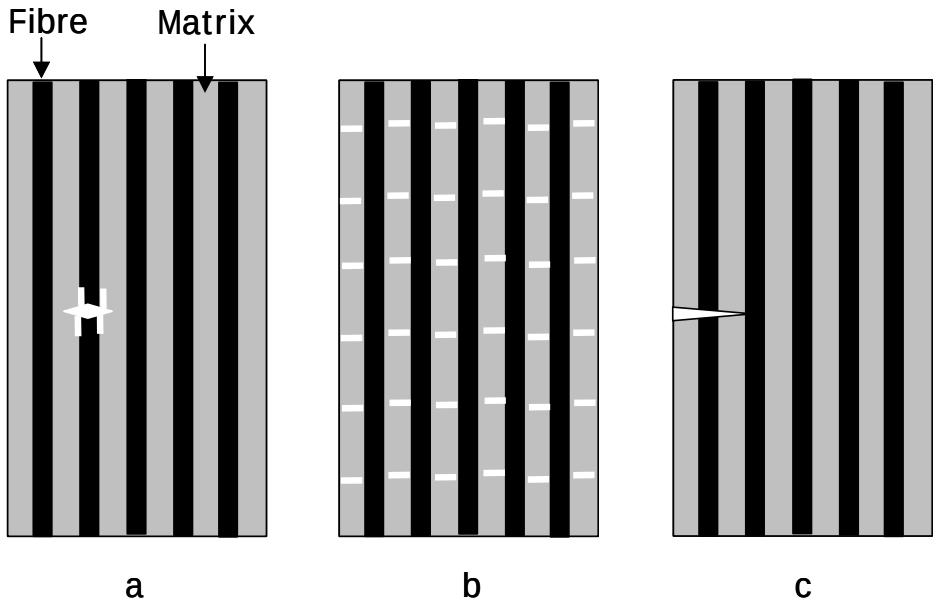

Figure 2-30: Fatigue damage mechanisms in unidirectional composite under tensile loading parallel to fibres. (a) fibre breakage and interfacial debonding, (b) matrix cracking, (c) interfacial shear failure.

Referring to Figure 2-30, fibre breakage (a) occurs at stresses exceeding the strength of the weakest fibre in the composite. An isolated fibre break causes shear-stress concentration at the interface close to the tip of the broken fibre. The interface may then fail, leading to

debonding of the fibre from the surrounding matrix. The debonding length depends on the interfacial shear strength of the fibre-matrix interface. The magnified tensile stress concentration at a debonded area may exceed the fracture stress of the matrix leading to a transverse crack in the matrix (b). A matrix crack would stop at the interface at low strains, while at high strains the stress at the crack tip might exceed the fracture stress of fibres, leading to fibre failure. The matrix crack may now propagate under fatigue as a macrocrack until it hits an interface, where the shear stresses may cause its propagation to a progressive failure of the interface (c).

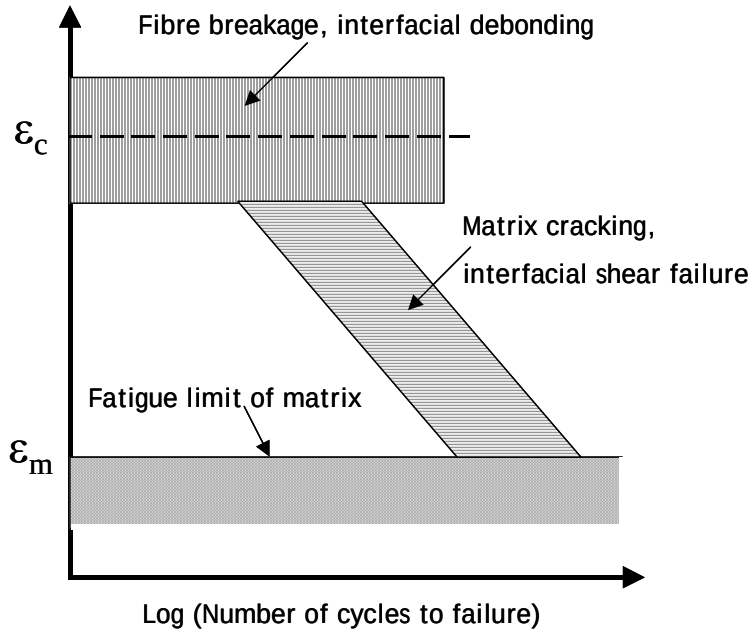

Figure 2-31: Fatigue-life diagram for unidirectional composites under tensile loading parallel to fibres.

Based on the above mechanisms, a fatigue-life diagram was proposed and demonstrated by Talreja. A schematic fatigue-life diagram with co-ordinates of maximum strain in the y-axis and the logarithmic number of cycles to failure in the x-axis is shown in Figure 2-31. Strain instead of stress was chosen as an independent variable, as both fibres and matrix would be subjected to the same strain while stresses in the two phases would differ depending on the volume fraction and the elastic moduli of the two phases. The diagram shows three different bands:

a) the horizontal band centred about the composite static failure strain, ε_c, corresponds to the fibre breakage and the resulting interfacial debonding. The failure in this band was said to be catastrophic damage;

b) the sloping band corresponds to matrix cracking and interfacial shear failure which is a progressive damage;

c) the horizontal line below the sloping band represents the fatigue strain limit of the matrix, ε_m.

Several sets of experimental data for different fibre stiffness were shown to agree with the basic pattern presented in Figure 2-31.

2.13 Summary

This chapter firstly presented a review of process-induced residual stresses and fibre waviness in composites. From the review, it was shown that residual stresses and fibre waviness could substantially degrade the structural performance of composite materials. Also various techniques to measure the residual stresses in composites were reviewed. A more detailed review was presented for embedded optical fibre sensor-based residual strain monitoring in composites.

Secondly, the various techniques for minimising the process-induced residual stresses and fibre waviness in composites were reviewed. From the discussion, it can be concluded that fibre prestressing is the only technique, which can counteract both process-induced residual stresses and fibre waviness.

Thirdly, a comprehensive review of the literature on fibre prestressing of composites was presented. In this review a detailed analysis of various fibre prestressing methods was presented. Of all the methods reviewed only a few methods monitored the applied pre-load to the fibres throughout the curing process. However, from the analysis it was found that none of the methods presented in the literature measured the residual strain in composites with fibre prestress.

The reported literature on the effect of prestress on static mechanical properties of composites was reviewed. From the literature, it was shown that by applying optimum fibre prestress, static mechanical properties such as flexural and impact strength of composites can be enhanced. It was shown previously in this Chapter that fibre waviness in composites could significantly reduce the compressive properties of composites. The fibre alignment in composites could be improved by fibre prestressing. This suggests that the compressive properties of the composites could be improved.

From the reported literature on the fatigue properties of metal-composite laminates it was shown that fibre prestressing enhanced the resistance to fatigue crack propagation and fatigue life. This suggests that fatigue resistance in polymer composites could also be improved by fibre prestressing.

In the research described in this thesis it was decided to monitor and measure both the applied fibre pre-load and residual stress development in composites during autoclave processing of composites.

CHAPTER 3

Design and development of the prestress methodology

OVERVIEW

In chapter 2, a review of the prestress methodologies reported in the literature was presented. From the study it was shown that fibre prestressing could be achieved by using many mechanical arrangements. The study also compared all the prestress methodologies and presented these in Table 2-4. From the review it was shown that none of the methods satisfied all the current design criteria. In this chapter, a new approach to fibre prestressing using flat-bed methodology is presented. This is presented in three sections.

- The current design criteria are presented and discussed.
- The working principle of the flat-bed prestress methodology is given.
- The design calculations pertinent to the prestress rig are presented with its limitations.

3.1 Design criteria

IN THIS RESEARCH, it was required to design a prestress methodology satisfying the criteria: (a) unidirectional fibre prestressing, (b) monitor the applied pre-load online, (c) measure the residual strain development, (d) manufacture prepreg-based composites using an autoclave and (e) vacuum-bagging using conventional methods.

3.1.1. Unidirectional fibre prestressing

In this research, it was required to investigate the effect of fibre prestress on process-induced residual stresses and fibre waviness, and the mechanical performance of unidirectional laminates. Because this will enable us to understand the fundamental phenomena of the effect of prestress in unidirectional laminates, which could then be used to predict the performance of multidirectional laminates using classical laminate plate theories. Therefore, the prestress methodology should be capable of applying a unidirectional fibre prestress.

3.1.2. Monitor and measure the applied pre-load online

In manufacturing prestressed composites, a pre-defined load is applied to the fibres prior to cure. This load is maintained throughout the curing process and released after the composite has been cooled to room temperature. During this manufacturing process due to the change in temperature, pressure and creep in the clamps, the load applied to the fibres prior to cure may not be the same as the load after the cure cycle. Most of the prestress methods presented in chapter 2 did not monitor or measure the load applied to the fibres during the curing process, or after the load was released. As a result, the load released to the composite is difficult to calculate. Therefore, it was required to measure the load applied to the fibres throughout the manufacturing process, in order to measure the final load released to the composite. Also a suitable load sensor which is temperature compensated (up to the cure temperature of the composite) was required.

3.1.3. Measure and quantify the residual strain development in composites

In this study, it was required to measure the residual stresses in composites in order to quantify the effect of fibre prestress on residual stresses. This was achieved by using embedded optical fibre EFPI and FBG strain sensors (see Chapter 4). These sensors were monitored throughout the curing process and during load release.

3.1.4. Manufacture prepreg-based composites using autoclave

Prepreg-based composites are used in aerospace industries because it is easy to control the fibre orientation, fibre content and easy to fabricate into prepreg laminates prior to curing. In this study, it was required to prepare high-quality prepreg-based composites to understand the fibre prestress effect. Autoclave processing is a widely used method of producing high-quality composites in the aerospace industry. Therefore, in this work, autoclave processing was used to prepare the prestressed composites.

3.1.5. Use of conventional vacuum-bagging method

In an autoclave curing process, it is required to apply a vacuum to the composite in order to release the entrapped air in the prepreg laminates during the curing process and also for consolidation of the laminates. This is achieved by using a conventional vacuum bagging method, which uses a plastic sheet as a vacuum bag, tacky tape, breather and bleeder cloth and porous film. One of the most important requirements for conventional vacuum bagging is that the composite part should have no sharp corners/protrusions, because this may burst the vacuum bag. Alternatively, a special vacuum bag made of a high peel resistant material such as rubber (e.g., silicone rubber) could be used. However, most aircraft products are manufactured using conventional vacuum bagging methods. Therefore, it was decided to use a conventional vacuum bagging method for the prestress rig. This dictated that an important criterion for the prestress rig design is that it should have no sharp corners/ protrusions, which would burst the vacuum bag.

In the following section a new approach to prestressing the fibres using a flat-bed methodology is presented. This method is evaluated to determine whether it satisfies all the above design criteria.

3.2 Flat-bed prestress methodology

The flat-bed prestress methodology (FBPM) is a basic principle of using a load screw to apply the prestress. A schematic illustration of the FBPM is presented in Figure 3-1. In this design, two blocks are used; of which one is fixed to a base plate and the other is movable. The moving block slides on guide bars, which are connected to the fixed block as shown in Figure 3-2. These guide bars are used to align the clamps of the moving and fixed blocks. The load screw is positioned in the moving block such that the screw end sits on a load cell positioned in the fixed block as shown in Figure 3-1. The locking bolts are used to lock the movement of the moving block by clamping it to the base plate after loading. An engineering two-dimensional drawing and three-dimensional solid model of FBPM are presented in Appendix B.

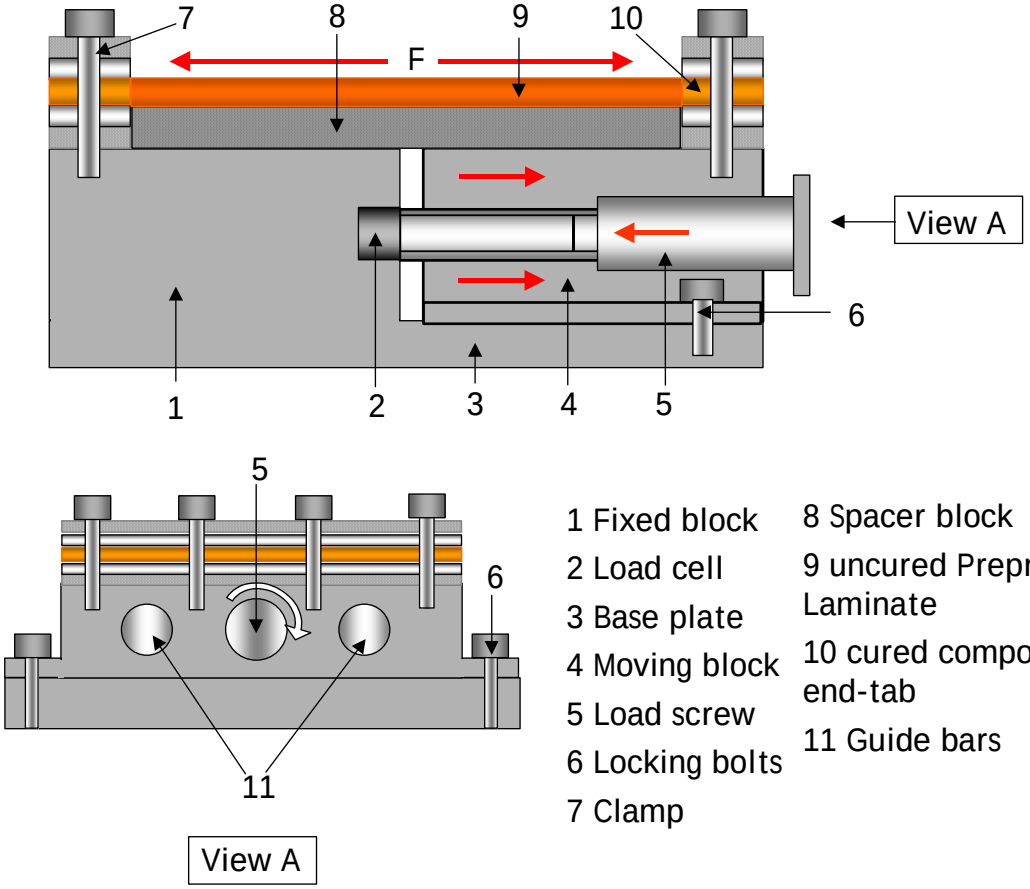

Figure 3-1: Schematic Illustration of flat-bed prestress methodology.

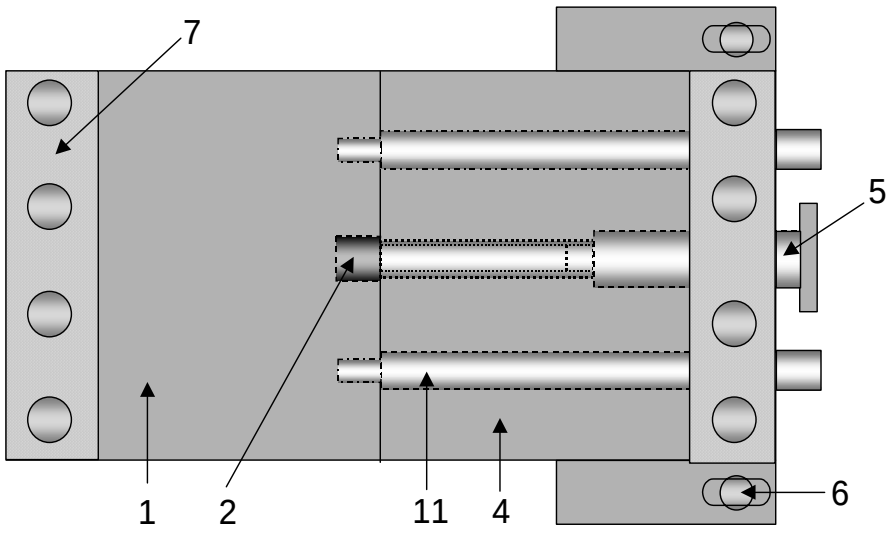

Figure 3-2: Plan view of the flat-bed prestress methodology.

Prestressed composites were manufactured by laying up a unidirectional prepreg laminate, and pre-curing the ends with aluminium tabs attached as shown in Figure 3-3. The ends of the prepreg were cured in order to clamp the prepreg onto the prestress rig and to transfer the applied load to the fibres. After curing the end tabs, holes were drilled (see Figure 3-3) for the clamp bolts. The end-tabbed prepreg was attached using serrated-faced clamp plates, which in turn were bolted to the prestress rig using M12 bolts. The load was applied by tightening the load screw in a clock-wise direction as shown in view-A in Figure 3-1. By tightening the load screw, the movable block moved in the tensile loading direction and as the prepreg is clamped to the moving block, the fibres were loaded. The applied load was directly measured from the load cell connected to the end of the load screw (see Figure 3-2). Once the required load was achieved, the locking bolts were tightened. This clamped the moving block to the base plate.

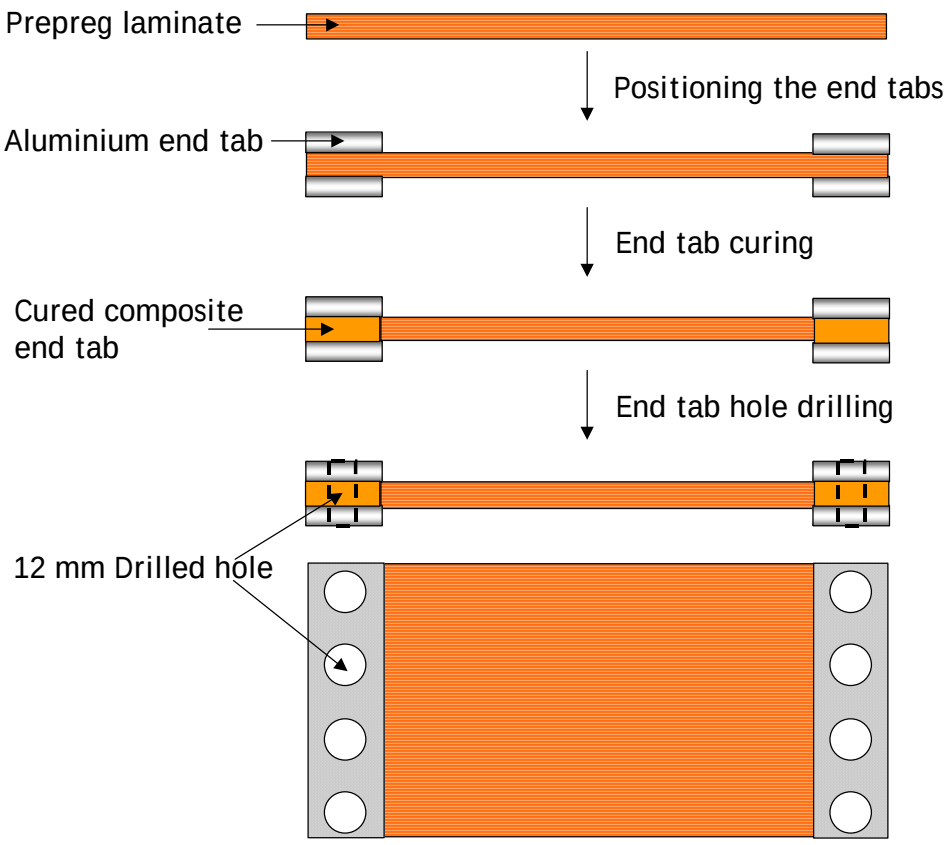

Figure 3-3: Schematic illustration of pre-fabrication stages involved prior to clamping the prepreg laminate onto the FBPM.

Once the prestress was applied to the fibres, silicone rubber spacers were used to cover the sharp corners of the FBPM as shown in Figure 3-4. This enabled conventional vacuum bagging of the prepreg laminate clamped to the FBPM. A photograph of a vacuum bagged prepreg laminate clamped to the FBPM in the autoclave is shown in Appendix B.

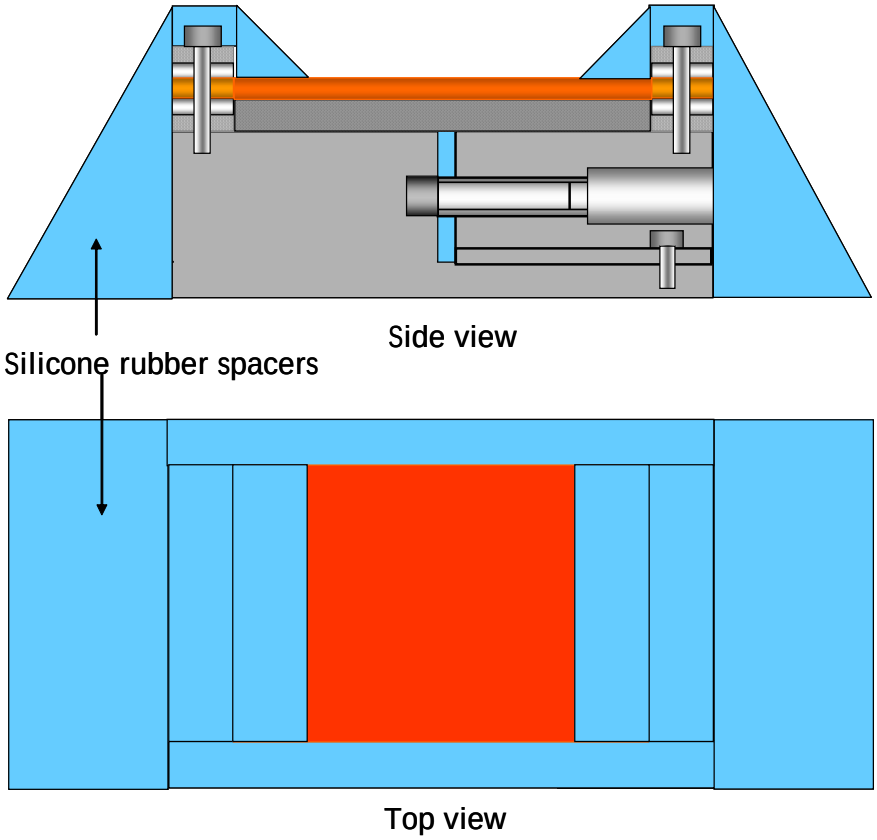

Figure 3-4: Silicone rubber spacer arrangement to enable conventional vacuum bagging.

3.3 Design calculations

This section will discuss the design calculations for determining the maximum load capacity of the FBPM and its limitations.

In the literature, for the unidirectional E-glass/epoxy composite systems, Mottahari and Cameron[76,79] showed that the mechanical properties of composites improve up to an optimum limit of fibre prestress and above this optimum limit the mechanical properties indicates a detrimental effect (see Chapter 2). These optimum limits for impact and flexural properties were shown to be 60 MPa and 20 MPa respectively. Therefore, the current FBPM should be capable of applying the optimum limit found by Mottahari and Cameron. In addition, it was also required to study the detrimental effect on mechanical properties above the optimum prestress limit. For this research, it was decided to apply a maximum prestress of 100 MPa to the fibres using FBPM.

Prepreg cross-sectional area (A_c)= 200 mm (width) × 2 mm (thickness) = 400 mm^2.

Fibre volume fraction (V_f) = 60%.

Fibre cross-sectional area (A_f) = $A_c \times V_f$ = 400 mm^2 × 0.6 = 240 mm^2.

The required force (F) to apply 100 MPa prestress to the fibres is given by[108]:

$$F = \sigma^{f}_{prestress} \times A_f = 100 \times 240 = 24kN \tag{3.1}$$

where $\sigma^{f}_{prestress}$ is the prestress applied to the fibres. In order to achieve a prestress of 100 MPa, it is required to obtain a final force of 24 kN in the fibres of 240 mm^2 cross-sectional area. The corresponding strain in the fibre (ε_f) is expressed by:

$$\varepsilon_f = \frac{\sigma_{prestress}}{E_f} \tag{3.2}$$

where E_f is the Young's modulus of fibres. The value of the fibre Young's modulus E_f is presented in Table 3-1.

From equation 3.2 the strain in the fibre for an applied prestress of 100 MPa is calculated to be ε_f = 1315.78 $\mu\varepsilon$. For a fibre length of L = 290 mm, the displacement is expressed as:

$$\Delta L = L \times \varepsilon_f = 0.3815 \text{ mm} \tag{3.3}$$

This suggested that the displacement of the moving block would be 0.3815 mm for a maximum prestress of 100 MPa. To allow for this, the moving block was designed to have a free movement of 5 mm.

After applying the pre-determined prestress, the locking bolts are tightened to the base plate. This applies a tensile load to the locking bolts. It is required to calculate the tensile load applied to the locking bolts in order to determine whether the tensile load in the locking bolt is within the maximum limit of the bolt strength.

Table 3-1: Properties of E-glass and steel.

Material	Young's Modulus E (GPa)	Thermal expansion coefficient (α) (/°C)
E-glass	76	4.9×10^{-6}
Steel	200	11.7×10^{-6}

3.3.1. Load in the locking bolts

Figure 3-5 shows a free-body diagram of the FBPM.

Force applied (F) = 24 kN.

Moment:

$$M = F_1 x_1 - F_2 x_2 + F_3 x_3 \quad (3.4)$$

x_1 = 25 mm, x_2 = 71.1 mm, and x_3 = 2 × 82 (as there are two locking bolts in the rig, one in the front and the other in rear side).

$M = 24 \times 25 - 24 \times 71.1 + (2 \times 82) F_3$

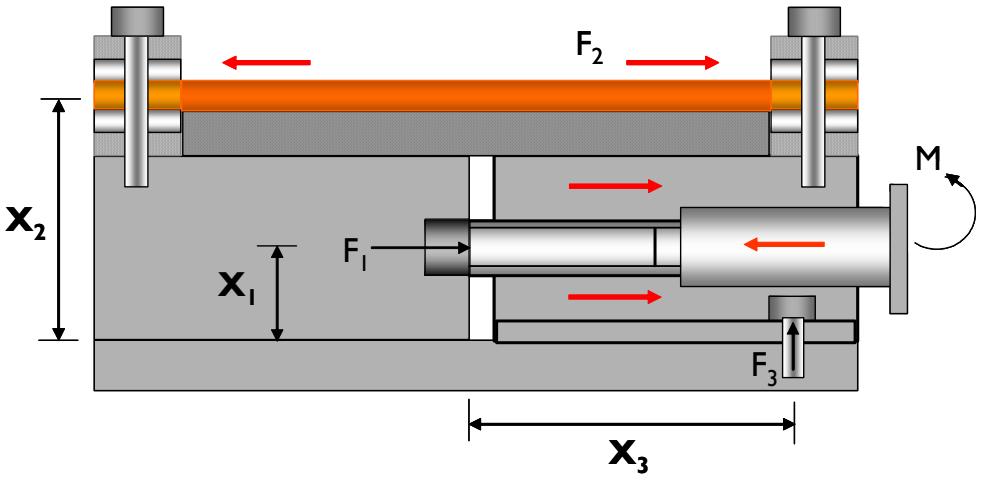

Figure 3-5: Free body diagram of FBPM.

In a static loading, Moment will be zero.

$0 = 24 \times 25 - 24 \times 71.1 + 164 F_3$

F_3 = 6.74 kN

The load in the locking bolt is 6.74 kN for an applied load of 24 kN in the fibres.

3.3.2. Shear stress in the bolt thread

The average shear stress on a screw-thread is obtained by assuming that the load is uniformly distributed over the nut height h, and that the threads would shear on the contact position (that is between minor and major diameter of the bolts) [109]. This gives:

$$\tau = \frac{2F}{\pi d_r h} \quad (3.5)$$

Shear stress in locking bolts

The locking bolt major diameter (d_m) = 10 mm, pitch = 1.5 mm and its height h = 20 mm. The minor diameter of the locking bolt is expressed by:

Minor diameter $d_r = d_m - 1.226869$ (pitch of the bolt)

$d_r = 10 - 1.226869\ (1.5) = 8.1596$ mm

Case	Shear Stress τ (MPa)
F = 6.74 kN	26.31
F = 15 kN	58.51

Shear stress in load screw

The load screw major diameter (dm)= 20 mm, pitch = 1.5 mm and its height h = 50 mm.

Minor diameter dr = 20 – 1.226869 (1.5) = 18.1596 mm

Case	Shear Stress τ (MPa)
F= 24 kN	16.82
F= 50 kN	35.05

The calculated shear stresses in the locking bolts and loading screw are 26.31 MPa and 16.82 MPa respectively. This is smaller than the yield strength of the bolts (220 MPa) respectively.

3.3.3. Calculation of the angle of rotation

In this work, the pre-load applied to the fibres using the load screw was directly measured from the load cell. This can also be theoretically predicted by calculating the load screw angle of rotation. The following Table 3-2 shows the calculation of the angle of rotation θ of the loading screw to apply a pre-determined load.

Table 3-2: Calculation of angle of rotation.

Input	Calculation	Output
Pitch = 1.5 mm, $\Delta L = 0.3815$ mm $a = \Delta L /$ Pitch, $\theta = a \times 360$	$0.3815/1.5 = 0.2543$ $\theta = 0.2543 * 360°$	**91.56°**

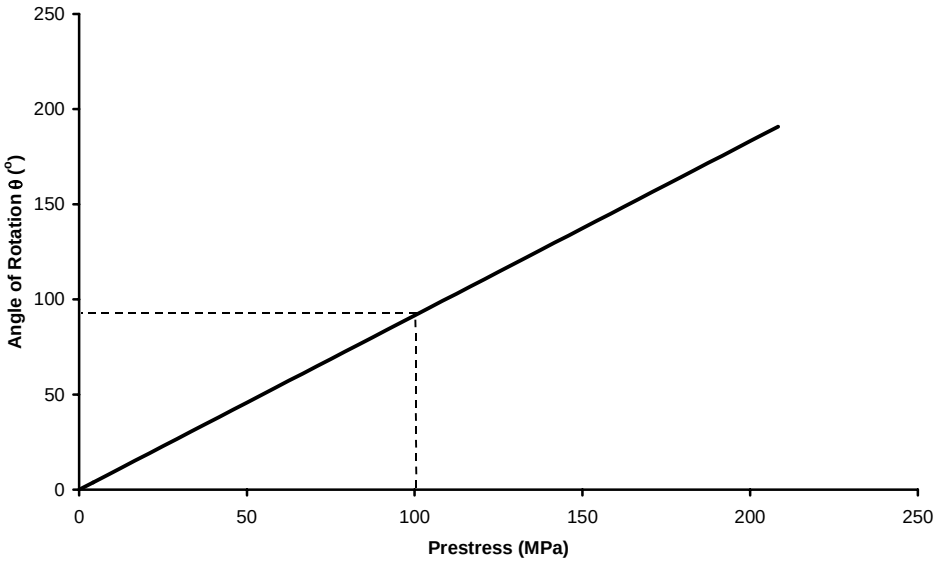

Figure 3-6: Angle of rotation of the load screw as a function of prestress.

The degree of rotation of the load screw for various loads is shown Figure 3-6. With reference to Figure 3-6 it can be observed that to apply a prestress of 100 MPa to the fibres, the load screw has to be rotated to an angle (θ) of 91.56°.

3.3.4. Pre-load calculation

When a load is applied to the fibres by tightening the load screw, due to the resulting moment created in the moving block (as shown in Figure 3-5) there will be a reduction in the applied load. This is calculated in this section by considering two cases:

- Case I: Considering the deflection caused by the moment at the moving block M_1 (as shown in Figure 3-7); and
- Case II: Considering the deflection caused by the moment at the base plate on the composite M_2 (as a worst case).

Consider the moving block and base plate as a cantilever beam as shown in Figure 3-8. When a moment M is applied to the end of the cantilever beam as a result the beam will deflect. This deflection of the beam would cause a change in the prestress applied to the fibres connected to the FBPM. This deflection of the beam caused by moment is expressed by:

$$\delta = \frac{ML^2}{2EI} \tag{3.6}$$

where L is the length of the beam, E is the Young's modulus, and I is the second moment of inertia.

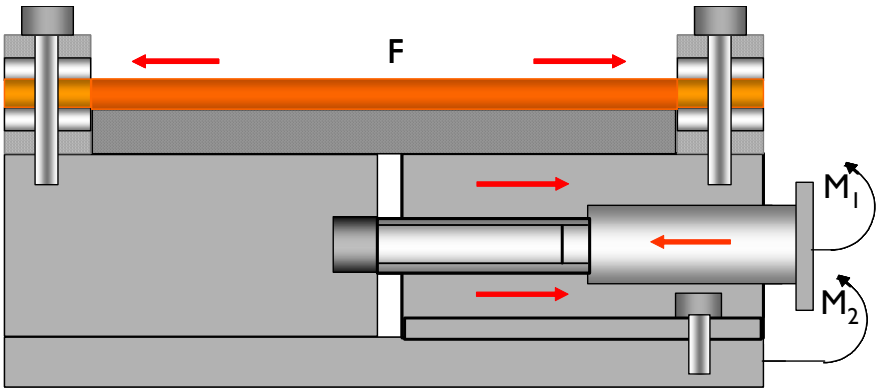

Figure 3-7: Free body diagram of FBPM.

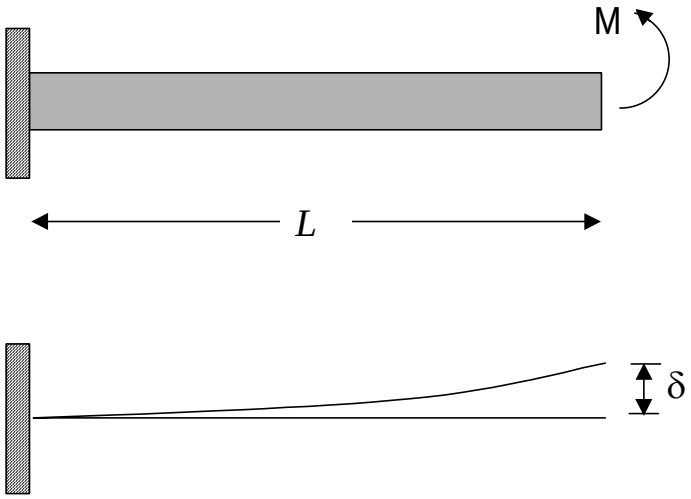

Figure 3-8: Schematic illustration of the deflection (δ) caused by the moment (M) in the cantilever beam.

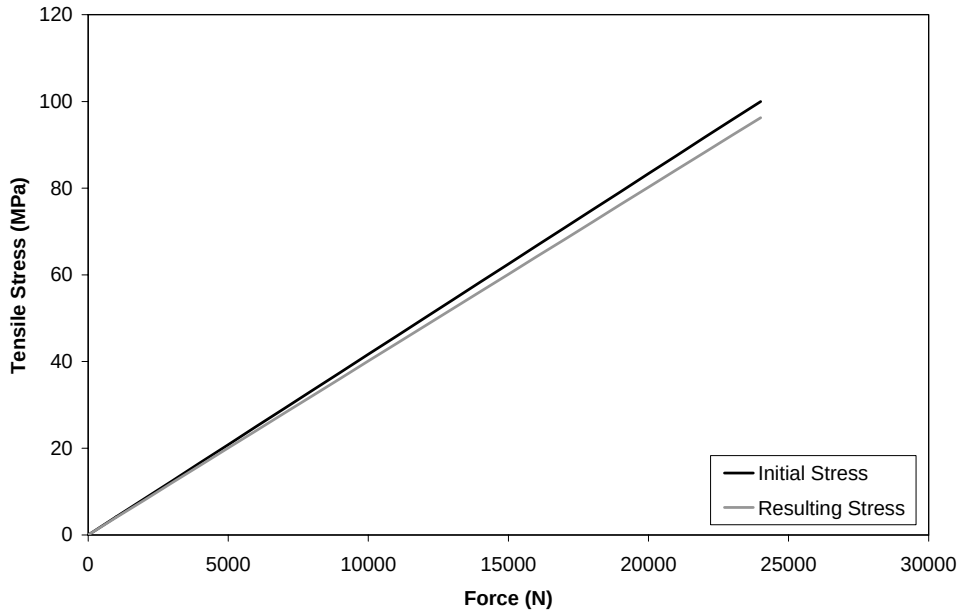

Figure 3-9: Fibre tensile stress as a function of applied pre-load.

The total deflection of the prestress rig per unit force was calculated to be 0.33 nm (Case I) and 0.63 nm for (Case II). This is negligible when compared to other rig systems reviewed in this work (see Section 2.9.7, Chapter 2). From Figure 3-9 it can also be observed that the reduction in the tensile stress in the fibres due to FBPM bending from case II is 4%.

3.3.5. Rig thermal expansion-induced prestress

The E-glass/epoxy prepreg system used in this study is cured at a temperature of 120°C. The flat-bed prestress rig was manufactured using mild steel material. When the prepreg is clamped to the flat-bed rig at room temperature (20°C) and subjected to the cure temperature of 120°C, thermal stresses are developed due to mismatch in the thermal expansion coefficient between E-glass fibre and steel prestress rig. The epoxy resin will not be subjected to any thermal stresses during heating cycle, because it has negligible stiffness. This will subject E-glass fibres to tension and steel prestress rig to compression as shown in Figure 3-10. This tensile stress applied to the E-glass fibres due to the change in temperature is referred to here as the thermally-induced prestress. This was calculated by using the well known composite bar model proposed by Timoshenko[110]. The assumptions used in this model were:

- Perfect bonding exist between the two materials under consideration;
- Linear elastic isotropic materials;
- Temperature-independent material properties;
- Uniform temperature distribution;

- No external force applied.

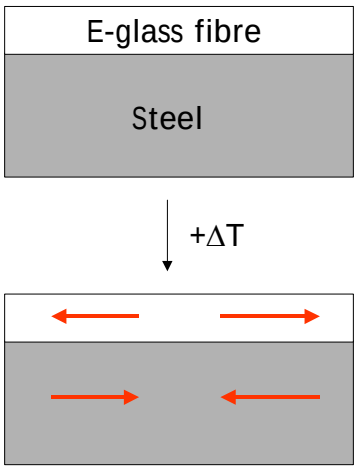

Figure 3-10: Model representation of prepreg clamped to prestress rig.

Consider two rectangular plates made from E-glass and steel, which are fastened together at their ends at a temperature T°C as shown in Figure 3-10. When there is a change in temperature ΔT, thermal stresses will be induced into the plates.

In equilibrium:

$$F_{\text{E-glass}} + F_{\text{Steel}} = 0, \tag{3.7}$$

i.e, $\sigma_{\text{E-glass}} A_{\text{E-glass}} + \sigma_{\text{Steel}} A_{\text{Steel}} = 0$.

Where F is the force, σ is the stress and A is the cross-sectional area. The stress-strain relationships for each material are:

$$\varepsilon_{E-glass} = \frac{\sigma_{E-glass}}{E_{E-glass}} + \alpha_{E-glass}\Delta T \tag{3.8}$$

$$\varepsilon_{Steel} = \frac{\sigma_{Steel}}{E_{Steel}} + \alpha_{Steel}\Delta T \tag{3.9}$$

where α, E and A represent the coefficient of thermal expansion, modulus and cross-sectional area respectively.

Combining the above stress-strain relationship equations gives:

$$\sigma_{Steel} = + \frac{E_{E-glass}E_{Steel}A_{E-glass}\left(\alpha_{Steel} - \alpha_{E-glass}\right)\Delta T}{E_{E-glass}A_{E-glass} + E_{Steel}A_{Steel}} \tag{3.10}$$

$$\sigma_{E-glass} = -\frac{E_{E-glass} E_{Steel} A_{Steel} \left(\alpha_{Steel} - \alpha_{E-glass}\right)\Delta T}{E_{E-glass} A_{E-glass} + E_{Steel} A_{Steel}} \tag{3.11}$$

By substituting the materials properties from Table 3-1 in equation 3.10 and 3.11 the thermal residual stresses in the E-glass (V_f = 60%) and steel (for $\Delta T = 100^o$ C) were calculated to be 51.21 MPa and –1.23 MPa respectively. In other words, the thermally-induced prestress in the as-clamped E-glass fibres was 51.21 MPa. Therefore, the total prestress will include both mechanical prestress (applied via the load screw at room temperature prior to prepreg cure) and thermal prestress (applied during the curing cycle due to the change in temperature).

3.4 Concluding remarks

In this chapter, a new approach to fibre prestressing was presented using a flat-bed prestress methodology for manufacturing prestressed composites. The FBPM was designed to apply a unidirectional prestress to the fibres. The design criteria for the current study were: 1) unidirectional fibre prestressing, 2) monitor and measure the applied load online, 3) measure and quantify the residual strain in composites, 4) manufacture prepreg-based composites in an autoclave and 5) use a conventional vacuum bagging method. All the current design criteria were satisfied by the FBPM design. From the design calculations, it was shown that the rig is capable of applying 100 MPa prestress to the fibres. At the maximum prestress of 100 MPa, the shear stress in the load screw and locking bolts were smaller than the yield strength of the bolts respectively. The reduction in tensile stress in the fibres due to prestress rig bending was shown to be small (4% reduction for case II). The FBPM is designed to monitor and measure the applied load to the fibres via the load cell. From classical mechanics, the rig thermal expansion-induced prestress to the fibres was calculated to be 51 MPa prestress for 100°C temperature change. The advantages of the flat-bed prestress methodology are 1) one parameter to control the applied load (load screw), 2) monitoring the applied load online, 3) enables conventional vacuum bagging and 4) allows processing prepreg-based composites in an autoclave.

CHAPTER 4

Experimental procedures

OVERVIEW

- This chapter presents the materials and equipment used in this research.
- The experimental procedure for manufacturing non-prestressed and prestressed composites is described.
- The experimental methodology for residual strain monitoring, static tensile and compression, and fatigue tests of composites are presented.

4.1 Materials

THE PREPREG MATERIAL USED in this study was Fibredux 913G-E-5-30% (E-glass fibre/ epoxy resin) supplied by Hexcel Composites Ltd, Duxford, Cambridge, UK. This material was chosen because it is used in aerospace structural components and helicopter blades[111], and also this material has been used in many of the previous research studies carried out in the Sensors and Composites Group, Cranfield University, Shrivenham Campus, UK. The prepreg was supplied as unidirectional reels with a 300 mm width and 0.125 mm ply thickness. The prepreg was stored in sealed polyethylene bags at -18°C in a freezer according to the manufacturer's recommendations. Silica gel was placed within the storage container to absorb any moisture. The prepreg storage container was removed from the freezer and left to thaw to room temperature prior to the removal of the prepreg from the container.

4.2 Sensors

4.2.1. Optical fibre sensors

Optical fibre sensors were used to measure the residual strain and the magnitude of pre-strain release in composites during processing. The optical fibre sensors used in this study were (i) extrinsic Fabry-Pérot interferometric (EFPI) strain sensors and (ii) Fibre Bragg grating (FBG) strain and temperature sensors. These sensors were manufactured in-house by Mr J Tetlow (EFPI) and Dr G Kister (FBG). The single mode optical fibres working at 800 nm and 1550 nm were supplied by Fibrecore Ltd, UK. The EFPI sensors were manufactured in single mode 800 nm optical fibres. In this study EFPI sensors with a gap length from 50 to 100 μm were used. The FBGs were manufactured using single mode 1550 nm optical fibres. Bragg grating wavelengths from 1530 to 1560 nm were used in this study.

4.2.2. Electrical resistance strain gauges

The electrical resistance strain gauges (ERSG) used in this study were supplied by TML Ltd. These were 120 Ω electrical resistance gauges with a 2 mm gauge length (used in static compression testing) and 5 mm (used in pre-strain release). ERSGs were bonded to the surface of the specimen after curing. They were used to compare the prestrain release measured from optical fibre sensors.

4.2.3. Load Cell

A compressive load cell was used to monitor and measure the applied pre-load to the reinforcing fibres during composite processing. The load cell (Model No: 060-4771-01-08) was supplied by RDP Electronics Ltd, UK. The capacity of the load cell used in this study was 44.5 kN in compression. The load cell is temperature compensated up to 121°C.

4.3 Preparation of composite

4.3.1. Laminate sequence

The laminate sequences used in this study are as follows:

- $[0]_{16}$
- $[0/90/0/90/90/0/90/0]_S$
- $[0/90/0/90/90/0/90/0]_{4S}$

The $[0]_{16}$ unidirectional laminate sequence was used to prepare non-prestressed and prestressed composites. The static and dynamic mechanical properties were determined for this unidirectional composite. The cross-ply laminate sequences ($[0/90/0/90/90/0/90/0]_S$ and $[0/90/0/90/90/0/90/0]_{4S}$) were used only to compare the residual strain development with those in unidirectional composites.

4.3.2. Lay-up

The day before prepreg lay-up, the prepreg reel was taken out of the freezer and kept at room temperature for 24hrs. This was carried out to prevent condensation onto and moisture-ingress into the prepreg and thermally equilibrated before use. The prepreg was cut to 300 × 300 mm (for non-prestressed composite) and 350 × 200 mm (for prestressed composite) using a rotary cutter. The composites manufactured in this study consisted of 16 plies of prepreg to obtain 2 mm thickness of laminate. The prepreg plies were stacked according to the laminate sequence using a vacuum assisted jig as shown in Figure 4-1. The vacuum assisted jig was used to aid in the alignment of the prepreg during lamination (see Figure 4-2). A roller was used to consolidate the prepregs during lamination and to expel the entrapped air in between the prepreg plies.

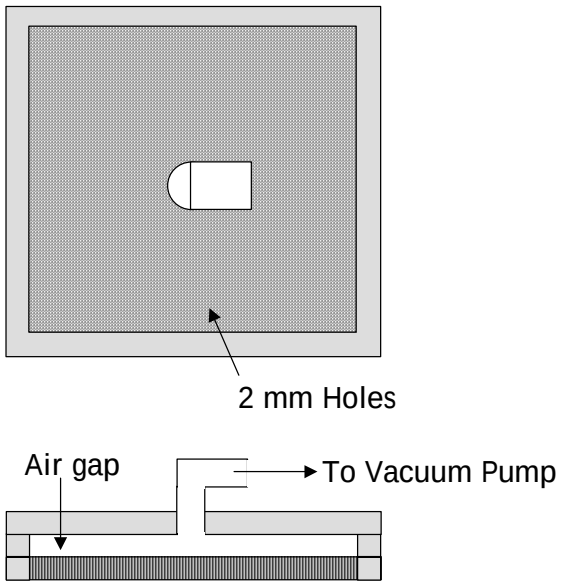

Figure 4-1: Vacuum jig used during prepreg lamination.

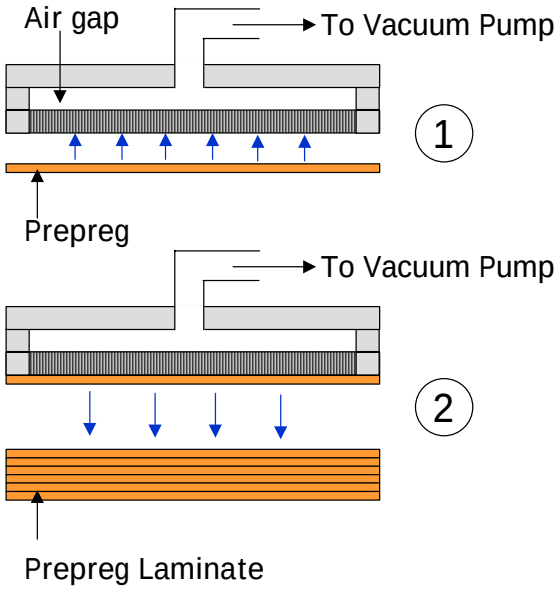

Figure 4-2: Prepreg lay-up process using vacuum assisted jig. 1) Prepreg ply holding to the vacuum jig and 2) Prepreg ply stacking using vacuum jig.

4.3.3. Embedding optical fibre sensors

The EFPI and FBG sensors were embedded in the 0° fibre direction in all the laminate sequences used in this study. The sensors were embedded in the mid-plane of the laminate to avoid any strain caused by bending. The positions of the embedded optical fibre sensors are as follows:

- between 8th and 9th plies of $[0]_{16}$ laminate.
- between 8th and 9th ply of $[0/90/0/90/90/0/90/0]_S$ laminate.
- between 32nd and 33rd plies of $[0/90/0/90/90/0/90/0]_{4S}$ laminate.

The prepreg layers were laminated into two parts, below and above the sensor. This was followed by careful placement of the optical fibre sensors on the surface of the bottom laminate and maintaining the alignment of the optical fibre with the fibre orientation in the laminate. Then the top laminate was sandwiched to the bottom laminate with careful alignment. Because of the fragile nature of the optical fibre sensors, due care and attention was essential during embedding of the sensors and processing in the autoclave. In order to avoid any optical fibre kink in the entry and exit point of the laminate during autoclave processing, poly (tetrafluroethylene) (PTFE) tubing was used to protect the optical fibre lead in and lead out. Also silicone rubber resin was used to seal both the ends of the PTFE to avoid resin getting inside the tube, which could make the ends brittle and fragile.

4.3.4. Prestress methodology

A flat-bed fibre prestress methodology was designed (as shown in Chapter 3) and developed in-house to manufacture fibre prestressed composites. In this study, fibre prestressing was applied in two ways: (i) by thermal expansion of the prestress rig, and, (ii) mechanical loading to a predetermined level using a load screw. The prestress induced by thermal expansion of the rig was calculated to be 51 MPa for the cure cycle of E-glass/913 epoxy resin (see Section 3.3.5, Chapter 3). Three different mechanical loads (7 kN, 14 kN and 24 kN) were applied. The total prestress applied to the fibres is the addition of the rig thermal expansion-induced prestress and the mechanically-induced prestress. In total four different prestressed composites (51 MPa, 80 MPa, 108 MPa and 150 MPa) were prepared apart from the non-prestressed (0 MPa or reference) composite.

In order to clamp the prepreg in the prestress rig (see Figure 3-1), aluminium tabs were bonded to both ends of the prepreg over a 30 mm length. The prepreg end-tabbing was carried out using an in-house designed end-tab jig (as shown in Figure 4-3 and Figure 4-4). This was to avoid any fibre misalignment and composite curing away from the end-tab region.

Once the prepreg laminate had been prepared using the procedure described in Section 4.3.2, it was then end-tabbed. Aluminium alloy (5251-H2 supplied by Metalfast Ltd, Swindon, UK) end-tabs were cut to size (30 (l) × 200 (w) × 1.5 (t) mm) and abraded on both sides, then degreased using acetone. The end-tabs were aligned with the ends of the prepreg laminate and cured (at 120°C for 1 hour) using the end-tab jig. Once the end-tabs were cured onto the prepreg ends, 12 mm diameter holes were drilled to enable clamping of the prepreg onto the prestress rig (see Figure 3-3). After drilling, the holes were cleaned using a de-burring tool. Prior to clamping the end-tabbed prepreg to the prestress rig, the rig was cleaned and a silicone release agent (Rocol, PR spray supplied by RS Consumables Ltd, UK) was applied. A torque of 20 N m was applied using a torque wrench to each of the clamp bolts to ensure uniform pressure distribution on the end-tab.

Mechanical prestress was applied to the reinforcing fibres (in the prepreg) to a predetermined load by means of the load screw. The load applied was monitored by use of the load cell. Once the required prestress was applied, the locking bolts were tightened to 20 Nm. The composite was then vacuum bagged using conventional procedures (see Section 4.3.5) and cured in the autoclave (see Section 4.3.6).

During composite curing the residual strain development was monitored *in-situ* using optical fibre sensors (EFPI and FBG sensors) (as explained in Section 4.6). After curing and being cooled to room temperature, the vacuum bag was removed. The ERSG sensors were positioned and aligned to the optical fibre sensors embedded in the composite as shown in Figure 4-5. These were then bonded onto the composite surface using Cyanoacrylate adhesive (supplied by TML Ltd, UK). The prestress was released by slackening the load screw, locking bolts and clamp bolts. The strain transferred to the

composite was monitored and recorded using optical fibre sensors (EFPI and Bragg grating) and ERSG sensors.

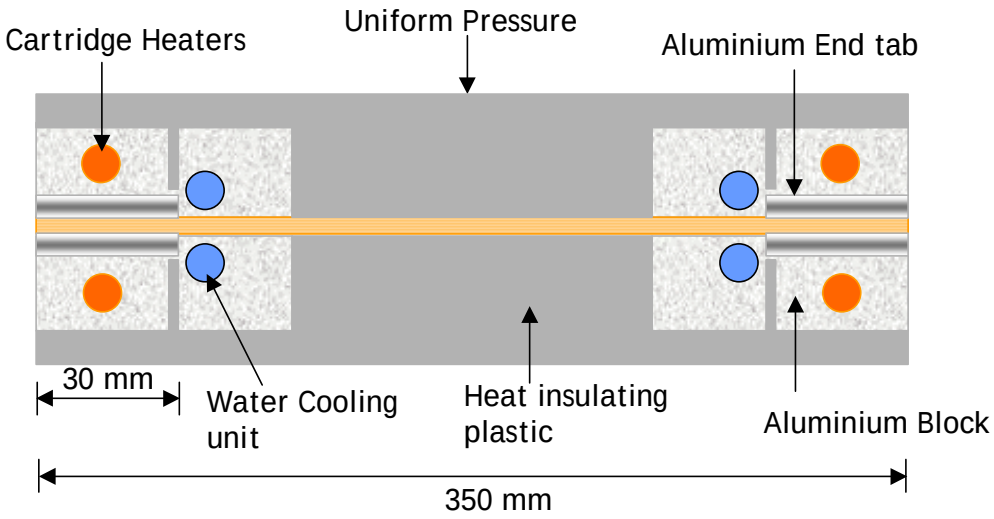

Figure 4-3: Side view of the End-tab Jig.

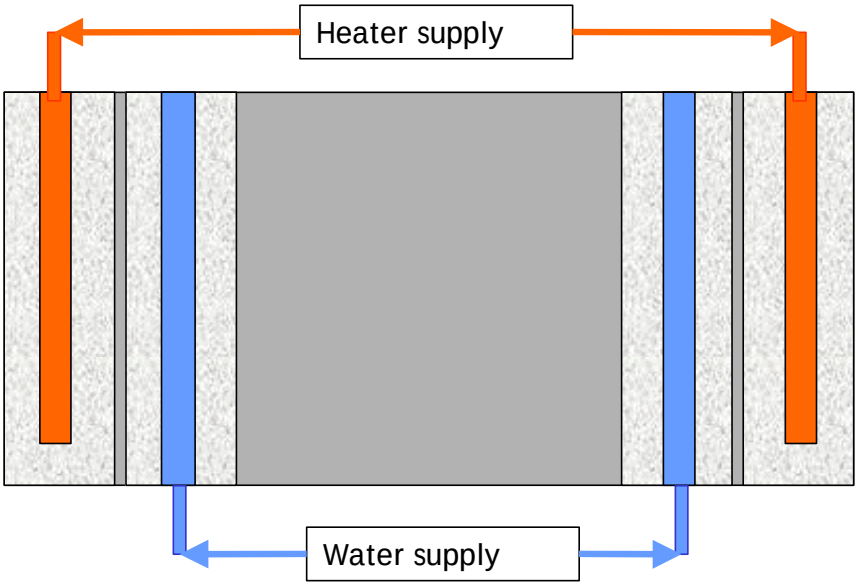

Figure 4-4: Top view of the End-tab jig.

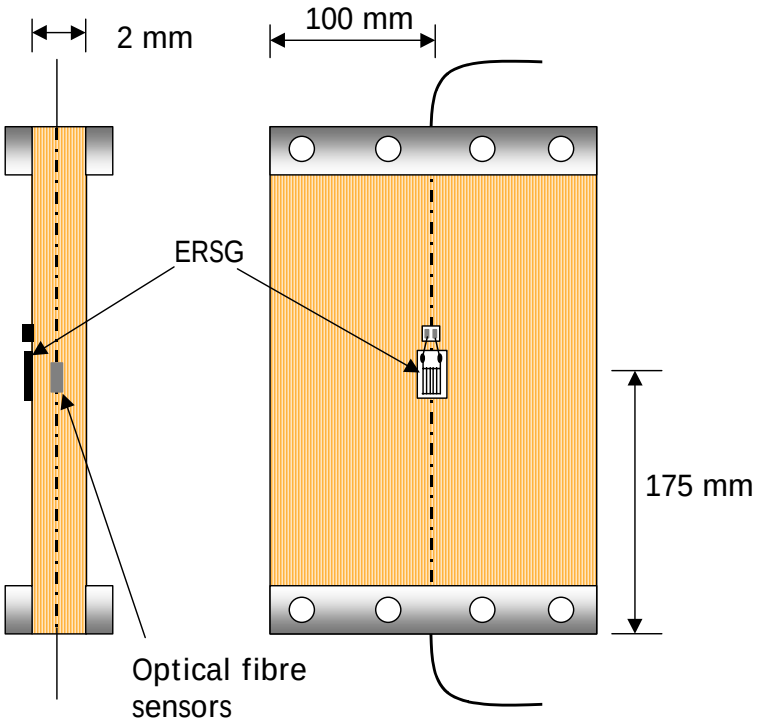

Figure 4-5: Position and alignment of ERSG sensors with embedded optical fibre sensors.

4.3.5. Vacuum bagging

The prepreg laminate was vacuum bagged using conventional techniques to enable the application of a vacuum during autoclave processing. The vacuum bag assembly used in this study is schematically represented in Figure 4-6. The vacuum bag materials used in this study were supplied by Aerovac Ltd, UK.

Peel ply: The peel ply is placed in direct contact with the composite surface. It is a Teflon coated porous Nylon fabric (product code: B100). The Teflon coating prevents the resin from adhering to the bagging materials.

Perforated release film: The perforated release film (product code: A2000) separates the laminate from breather/bleeder cloth. They are perforated in order to remove air, volatiles or excess resin out of the laminate.

Bleeder and breather cloth: These are made of non-woven polyester fabrics (product code: Airbleed 10). The cloth serves two purposes in composites processing. Firstly, it allows air and volatiles to be removed from within the vacuum bag throughout the cure cycle. Secondly, they may also be used to absorb excess resin present in some composite lay-ups.

Caul Plate: A caul plate must be the same size and shape of the prepreg lay-up. This was used in the lay-up process to transmit normal pressure throughout the laminate. The application of a uniform pressure on both sides of the laminate compacts the fibres, and maintains a uniform fibre-to-resin ratio throughout the composite. A smooth aluminium caul plate free from surface defects was used (supplied by Metalfast Ltd, Swindon, UK).

Teflon film: This is porous Teflon coated glass fabric (produce code: 200TFP-I). Teflon is a polymer of a tetrafluoroethylene monomer. This Teflon film ensures easy removal of the laminate from the tool plate. This film was used as a release film on tool plates.

Vacuum Bag Sealant: The vacuum bag sealant tapes are rubber-based adhesives that are used to form a tight seal between the vacuum bag and the tool plate (product code: LTS90B).

Vacuum Bag Film: This is a film used to contain the vacuum during the cure process. A Nylon-based vacuum bag film was used in this work (product code: Capran 512).

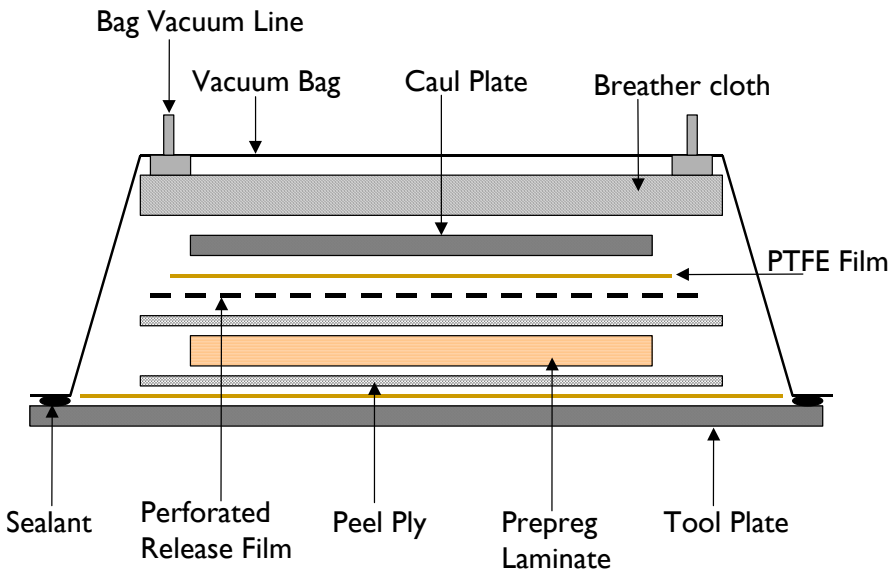

Figure 4-6: Detail of vacuum bag lay-up.

4.3.6. Autoclave processing of composites

In this study composites were prepared using an autoclave. The autoclave (Serial No: 1519) was supplied by Aeroform Ltd, UK. After vacuum bagging the composite, it was placed inside the autoclave bed and a vacuum (-0.084MPa (-850 millibars)) was applied. The manufacturer's recommended cure cycle for the E-glass/913 epoxy prepreg system[112] is 1 hour at 120°C, reached at a rate of ~2 K·minute^{-1}, with a pressure of 0.69 MPa (101 PSI) as shown in Figure 4-7.

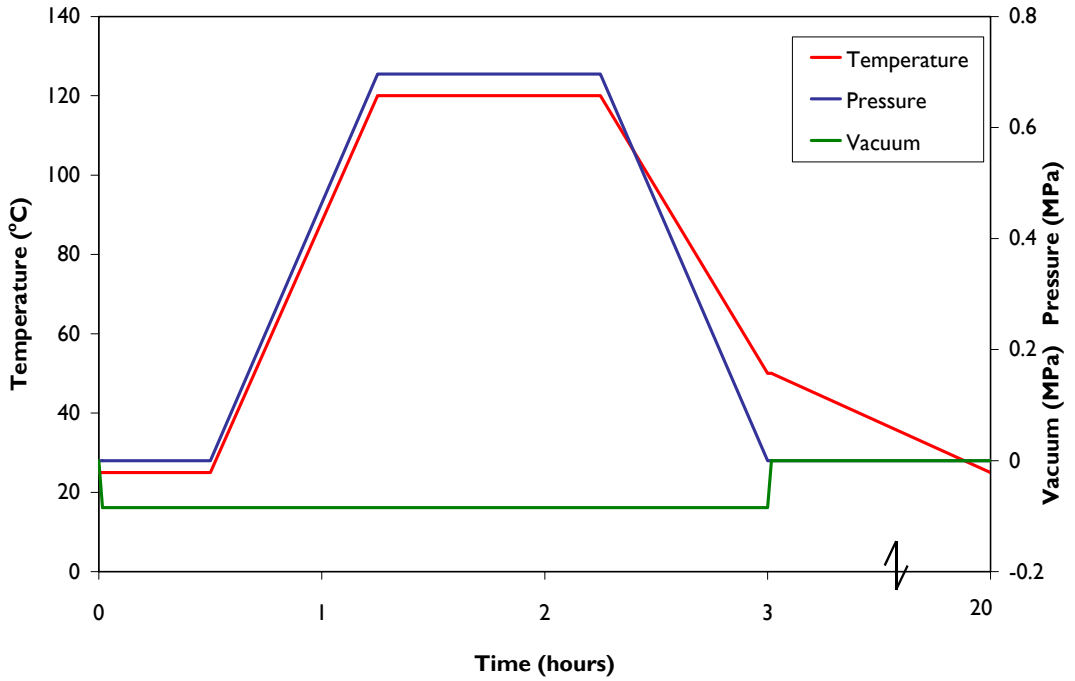

Figure 4-7: The cure cycle for E-glass/913 epoxy prepreg system.

4.3.7. Coding of the composite panels

In order to identify the composites with different levels of prestress from each other, a code system was used. This is described as follows

URX where U = unidirectional, R = reference (non-prestressed), X = panel number.

For example, UR6 represents unidirectional reference panel number 6.

UPTX where P = prestressed and T= prestress rig thermal expansion-induced prestress.

UPX_FkN where P = prestressed, FkN = pre-load in kN

For example, UP6_14kN represents unidirectional prestressed panel number 6 with 14 kN pre-load.

4.4 Evaluation of prestress methodology

In this section the procedure for evaluation of prestress rig is presented. The evaluation of prestress rig involves (i) calibration of load cell at room temperature and elevated temperatures and (ii) evaluation of strain distribution in the prestress rig.

4.4.1. Load cell calibration

The load cell was calibrated by applying a static compression load using an Instron testing machine, model 8501, and comparing the load from the load cell and the Instron testing machine. The test was conducted at room temperature. The test rate was 0.125 kN/second. The static compression test was also conducted at 70, 100 and 121°C, to verify the temperature compensation of the load cell. This temperature compensation test of the load cell was carried out using an Instron model 1195 equipped with an oven.

4.4.2. Prestress rig evaluation

The flat-bed prestress rig designed and developed in this study (as shown in Chapter 3) was evaluated by applying a tensile load to a steel plate (clamped in the prestress rig) and measuring the strain distribution through the width of the plate. The steel plate was instrumented with ERSGs in the positions as shown in Figure 4-8. The static tensile test was conducted at room temperature. In order to enable clamping of the steel plate, holes (12 mm diameter) were drilled. The steel plate was secured into the clamps by tightening the bolts to 20 Nm torque. Pre-tension was applied to the steel plate by tightening the load screw while monitoring the load from the load cell. The strain from ERSGs bonded in different positions on the steel plate was recorded during the tensile test.

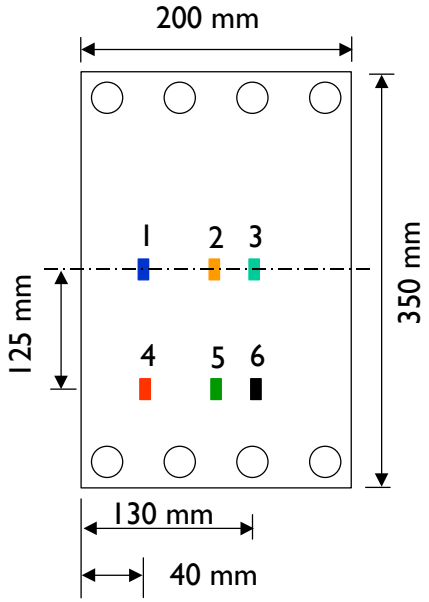

Figure 4-8: Position of ERSG sensors in steel plate.

4.5 Evaluation of sensors

Optical fibre sensors and load cell were used during processing of composites to monitor and measure the residual strain development and applied pre-load respectively. Because the composites are processed in an autoclave at elevated temperature (120°C) with air pressure and a vacuum, the effect of these process parameters on the sensors needed to be investigated prior to using these sensors to monitor residual strain development. This section gives the experimental procedure to evaluate these sensors.

4.5.1. Temperature and pressure tests

The test was conducted on a cured composite panel (290 mm × 200 mm × 2 mm). The sensors used in this test and their positions are described in the following:

Embedded Sensors: EFPI strain sensor and FBG (strain and temperature) sensors are embedded between the 8th and 9th ply of a 16 ply unidirectional composite and placed in the position as shown in the Figure 4-9.

Reference sensors: The reference EFPI strain and FBG (strain and temperature) sensors were placed on top of the composite in the same position as the embedded sensors. They were secured using high temperature polyimide tape.

Load Cell: The load cell was placed at the end of the loading screw in the flat-bed prestress rig as shown in Figure 3-1. The load cell is used in pressure test. No prestress is applied. The Load cell was not in contact with the load screw.

Thermocouple: A thermocouple (K type) was surface mounted on top of the composite and placed in the position shown in Figure 4-9, using high temperature polyimide tape.

The test conditions were the same as the composite cure cycle (Temperature - 120°C for 1 hour with a heating rate of 2 K. minute^{-1}, Pressure - 0.69 MPa for 1 hour with a pressure rate of 0.015 MPa per minute). The temperature and pressure tests were carried out for two repetitions.

4.5.2. Vacuum test

The test was conducted on a prepreg (un-cured) laminate. Before starting the curing process vacuum is applied to the composite in order to remove the entrapped air in the prepreg laminate. In order to understand the effect of a vacuum on the optical fibre sensors during this process, the vacuum test was conducted on the prepreg. An FBG strain sensor was embedded between the 8th and 9th ply of 16 ply prepreg, and placed in the position as shown in the Figure 4-9. The vacuum test conditions are -850 millibars (-0.084 MPa) for 1 hour. The load cell was in contact with the end of the loading screw in the flat-bed prestress rig as shown in Figure 3-1.

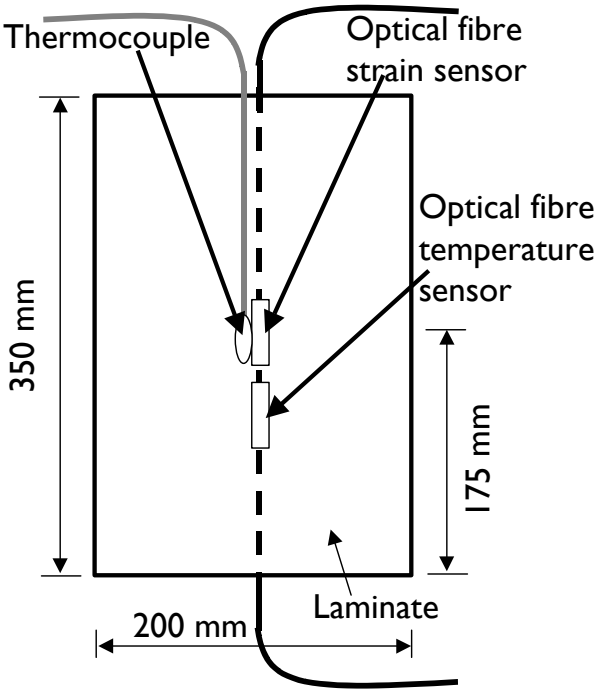

Figure 4-9: Position of sensors in the laminate.

4.5.3. Cure cycle test

The test was conducted on a cured composite panel (290 mm × 200 mm × 2 mm).

Embedded Sensors: EFPI strain sensor was embedded between 8th and 9th ply of 16 ply laminate and placed in the position as shown in the Figure 4-9.

Reference sensors: The reference EFPI strain sensors were placed on top of the vacuum bag in the same position as the embedded sensors. They were secured using high temperature polyimide tape.

Load Cell: The load cell was placed at the end of the loading screw in the flat-bed prestress rig as shown in Figure 3-1.

Thermocouple: A thermocouple was surface mounted on top of the vacuum bag and placed in the position as shown in Figure 4-9, using high temperature polyimide tape.

The test conditions were the same as the composite cure cycle (Temperature - 120°C for 1 hour with a heating rate of 2 K. minute^{-1}, Pressure - 0.69 MPa for 1 hour with a pressure rate of 0.015 MPa per minute and vacuum -850 millibars (-0.084 MPa) maintained throughout the test).

4.6 Residual strain monitoring

The process-induced residual strain in composites was monitored *in-situ* using EFPI and FBG grating sensors. The residual strain development was monitored in unidirectional $[0]_{16}$ and cross-ply $[0/90/0/90/90/0/90/0]_S$, $[0/90/0/90/90/0/90/0]_{4S}$ laminates. Table 4-1 shows the number of panels used to record *in-situ* residual strain development, and the sensor type and position in each panel.

The EFPI and FBG interrogation systems used to monitor the gap length and Bragg wavelength shift respectively are shown in Figure 4-10 and Figure 4-11. Interference spectra from the EFPI sensors were recorded using a charged-coupling-device (CCD) spectrometer (supplied by Ocean Optics Inc., The Netherlands) and was powered by an super-luminescence diode (SLD) light source with a centre wavelength of 850 nm. The wavelength of the reflected narrow band spectrum from the FBG was monitored using a FBG interrogation system (supplied by Fiberpro Ltd., South Korea) and was powered by a class 3A Laser diode. The 2 × 2 coupler was manufactured in-house by Dr R Chen. A custom-written LabVIEW™ (version 6.1) program was used to record the data from the interrogation unit.

Table 4-1: Summary of the panels used to record *in-situ* residual strain development, and the type of sensor and its position in the panel.

Panel Code	Middle	40 mm from the edge
UR1	EFPI	
UR8	EFPI	
UR9	EFPI	
UPT8	EFPI	
UPT11	EFPI	
UP1_7kN	EFPI	
UP2_7kN	EFPI	
UP2_14kN	EFPI	EFPI
UP3_14kN	EFPI	EFPI
UP4_14kN	EFPI	
UP5_14kN	EFPI	
UP6_14kN	EFPI	
UP7_14kN	EFPI	
UP9_14kN	EFPI + FBG	
UP12_14kN	FBG	
UP1_24 kN	EFPI	

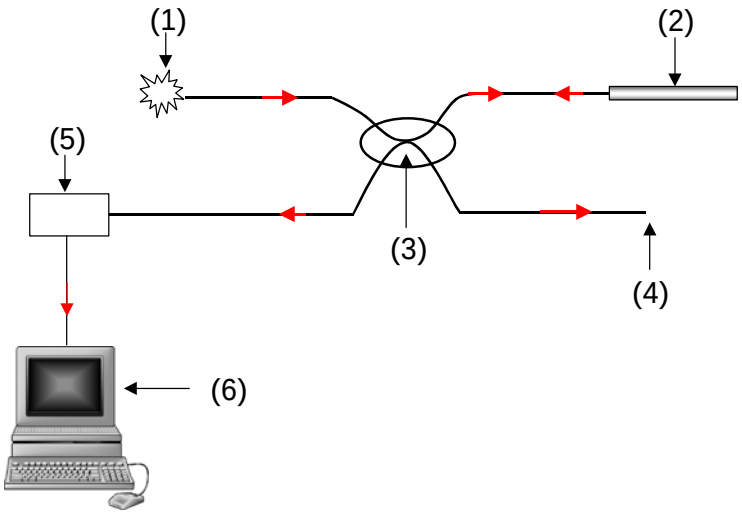

Figure 4-10: Schematic of the arrangement used to record spectra from the EFPI sensor: (1) the SLD light source, (2) the EFPI sensor, (3) the 2 × 2 coupler, (4) anti-reflection terminal (broken fibre covered with index matching gel) used to prevent any back-reflection, (5) CCD spectrometer, and (6) data acquisition.

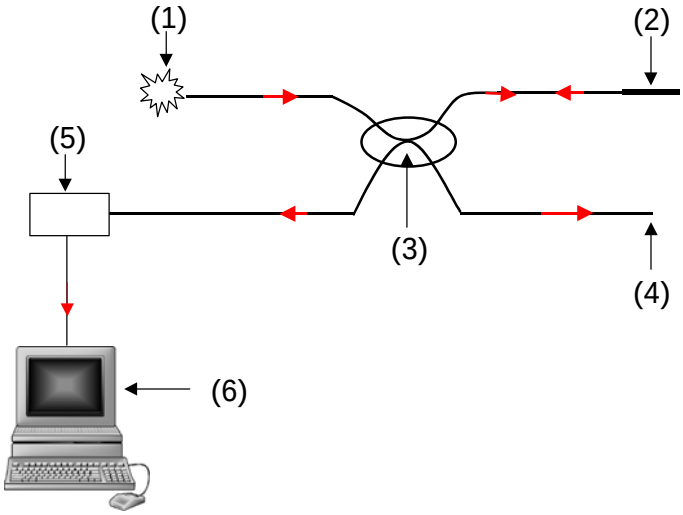

Figure 4-11: Schematic of the arrangement used to record spectra from the FBG sensor: (1) the 1550 nm Laser diode, (2) the FBG sensor, (3) the 2 × 2 coupler, (4) anti-reflection terminal (broken fibre covered with index matching gel) used to prevent any back-reflection, (5) the FBG interrogation unit, and (6) the data acquisition.

4.7 Differential scanning calorimetry

A differential scanning calorimeter (Diamond DSC supplied by Perkin Elmer Ltd, UK) was used to study the 913 epoxy resin cure characteristics. The DSC was calibrated using high purity indium and tin. A 5 mg sample was cured in a conventional aluminium pan, using the 913 epoxy resin cure temperature cycle (see Section 4.3.6). The heating rate used was 2 $K.minute^{-1}$.

4.8 Quality control and specimen preparation

After preparation of the composite panel, the quality of the panel was checked, prior to specimen cutting, polishing and end-tabbing. This section explains the procedures used for panel quality control and specimen preparation.

4.8.1. Quality control

The quality of the composite panels was examined by employing both non-destructive (ultrasonic C-Scanning) and destructive (optical microscopy, scanning electron microscopy and resin burn-off) methods. This is described in the following section.

Non-destructive testing

An ultrasonic C-Scan was used to examine the extent of void and delamination defects in composite materials. The C-Scan equipment (Model No: UPK-II/D) was supplied by Physical Acoustics Corporation, UK. The composite panel was placed in a water tank and an ultrasonic transducer working at 5 MHz was used to scan the panel. Distilled water was used as a coupling medium between the ultrasonic transducer and the composite panel. When the signal reaches a void or a delamination, the signal is attenuated. This information is processed to produce a two-dimensional image of the panel showing the void and defect positions.

Destructive testing

Destructive testing methods were used to measure the fibre volume fraction, void volume fraction and fibre alignment of composite panels. Optical microscopy, scanning electron microscopy (SEM) and resin burn-off (pyrolysis) methods were used to destructively examine the composite panels. For microscopy examination, samples of 15 × 15 mm dimensions were sectioned from the composite panel and mounted in a polyester resin supplied by Struers Ltd, UK. The specimens were polished using different grades of SiC abrasive paper from 220 to 2400 grit. The final polishing stage was carried out using water-

based diamond suspensions, starting from 6 μm and going down to 0.25 μm. The polishing equipment (Rotopol-21 and RotoForce-4) was supplied by Struers Ltd, UK.

Once the samples were polished they were dried and stored in laboratory conditions. The polished samples were then examined using optical microscopy and SEM. The optical microscope used in this study was a Leica DMLM set with a camera and image acquisition software Leica Qwin (version 2.3) supplied by Leica Ltd, UK. The SEM used in this study was a LEO 435VP supplied by Carl Zeiss SMT Ltd, UK.

(i) *Fibre volume fraction (V_f)*

The fibre volume fractions of manufactured composites were determined using two techniques namely, (i) burn-off and (ii) image analysis.

In the burn-off method, a piece of composite (15 (l) × 15 (w) × 2 (t) mm), conditioned at ambient laboratory conditions, was weighed accurately using an electronic balance with a measurement accuracy of 0.0001 gm. This was placed in a clean heat-resistance crucible in the furnace. The furnace temperature was increased from room temperature to 650°C and held for 6 hours until all the resin was decomposed. The residue, which consisted of glass fibres, was weighed and the resin weight was calculated. The fibre volume fraction of glass (V_f) was determined using the following equation:[113]

$$V_f = \frac{\left(\frac{W_f}{\rho_f}\right)}{\left(\frac{W_f}{\rho_f}\right)+\left(\frac{W_m}{\rho_m}\right)} \tag{4.1}$$

where W_f, W_m, ρ_f and ρ_m are the weight fraction and densities of the fibre and matrix resin, respectively. The average fibre volume fraction was calculated from ten individual specimens.

In the image analysis method, a transverse cross-section of the unidirectional composite taken from the scanning electron microscope (SEM) was examined using Leica image analysis software. The average fibre volume fraction was calculated from a minimum of ten micro-frames (540 × 360 μm) for each prestress level.

(ii) *Void volume fraction (V_v)*

Microscopic images from the SEM were used to calculate the void volume fraction using the Leica image analysis software. The average void volume fraction was calculated from a minimum of ten micro-frames (540 × 360 μm) for each prestress level.

(iii) *Measurement of fibre alignment*

In this work, the Yurgartis method for measuring the fibre alignment in composites was used. The principle of Yurgartis method was presented in Section 2.5.1, Chapter 2. The specimens were prepared by cutting samples from the unidirectional laminate parallel to the fibres (see cross-section A-A in Figure 4-12). The samples were then potted in a room temperature curable polyester resin (supplied by Struers Ltd) with the fibres aligned parallel to the polishing direction as shown in Figure 4-13. This specimen was then polished using the procedure described above. This polished section (A-A) was then examined under the scanning electron microscope. The major axis length *l* was measured manually and substituted in equation 2.8 to determine the fibre orientation. The fibre, which is spanning throughout the length of the micro-frame, is assumed to have aligned in the 0° direction. The average fibre alignment was calculated from a minimum of six micro-frames (876 × 660 μm) for each prestress level.

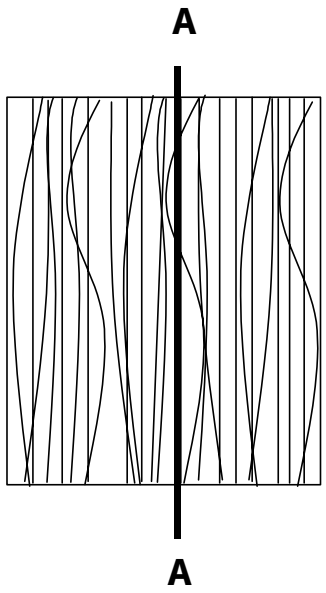

Figure 4-12: Definition of the parallel cutting angle.

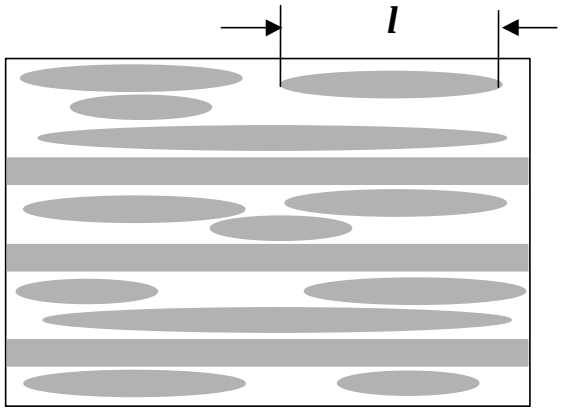

Figure 4-13: Illustration of fibre orientation in the cross-section A-A of Figure 4-12.

4.8.2. Specimen cutting and polishing

The laminates were cut to size for testing with a water-cooled diamond saw, avoiding plate edges and areas indicated as defective by the ultrasonic C-scan technique. Both sides of each specimen were polished to 2400 grit SiC abrasive paper to avoid any edge defects that could initiate premature failure.

4.8.3. Coding of composite specimens

In order to identify the composite specimen position from the composite panel, a coding system of numbers was used. The specimen numbers in a composite panel are shown in Figure 4-14. This number was added to the composite panel code as shown below.

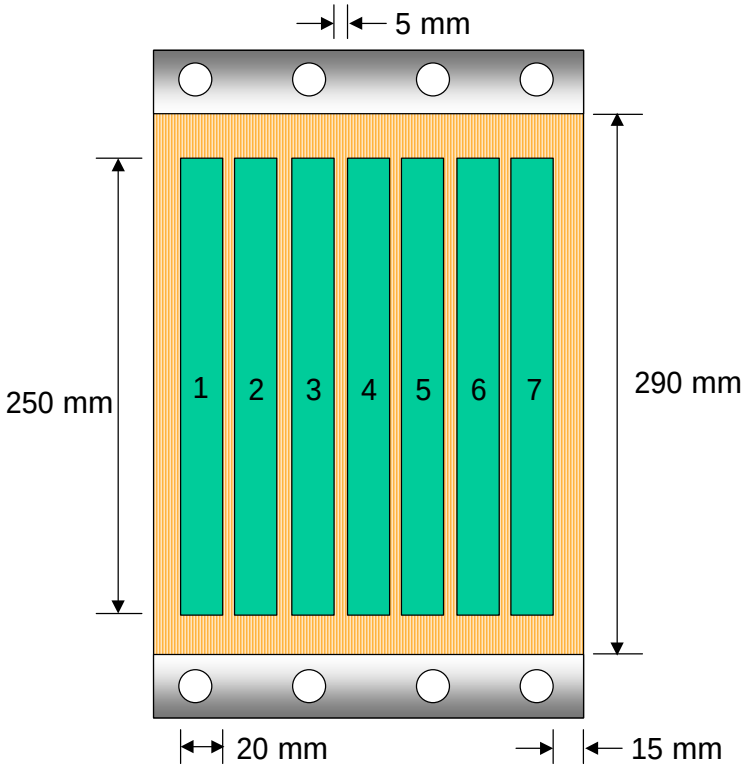

Figure 4-14: The position of specimens taken from the composite panel.

URX_Y where U = unidirectional, R = reference (non-prestressed), X = panel number and Y= specimen number. For example, UR6_5 represents specimen number 5 taken from unidirectional reference panel number 6.

UPTX_Y where U = unidirectional, P = prestressed, T = prestress rig thermal expansion-induced prestress and Y = specimen number.

UPX_FkN_Y where P = prestressed, FkN = pre-load in kN and Y= specimen number.

For example, UP6_14kN_5 represents specimen number 5 taken from unidirectional prestressed panel number 6 with 14 kN pre-load.

4.8.4. End-tabbing

The static tension and fatigue test specimens were end-tabbed with aluminium alloy tabs and for the static compression test GFRP (woven-fabric) end-tabs were used. Conventional

end-tabbing procedures were used. The adhesive, 3M Scotch-weld epoxy-based system was used to bond end-tabs on the composite specimen. The end-tabs were cured at room temperature for 24 hours, followed by post-curing at 65°C for 2 hours. Specimens were stored in a desiccator at ambient laboratory conditions until required.

4.9 Mechanical testing

All tests were carried out in ambient laboratory atmospheric conditions.

4.9.1. Quasi-static tensile test

The static tensile properties were obtained using a servo-hydraulic Instron testing machine (model 8501). The static tensile tests were conducted according to the Composite Research Advisory Group [114] (CRAG) standard. The dimensions of the static tensile test specimens were 250 mm (l) × 20 mm (w) × 2 mm (t) with a gauge length of 150 mm as shown in Figure 4-15. The tensile tests were conducted under position control with a crosshead speed of 5mm.min^{-1}. The strain was measured with an extensometer over a 50 mm gauge length. The load, strain, position and time were recorded using custom-written LabVIEW™ software (version 6.1). Six specimens were tested with the aforementioned conditions to measure the tensile properties of each prestressed composite.

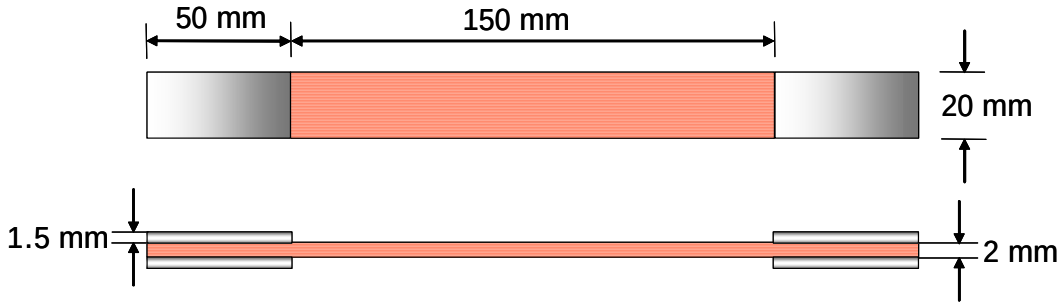

Figure 4-15: Test specimen geometry for static tension and tension-tension fatigue testing.

The properties measured from the tensile test were: 1) secant modulus, 2) ultimate tensile strength, 3) failure strain and 4) strain at deviation from linearity. The strain at deviation from linearity (ε_{SDL}) is defined as the strain at which the onset of non-linearity occurs in the stress-strain curve during a tensile test of a composite specimen. This is illustrated in Figure 4-16.

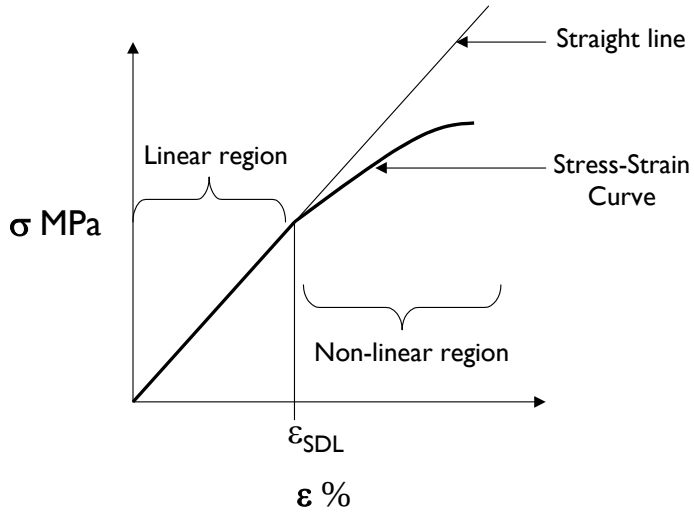

Figure 4-16: Illustration of strain at deviation from linearity.

4.9.2. Quasi-static compression test

The compressive test was carried out in a Zwick machine model 1488 at the Department of Aerospace Engineering, Imperial College, London. The compression test was conducted using the Imperial College of science, technology and medicine[115] (ICSTM) fixture. The dimensions of the compressive test specimens were 90 mm (l) × 10 mm (w) × 2 mm (t) with a gauge length of 10 mm as shown in Figure 4-17.

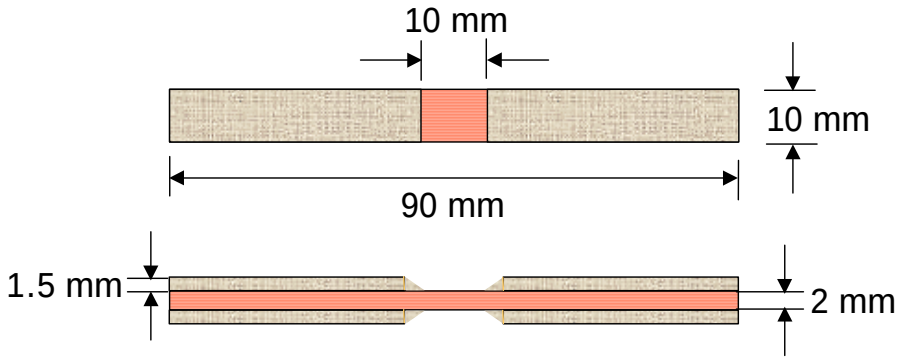

Figure 4-17: Test specimen geometry for static compression testing.

Both ends of each specimen were ground using a surface grinding machine to avoid any edge defects that could initiate premature failure. The specimens were instrumented with two ERSG sensors of 2mm gauge length (one in the front and the other in rear). The compression tests were conducted under position control with a crosshead speed of 1mm/minute. The load and strain were recorded during the test. A minimum of five specimens were tested to measure the compressive properties for each prestress level. The

properties studied in a compression test were 1) ultimate compressive strength, 2) modulus of elasticity.

4.9.3. Fatigue test

The fatigue tests were carried out in a servo-hydraulic Instron testing machine (model 8501). The specimen dimensions for tension-tension fatigue were the same as the static tensile specimens (see Figure 4-15) and for tension-compression fatigue the dimensions used were 200 mm (l) × 20 mm (w) × 2 mm (t) as shown in Figure 4-18.

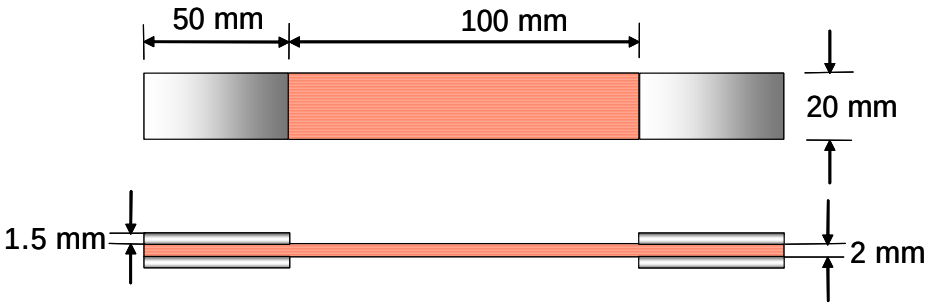

Figure 4-18: Test specimen geometry for tension-compression fatigue testing.

The fatigue tests were conducted according to CRAG and ISO 13003[116]. Stress ratios (R) of +0.1 and –0.3 were employed in this investigation. The fatigue tests were carried out under constant amplitude loading with a sinusoidal waveform, and a loading rate of 250 kN s^{-1}. Seven different stress levels (from 35% to 90% of the ultimate strength of the composite) were used to determine the fatigue life diagram. At each stress level, three specimens were tested. A custom-written LabVIEW™ (version 6.1) program was used to monitor stiffness, amplitude stress and strain, and surface temperature changes as a function of fatigue life in real-time.

CHAPTER 5

Evaluation of prestress methodology and sensors

OVERVIEW

- Results from the evaluation of strain distribution in the flat-bed prestress rig at different tensile loads to a rectangular steel plate instrumented with strain gauges are discussed.
- The design and development of an end-tab jig to circumvent (i) fibre misalignment in and near the end-tab region and (ii) pre-cure away from end-tab region are described.
- The effect of autoclave process parameters such as temperature, pressure and vacuum on the load cell and optical fibre (EFPI and FBG) sensors are presented.

5.1 Results and discussions on prestress rig evaluation

5.1.1. Load cell calibration

The load cell calibration was carried-out according to the experimental procedure given in Section 4.4.1, Chapter 4. Figure 5-1 shows the results from the load cell calibration test. From Figure 5-1 it can be observed that the load recorded from the load cell is in good agreement with the load measured from the Instron machine.

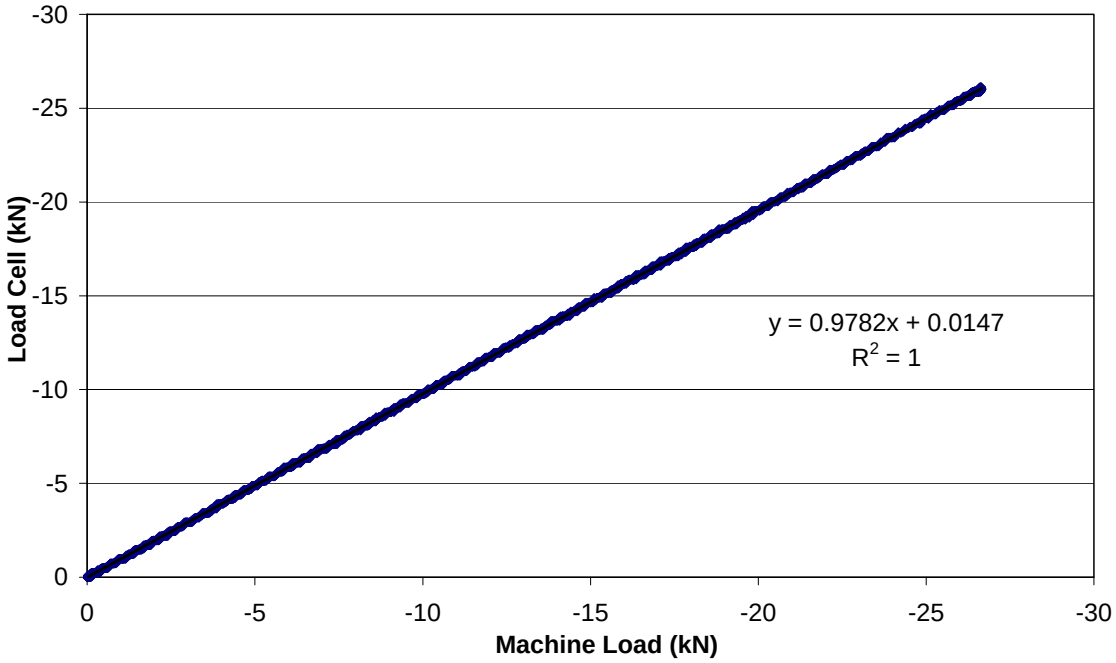

Figure 5-1: Comparison of load from load cell and Instron testing machine.

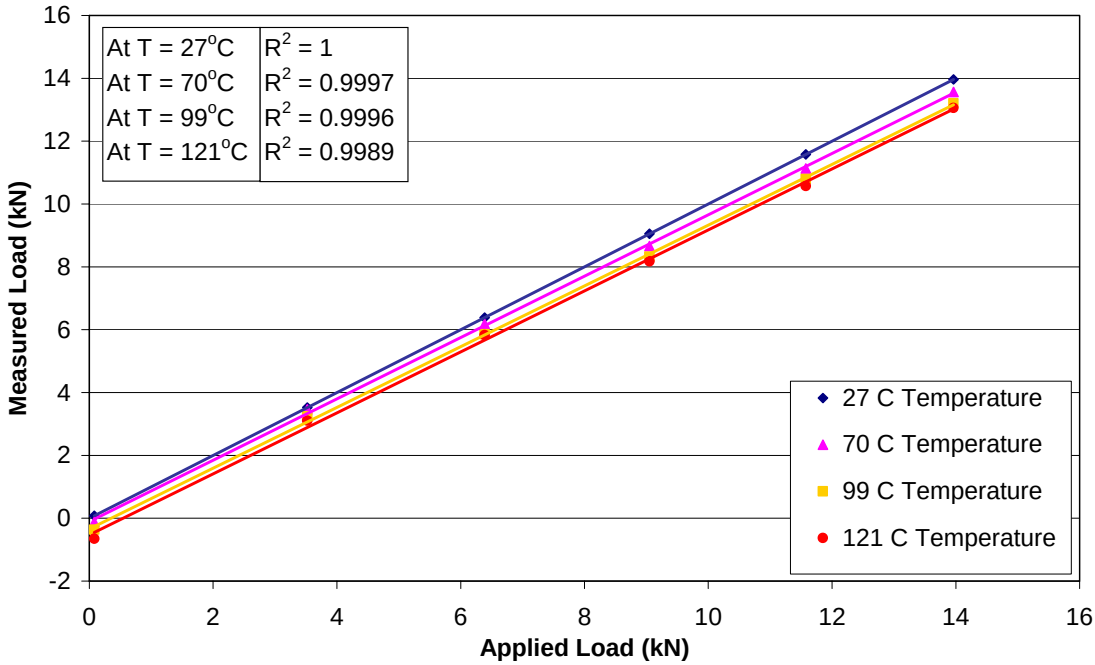

Figure 5-2: Comparison of load measured from the load cell and the applied load (Instron machine) at different temperatures.

The temperature effect on the response of the load cell was also studied according to the procedure given in Section 4.4.1. Figure 5-2 presents the results from the temperature

response of the load cell. With reference to the figure it can be observed that the load cell responds linearly during the static tests conducted at different temperatures (27°C, 70°C, 99°C and 121°C). It can be observed that there is a change in load of about -0.8 kN for a 94°C temperature difference. This shows that for a 94°C temperature difference the load measured will change by -0.8 kN.

5.1.2. Prestress rig evaluation

The calibrated load cell was used in the prestress rig to apply a pre-defined static tensile load to a steel plate (clamped to the prestress rig) to study the strain distrubution in the steel plate. Figure 5-3 shows the strain measured at different positions (see Figure 4-8) in the steel plate during the static tensile test in the prestress rig. With reference to Figure 5-3 it can be observed that the strain measured at different positions on the steel plate for an applied load are in good agreement. This shows that the strain distribution through the width of the steel plate is uniform. The load-strain curve is linear because the applied loads were within the elastic region of the steel plate.

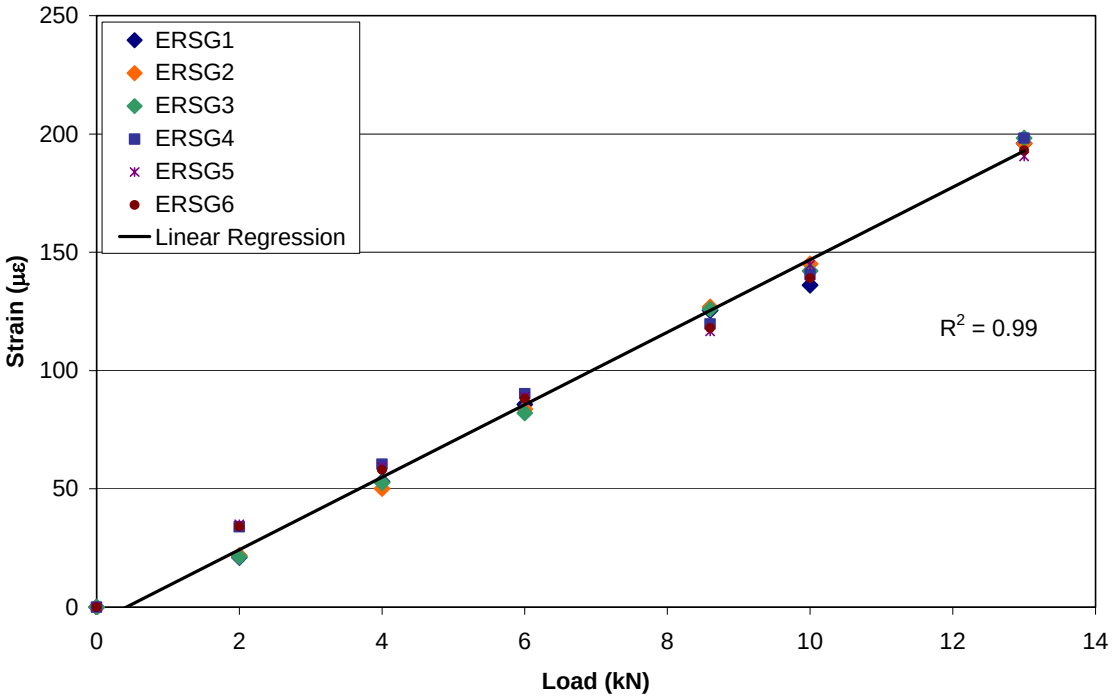

Figure 5-3: Strain measured from the ERSG as a function of the applied load measured from the load cell.

In order to visualise the strain distribution through the plate area two-dimensional plots were drawn at different load levels as shown in Figure 5-5, Figure 5-6 and Figure 5-7. It was assumed that the strain distribution is symmetric throughout the plate. Figure 5-4

shows the positions of the ERSGs and the corresponding symmetrical positions (marked with superscript-1).

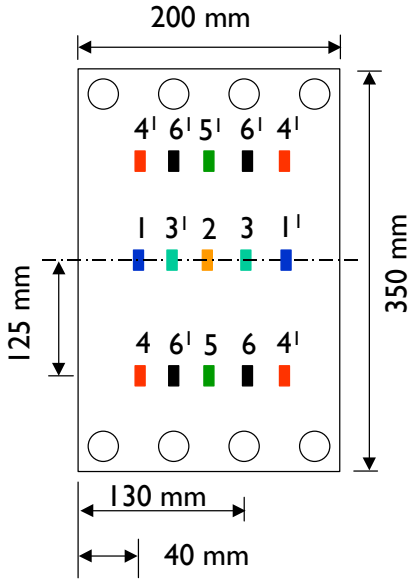

Figure 5-4: Position of ERSGs and the corresponding symmetrical positions in steel plate.

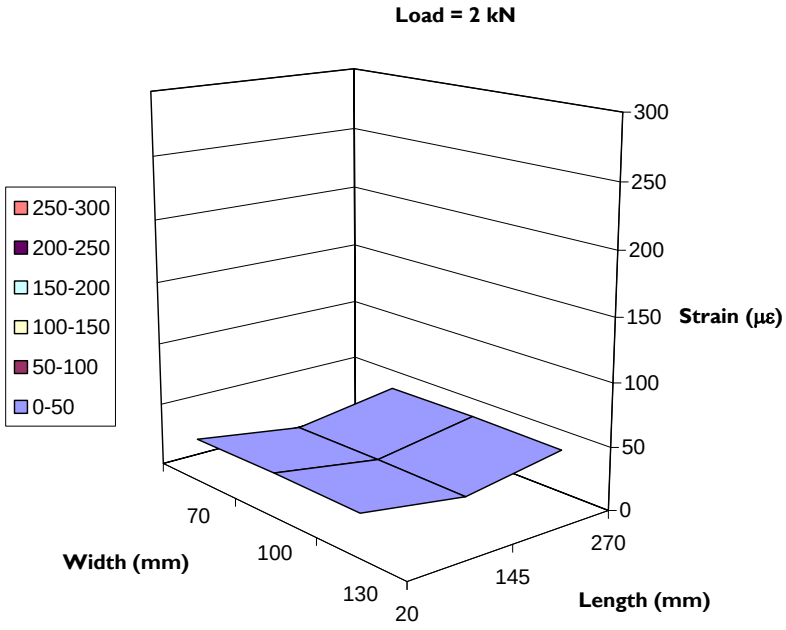

Figure 5-5: Strain distribution in steel plate at an applied load of 2 kN.

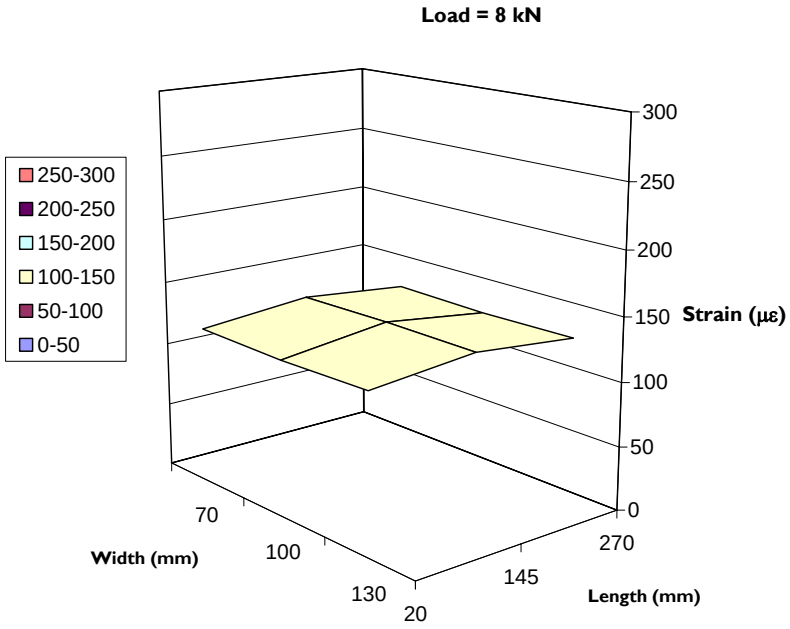

Figure 5-6: Strain distribution in steel plate at an applied load of 8 kN.

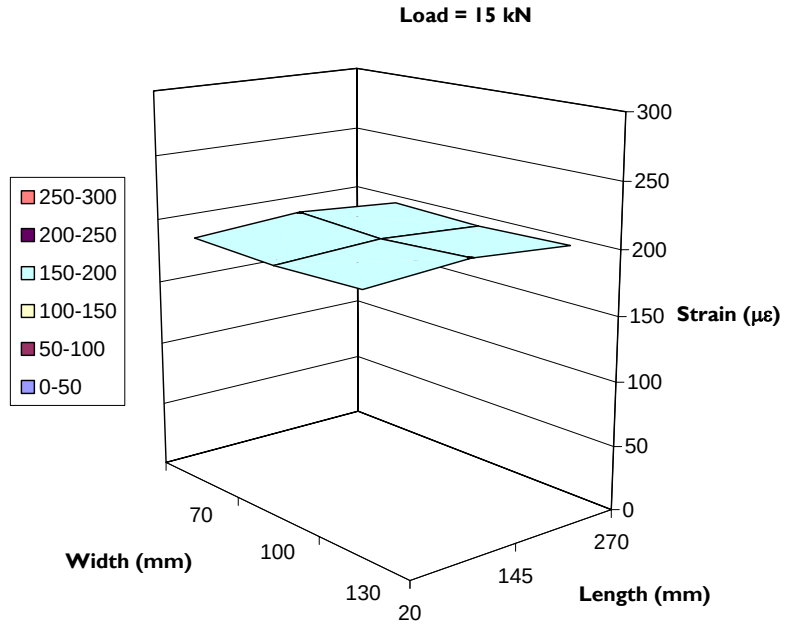

Figure 5-7: Strain distribution in steel plate at an applied load of 15 kN.

From Figure 5-5 to Figure 5-7 it can be observed that the strain distribution in the plate is uniform with a variation of about 10% in strain through the length and 4% variation through the width of the plate. This small variation in the strain distribution in the steel

plate could be due to Poisson's effect and small misalignment of the strain gauge surface-mounted on the steel plate.

5.2 Prepreg end-tab jig design and evaluation

In this study initially, prepreg end-tab curing was carried out using the hot-press method. During this curing process only the end-tab region was placed in the hot-press. The rest of the prepreg laminate was supported using an aluminium plate with PTFE spacers (to prevent the curing of the prepreg away from the end-tab region). Once the end-tab was cured, the prepreg laminate was clamped onto the flat-prestress rig and cured in the autoclave. The first prestressed composite panel was prepared after designing and evaluating the flat-bed prestress rig. The composite panel manufactured was warped as shown in Figure 5-8. This section investigates the cause of composite warping and presents a design and development of a flat-bed end-tab jig to eliminate warping in composites.

The major reason for the composite bending during manufacturing could be due to the eccentric release of prestress caused by fibre misalignment near the end-tab regions. In order to identify the cause of the bending, at first samples were cut in the end-tab region and examined in an optical microscope. From the examination (see Figure 5-9), it was found that fibre misalignment exists near the end-tab region. This was observed throughout the width of the composite near the end-tab region.

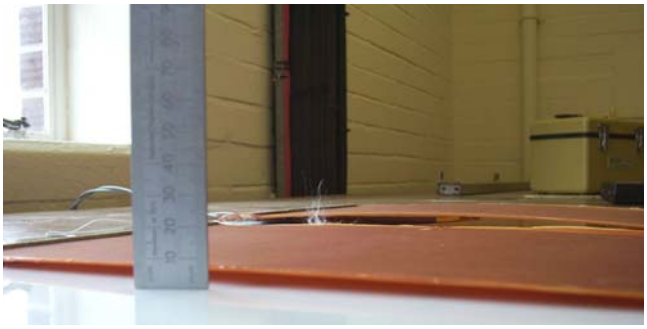

Figure 5-8: Warped composite.

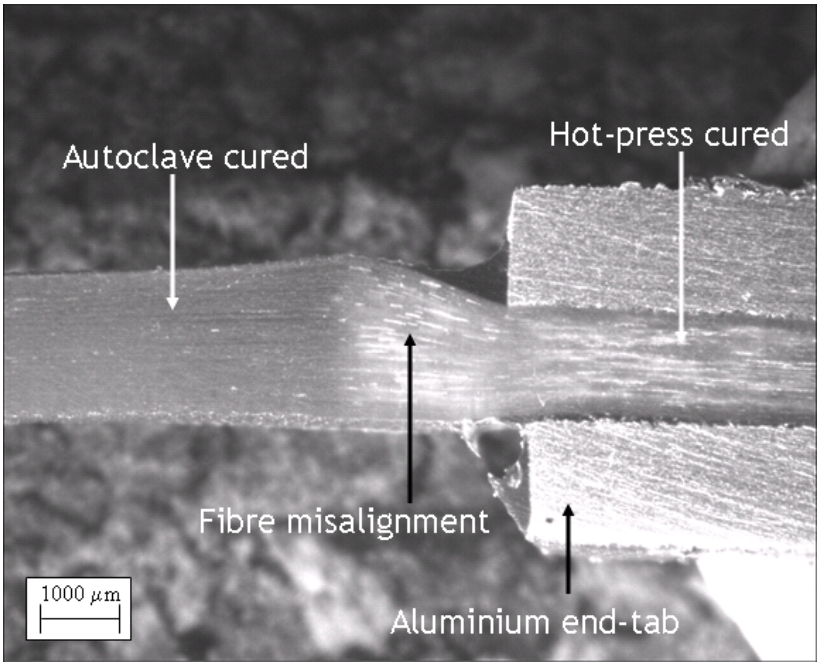

Figure 5-9: Microscopic evidence of fibre misalignment near end-tab region.

From Figure 5-9 it is also apparent that there exists a difference in the thickness of the composite panel between the hot-press cured and the autoclave cured regions. This is due to high pressure being applied in the end-tab region during the hot-press cure. Also during the hot-press cure, the heat is transferred away from the end-tab region. This leads to resin melting, which instigates fibre movement, and subsequently the resin near the end-tab region cures. This freezes the fibre misalignment near the end-tab region. When a pretension is applied there may be a possibility of reducing the fibre misalignment near the end-tab region but not completely, because the composite near the end-tab region is pre-cured. Once the composite is processed in autoclave and cooled-down to room temperature, the prestress is released. This induces compressive stress to the composite in the direction of the fibres. Because the fibres near the end-tab region are misaligned, the prestress is released eccentrically, which caused composite bending.

5.2.1. End-tab jig design

In order to circumvent the fibre misalignment near the end-tab region and composite pre-curing away from the end-tab region, a custom-designed end-tab jig was manufactured as shown in Figure 5-10. The jig consists of a heating and cooling unit in both the ends of the jig. The heating element is connected to a temperature controller and the cooling system is connected to a temperature-controlled water cooler. After laminating the prepreg the aluminium end tabs were carefully attached to the ends of the prepreg. This was then placed inside the end-tab jig such that the end-tabs sits between the heating blocks and the

prepreg near the end-tab region sits between the cooling blocks. The end-tab is then cured according to the manufacturer's recommended cure cycle. The end-tabbed prepreg was then clamped in the prestress rig and the prepreg laminate was then cured in an autoclave.

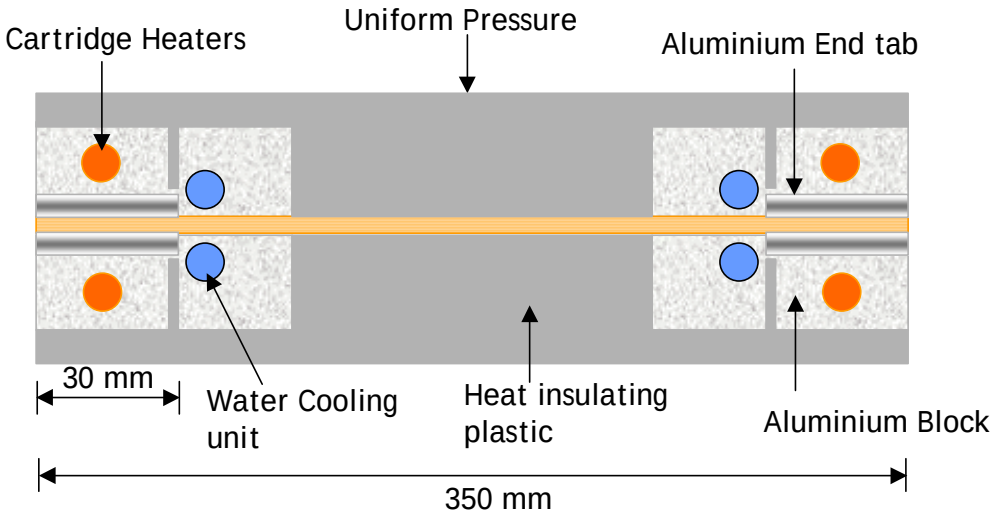

Figure 5-10: Schematic illustration of End-tab jig design.

Figure 5-11 shows a cross-section of the end-tab cured using the end-tab jig. From Figure 5-11 it can be observed that the fibre misalignment was eliminated near the end tab region. The surface profile of composite panels was measured using a dial gauge for composites manufactured with and without using the end-tab jig. The results from the surface profile measurements are shown in Figure 5-12. In Figure 5-12 the prestressed composites with hot-press cured end-tabs are coded as HPCET and end-tab jig cured end-tab are coded as ETJCET. The non-prestressed composite in Figure 5-12 refers to the composite cured out-of-prestress rig and without any end-tab. The measured surface profile of non-prestressed composites shows the variation in thickness of the composite through the length. From Figure 5-12 it is apparent that composites prepared using the end-tab jig show a significantly reduced bending of the composite.

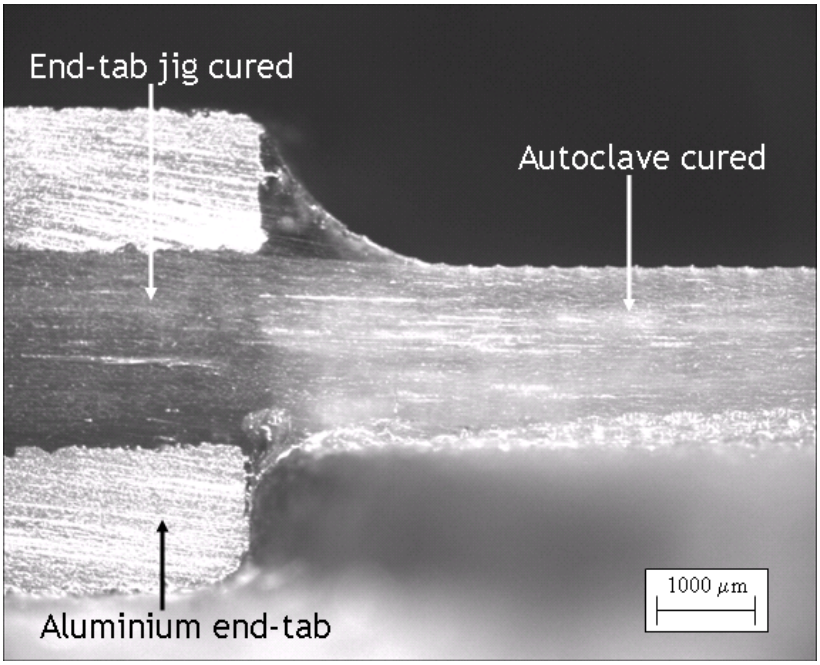

Figure 5-11: Microscopic evidence of improved fibre alignment near end-tab region.

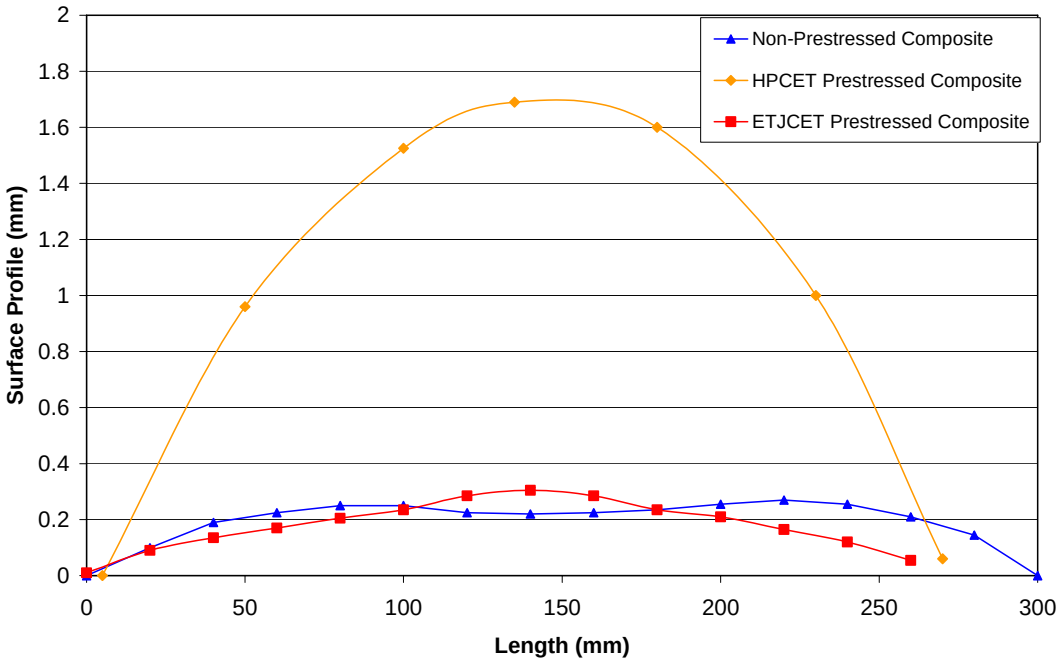

Figure 5-12: Surface profile of non-prestressed and prestressed unidirectional composites.

5.3 Results and discussions on sensor evaluation

The optical fibre sensors and load cell were used during processing of composites to monitor and measure the residual strain development and applied pretension respectively. Because the composites are processed in an autoclave at elevated temperature (120°C) with air pressure and vacuum, the effect of these process parameters on the sensors needed to be investigated. This section discusses the preliminary results from the effect of autoclave process parameters on sensors. The results from the sensor behaviour during temperature, pressure, vacuum and cure cycles are discussed in the following sections.

5.3.1. Effect of temperature on sensors

Optical fibre sensors

The effect of temperature on optical fibre sensors was studied according to the experimental procedure given in Section 4.5.1 of Chapter 4. Figure 5-13 shows the response of embedded and reference sensors during autoclave temperature tests. With reference to Figure 5-13 it can be observed that the temperature measured from the embedded FBG temperature sensor is in good agreement with the temperature measured from the thermocouple in the autoclave.

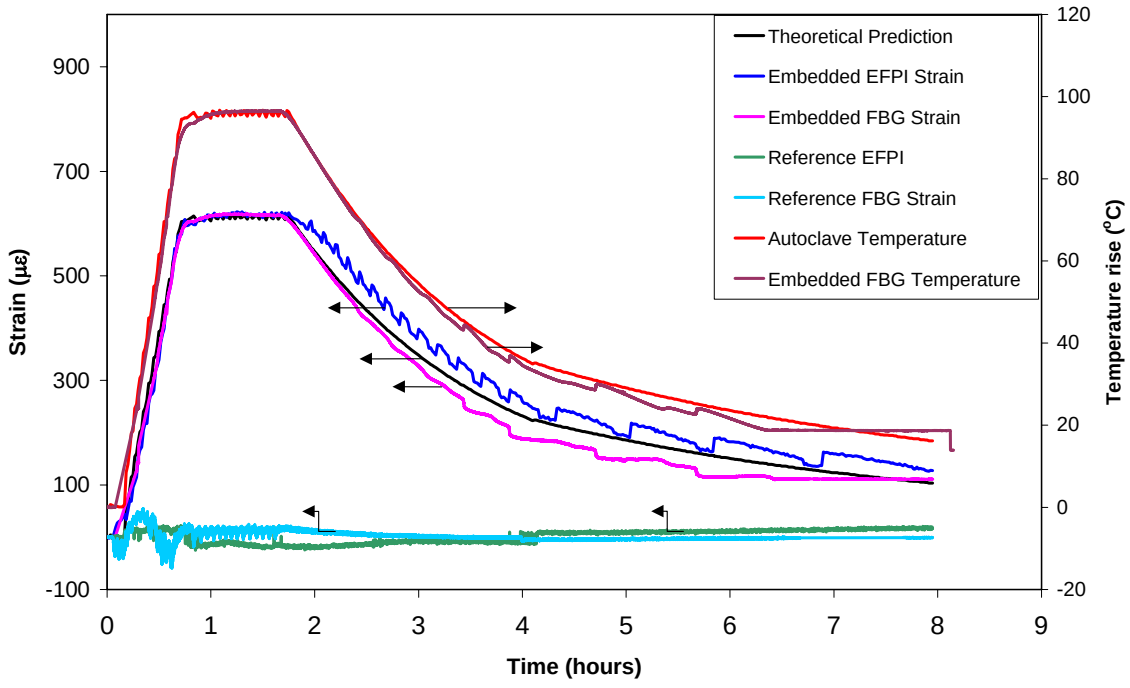

Figure 5-13: Relationship between optical sensors (embedded and reference) and temperature.

From Figure 5-13 it can be observed that there is no significant change in strain measured from the reference sensor during the temperature test. A small variation in measured strain of about ± 25 με and ± 50 με in EFPI and FBG sensors were recorded respectively. This variation in strain measured from the reference sensors could be due to (i) the influence of the polyimide tape bonding-resin on the reference sensors, (ii) the transverse sensitivity of the FBG sensor and (iii) the error in the measurement. This small variation is negligible and therefore it can be concluded that the temperature does not influence the response of optical fibre strain sensors.

With reference to Figure 5-13 it can be seen that the embedded strain sensors measures the thermal expansion of the cured unidirectional composite. Theoretically, the thermal expansion of a unidirectional composite (α_C), in the fibre direction is given by the following equation:

$$\alpha_C = \frac{\alpha_m \nu_m E_m + \alpha_f \nu_f E_f}{E_m \nu_m + E_f \nu_f} \left(K^{-1}\right) \tag{5.1}$$

where α, ν and E are the thermal expansion coefficient, Poisson's ratio and modulus respectively. The subscript *m* and *f* stand for matrix and fibre respectively.

Table 5-1: Material properties used.

Properties	E-glass	Epoxy Resin
Young's Modulus [MPa]	72500	4000
Poisson's ratio [-]	0.22	0.4
Thermal expansion coefficient [°C^{-1}]	5.00×10^{-06}	60.0×10^{-06}
Volume fraction	0.6	0.4

Table 5-2: Summary of thermal expansion measured experimentally and calculated theoretically.

Method	Thermal expansion ($\times10^{-06}$ K^{-1})
Theoretical prediction (equation 5.1)	6.38
Experimental measurement (EFPI and FBG)	6.45

Equation 5.1 is based on a micro-mechanics theory of composites. The material properties from Table 5-1 are used to predict the thermal expansion of the composite (using equation 5.1) for the temperature rise shown in Figure 5-13. The theoretical prediction of thermal expansion (strain) of the composite is included in Figure 5-13. A summary of the thermal expansion predicted from equation 5.1 and measured from experiments is presented in Table 5-2. It can be observed that the theoretically-predicted thermal expansion of the

composite during the heating and isothermal cycles is in good agreement with the measured EFPI and FBG strain sensors. Also from Table 5-2 it can be seen that the experimental measurement of thermal expansion of composite is in good agreement with theoretical prediction. During the heating and cooling cycle, perturbations are observed in the strain measured from both the EFPI and FBG strain sensors. The perturbation observed in the EFPI sensor response may be due to the time-delay for the optical fibres inside the capillary to respond to the thermal strain induced by the composite to the sensor. However, the measured strain from optical fibre sensors was within ± 50 με of the theoretical prediction.

5.3.2. Effect of pressure on sensors

a) Load cell

The effect of pressure on the load cell was studied. From the pressure test it was found that a change of 0.04 kN was recorded for an increase in pressure of 0.69 MPa. During this test the load cell was positioned at the end of the load screw, but the load screw was not touching the load cell. This shows that there is no significant effect of pressure on the load cell.

b) Optical fibre sensors

The effect of pressure on optical fibre sensors was studied according to the experimental procedure given in Section 4.5.1, Chapter 4. Figure 5-14 shows the effect of pressure on the reference optical fibre EFPI and FBG sensors. From Figure 5-14 it can be observed that there is no significant effect of pressure on the EFPI and FBG sensors. The recorded strain of ± 20 $\mu\varepsilon$ in both the reference optical fibre sensors was within the accuracy of the instrumentation used.

Figure 5-15 shows the response of embedded FBG temperature and strain sensors on the effect of autoclave pressure. From figure it can be observed that with increase in pressure there is a change in strain of about ± 20 $\mu\varepsilon$ was observed. This is very similar to the reference optical fibre sensors. It can also be observed that with increase in pressure an increase in temperature of about 4.8°C was observed. The increase in temperature may also have influenced the change in strain measured in the embedded sensor. The temperature measured from thermocouple and FBG temperature sensors are in good agreement. The observed change in the measured strain from embedded and reference optical fibre sensors on the effect of pressure are negligible.

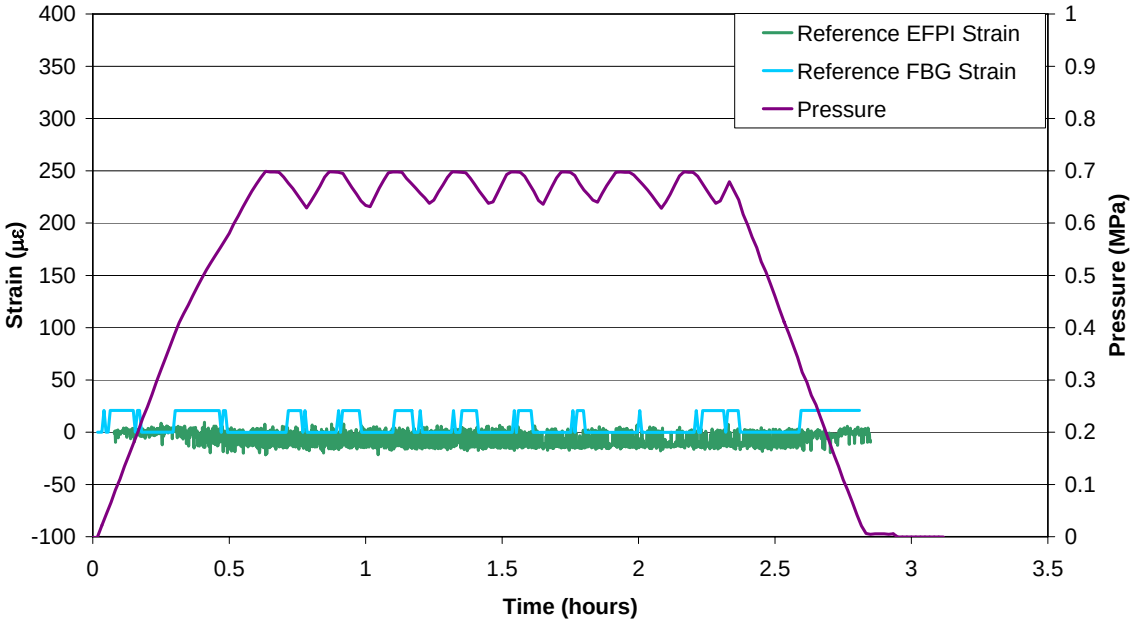

Figure 5-14: Relationship between reference optical fibre sensors and pressure.

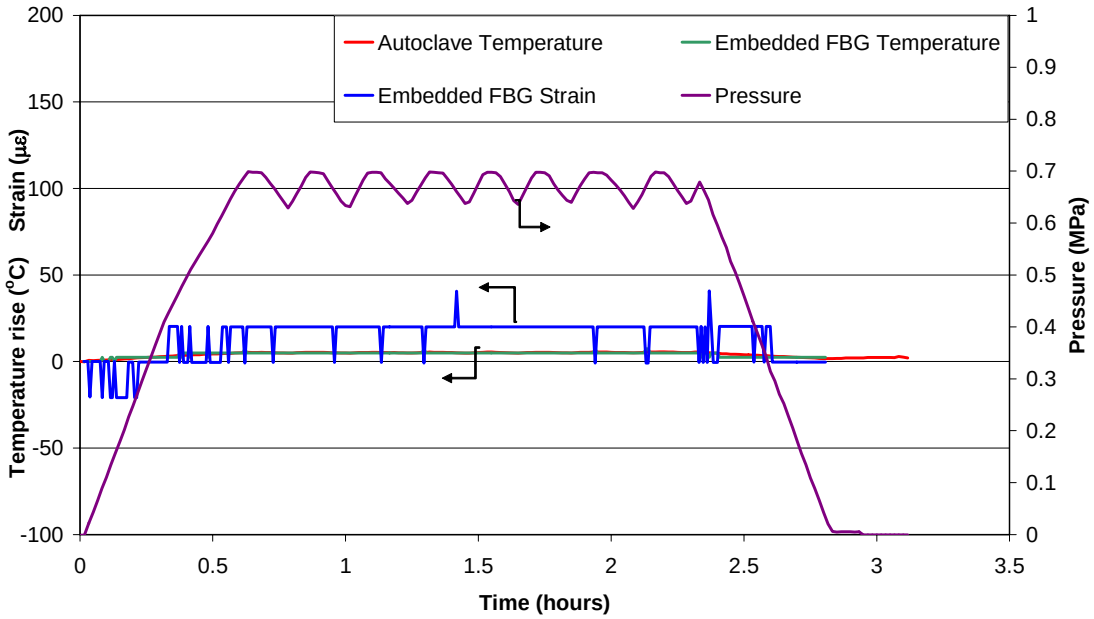

Figure 5-15: Relationship between embedded optical fibre sensors and pressure.

5.3.3. Effect of vacuum on sensors

a) Load cell

Figure 5-16 presents the relationship between the load measured from the load cell and the applied vacuum. From Figure 5-16 it can be observed that a linear relationship exists between the load and the vacuum.

In this vacuum test the sample was not clamped to the prestress rig. The load cell was positioned such that the load screw was just in contact with the sensor face of the load cell. Initially no load was applied to the load cell. When vacuum was applied, a uniformly distributed compressive load was induced to the vacuum bagged flat-bed rig. The load cell through the contact of the load screw recorded the compressive load applied by the vacuum.

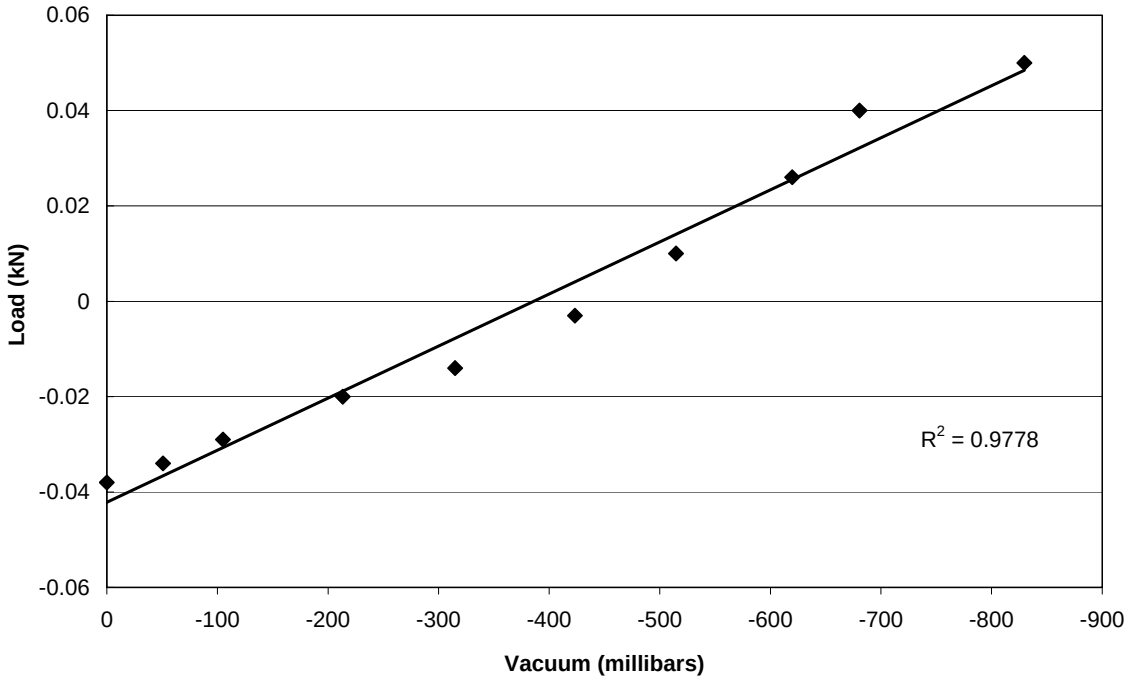

Figure 5-16: Relationship between load measured from the load cell and vacuum.

b) Optical fibre sensors

Figure 5-17 presents the observed relationship between the optical fibre sensors and the vacuum. From Figure 5-17 it can be observed that the optical fibre sensor experienced a compressive strain of about 80 $\mu\varepsilon$ for an applied vacuum of 826 millibars (-0.084 MPa).

When the vacuum is removed not all the compressive strain induced in the optical fibre sensor during the application of the vacuum is recovered. This is because prior to the solidification of the resin, it is very difficult to control the relative orientation of the FBG sensor. This could be the reason why the FBG sensor did not return to its initial value (at the start of the vacuum test). No repetitions were carried out on this test. Only FBG sensors were used. Therefore further investigations are required to confirm the reproducibility of the results.

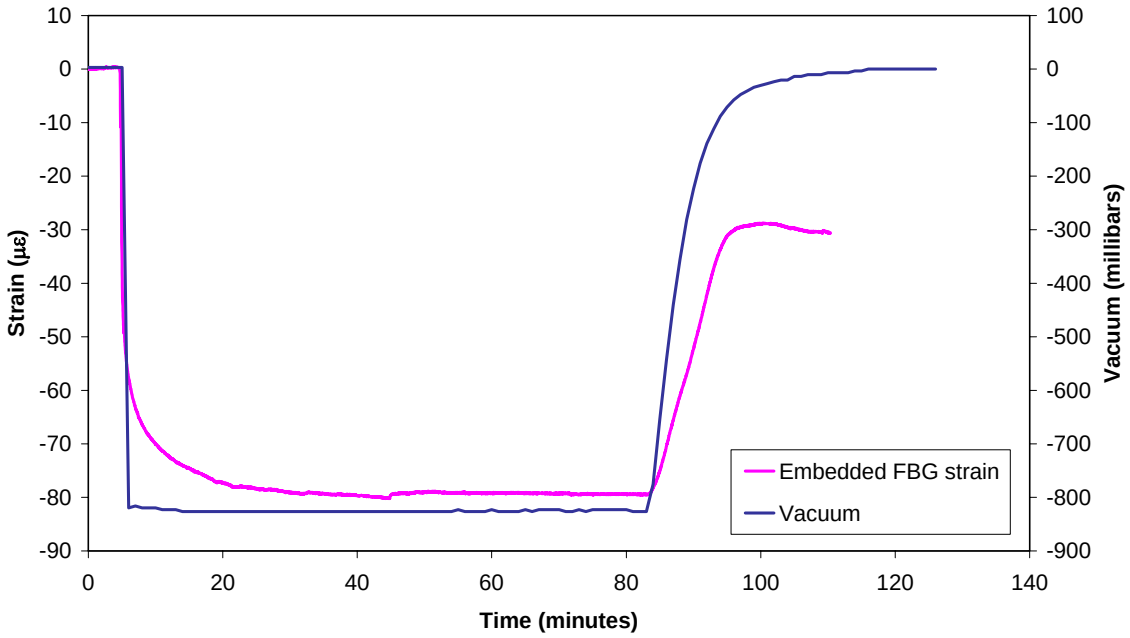

Figure 5-17: Relationship between embedded sensors and vacuum.

5.3.4. Effect of cure cycle on sensors

a) Load cell

The effect of cure cycle on the load cell was studied according to the procedure described in Section 4.5.3, Chapter 4. From the cure cycle test it was found that a change in load of about 0.4 kN was observed. This shows that the cure cycle does not have a significant influence on the load recorded from the load cell.

b) Optical fibre sensors

Figure 5-18 shows the relationship between the cure cycle parameters on the reference EFPI and FBG sensors. From Figure 5-18 it can be observed that a variation in strain of about ± 25 με and ± 50 με was recorded in EFPI and FBG sensors respectively. This variation was also observed in the temperature and pressure tests. This could be due to the effect of the polyimide bonding tape on the sensors during the cure cycle. In the embedded sensor the thermal expansion of the composite was measured to be 7.30 $\times 10^{-6}$ K^{-1}. This measured thermal expansion is 1 $\times 10^{-6}$ K^{-1} greater than the thermal expansion measured from embedded sensors during temperature test. This increase in thermal expansion could be the effect of pressure and vacuum combined with temperature.

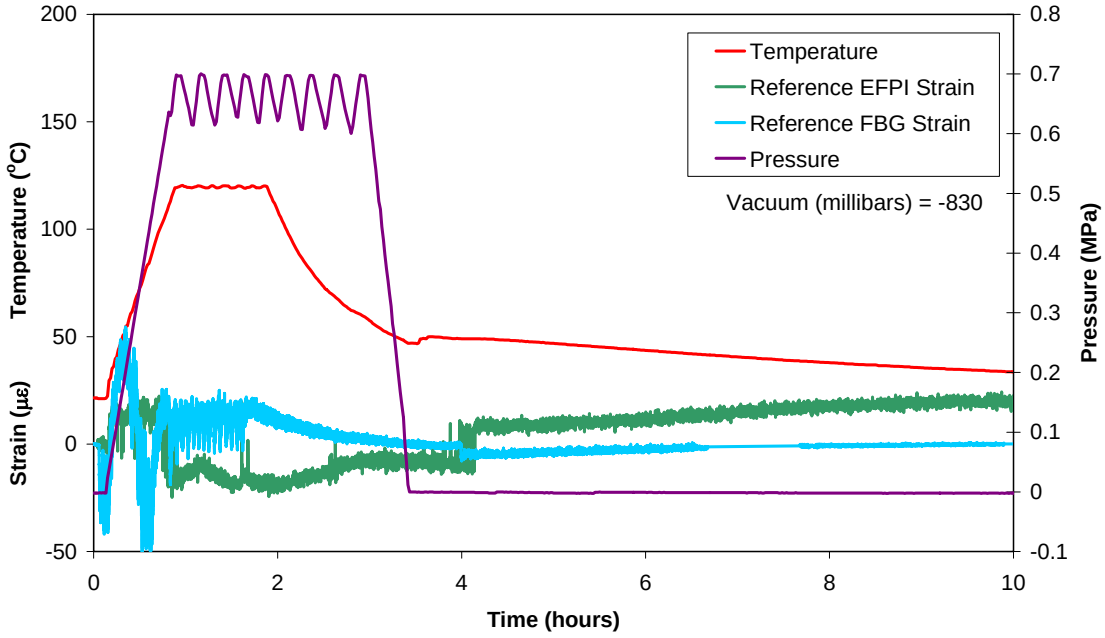

Figure 5-18: Relationship between reference EFPI sensor and the cure cycle parameters.

5.4 Concluding remarks

The evaluation of the prestress methodology was carried out in three stages. Firstly, the load cell calibration (at different temperatures) and strain distribution in a steel plate during an application of tensile load was investigated. Secondly, the end-tab jig design to circumvent fibre misalignment near the end-tab jig and resin pre-cure away from the end-tab region was presented. Finally, the effect of the autoclave process parameters on sensors

used in this work (load cell and optical fibre sensors) was studied. From the above study the following conclusions can be made.

Load cell calibration

From the static compression calibration test it was shown that the load recorded from the load cell is in good agreement with the applied machine load. A linear relationship was observed from the load cell during the static tests conducted at different temperatures (27°C, 70°C, 99°C and 121°C). A small change in load of about -0.8 kN for a 94°C temperature difference was found.

Prestress rig evaluation:

From the static tensile prestress rig evaluation test, it can be concluded that the strain distribution in the steel plate is uniform with a variation of 4% strain through the width of the panel. This variation in the strain could be due to (i) the Poisson's effect, (ii) any misalignment in the ERSGs during bonding and (iii) measurement errors. A linear relationship was found between the strain measured from the steel plate and the applied load using the load screw in a prestress rig. This is because the load applied is within the elastic region of the steel plate. Furthermore, this shows that this prestress rig system responds linearly.

Prepreg end-tab jig design and evaluation:

Evidence of fibre misalignment near the end-tab region was found to be the cause of composite bending. It was shown that as a result of fibre misalignment near the end-tab region, the compressive load was induced eccentrically to the composite during prestress release. This results in composite bending.

A flat-bed end-tab jig was designed to circumvent the fibre misalignment near the end-tab region. Using this end-tab jig it was shown that fibre misalignment near the end-tab region was eliminated.

Results from the surface profile of the composite shows that the surface profile of the prestressed composite manufactured with the aid of an end-tab jig is in agreement with the surface profile of the non-prestressed composite.

Sensor evaluation:

From the preliminary investigation of the effect of cure cycle parameters on the optical fibre sensors, the following conclusions can be made.

Effect of temperature:

No significant change in the measured strain from the reference optical fibre sensors during the temperature test. Therefore it can be concluded that the response of the optical fibre strain sensors are not influenced by temperature.

Embedded optical fibre sensors measured the thermal expansion of the composite. The measured thermal expansions from optical fibre sensors are in good agreement with the theoretically-predicted thermal expansion from the micro-mechanical model.

The temperature measured from the embedded FBG temperature sensor is in good agreement with the temperature measured from the thermocouple in the autoclave.

Effect of pressure:

During the pressure test a small change of about 0.04 kN was measured from the load cell. This shows that there is no significant effect of pressure on the load cell.

It was found that there is no significant change in the measured strain from the reference and embedded optical fibre sensors during the pressure test. This shows that the responses of the optical fibre sensors are not influenced by the pressure.

Effect of vacuum:

The load cell showed a linear relationship with the application of a vacuum. An increase of about 0.09 kN load in compression was measured for an increase in vacuum to -830 milibars (-0.084 MPa). This is because the uniform distribution of compressive load applied by application of vacuum to the prestress rig was measured through the contact of the load screw to the load cell.

An embedded optical fibre sensor in the prepreg recorded a compressive strain of about 80 με for -830 milibars (-0.084 MPa) vacuum. However, when the vacuum was released not all the compressive strain in the optical fibre was removed. This is because prior to the solidification of the resin it is difficult to control the relative orientation of the FBG sensor.

Effect of cure cycle:

The load cell showed an increase of 0.4 kN during the cure cycle. This variation in load is due to the combined effect of temperature, pressure and vacuum.

No significant variation was observed in the strain measured from the reference optical fibre sensor throughout the cure cycle. A small variation of about ± 25 με from EFPI and ± 50 μεfrom FBG was recorded. This could be due to the effect of the bonding tape and optical fibre sensor during the cure cycle.

CHAPTER 6

Residual strain and fibre alignment in the composites

OVERVIEW

This chapter presents the residual strain and fibre alignment results on the effect of prestress.

- The first part of the chapter presents the residual strain development in non-prestressed and prestressed composites. The development of residual strain during autoclave processing of a non-prestressed composite (unidirectional and cross-ply) is discussed in four stages.
- This is followed by the discussion of the residual strain results on the effect of four different prestress levels in unidirectional composites. The results from the strain released to the composite recorded from optical fibre sensors and ERSG are discussed and compared.
- The second part of this chapter investigates the effect of fibre prestress on the alignment of fibres in the composite. The measured fibre alignment and micrographs are presented for all the prestressed composites and discussed.
- Finally, the conclusions were drawn from the residual strain and fibre alignment results.

6.1 Residual strain development in non-prestressed composite

6.1.1. Unidirectional composite

Figure 6-1 presents the residual strain development measured using embedded EFPI sensor in $[0^o]_{16}$ laminate during the autoclave curing process. Table 6-1 summarises the residual strain measured using the embedded EFPI sensors in unidirectional non-prestressed composites at different stages of the cure cycle. The residual strain measurement using EFPI sensors during the autoclave curing process could be considered in four stages: a) before curing, b) heating cycle, c) isothermal and d) cooling cycle.

Prior to embedding the EFPI sensors into the prepreg, the strain recorded was zero (start of the cure cycle in Figure 6-1). After embedding the EFPI sensor in the prepreg laminate, a compressive residual strain was measured as shown in the Figure 6-1 and Table 2-1. During embedding sensors, rollers were used to expel the air between the laminates. The back and forth movement of the roller during the prepreg laying processes could have caused the compressive strains in the EFPI sensor. From Table 6-1 it can also be noticed that the compressive strain recorded from the EFPI sensor after embedding changes at different times in the same prepreg. This is because of the manual lay-up and rolling process. During the heating cycle, the viscosity of the resin initially decreases. The compressive strain in the sensor decreases and above 100ºC the sensor is subjected to a tensile strain. This suggests that the reduction in the resin viscosity could have released the compressive strain induced in the sensor during the embedding process. During the heating cycle, the resin and fibre also expands. The tensile strain recorded from the sensors could be due to the friction between the sensor and the constituent materials in the laminate.

Table 6-1: Presents the EFPI strain measured at different stages of the cure cycle in non-prestressed composites.

Reference panels	Before embedding (με)	After embedding (με)	at 120ºC (με)	Final residual strain at RT (με)
UR1	0	-71	40	-587
UR8	0	-63	42	-640
UR9	0	-101	24	-586

In the isothermal stage, the exothermic reaction of the resin begins, and this increases the resin viscosity. The exothermic reaction increases the temperature of the composite from 120ºC (cure temperature) to 127ºC. Figure 6-2 shows the result from differential scanning calorimetry for the 913 epoxy resin system. From Figure 6-2 it can be seen that when the resin temperature reaches 120°C an exothermic peak is observed. In this stage, the resin

reacts to form a polymeric three dimensional cross-linked network structure. These cross-linking reactions induce shrinkage of the resin, which induces a compressive residual strain as shown in Figure 6-1. This was also observed by many researchers[12,13,36]. This is called cure-induced shrinkage.

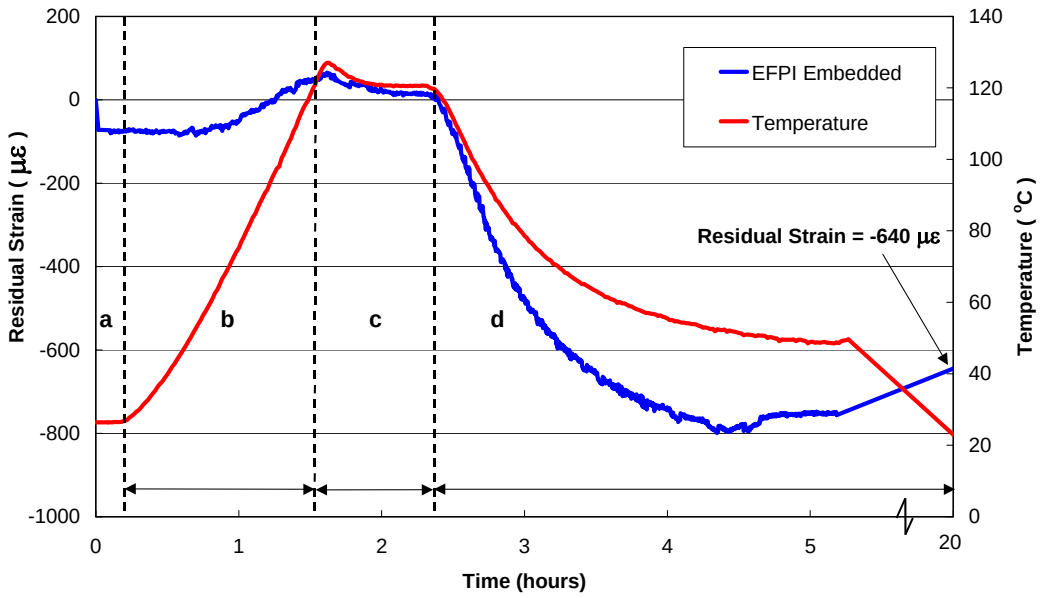

Figure 6-1: Residual strain measured using embedded EFPI sensor in non-prestressed $[0]_{16}$ laminate during the autoclave curing process. a) before curing, b) heating cycle, c) isothermal and d) cooling cycle.

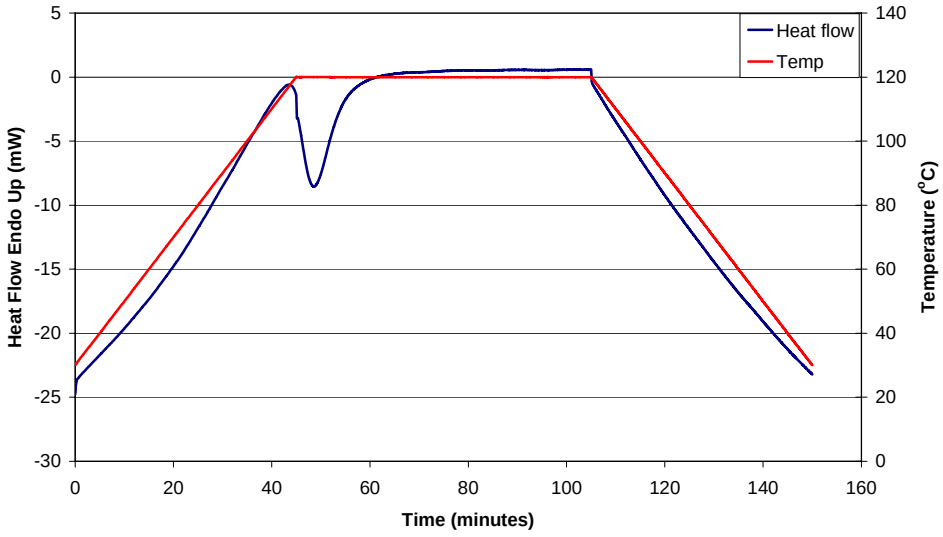

Figure 6-2: Differential Scanning Calorimetry (DSC) results for the 913 epoxy resin.

Once the temperature in the composite is reduced from the exotherm to the cure temperature, the residual strain stabilises (see Figure 6-1). At the end of the isothermal stage, the cooling cycle of the process commences. From Figure 6-1 it can be observed that the compressive residual strain measured by the EFPI sensors increases. Because of the mismatch in thermal expansion between the fibre and matrix, as the matrix shrinks, the fibres in the matrix are compressed as illustrated in Figure 6-3. The arrow marks show the direction of the residual stress. Because of the presence of rigid fibres, the matrix is restrained from shrinking, which induces tensile strains in the matrix. This is called thermally-induced residual strain. It can be seen that the thermally-induced residual strain is significantly higher than the cure-induced residual strain. Previous researchers[36,37] have also reported this phenomena.

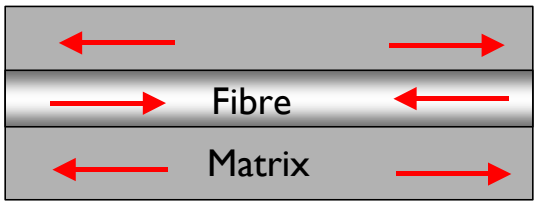

Figure 6-3: Illustration of residual stress development in a unidirectional composite.

When the temperature cooled down to 55°C, a slight decrease in the measured compressive strain was observed, this coincides with the decrease in pressure (see Figure 6-4). Once the pressure reaches zero the residual strain stabilises. The final average residual strain measured from three $[0]_{16}$ non-prestressed composite was –604 με at room temperature (RT).

The results from EFPI sensors show that the reinforcing fibres in the composite are subjected to a compressive strain during the curing process. In Chapter 7 the experimental results from optical fibre sensors are compared with theoretical models from the literature (for predicting residual strain in composites).

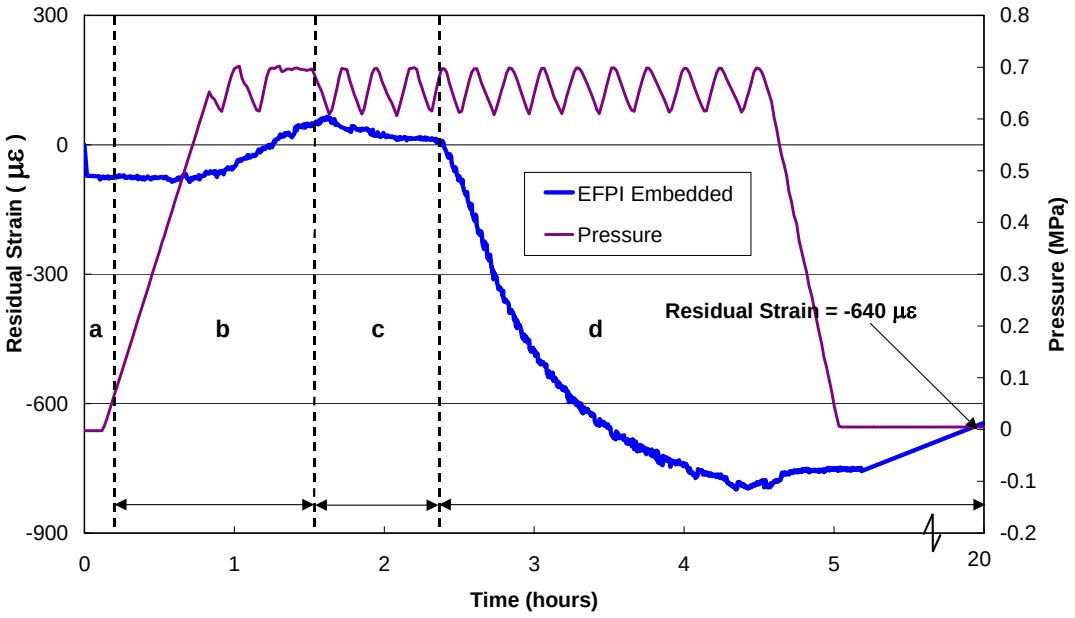

Figure 6-4: Residual strain and autoclave pressure recorded during the cure cycle.

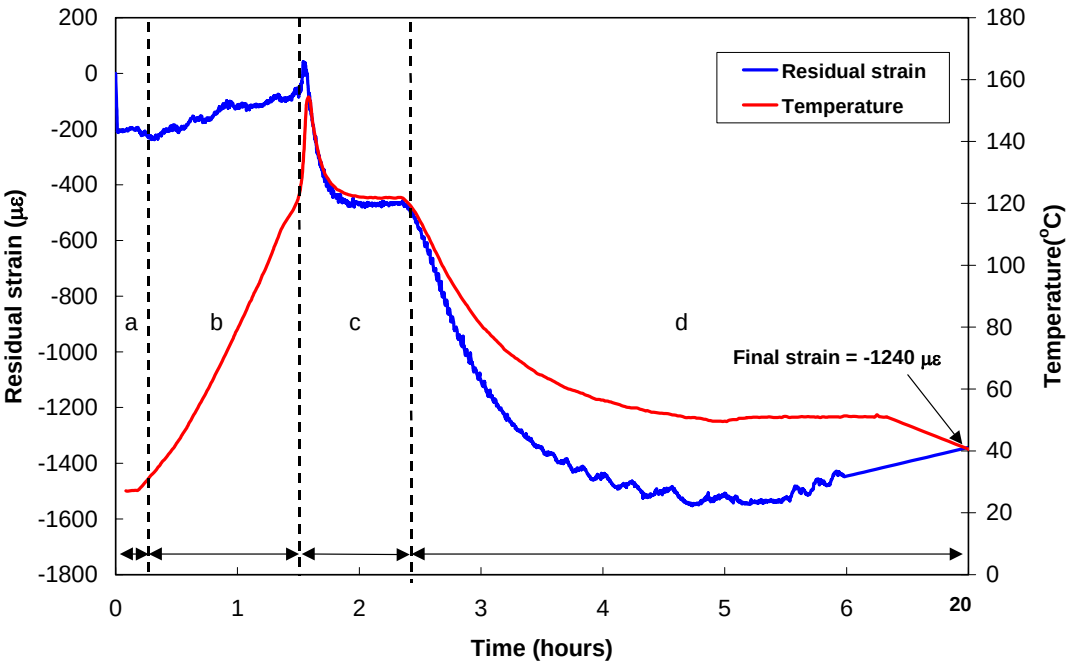

Figure 6-5: Residual strain development in cross-ply composite. a) before curing, b) heating cycle, c) isothermal and d) cooling cycle.

6.1.2. Cross-ply composite

The residual strain development was studied in a cross-ply laminate to compare the magnitude with the unidirectional laminates. Figure 6-5 presents the residual strain from the EFPI sensors for a $[0/90/0/90/90/0/90/0]_{4S}$ glass/epoxy with the corresponding processing temperature. This is a thick laminate of 64-ply thickness (8 mm). The shape of the residual strain development curve for the cross-ply composite is very similar to the unidirectional composite presented in Figure 6-1. However, the magnitude of the exotherm temperature (stage c) and the residual strain development recorded in the cross-ply composite is twice the unidirectional composite. This is expected because it is a cross-ply laminate and a thick composite system. Many researchers also observed this difference in residual strain between unidirectional and cross-ply composites. Because the 90º ply have a much greater stiffness than the resin matrix, the 0º ply contraction during cooling cycle will be restrained by the 90º ply and vise versa.

It can be observed that when the temperature reached 120°C (which is the cure temperature of the resin) there was a sudden increase in the mould temperature to 154°C, due to the exothermic reaction of the resin. This increase of 34°C in composite temperature is possible because of the 64-ply thick composite. This cross-linking reaction of the epoxy resin induces compressive strain to the composite, which is due to the cure-induced shrinkage. With reference to Figure 6-5, it can be seen that a compressive strain of about 400 με was recorded. Jinno *et al.* and Kang *et al.* have shown that this compressive strain is due to cure-induced shrinkage of the epoxy resin and they have shown that this could be related to the degree of cure of the resin. However, looking at Figure 6-5 again, it can be seen that this is not only due to cure-induced shrinkage but also due to thermally-induced shrinkage. Because the temperature after reaching the exotherm peak cools down to the cure temperature (the temperature difference is 34°C), which induces a thermal shrinkage of the fibre and matrix (which may also be bonded to each other due to the start of the curing reaction). Therefore, it will be difficult to separate the cure-induced and thermally-induced residual strain in the composite.

During the cooling cycle (stage d), a compressive strain was recorded from the EFPI sensors. This compressive strain is due to 1) mismatch in the thermal expansion between fibre and matrix at a micro-scale and 2) mismatch in the thermal expansion between the adjacent plies of different orientations (0° and 90°) in the ply-scale. The final residual strain measured in the cross-ply non-prestressed composite was –1240 με at room temperature.

The residual strain was also measured in a $[0/90/0/90/90/0/90/0]_S$ laminate. The residual strain development was similar to the $[0/90/0/90/90/0/90/0]_{4S}$ laminate shown in Figure 6-5. The final measured residual strain for the $[0/90/0/90/90/0/90/0]_S$ laminate was –1277 με at room temperature.

6.2 Residual strain development in prestressed composite

This study concentrates on unidirectional prestressed composites. The fibre prestressing of cross-ply laminates was not studied in this work. In the unidirectional $[0^o]_{16}$ prestressed composite, residual strains were measured using optical fibre (EFPI and FBG) sensors. After composite curing and cool down to room temperature, ERSGs were bonded onto the surface of the composite, in the same place as optical fibre sensors (as shown in Figure 4-5). The magnitude of the strain released to the composite when it was removed from the prestress rig was recorded and quantified by using optical fibre sensors and surface-mounted ERSG sensors. In this study composites were manufactured with four different prestress levels. The residual strain and strain release measurements were carried out at all the prestress levels and are presented in Table 6-2 and Table 6-3 respectively. The FBG sensor was used (only in two panels with 108 MPa prestress) to compare the results with EFPI sensors. Figure 6-6 shows the recorded pre-load from the load cell, residual strain from EFPI sensors and strain release from ERSG sensors during the processing of unidirectional composite prestressed to 150 MPa.

Table 6-2: Residual strain measured from four different prestress levels of the unidirectional composites at room temperature prior to prestress release.

Panel Code	Residual strain		
	EFPI Middle	FBG Middle	EFPI 40 mm from the edge
UPT8	-566		
UPT11	-581		
UP1_7kN	-586		
UP2_7kN	-574		
UP2_14kN	-564		-643
UP3_14kN	-503		-653
UP4_14kN	-573		
UP5_14kN	-553		
UP6_14kN	-520		
UP7_14kN	-605		
UP9_14kN	-529	-742	
UP12_14kN		-714	
UP1_24 kN	-592		

Table 6-3: Strain release recorded from EFPI, FBG and ERSG sensors during prestress release at room temperature. * Rig thermal expansion induced prestress calculated from the classical mechanics.

Panel code	Prestress released (MPa)	Strain released (με)				
		EFPI middle	FBG middle	EFPI 40 mm from the edge	ERSG middle	ERSG 40 mm from the edge
UPT8	51.21*	-			-109	-160
UPT11	51.21*	-108			-194	-221
UP1_7kN	79.95	-184				
UP2_7kN	80.36	-190			-223	
UP2_14kN	108.50			-630	-656	-696
UP3_14kN	107.22	-637		-685	-602	-763
UP4_14kN	108.62	-579			-628	
UP5_14kN	108.41	-537			-548	
UP6_14kN	112.89	-552			-613	
UP7_14kN	108.45	-600			-639	
UP9_14kN	113.57	-551	-684		-677	
UP12_14kN	107.61	-	-608		-600	
UP1_24 kN	150.07	-944			-958	-1113

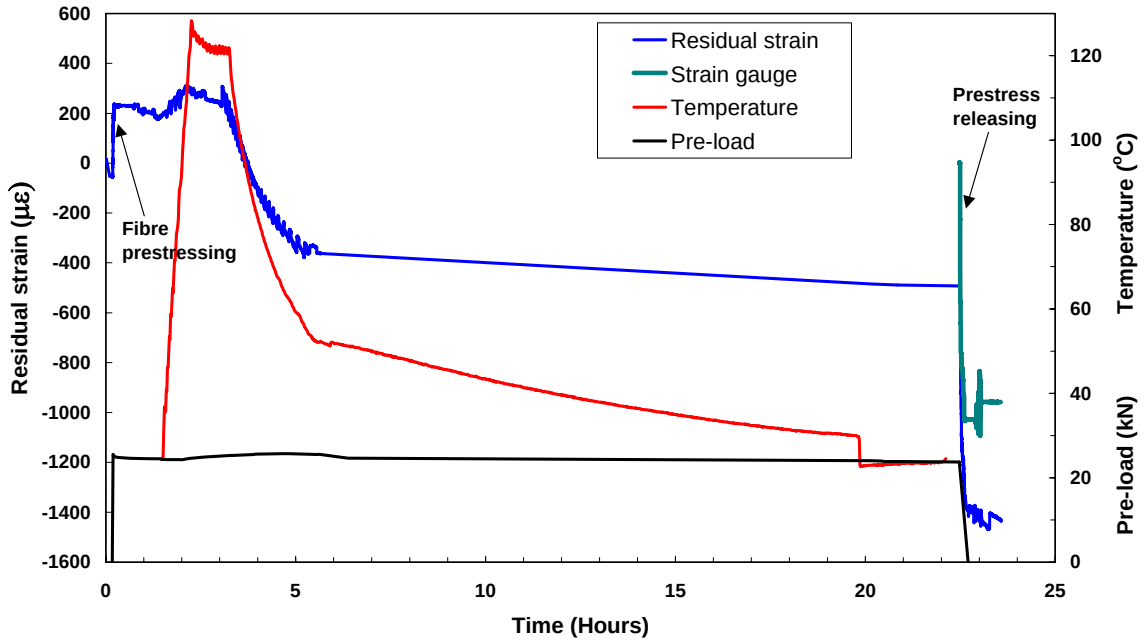

Figure 6-6: Residual strain development throughout the processing of 150 MPa prestressed composite.

From Figure 6-6 it can be seen that the recorded strain from EFPI sensors during the application of pre-load is small because the EFPI sensors are not bonded to the prepreg. It can be observed from Figure 6-6 that the applied pre-load was maintained throughout the curing process to within 1 kN. During the heating cycle, the load cell did not record the prestress induced in the fibres due to thermal expansion of the rig. This is because in the current set-up there is no frame of reference for the load cell to record the thermally-induced prestress to the fibres. When there is a temperature rise the whole prestress rig set-up expands, this will induce prestress to the glass fibres. However, the load applied to the glass fibres due to thermal expansion of the rig will not be recorded by the load cell.

The residual strain development curve and its magnitude in unidirectional prestressed composites (see Figure 6-6 and Table 6-2) are very similar to the non-prestressed composites as shown in Figure 6-1 and Table 6-1. After curing and cool-down to room temperature the prestress is released. On the release of the prestress, a compressive strain is induced into the composite. Figure 6-7 shows the strain release recorded from the EFPI, FBG and ERSG sensors when a prestress of 108 MPa was released (Panel code UP9_14kN). The pre-load was released in steps.

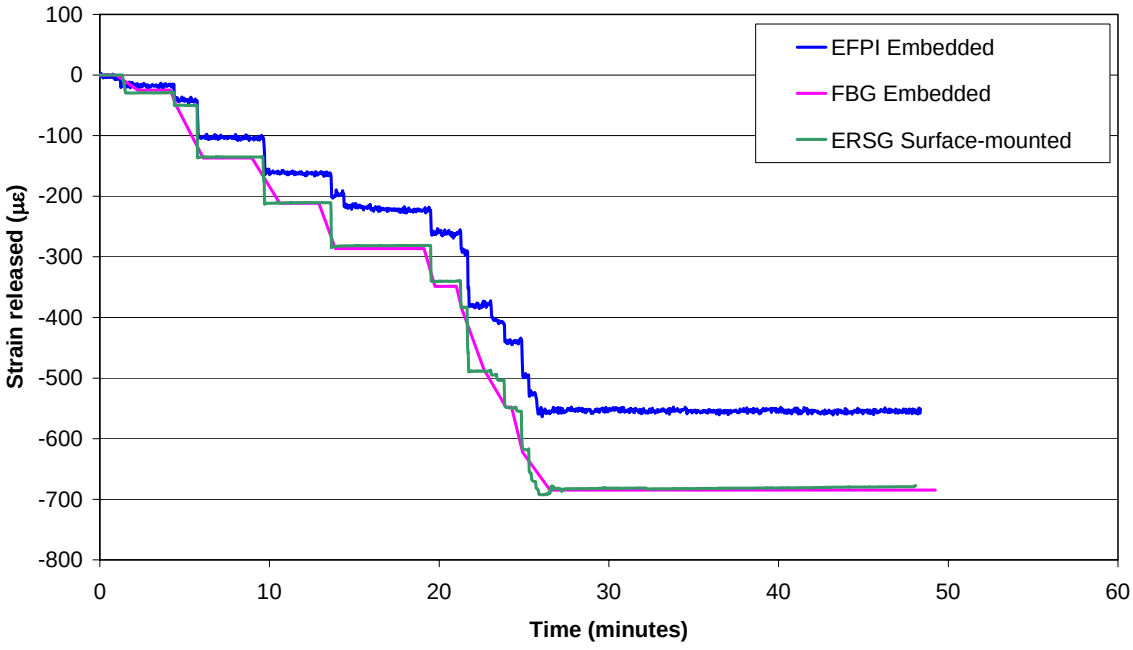

Figure 6-7: The strain release measured from optical fibre sensors and ERSG. This was recorded during 108 MPa prestress release.

From the Figure 6-7 it can be seen that initially the strain measured from EFPI, FBG and ERSG are in agreement with each other. However, as the magnitude of the pre-load release increases the EFPI sensor records slightly less compressive strain when compared to FBG and ERSG sensors. On the other hand the FBG and ERSG sensors are in very good

agreement. Also from Table 6-2 it could be observed that the compressive residual strains recorded during the autoclave curing cycle from FBG sensors are slightly higher than the EFPI results. This difference in the strain recorded from EFPI and FBG sensors could be due to one or more of the following reasons.

a) The difference in configuration of the optical fibre sensors (as shown in Figure 6-8) could have an effect on the measured residual strain.

b) Difficult in accurately measuring the gauge length of EFPI sensors. The change in measurement of the gauge length in an EFPI sensor will lead to a change in the strain measured. In order for the effective gauge length to be equal to *L* as shown in Figure 6-8, there would be need to satisfy the following. a) perfect bond at fusion points, b) void-free fusion points (the presence of voids could transport foregin material into the cavity) and c) friction-free surfaces between fibre and capillary. If all the above conditions are not satisfied, the effective gauge length will change, and this will lead to a change in the strain measured by the EFPI sensor.

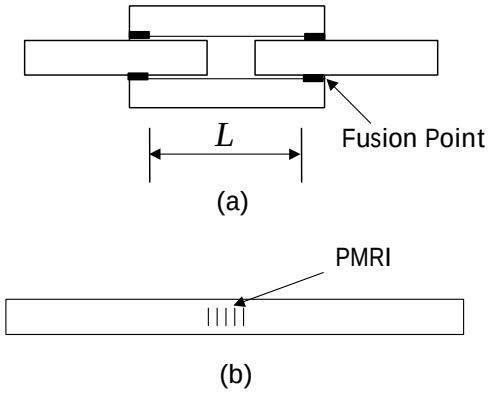

Figure 6-8: Sensor configuration, a) EFPI strain sensor and b) FBG strain sensor. PMRI – periodic modulation of the refractive index of the optical fibre core.

Also from Figure 6-7 it could be observed that the data recorded from the FBG sensor did not follow the stepwise pre-load release similar to EFPI and ERSG sensors. This is because the rate of data acquisition in FBG sensors was very low (2 measurements per minute) when compared to the EFPI and ERSG sensor data acquisition rate (1 measurement per second). Table 6-4 presents the average strain release measured from EFPI, FBG and ERSG sensors in 108 MPa prestressed composite. From Table 6-4 it can be observed that the average strain release measured from FBG is slightly higher than from the EFPI sensor. However, by considering the standard deviation and the number of samples it can be seen that the strain recorded from the optical fibre (EFPI and FBG) and ERSG sensors are all in good agreement.

Table 6-4: The average strain release recorded using EFPI, FBG and ERSG sensors in a 108 MPa prestressed composite.

Sensors	Number of samples	Average strain release (με)	Standard deviation (με)
EFPI	6	-592.8	56
FBG	2	-646.0	54
ERSG	7	-616.2	35

After releasing the prestress, the residual strain of the composite changes. Therefore, the final residual strain ε_{final} in the fibre is expressed as:

$$\varepsilon_{final} = \varepsilon_r - \varepsilon_p \tag{6.1}$$

where, ε_r is the residual strain measured before releasing (that is cure-induced and thermally-induced residual stresses) and ε_p is the strain measured during pre-load release.

Figure 6-9 shows the final residual compressive strain in the fibres calculated for all the prestressed composites. From this figure it can be seen that the compressive strain in the fibre reduces as the applied prestress increases. It can also be observed that with the application of a fibre prestress of about 108 MPa, fibres with approximately zero final residual strain can be achieved. Above 108 MPa prestress, the final residual strain becomes tensile. This demonstrates that fibre prestressing enables the control of final residual strain in the composite.

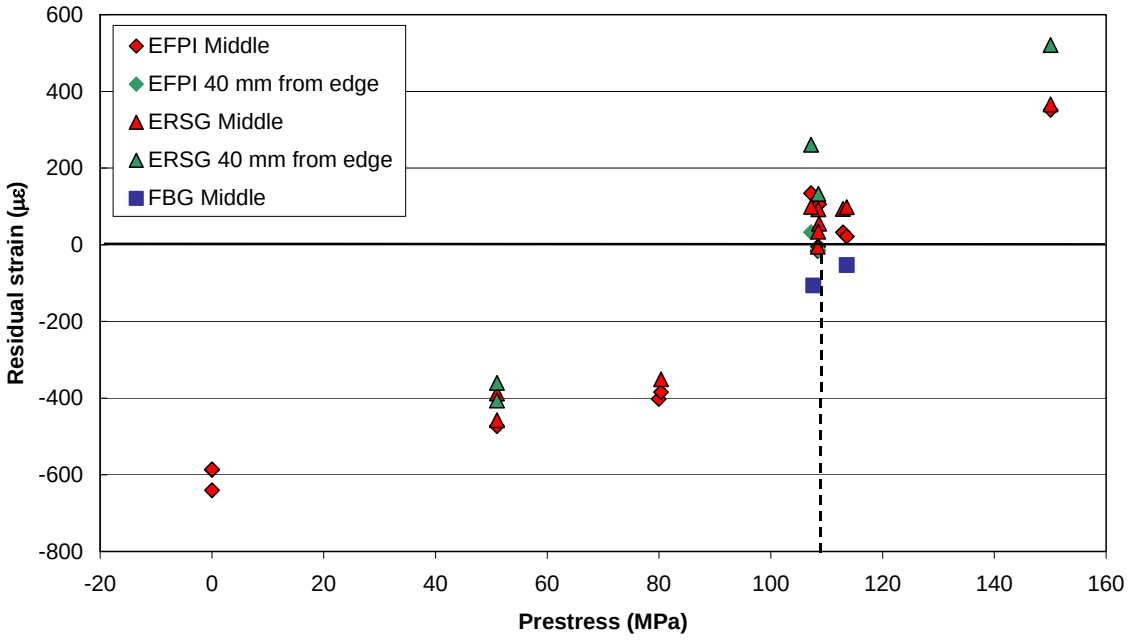

Figure 6-9: The final residual strain in the composite for different prestress levels.

From Figure 6-9 and Table 6-3 it can be observed that the strain gradient across the panel (middle and 40 mm from edge) increases with an increase in prestress. This variation in strain reaches a maximum of 14% at 150 MPa prestress. We conjecture that this difference in the measured strain release is due to an edge effect caused by the variation in Poisson's contraction at an unconstrained edge. When the pre-load is released, a compressive force is induced in the matrix. This results in a transverse expansion of the composite. At the edges uniaxial compressive stresses exist. However, in the centre, some transverse stress will exist due to the transverse stiffness of the composite. These transverse compressive stresses produce tensile longitudinal strains, which reduce the measured value of the strain released in the centre. This is mathematically modelled and presented in Chapter 7.

6.3 Results of fibre alignment

It was shown in Chapter 2 that fibre waviness or misalignments in composites are caused by many factors during the processing of composites. In manufacturing prestressed composites, prior to composite curing, the reinforcing fibres are mechanically prestressed. This firstly straightens the wavy fibres present in the prepreg and secondly avoids movement of fibres during the composite curing process. As a result, the reinforcing fibres would be more aligned to the direction of the applied load.

The fibre alignment in all the prestressed composites were measured according to the procedure described in Section 4.8.1 (iii), Chapter 4. Figure 6-10 shows the fibre orientation angle measured in all the composites. From Figure 6-10 it can be observed that in non-prestressed composite the fibres are aligned between 0° to 6°. Yurgartis[117] also reported a similar degree of fibre misalignment in prepreg systems. A representative micrograph of a non-prestressed composite, taken from the transverse direction is shown in Figure 6-11.

From Figure 6-10 it can also be observed that with an increase in prestress the percentage of fibres accurately aligned increases. Figure 6-12 to Figure 6-15 show representative micrographs taken from the transverse direction of prestressed composites. From Figure 6-10 and Figure 6-12 to Figure 6-15 it can be clearly seen that fibre prestressing improved the fibre alignment in composites. It can also be observed that the 0° fibre alignment reaches a maximum of about 75% in a composite with a prestress of 108 MPa, above which no further improvement was observed. This is because of the original fibre alignment in the prepreg. A certain percentage of fibres are so misaligned that no matter what prestress is applied they will not be oriented parallel to the loading direction. For this composite, the results show that 25% of fibres fall into this category.

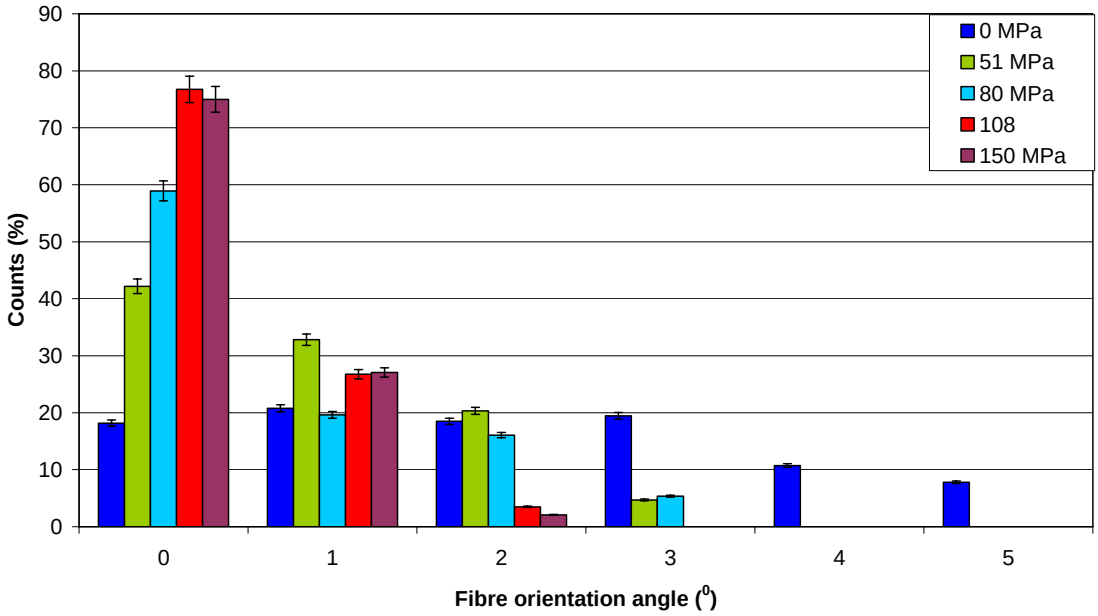

Figure 6-10: The measured fibre orientation in a composite as a function of applied prestress.

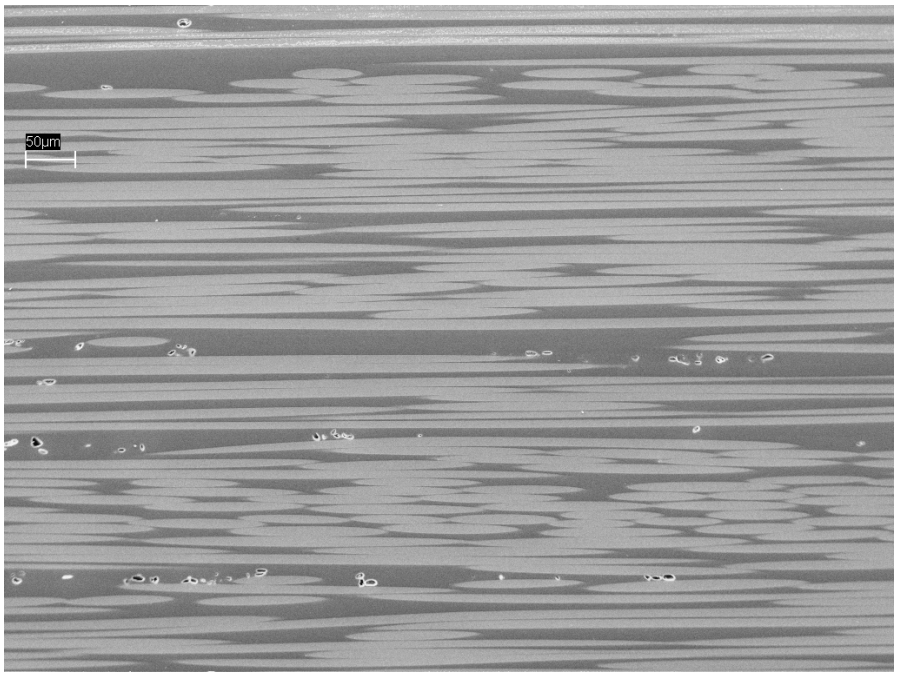

Figure 6-11: A representative micrograph of a transverse section of a non-prestressed (0 MPa) composite.

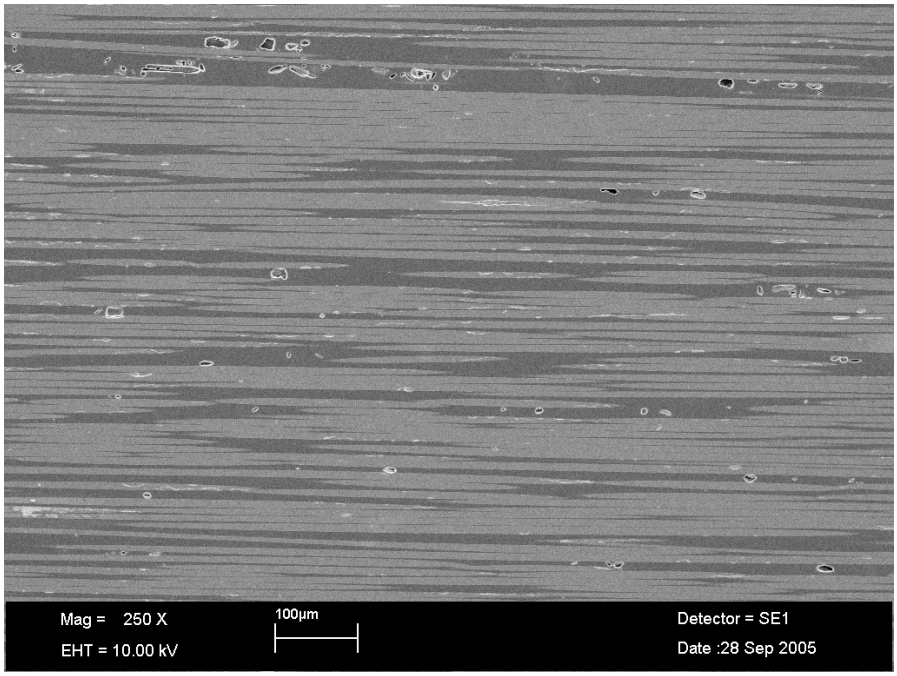

Figure 6-12: A representative micrograph of a transverse section of the 51 MPa prestressed composite.

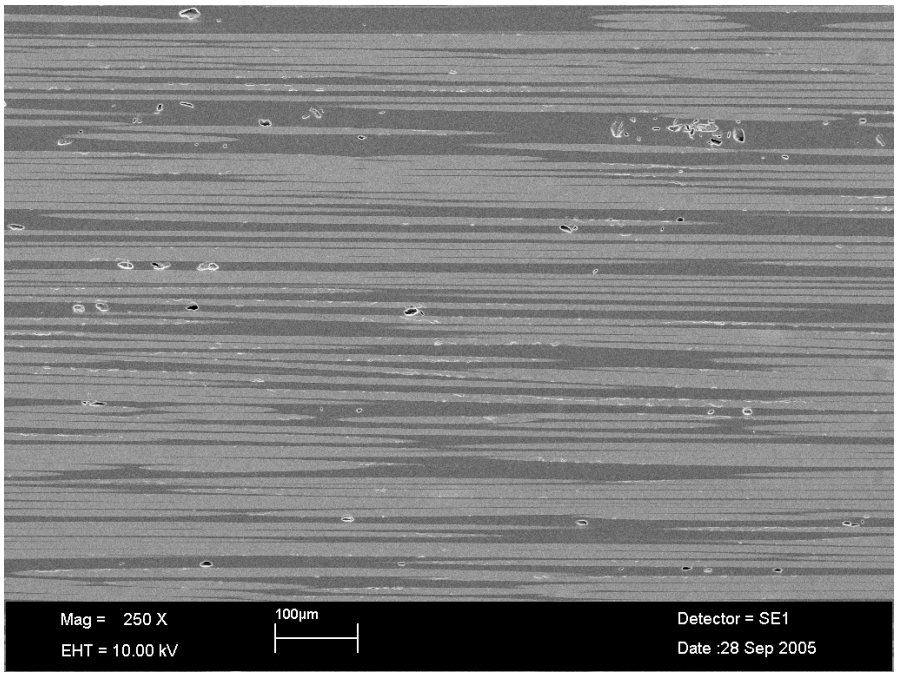

Figure 6-13: A representative micrograph of a transverse section of the 80 MPa prestressed composite.

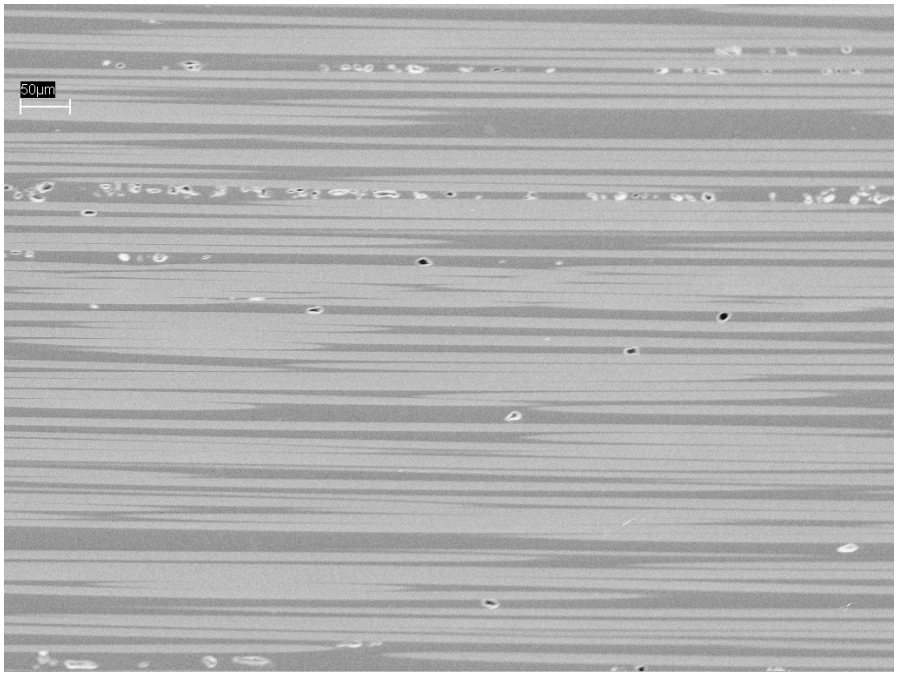

Figure 6-14: A representative micrograph of a transverse section of the 108 MPa prestressed composite.

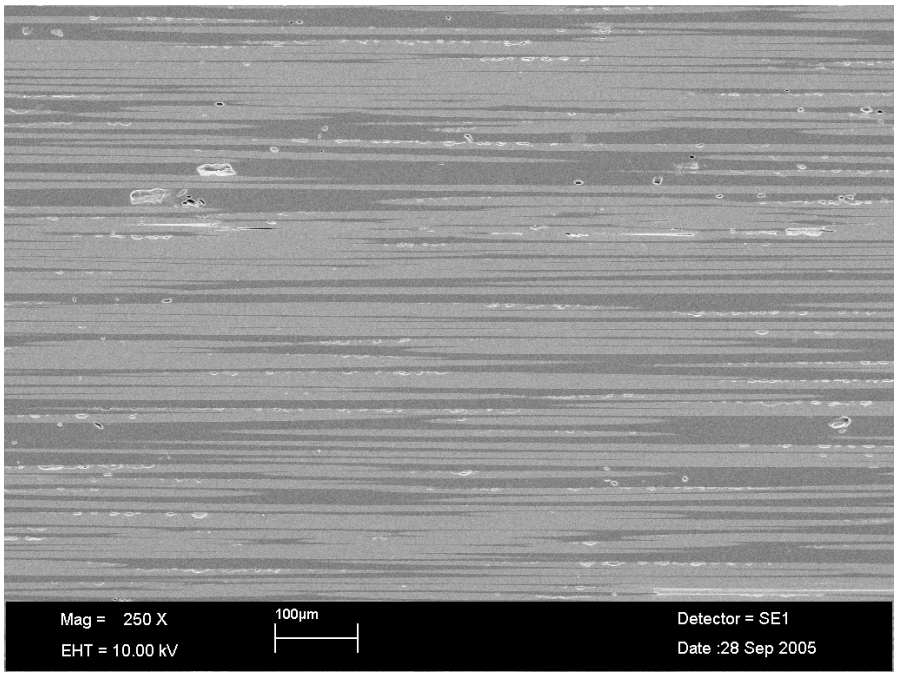

Figure 6-15: A representative micrograph of a transverse section of the 150 MPa prestressed composite.

6.4 Concluding remarks

The present study was aimed at an investigation of the effect of fibre prestress on residual strain and fibre alignment in glass/epoxy composites. From the results presented the following conclusions can be made.

Residual strain

Residual strain development in two different lay-ups (unidirectional and cross-ply) of glass fibre/epoxy composite panels was measured using optical fibre EFPI sensors. From the residual strain data, it was shown that two types of residual strains are developed (i) due to shrinkage of the resin during cure and (ii) due to the thermal mismatch between fibre and matrix. The residual strain development curve was similar for both the laminate types. However, the magnitude of the measured residual strain for a cross-ply composite panel was twice the residual strain of a unidirectional composite. This is because the 90º plies have a much greater stiffness than the resin matrix.

Results from the residual strain measurement using the EFPI sensors in non-prestressed and prestressed unidirectional $[0^{\circ}_{16}]$ composite panels show that fibre prestressing methodology can be used to reduce or control the residual strain development in composites. For example, by applying about 108 MPa prestress, a composite panel with approximately zero final residual strain can be prepared.

Experimentally, it was also shown that the measured strain release from EFPI, FBG and ERSG sensors were in good agreement with each other. The difference in strain measured through the width of the composite is conjectured that to be due to Poisson's ratio and edge effects and this is discussed in Chapter 7. It was also shown that the strain release measured from embedded EFPI and FBG sensors in the composite are in good agreement.

Fibre alignment

From the experimental results it was shown that fibre prestressing improved the alignment of fibres in composites. This improvement in fibre alignment resulted in an increase from 20% for non-prestressed to 75% of fibres oriented in the 0° direction for a 108 MPa prestress. Above this prestress level no further improvement in the fibre alignment was observed.

CHAPTER 7

Theoretical analysis of prestressed composites

OVERVIEW

- This chapter concentrates on (i) a theoretical analysis of the effect of fibre prestress on residual stresses in composites and (ii) compares the theoretical prediction with experimental results.
- The theory predicts the final residual stress in fibre and matrix after releasing the prestress. The theory is further extended to predict the strain distribution through the width of the composite panel.
- Experimental results from extrinsic Fabry-Pérot interferometric (EFPI) strain sensors, Fibre Bragg Grating (FBG) strain sensors and electrical resistance strain gauges (ERSG) are in good agreement with theoretical predictions.
- A small variation of 1% in the strain distribution across the width of the composite panel is predicted.

7.1 Introduction

PRESTRESSED COMPOSITES ARE PREPARED by applying a pre-load to the reinforcing fibres prior to cure. Since the uncured polymeric matrix possesses negligible stiffness, essentially all the pre-load applied would be carried by the fibres. The composite would then be cured, causing the polymeric matrix to gel and solidify. Following cure and cool down the fibre pre-load is released, and the resulting elastic contraction of

fibres relieves the tensile residual stress in the matrix resulting from the cure cycle by inducing compressive stresses.

The theoretical prediction is described in three stages namely,

1. Application of pre-load to the fibres
2. Process-induced residual stress development during elevated temperature processing of composites.
3. Fibre pre-load release

The following model assumes that perfect bonding exists between fibre and matrix.

The above three steps of fibre prestressed composite preparation can be mathematically described as follows

Step 1:

Pre-load is applied to the reinforcing fibres. This applied pre-load is maintained throughout the curing process. Prior to curing, the stress in the fibre and matrix are:

$$\sigma^{f} = \sigma^{f}{}_{prestress}$$

$$\text{where } \sigma^{f}{}_{prestress} = \frac{W}{A_f} \tag{7.1}$$

$$\sigma^{m} = 0 \tag{7.2}$$

where σ^{f} and σ^{m} are the stresses in the fibre and matrix, $\sigma^{f}{}_{prestress}$ is the applied prestress to the fibres and W and A_f are the pre-load applied to the fibre and cross-sectional area of the fibre.

Step 2:

During composite processing, residual stresses are developed. This is due to resin cure-induced volume changes and thermal expansion mismatch (between fibre and matrix) induced volume changes. The stresses in the fibre and matrix after curing can be written as:

$$\left(\sigma^{f}\right)_{ac} = \sigma^{f}{}_{prestress} + \sigma^{f}{}_{R} \tag{7.3}$$

$$\left(\sigma^{m}\right)_{ac} = \sigma^{m}{}_{R} \tag{7.4}$$

where $(\sigma^{f})_{ac}$ and $(\sigma^{m})_{ac}$ are the values of σ^{f} and σ^{m} after curing; and σ^{f}_{R} and σ^{m}_{R} are the residual stresses in the fibre and matrix. The residual strain development in the fibre and matrix was calculated using the one-dimensional Tsai and Hahn model and the three-dimensional concentric cylinder Wagner model.

The Tsai and Hahn model assumptions were:

- Both fibre and matrix are isotropic materials.
- The system is a unidirectional composite in a state of plane stress corresponding to thin laminates, under a thermal strain.
- No mechanical stress is applied.
- There is perfect bonding between fibre and matrix.
- The modulus and thermal expansion coefficients of fibre and matrix are independent of temperature.

Most of the Tsai and Hahn assumptions were considered in the Wagner model except that the Wagner model considers that the fibre and matrix are transversely isotropic. Transversely isotropic materials are a special class of orthotropic materials that have the same properties in one plane (e.g. the *x*-*y* plane) and different properties in the direction normal to this plane (e.g. the *z*-axis fibre direction). Both these models predict only the thermally-induced residual stresses and not the cure-induced residual stresses.

The residual strain predicted from these models for E-glass/epoxy composite is presented in section 7.4.1.

Step 3:

After composite curing and cool-down to room temperature the applied pretension in the fibres is removed. This induces compressive stresses to the matrix. During pretension release, not all the fibre prestress is released to the matrix. Some of the prestress remains in the fibre as tensile residual stress $(\sigma_f)^P$. Hence, the resulting stresses in the fibre and matrix can be written as:

$$\left(\sigma^f\right)_{apr} = \sigma^f{}_R + \left(\sigma_f\right)^P \tag{7.5}$$

$$\left(\sigma^m\right)_{apr} = \sigma^m{}_R + \Delta\sigma \tag{7.6}$$

$$\sigma^f{}_{prestress} = \left(\sigma_f\right)^P + \Delta\sigma \tag{7.7}$$

where $(\sigma^f)_{apr}$ and $(\sigma^m)_{apr}$ are the values of σ^f and σ^m after pretension release; and $\Delta\sigma$ is the stress released to the matrix.

The tensile residual stress in the fibre resulting from pretension release is calculated as follows. In the following analysis the process-induced residual stresses will be omitted initially for simplicity and added later (see equations 7.18 and 7.19).

The change in strain due to pretension release is expressed as $\Delta\varepsilon$. The strain released in the fibre (ε^f) and matrix (ε^m) will be equal.

$$\varepsilon^f = \frac{(\sigma_f)^P}{E_f} = \frac{W}{A_f E_f} - \Delta\varepsilon \tag{7.8}$$

where E_f is the modulus of fibre. Equation 7.8 can be rewritten as:

$$\frac{(\sigma_f)^P}{E_f} + \Delta\varepsilon = \frac{W}{A_f E_f} \tag{7.9}$$

$$\varepsilon^m = \frac{(\sigma_m)^P}{E_m} = \Delta\varepsilon \tag{7.10}$$

As there are no external forces applied to the composite, at equilibrium:

$$(\sigma_f)^P \phi_f + (\sigma_m)^P \phi_m = 0 \tag{7.11}$$

where ϕ_f and ϕ_m are the volume fraction of fibre and matrix present in the composite that is

$$(\sigma_m)^P = -(\sigma_f)^P \frac{\phi_f}{\phi_m} \tag{7.12}$$

Substituting equation 7.12 in 7.10 gives:

$$\Delta\varepsilon = \frac{(\sigma_m)^P}{E_m} = -\frac{(\sigma_f)^P}{E_m} \times \frac{\phi_f}{\phi_m} \tag{7.13}$$

Substituting equation 7.13 in 7.9 gives:

$$\frac{(\sigma_f)^P}{E_f} - \frac{(\sigma_f)^P}{E_m} \times \frac{\phi_f}{\phi_m} = \frac{W}{A_f E_f} \tag{7.14}$$

$$(\sigma_f)^P \left(\frac{1}{E_f} - \frac{\phi_f}{E_m \phi_m} \right) = \frac{W}{A_f E_f} \tag{7.15}$$

$$(\sigma_f)^P \left(\frac{E_m \phi_m - E_f \phi_f}{E_f E_m \phi_m} \right) = \frac{W}{A_f E_f} \tag{7.16}$$

$$\frac{(\sigma_f)^P}{E_f} = \frac{W}{A_f E_f} \times \left(\frac{E_m \phi_m}{E_m \phi_m - E_f \phi_f} \right) \tag{7.17}$$

From equation 7.17, the tensile residual strain in the fibre resulting from pretension release can be calculated. Now adding together the process-induced residual strain and the strain resulting from pretension release, the strain in the fibre and matrix after pretension release become:

$$\left(\varepsilon^{f}\right)_{apr} = \varepsilon^{f}{}_{R} + \frac{W}{A_f E_f} \times \left(\frac{E_m \phi_m}{E_m \phi_m - E_f \phi_f} \right) \tag{7.18}$$

$$\left(\varepsilon^{m}\right)_{apr} = \varepsilon^{m}{}_{R} + \Delta\varepsilon \tag{7.19}$$

where ε^{f}_{R} and ε^{m}_{R} are the process-induced residual strain in the fibre and matrix respectively.

7.2 Composite strain

The pretension is released in the longitudinal direction (direction 1 in Figure 7-1) of the composite, so the resulting strain of the composite (ε^{c}_{1}) in the longitudinal direction is given by:

$$\varepsilon^{C}{}_{1} = \Delta\varepsilon \tag{7.20}$$

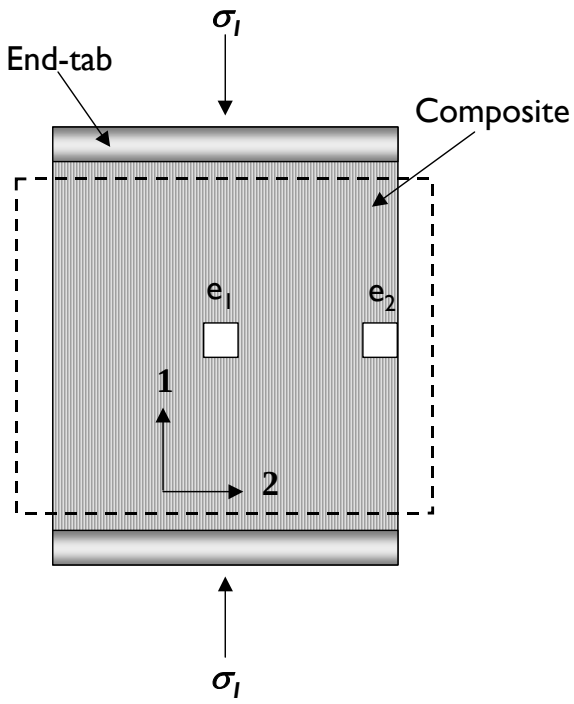

Figure 7-1: Strain release to the composite.

The dimensions of the composite panels prepared in this study are 290 mm *(l)* × 200 mm *(w)* × 2 mm *(t)* and so the panels can be considered to be thin and the stress system to be plane stress. When pretension is released to such a system, there will be a variation in the residual strain at various locations across the width of the composite due to Poisson's effect.

Consider the element e_1 and e_2 in Figure 7-1. When a prestress σ_1 is released to the composite, the elements e_1 and e_2 will undergo compression. Also due to the Poisson's effect there will be an expansion in the transverse direction (direction 2), shown as dotted lines in Figure 7-1. Because of the free-edge, the element e_2 can easily expand in the transverse direction (it does not have any constraint against expansion). However, the element e_1 will be constrained in the transverse direction by the transverse stiffness of the composite. As an approximation it is assumed that element e_1 is prevented from expanding in the transverse direction (that is $\varepsilon_2 = 0$). The material adjacent to element e_1 imposes a transverse compressive stress, σ_2, as shown in the Figure 7-2. This in turn will reduce the strain released in the longitudinal direction.

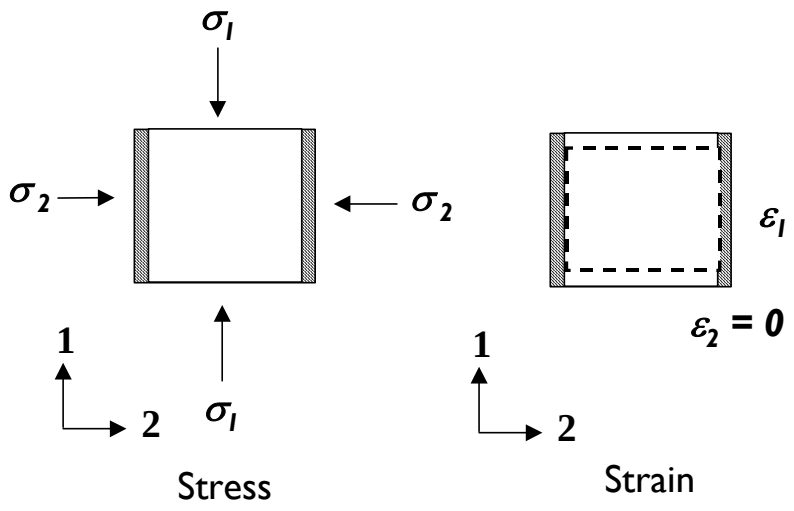

Figure 7-2: Prestress release in element e_1.

Assuming that the composite is an orthotropic material the stress-strain relationship can be written as:

$$\begin{pmatrix} \varepsilon_1 \\ \varepsilon_2 \\ \gamma_{12} \end{pmatrix} = \begin{pmatrix} \frac{1}{E_1} & \frac{-\nu_{21}}{E_2} & 0 \\ \frac{-\nu_{12}}{E_1} & \frac{1}{E_2} & 0 \\ 0 & 0 & \frac{1}{G_{12}} \end{pmatrix} \times \begin{pmatrix} \sigma_1 \\ \sigma_2 \\ \tau_{12} \end{pmatrix} \tag{7.21}$$

where σ, τ are the direct and shear stresses. ε and γ are the direct and shear strains, E and G are the direct and shear moduli. Subscripts 1 and 2 denote the longitudinal and transverse directions respectively. ν_{12} and ν_{21} are the major and minor Poisson's ratios of the composite.

From equation 7.21, the strain in the longitudinal direction resulting from pretension release can be expressed as:

$$\varepsilon_1 = \frac{\sigma_1}{E_1} - \frac{\nu_{21}}{E_2}\sigma_2 \tag{7.22}$$

therefore the strain in the element e_1 is given by:

$$\varepsilon^C{}_1 = \Delta\varepsilon - \frac{\nu_{21}}{E_2}\sigma_2 \tag{7.23}$$

where σ_2 is the stress induced in the lateral direction because of the Poisson's effect (due to the greater width of the specimen) and E_2 is the transverse stiffness of the composite.

Calculation of σ_2

Consider the element e_1 at the centre. If the strip were infinitely wide then no transverse strain would be possible. The element would be 100% laterally constrained ($\varepsilon_2 = 0$).

From equation 7.21, the strain in the transverse direction is given by:

$$\varepsilon_2 = -\frac{\nu_{12}}{E_1}\sigma_1 + \frac{1}{E_2}\sigma_2 \tag{7.24}$$

Since $\varepsilon_2 = 0$, :

$$\sigma_2 = \left(\frac{E_2}{E_1}\right)\nu_{12}\sigma_1 \tag{7.25}$$

So, returning to equation 7.8 and 7.10, but applying it to the element in the centre (e_1):

$$\varepsilon_f = \frac{(\sigma_f)^P}{E_f} - \frac{\nu_f}{E_f}\sigma_2 = \frac{W}{A_f E_f} - \Delta\varepsilon \tag{7.26}$$

$$\varepsilon_m = \frac{(\sigma_m)^P}{E_m} - \frac{\nu_m}{E_m}\sigma_2 = \Delta\varepsilon \tag{7.27}$$

$$\frac{(\sigma_f)^P}{E_f} - \frac{\nu_f}{E_f}\sigma_2 = \frac{W}{A_f E_f} - \frac{(\sigma_m)^P}{E_m} + \frac{\nu_m}{E_m}\sigma_2 \tag{7.28}$$

Also the strain in the matrix in the transverse direction is zero ($\varepsilon_m = 0$):

$$\frac{\sigma_2}{E_m} - \nu_m\frac{(\sigma_m)^P}{E_m} = 0 \tag{7.29}$$

$$\sigma_2 = \nu_m(\sigma_m)^P \tag{7.30}$$

From equation 7.11 $(\sigma_f)^P$ can be expressed as:

$$(\sigma_f)^P = -(\sigma_m)^P \frac{\phi_m}{\phi_f} \tag{7.31}$$

Substituting equation 7.30 and 7.31 in equation 7.28 we get:

$$(\sigma_m)^P \left(\frac{1}{E_m} - \frac{\phi_m}{E_f \phi_f} - \nu_m \left(\frac{\nu_f}{E_f} + \frac{\nu_m}{E_m} \right) \right) = \frac{W}{A_f E_f} \tag{7.32}$$

$$(\sigma_m)^P = \frac{W}{A_f E_f} \left(\frac{E_m E_f \phi_f}{E_f \phi_f - E_m \phi_m - \nu_m \phi_f (\nu_f E_m - \nu_m E_f)} \right) \tag{7.33}$$

The value of $(\sigma_m)^P$ calculated from equation 7.33 is substituted into equation 7.30 to determine the transverse stress (σ_2) induced to the element e_1 due to lateral constraint.

The strain released to the free-edge of the composite panel (element e_2) and centre of the composite panel (element e_1) can be calculated from equations 7.20 and 7.23 respectively.

7.3 Results and discussions

7.3.1. Residual strain

The residual strain predicted from the Tsai and Hahn one-dimensional model and the Wagner three-dimensional model using the materials parameters from Table 7-1 are presented along with the experimentally-measured residual strain (using EFPI and FBG strain sensors) in Table 7-2.

From Table 7-2, it is apparent that the experimentally measured residual strain is higher than the predicted residual strain from the Tsai and Hahn and Wagner models. The reason for this difference between models and experimental results are as follows.

- The Tsai and Hahn and Wagner residual strain models include only the thermal mismatch effects on residual strains, whereas the experimental results include both thermal strains and cure-induced (resin shrinkage) residual strains. The magnitude of the cure-induced residual strain development varies greatly between different polymer matrix materials. In general, the higher the cross-link density, the higher the strain development[118]. Researchers have shown that cure-induced residual strain can range from 1% to as much as 30% of the total residual strain and may be even higher.
- The interaction between the neighbouring fibres and the host fibre on the residual strain measurement were not included in the models (because they are concentrated on a micro-mechanical scale).

- The variation of fibre and matrix modulus and thermal expansion with temperature has been ignored.
- Any variation in fibre volume fraction within the composite panel is ignored.

Table 7-1: Material parameters used

Properties	E-glass	Epoxy Resin
Young's Modulus [MPa]	72500	4000
Poisson's ratio [-]	0.22	0.4
Thermal expansion coefficient [°C^{-1}]	5.00×10^{-06}	60.0×10^{-06}

Table 7-2: Residual strain results.

Models	Residual strain in fibre (με)
Tsai and Hahn	-195
Wagner	-280
Experimental EFPI results	-600 ± 58
Experimental FBG results	-737 ± 35

From Table 7-2, it can also be observed that there is a small difference in the residual strain measured from EFPI and FBG strain sensors. The possible reasons for the differences in residual strain measurements are:

a) The difficulty to measure accurately the gauge length of EFPI sensors. The change in measurement of the gauge length of an EFPI sensor will lead to a change in the strain measured. In order for the effective gauge length to be equal to A as shown in the Figure 7-3, there would need to be perfect bond at fusion points and friction-free surfaces between fibre and capillary. If both of these conditions are not satisfied, the effective gauge length will be less, so the strain measured should be greater.

b) The possibility of resin-wicking in to the EFPI capillary, which could reduce the gauge length.

c) The configuration of optical sensors (as shown in Figure 7-3) could have an effect on the measured residual strain.

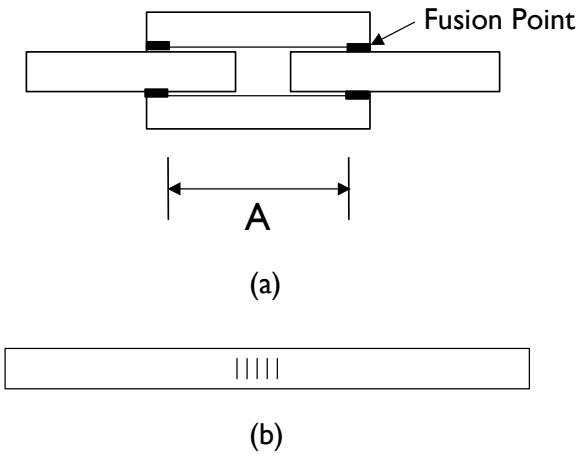

Figure 7-3: Sensor configuration, a) EFPI strain sensor and b) FBG strain sensor.

7.3.2. Strain release

The prestress is released to the composite after curing and cool-down to room temperature. The release of prestress induces compressive stresses to the polymer matrix. The effect of prestress on the residual stress in fibre and matrix are shown in Figure 7-4. The theoretical residual stress in the fibre and matrix was calculated from the Wagner model. From Figure 7-4, it can be observed that with an increase in prestress, the tensile residual stress in the matrix reduces and above 21 MPa prestress the matrix is subjected to compressive stresses. This change in matrix residual stress with prestress could increase the resistance to crack initiation and propagation during mechanical loading. On the other hand, the compressive residual stress in the fibre reduces with prestress and above 21 MPa prestress, the fibre is subjected to a tensile residual stress. The experimentally-measured fibre residual strain from EFPI and FBG strain sensors is converted to stress and plotted along with the theoretical prediction in Figure 7-4. From Figure 7-4, it can be seen that there is a constant difference between the experimental results and the theoretical predictions of fibre residual stress. This could be due to the cure-induced residual stress build-up during resin shrinkage. The Wagner model predicts only the thermally-induced residual stress.

The experimentally-measured fibre residual strain using EFPI and FBG strain sensor includes both cure-induced and thermally-induced residual strains. When the experimentally-measured fibre residual strain is included in the theoretical prediction at 0 MPa prestress, it can be observed that the experimental results are in agreement with the theoretical prediction as shown in Figure 7-5. Also it can be observed that the zero-residual stress in fibre and matrix occurs at 45 MPa prestress.

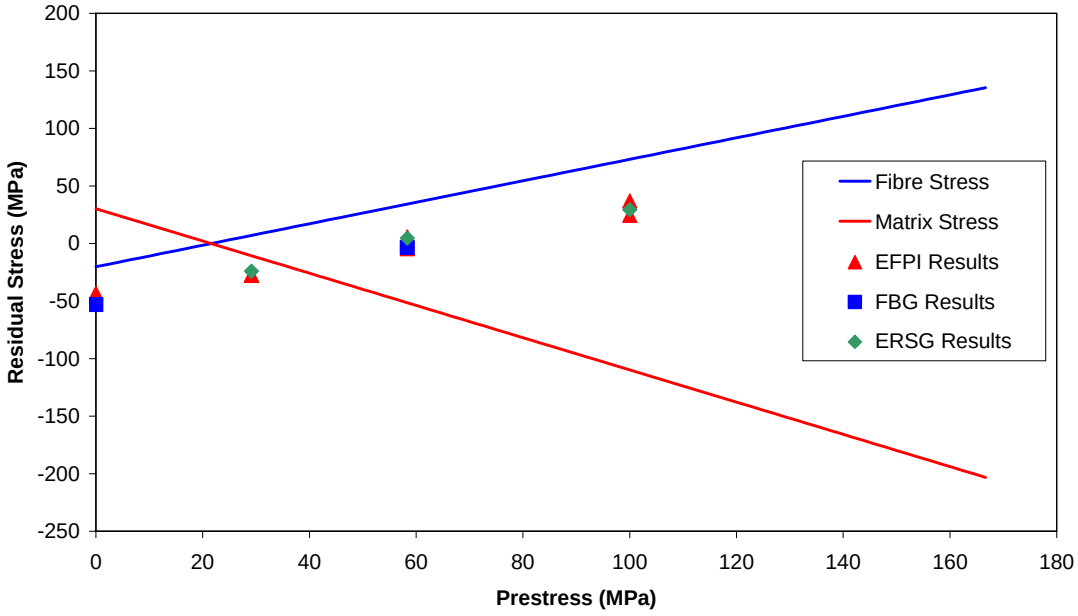

Figure 7-4: Residual stress in the fibre and matrix with prestress. The theoretical residual stress at 0 MPa prestress in fibre and matrix was calculated from the Wagner model.

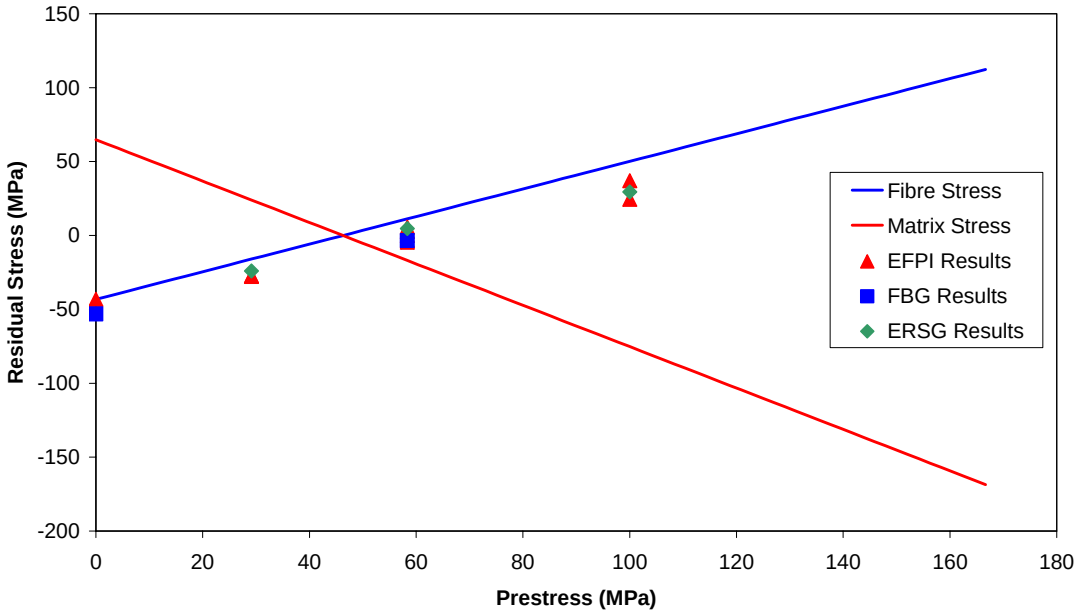

Figure 7-5: Residual stress in the fibre and matrix with prestress. The experimentally-measured residual stress at 0 MPa prestress is included in the theoretical prediction.

The small difference between the theoretical predictions and experimental results of the residual stress in the fibre with prestress could be due to 1) a small misalignment in the strain sensors (EFPI and FBG) during embedding and 2) error in the measurements.

The release of prestress to the composite, is very similar to applying a compressive stress to the composite. Before releasing the prestress, ERSG sensors were surface-mounted on the composite to compare the strain released from the optical sensors (EFPI and FBG) and ERSG.

Due to the greater width of the composite there will be a small variation in the strain distribution across the width of the composite panel due to Poisson's effect. This is explained in Setion 7.2. The strain induced in the free-edge and middle of the composite width are calculated from equations 7.20 and 7.23 respectively. The calculated strain released to the composite panel with applied prestress is plotted along with the measured strain release from EFPI, FBG and ERSG sensors in Figure 7-6. The experimental results are plotted with prestress measured before releasing.

In this research, prestress is applied to the fibres not only by mechnical load but also by the thermal expansion of the prestress rig. Using classical mechanics, the flat-bed prestress rig thermal-expansion-induced-prestress to the fibres was calculated to be 51 MPa (see Section 3.3.5, Chapter 3). However, the thermal-expansion-induced-prestress calculated above is the stress applied to the fibres at 120°C (which is the curing temperature of the composite). During the cool-down cycle, as the temperature decreases to room-temperature, the rig thermal-expansion-induced-prestress is released. When the composite is released from the prestress rig, a small strain release of about 110 με is recorded. This corresponds to 9 MPa prestress from the theoretical prediction as shown in Figure 7-6.

The predicted strain distribution across the width of the composite is plotted at three different prestress levels (29, 60 and 100 MPa) as shown in Figure 7-7, Figure 7-8 and Figure 7-9. It can be observed that there is a variation of about 1% strain release between the free-edge to the centre of the composite panels at all prestress levels.

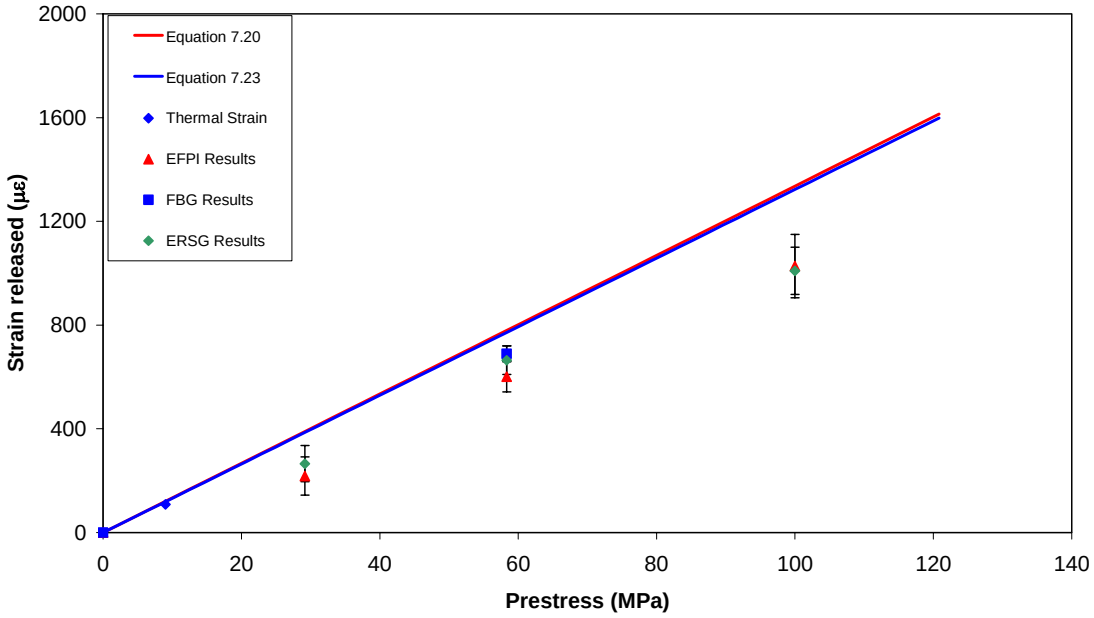

Figure 7-6: Strain released to the composite.

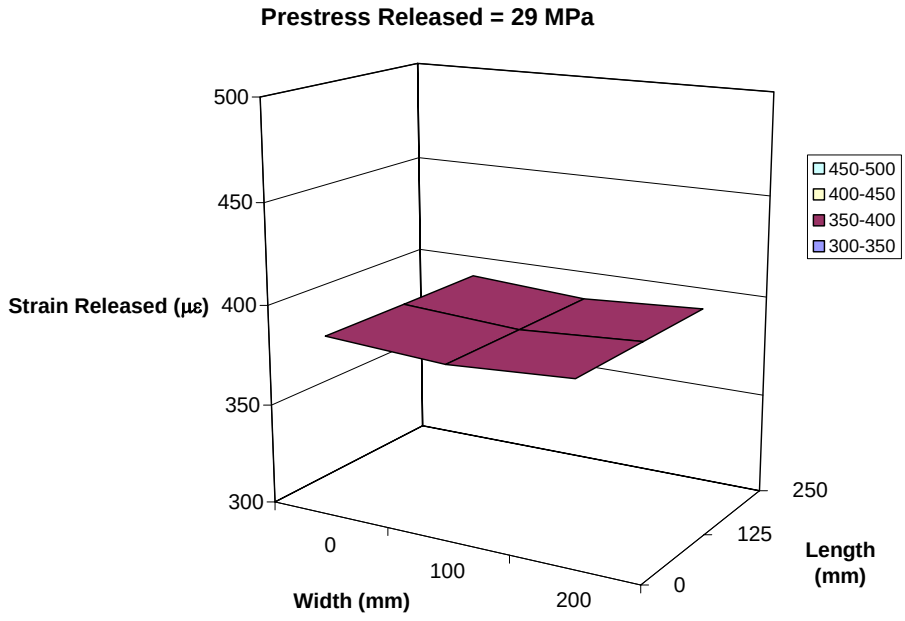

Figure 7-7: Strain distribution across the width of the composite panel for 29 MPa prestress release.

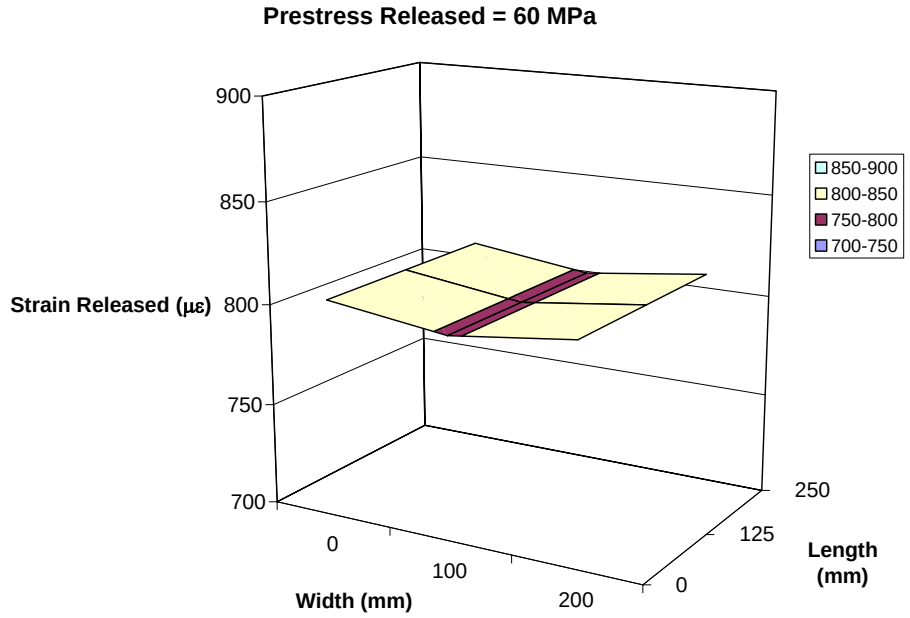

Figure 7-8: Strain distribution across the width of the composite panel for 60 MPa prestress release.

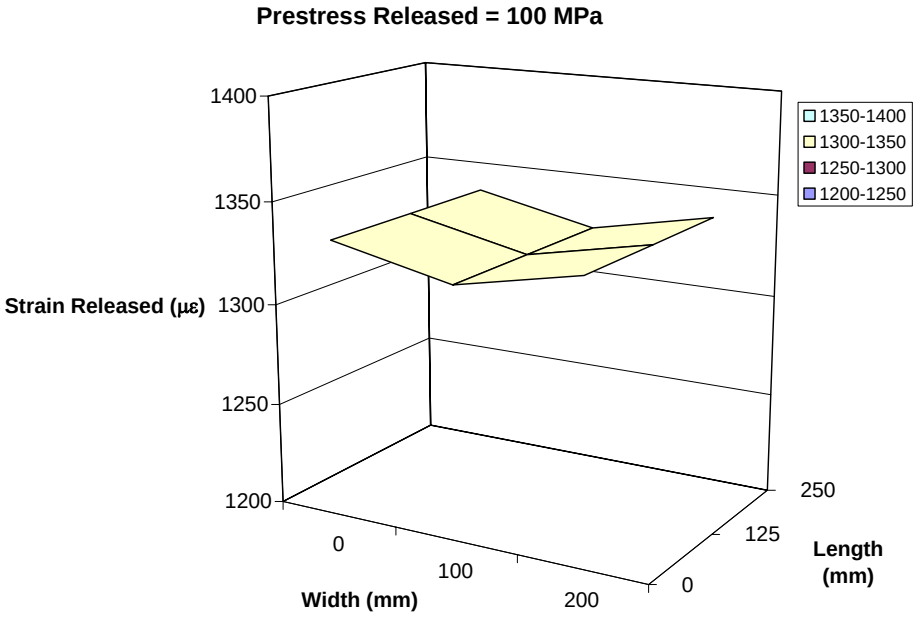

Figure 7-9: Strain distribution across the width of the composite panel for 100 MPa prestress release.

7.4 Concluding remarks

The present theoretical analysis is aimed at predicting (i) the effect of prestress on the residual stress in the fibre and matrix and (ii) the distribution of the strain released across the width of the composite panel during prestress release. Experimental results from residual strain measurements and strain release measured using strain sensors are compared with the theoretical analysis. From the theoretical analysis and experimental results the following conclusions can be made.

- Fibre prestress methodology can be used to minimise the process-induced residual stress in fibre and matrix present in the composite.
- Experimental residual strain results measured using EFPI and FBG strain sensors are greater than those predicted from the Tsai and Hahn and Wagner models. This is because these models predicts only the thermal stresses and on a micro-mechanical scale. On the other hand the experimental results measured using optical fibre sensors include both the cure-induced and thermally-induced residual stresses.
- The theoretical prediction of strain release to the composite is in good agreement with the experimental results.
- During prestress release, due to Poisson's effect, a small variation in strain distribution of about 1% across the width of the composite panel is predicted.

CHAPTER 8

Static mechanical properties

OVERVIEW

This chapter discusses the results of the effect of fibre prestress on static tensile and compression properties of composites.

- The tensile properties such as strength, modulus, and strain at deviation from linearity are discussed.
- The effect of prestress on macroscopic and microscopic tensile damage is discussed.
- The compressive properties such as strength and modulus are discussed.
- The influence of prestress on macroscopic and microscopic compressive damage of composites is discussed.
- The conclusions are drawn from the observed results for the effect of fibre prestress on tensile and compressive performance of composites.

8.1 Static tensile results and discussion

A SELECTION OF REPRESENTATIVE STRESS-STRAIN curves for all prestressed unidirectional $[0°]_{16}$ composite panels are shown in Figure 8-1. A summary of the tensile test results is presented in Table 8-1. The individual sample tensile test results for all the prestressed composites are presented in Appendix C.

8.1.1. Strain at deviation from linearity

With reference to Figure 8-1, a degree of non-linearity can be observed for all the prestressed composite panels studied. The average strain at which the non-linearity was

observed is summarised in Table 8-1 and plotted in Figure 8-2. From Table 8-1 and Figure 8-2 it can be observed that the average ε_{SDL} increases with increase in fibre prestress up to 108 MPa prestress, above which there is an indication of a reduction. However, from the statistical analysis student *t*-test it was found that there is no significant difference in ε_{SDL} measured between 108 MPa and 150 MPa.

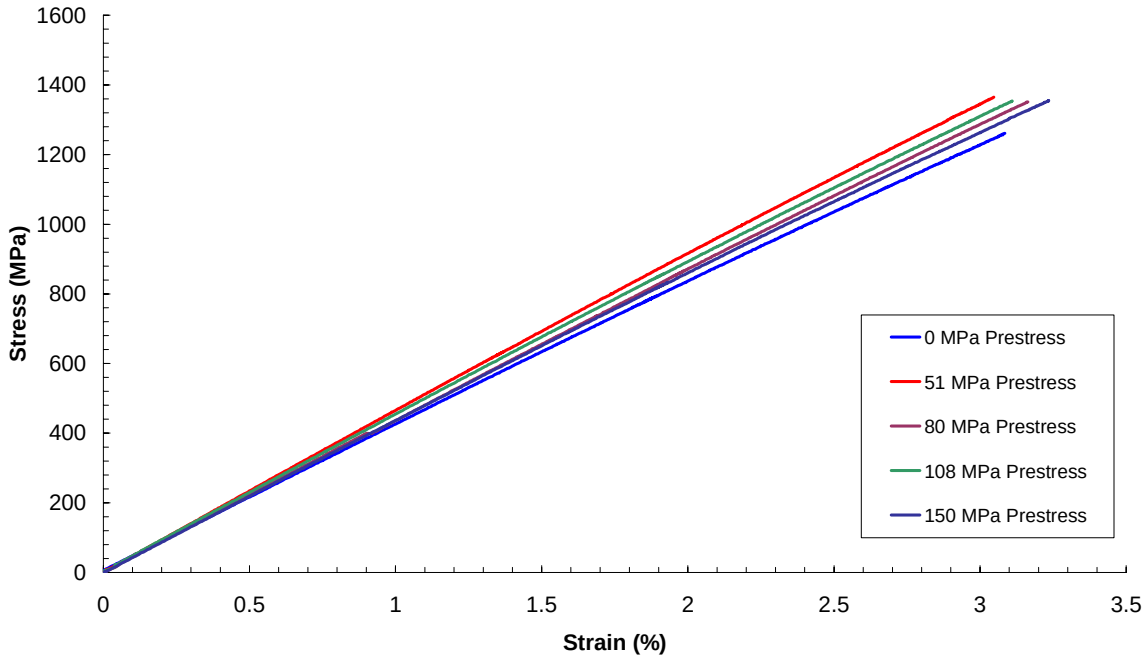

Figure 8-1: Stress-strain curve for all prestressed composite panels.

This deviation from linearity in the stress-strain curve during tensile loading may be attributed to the following reasons: a) non-linear behaviour of the matrix and b) fibre waviness.

(i) *Non-linear behaviour of the matrix*

It is possible to expect the non-linear behaviour of the epoxy matrix (because of its viscoelastic behaviour) to influence the stress-strain curve of the unidirectional composite. Goutianos *et al.*[119] studied the linear and non-linear behaviour in single fibre carbon/epoxy composites in tensile and compressive loadings. From their investigation, they showed that during tensile loading, the deviation from linearity is due to the on-set of matrix plasticity and the reduction in shear modulus.

This strain to non-linear behaviour of the matrix could be influenced by the process-induced residual stresses. The possible reason for the observed improvement in ε_{SDL} (see Table 8-1) could be attributed to a reduction in the tensile residual stress of the matrix with fibre prestress. Motahhari and Cameron showed that the reduction in matrix and interface

residual stresses with prestressing enhances the mechanical properties. They suggested that reducing matrix and interface residual stresses could prevent the opening of micro-cracks in the matrix and debonding at the interface.

On the other hand, above an optimum prestress level residual stress at the interface increases, which makes the interface vulnerable and causes fibre-matrix debonding. From Table 8-1 it can be observed that above 108 MPa prestress, the average ε_{SDL} indicates a reduction. This suggests that there is an optimum prestress level for the improvement in ε_{SDL}. Previous researchers[76,77,79] have shown that there is an optimum prestress level for the improvement in flexural and impact behaviour of composites.

Table 8-1: Summary of tensile properties of composites studied in this programme. The number in parentheses represents the standard deviation.

Prestress (MPa)	Ultimate tensile strength (MPa)	Secant modulus at ε = 0.25% (GPa)	Failure strain (%)	Strain at deviation from linearity ε_{SDL} (%)	Fibre volume fraction (%)	Void volume fraction (%)
0	1311 (±80)	43.37 (±2.64)	3.18 (±0.10)	1.49 (±0.05)	58 (±1)	0.34 (±0.09)
51	1244 (±110)	41.69 (±3.44)	3.05 (±0.15)	1.73 (±0.06)	58 (±1)	1.13 (±0.40)
80	1295 (±65)	43.69 (±2.48)	3.11 (±0.10)	1.78 (±0.04)	58 (±1)	1.13 (±0.37)
108	1285 (±138)	43.20 (±2.62)	3.10 (±0.17)	1.92 (±0.15)	58 (±2)	0.93 (±0.18)
150	1273 (±66)	42.60 (±1.52)	3.08 (±0.13)	1.80 (±0.05)	59 (±2)	0.78 (±0.32)

(ii) *Fibre misalignment*

Fibre prestressing prior to cure and maintaining this throughout the curing process could reduce fibre misalignment (both in-plane and out-of-plane) and this could have also contributed to the increase in ε_{SDL}. In non-prestressed composites, during processing, fibre misalignment can be instigated due a number of reasons. For example: (i) fibre movement during pressurisation and/or during the minimum viscosity phase of the resin matrix, (ii) differential thermal expansion of various constituent materials, (iii) low fibre volume fraction, (iv) excessive resin-bleeding inducing fibre movement and (v) over-pressurisation during processing.

Fernando and Al-Khodairi studied the ε_{SDL} for the same material used in this study. They reported that the average ε_{SDL} for E-glass/913 epoxy was 1.37 ± 0.08%. The average ε_{SDL} reported by Fernando and Al-Khodairi is smaller when compared to the current work (1.49 ± 0.05%). The possible reason could be different processing methods. In the current study the composites are prepared using an autoclave process, which is accepted as a process for manufacturing high quality composites and also mostly used by aerospace industries. However, in Fernando and Al-Khodairi's work, composites were prepared using the hot-press moulding process. Fernando and Al-Khodairi reported that during the hot-press moulding process it was not possible to control the leakage of matrix resin on a consistent basis. It is generally recognised that the hot-press moulding process is prone to induce more fibre waviness and voids in composites. This could have reduced the ε_{SDL} in Fernando and Al-Khodairi's work. Also no details were given regarding the extent of fibre waviness in their composites to compare with the current work.

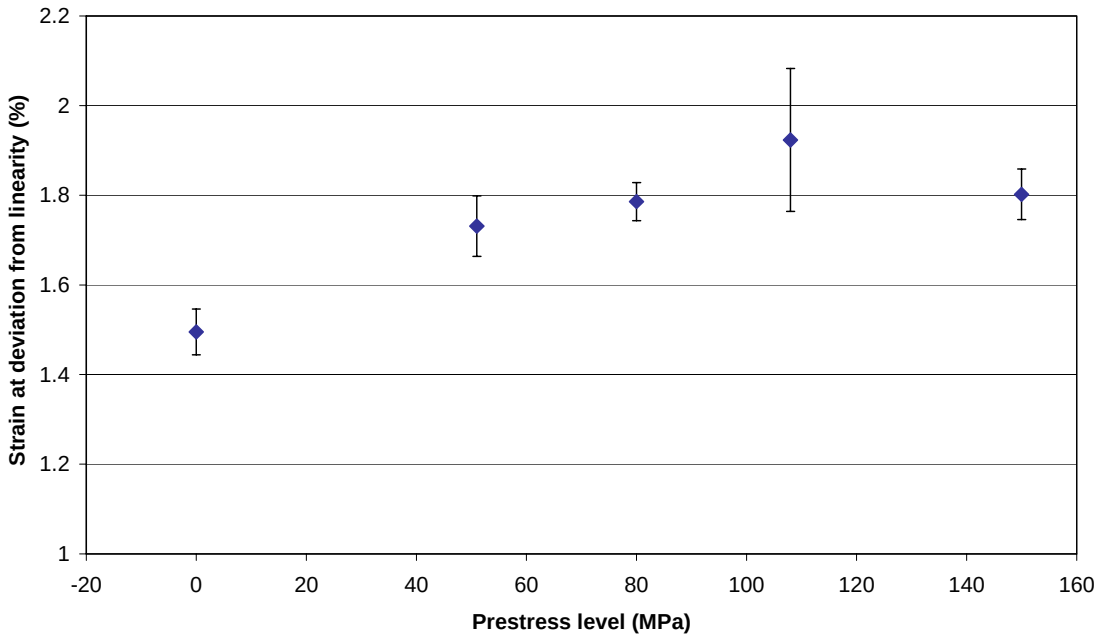

Figure 8-2: The measured strain at the deviation from linearity in stress-strain curve as a function of prestress. The error bars represents the standard deviation.

The fibre alignment of non-prestressed and prestressed composites are presented in Figure 6-10. It was shown that the number of fibres aligned to 0° direction of the composite increases with fibre prestress. Also the strain at deviation from linearity shows an improvement with fibre prestress (see Figure 8-2). This suggests that the fibre alignment could influence the non-linear behaviour of the composite. With reference to Figure 6-10,

it can also be observed that the fibres aligned to 0° direction of the composite reaches a maximum of about 75% in 108 MPa prestressed composite and above which no further improvement was observed. This also correlates with the observed optimum prestress limit to attain higher strain to on-set of non-linearity.

8.1.2. Tensile strength and modulus

The measured tensile strength for the 0 MPa prestressed E-glass/913 epoxy material in the current work is compared with the published literature results for the same material in Table 8-2.

Table 8-2: Tensile strength comparison.

Researchers	Tensile Strength (MPa)	V_f (%)
Current Work	1311 (80)	58.2 (1.5)
Fernando and Al-Khodairi	1160 (40)	62.2 (1.6)
Patridge *et al.*[120]	1337 (63)	69.0 (1)
Dickson *et al.*[121]	1400 (-)	~ 60.0 (-)
Broughton and Lodeiro[122]	1210 (-)	51 (-)

From Table 8-1 it can be observed that the average tensile strength and secant modulus are independent of applied prestress. In the literature there is a contradiction in tensile properties with fibre prestress. Zhao and Cameron studied the effect of fibre prestress on tensile properties in co-mingled PP/glass fibre composite. They showed that with fibre prestressing, the tensile strength and modulus increases. They suggested that this improvement is due to the reduction in residual stresses.

Schulte and Marissen studied the effect of fibre prestress on hybrid (Kevlar/Carbon) epoxy cross-ply composites. They studied two prestress levels 0 MPa and 341 MPa (1.1% prestrained) in composites. From their study, they have shown that fibre prestressing has minimised the transverse matrix cracking during tensile loading and improved the tensile fracture strength and strain of composites. From Table 2-6 reproduced from their paper, it can be observed that the average strength and modulus show an improvement. However, the standard deviation of their measurements shows that the properties of prestressed composites are within the limits of non-prestressed composites.

Tuttle *et al.* showed that in unsymmetrical carbon fibre/epoxy laminate, fibre prestressing minimised the transverse matrix cracks during tensile loading. This correlates with Schulte and Marrissen's results. However, they showed that no correlation was observed in tensile properties with an increase in fibre prestress.

Lee and Ali studied the effect of prestress on tensile properties of Kevlar49/epoxy and Twaron/epoxy composites respectively. They both showed that tensile modulus and fracture strain decreases with an increase in fibre prestress.

It was shown in Chapter 7 that after composite curing and releasing the prestress, the residual strains in the fibre is given by:

$$\varepsilon^{f} = \varepsilon^{f}{}_{R} + \varepsilon^{f}{}_{T} \tag{8.1}$$

where ε^{f}_{R} is the residual strain developed due to curing process and ε^{f}_{T} is the tensile residual strain remaining in the fibre due to release of prestress, which can be expressed as:

$$\varepsilon^{f}{}_{T} = \frac{W}{A_f E_f} \times \left(\frac{E_m \phi_m}{E_m \phi_m - E_f \phi_f} \right) \tag{8.2}$$

Therefore, the tensile failure strain of the prestressed composite to the first approximation can be given by:

$$\varepsilon^{F}_{PC} = \varepsilon^{F}_{NPC} - \varepsilon^{f} \tag{8.3}$$

where, ε^{F}_{NPC} is the average tensile failure strain of the non-prestressed (0 MPa) composite.

From the experimental results presented in Chapter 6, it was also confirmed that as the applied fibre prestress increases, the residual tensile stress in the fibre increases; this was also observed by Motahhari and Cameron. Figure 8-3 shows the theoretical prediction given by equation 8.3 of the effect of the prestress on the tensile failure strain along with the experimentally-measured results. From Figure 8-3 it can be observed that from the theoretical prediction there is a reduction in the composite failure strain with increasing fibre prestress. The experimental results are presented with standard deviations (99% confidence limits). Considering the greater standard deviation in the experimental results for all the prestressed composites, it can be concluded that no significant difference in the failure strain was observed with prestress. This correlates with the results of Tuttle *et al.*.

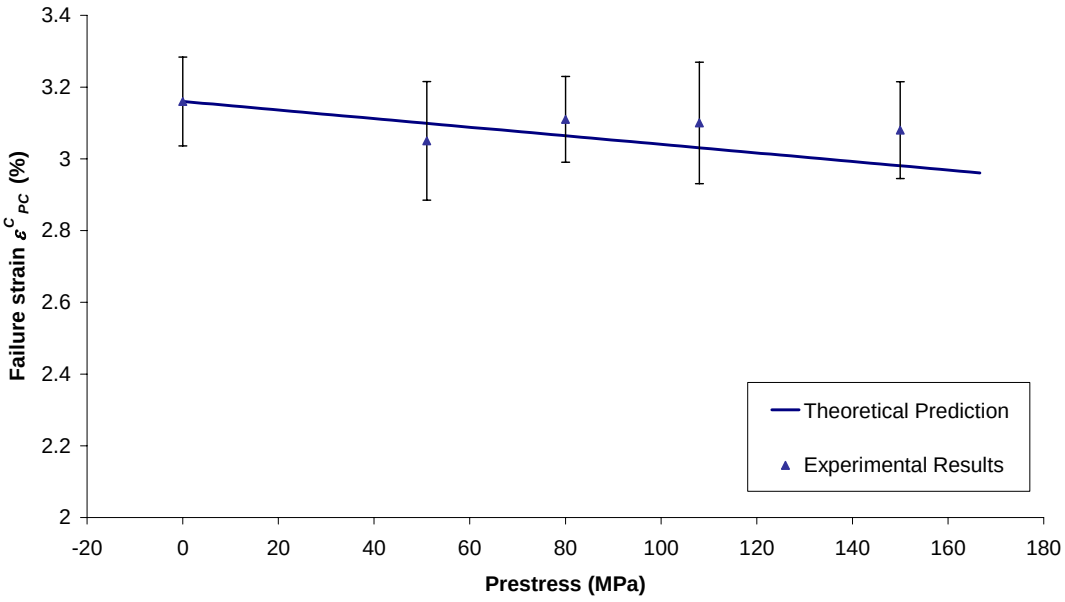

Figure 8-3: The effect of fibre prestress on composite failure strain.

8.2 Post-tensile failure analysis

The tensile fracture of the composites was examined from the macroscopic (by visual inspection) to the microscopic (scanning electron microscopy) scale. The results from the examination are discussed as follows.

8.2.1. Macroscopic examination

A representative tensile failure from each prestressed composite investigated in this study is presented in Figure 8-4. Macroscopically all the prestressed composites fractured by longitudinal splitting, which is a typical fracture of unidirectional E-glass/epoxy composite, also known as "brush-like" failure; this type of failure has been reported by many researchers[85,122]. From Figure 8-4, it can be observed that macroscopically there is no difference in the tensile fracture of composite samples with fibre prestress.

Figure 8-4: Photo macrograph of static tensile specimens.

8.2.2. Microscopic examination

Samples for microscopic examination were taken from the representative specimens from each prestressed composite. They were examined using a scanning electron microscope. Figure 8-5 shows the micrographs from all the prestressed composites.

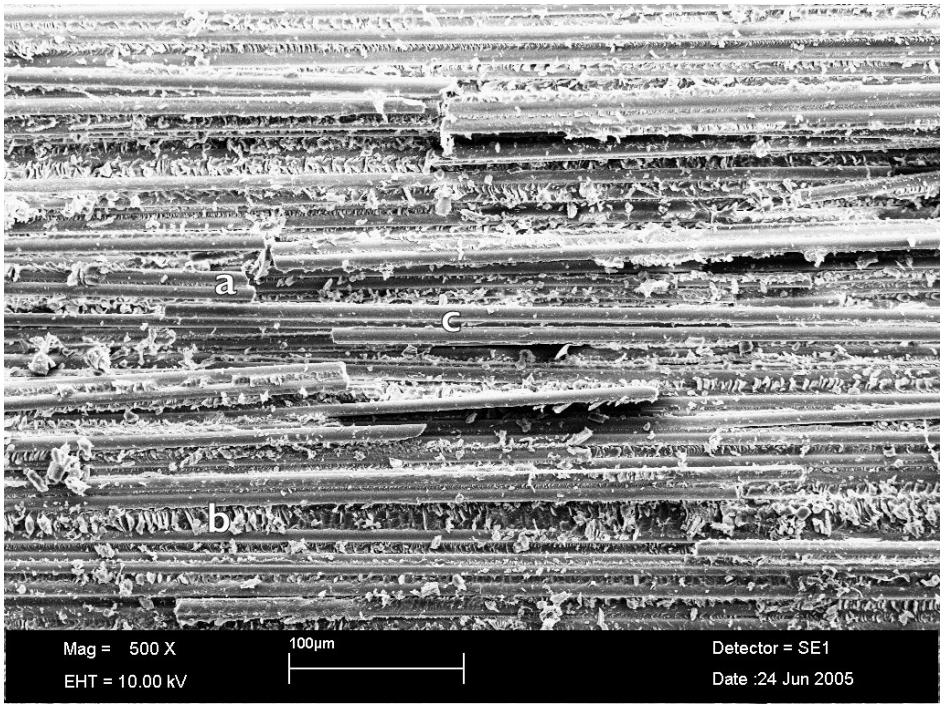

(i) – 0 MPa

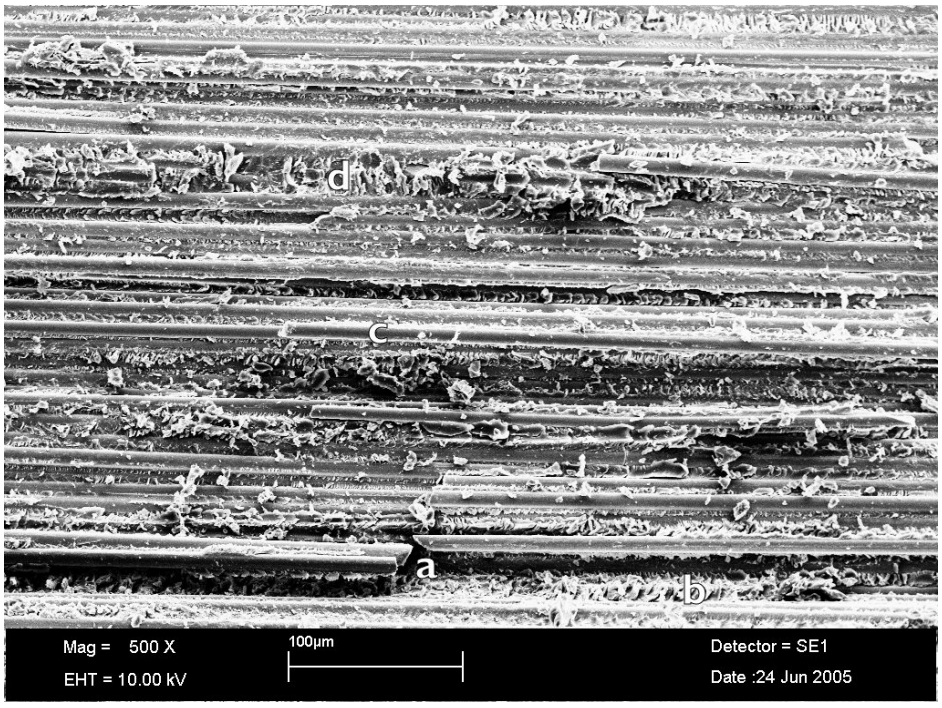

(ii) – 51 MPa

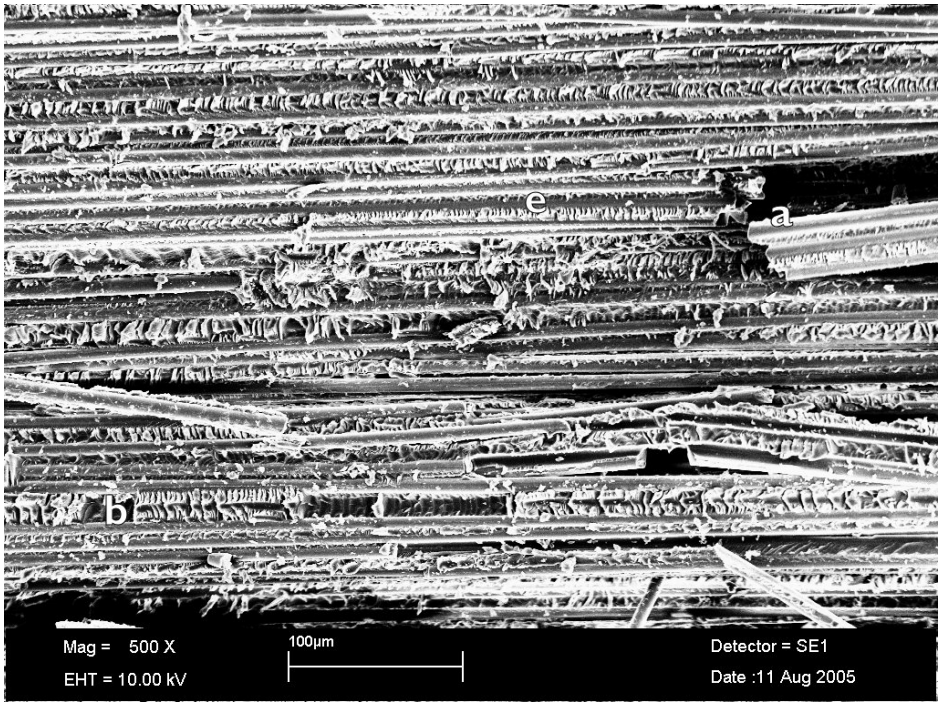

(iii) – 80 MPa

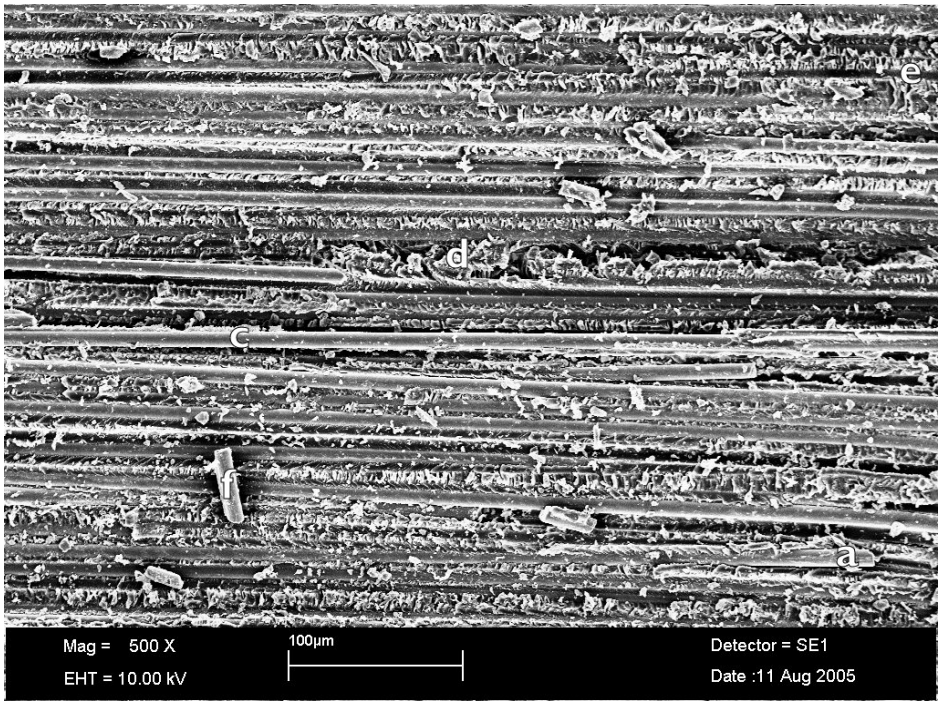

(iv) – 108 MPa

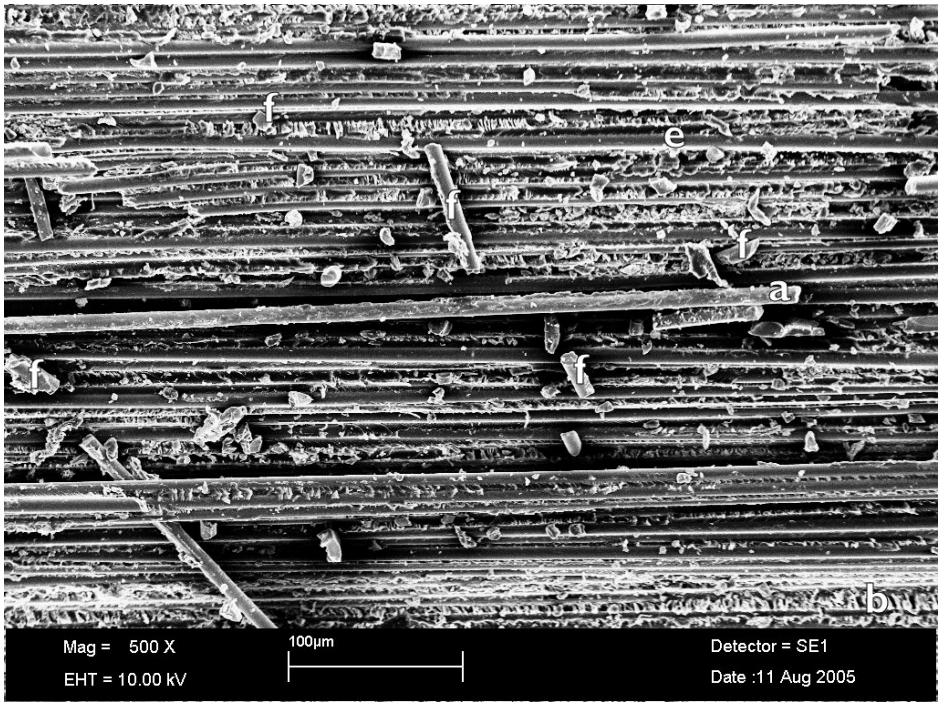

(v) - 150 MPa

Figure 8-5: Micrographs of specimens tested in tension, (i) 0 MPa, (ii) 51 MPa, (iii) 80 MPa, (iv) 108 MPa and (v) 150 MPa prestressed composites. The failure mechanisms are denoted thus in each figure: a – fibre fracture/pull-out, b – matrix hackle formation, c – clean fibre surface, d – matrix plasticity, e – fibre impression and f – fibre fragment.

From Figure 8-5 it can be observed that in general in all the prestressed composite specimens tensile failure mechanisms like fibre/matrix debonding, fibre fracture/pull-out, matrix hackle formation and matrix plastic deformation are present. The mechanism of hackle formation is presented in Chapter 9. A clean fibre surface indicates a weak interfacial bonding between fibre and matrix, which is a typical behaviour of E-glass/epoxy composites. These tensile failure modes were also reported by many researchers. There is a difference in the fibre damage at high prestress levels (108 and 150 MPa) when compared to low prestress levels (0, 51 and 80 MPa). At a high prestress level a greater number of fibre fragments can be observed (as shown in Figure 8-5 (iv) and (v)).

The possible reasons for the observed greater number of fibre fragments at high prestress levels are: (i) a reduction in the number of weak fibres during prestressing and (ii) some tensile residual strain in the fibre.

(i) *Reduction in weak fibres*

In a non-prestressed composite both weak and strong fibres are present. This difference in the strength of glass fibres is due to the presence of surface flaws. This strength distribution is also present along the length of a fibre. Therefore, fibres may fail at their weakest point, at stresses below the fracture stress of the bulk composite. When a non-prestressed composite is subjected to a tensile load, fibre failure first occurs in the weakest fibres. This may be simultaneous with matrix cracking and interfacial debonding.

Prior to composite curing, when a prestress is applied to the fibres, the weak fibres will fracture leaving predominantly strong fibres. The higher the prestress level applied the more weak fibres break. When a prestressed composite is subjected to a tensile load, the first failure of the fibres will occur at a higher applied tensile stress level, compared to the fibre failure in a non-prestressed composite. The fracture of the fibre will release strain energy and this is dissipated in various ways, depending on the strength of the fibre/matrix adhesion. In this study, all the prestressed composites were manufactured from the same prepreg material. Therefore, there is no chemical change in the fibre/matrix adhesion. The energy released by the fibre fracture in a prestressed composite will be greater than the energy released by the fibre fracture in a non-prestressed composite. This release of energy will increase with an increase in fibre prestress. At a very high-energy release rate, possibly a "shock wave" effect would be induced in the neighbouring fibres and also along the fractured fibre length, which would lead to an increase in the number of fibre fragments present in the fractured surface.

(ii) *Tensile residual strain in fibre*

In Chapter 7 it was shown that the residual tensile stress in fibres increases with applied prestress. This was also observed by Motahhari and Cameron. Scherf and Wagner[123] have studied the effect of fibre prestress on interfacial shear strength of single fibre micro-composites using a fibre fragmentation method. They have shown that at a higher applied fibre prestress, the number of fibre fragments increased. Their measurement of interfacial shear stress increases with an increase in fibre prestress. They explained that "the apparent increase in the value of the interfacial shear strength does not mean that stronger interfaces are created by fibre pre-loading; rather, the larger value obtained is an artefact arising from the increased number of fibre breaks obtained". They showed that with the applied prestress the residual tensile stress increases. This is stored as additional strain energy in the fibres, which might induce dynamic recoil effects upon fibre breakage. This could induce supplementary fibre breaks (possibly by a "shock wave" effect) and therefore an increased number of fragments. This means that composites with a higher applied prestress will have greater strain energy stored in the fibres.

8.3 Static compression results and discussion

Static compression tests are conducted in prestressed composites according to the procedure explained in section 4.9.2. Figure 8-6 and Figure 8-7 show the compressive strength and modulus results of prestressed composites. The individual sample compression test results are presented in Appendix C. Typical axial compressive stress-strain responses of all the prestressed composites are shown in Figure 8-8.

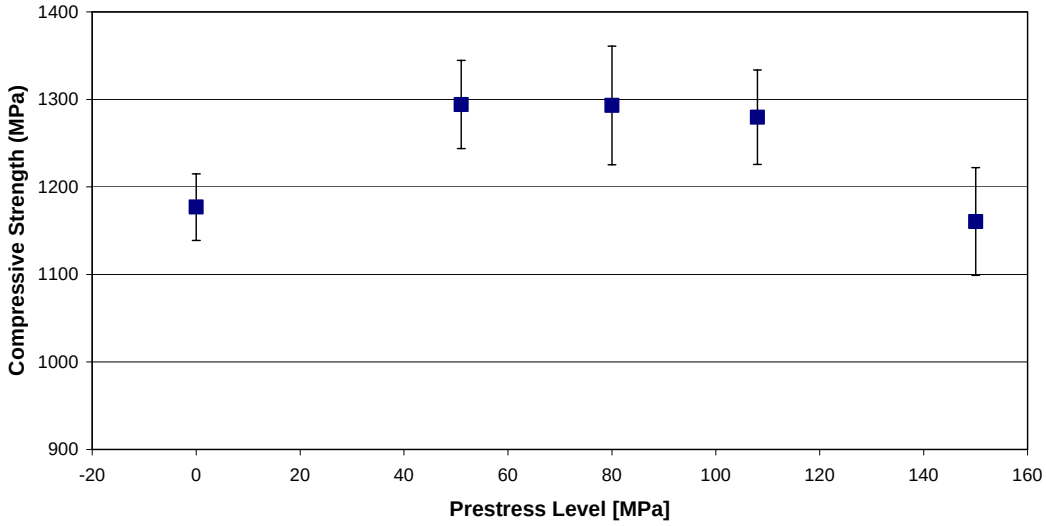

Figure 8-6: Compression strength of prestressed composites.

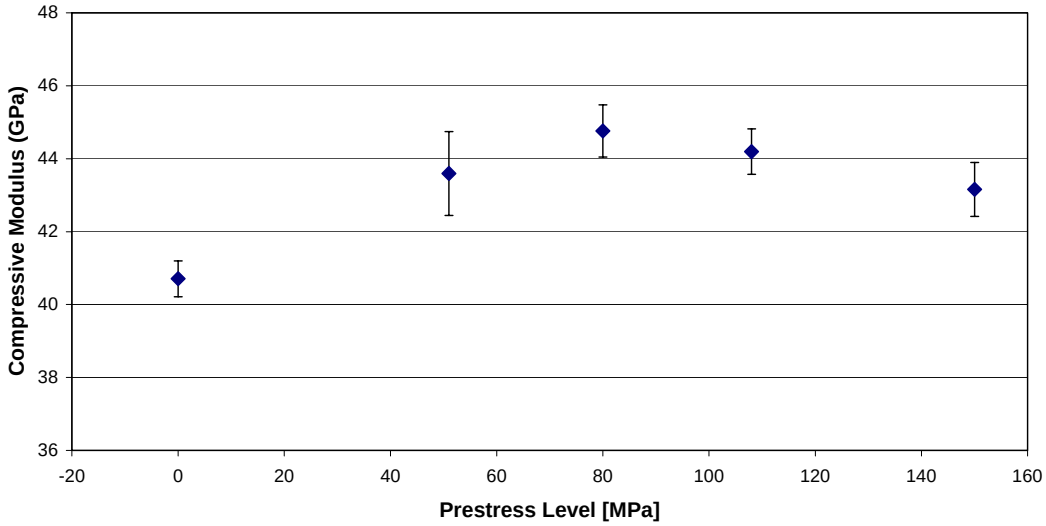

Figure 8-7: Compression modulus of prestressed composites

From Figure 8-6 and Figure 8-7 it can be observed that there is an increase of 9% in average ultimate compressive strength (UCS) and 9% in average compressive modulus of composites up to 80 MPa prestress. This increase in the compressive properties with prestress could be due to (i) an improvement in the fibre alignment and (ii) a reduction in the tensile matrix residual stresses. Previous researchers have shown that fibre misalignment can significantly reduce the compressive properties of unidirectional composites. Above an optimum prestress level (108 MPa for compressive strength and 80 MPa for compressive modulus) the compressive properties decrease. This reduction in compressive properties could be due to the increase in the interfacial shear residual stresses in the composite, which arise due to increased tensile residual stresses in the fibre and compressive residual stresses in the matrix. This increase in interfacial shear residual stresses could reduce the resistance to interfacial crack initiation and propagation. This could lead to the onset of fibre-matrix cracking at a very early stage of the loading. This will result in a reduction in the compressive properties of the composite. This reduction in compressive properties suggests that an optimum limit of prestress exists for the improvement. Motahhari and Cameron[76, 79], and Zhao and Cameron observed this phenomenon of optimum prestress limit in tensile, flexural, impact and inter-laminar shear strength.

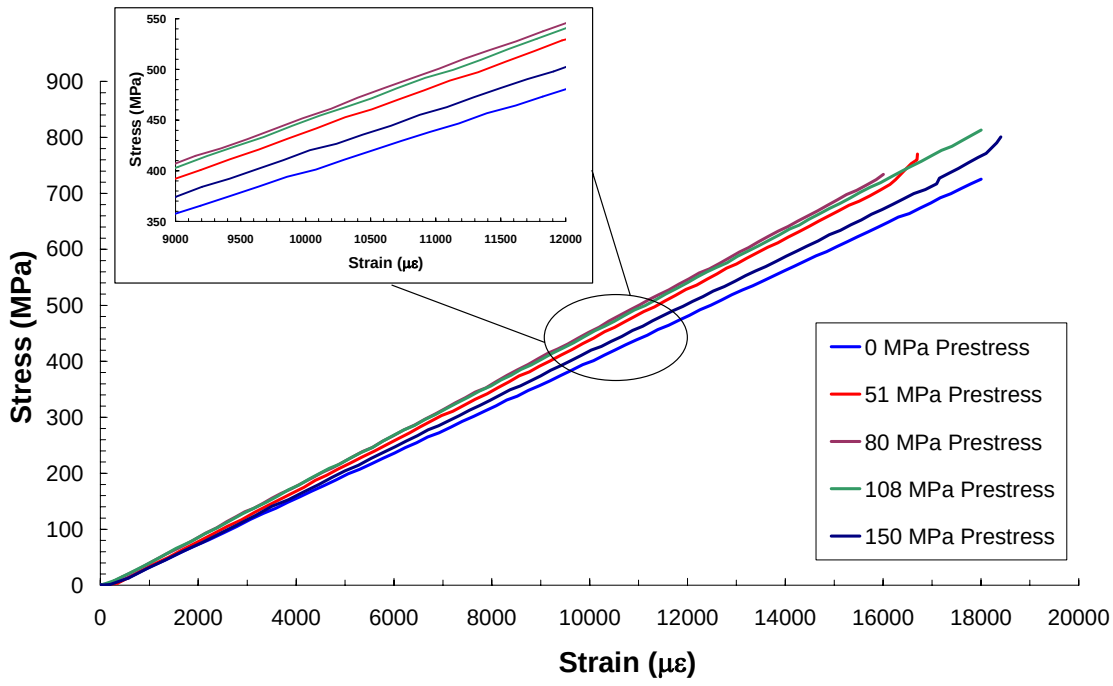

Figure 8-8: A typical compressive stress/strain curve for $[0°]_{16}$ prestressed composites.

From Figure 8-8 and Table 8-3 it can be observed that there is an increase in slope for all prestressed composite when compared to 0 MPa prestressed composite. The slope of the

stress-strain curve increased up to 80 MPa prestressed composite. This shows that there is an optimum limit for the increase in the slope. Above this optimum limit, the slope of the composite decreased.

Table 8-3: The slope calculated from linear regression analysis for each prestressed composite presented in Figure 8-8.

Prestress (MPa)	Slope (m)
0	0.0407
51	0.0453
80	0.046
108	0.0454
150	0.0429

In this study the compressive strain was measured using electrical resistance strain gauges on both sides of the specimen. The strain measured from both sides of the specimen showed a variation of 5% and is the standard variation found in the testing. A comparison of front and rear strain measurement during a compressive test is shown in Figure 8-9.

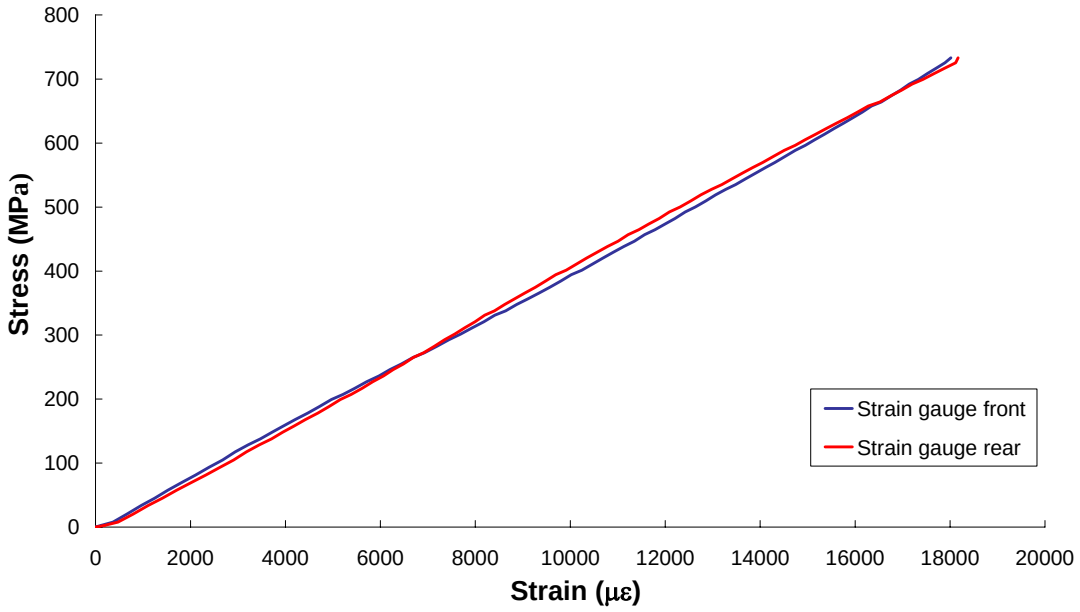

Figure 8-9: Comparison of compressive strain measured in front and back of the composite.

8.4 Compressive strength comparison

Compressive strength measured in this study and the values available in the literature[124] for the same material are summarised in Table 8-4. From Table 8-4 it can be observed that the compressive strength values measured in the current study is similar to the CRAG standard, but higher than the ASTM methods. It can also be noticed that the deviation of UCS measured in the current study (using the ICSTM rig) is small (4%) when compared to the CRAG value (15%). The large discrepancy between the ASTM and the current work could be due to the specimen misalignment during testing, and manufacturing problems like fibre waviness. Mrse and Piggott have shown that fibre waviness can significantly reduce the compressive strength of composites. In their experiments on carbon/PEEK composites with four different prepreg types, deviations ranging from 1° to ~6° in fibre waviness were obtained, with corresponding strengths from 1.9 GPa to 1.5 GPa. Matthews studied the effect of different compression test methods and specimen configurations on the compressive strength of carbonXAS/914 epoxy composite. He showed that out of the 12 different test methods investigated, the ICSTM test method and specimen configuration gave the higher mean strength, together with low scatter. He concluded that the discrepancy in the compression strength results is due to specimen misalignment, stability problems and operator inexperience.

Table 8-4: Comparison of UCS of unidirectional control specimens with different test methods. The number in parentheses represents the standard deviation. * *l* – gauge length, *w* – width, *t* – thickness.

Test method	Specimen dimension ($l \times w \times t$)* mm	Test speed [mm/min]	UCS [MPa]
ASTM D3410	12.7 x 6.35 x 3	1.26	642 (46)
ASTM D695 (mod)	80 x 19/12 x 2	1	592 (45)
CRAG 400 (Celanese)	10 x 10 x 2	3.25	1230 (188)
Current Work (ICSTM)	10 x 10 x 2	1	1177 (47)

8.5 Post-compressive failure analysis

8.5.1. Macroscopic examination

Figure 8-10, shows representative macroscopic compressive failures of all prestressed composites. It can be observed that all the prestressed composites show longitudinal splitting and fibre fracture except the 0 MPa prestressed composite. Under close examination it was found that the 0 MPa prestressed composites have failed in the fibre

microbuckling mode as shown in Figure 8-11, whereas all the rest of the prestressed composites show extensive longitudinal fibre splitting and minimal global buckling (see Figure 8-11). The sudden catastrophic nature of the failure made detection of any failure initiation event extremely difficult.

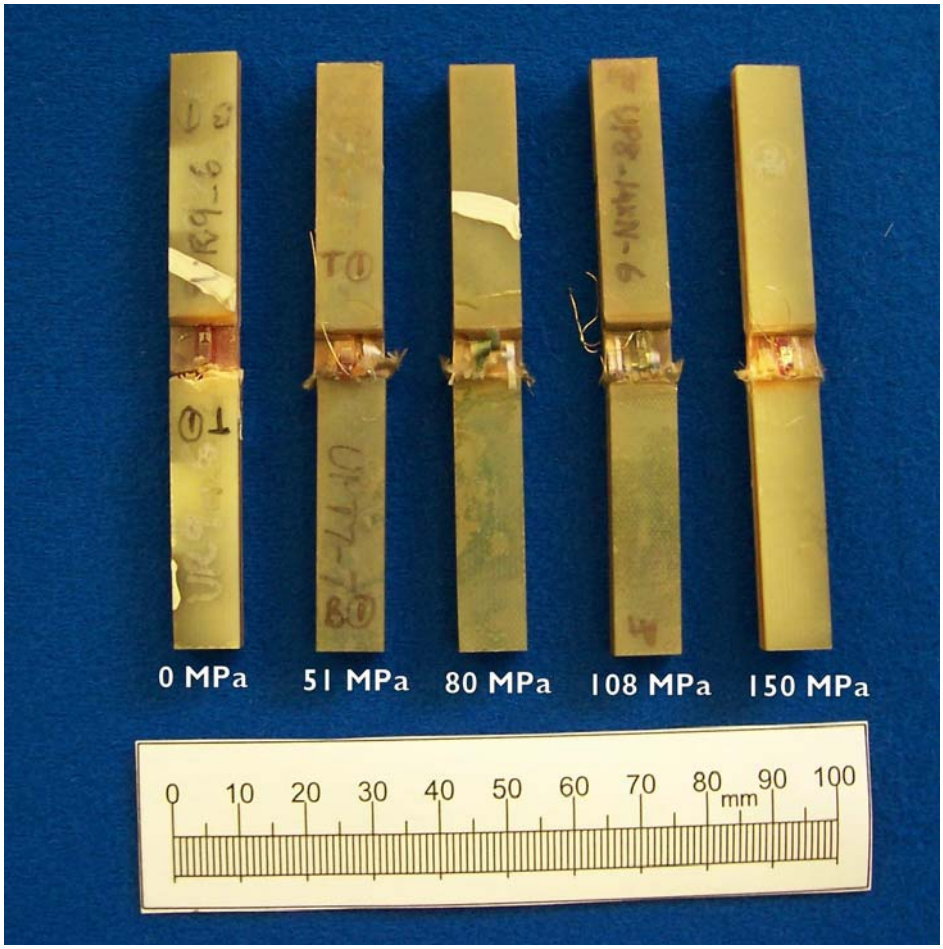

Figure 8-10: Representative compressive failures of 0, 51, 80, 108 and 150 MPa prestressed composites.

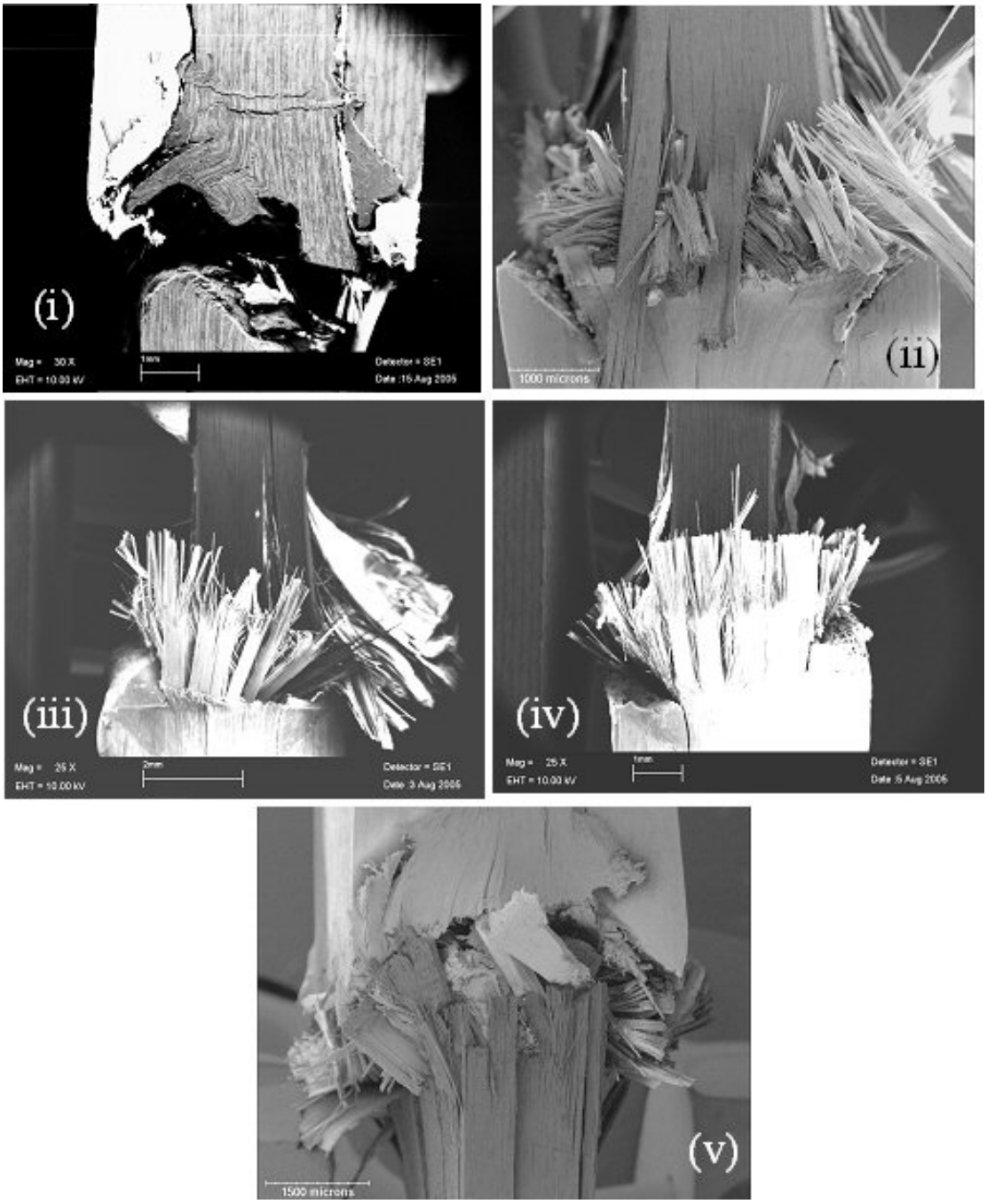

Figure 8-11: A magnified view of the macroscopic failure of all the prestressed composites. (i) 0 MPa, (ii) 51 MPa, (iii) 80 MPa, (iv) 108 MPa and (v) 150 MPa.

The possible reasons for the observed change in the damage mechanism could be due to the improvement in fibre alignment and reduction in matrix residual stresses.

Fibre misalignment or waviness can occur during the manufacturing process (as explained in section 2.5). When a compressive load is applied, the misaligned or wavy fibres start to buckle. Hahn and Williams and Lankford[125] have shown that in a unidirectional composite

the in-plane buckling of the fibres places the matrix pre-dominantly in shear. This leads to a shear mode of fibre "microbuckling or kink-band" failure, which is described in section 8.5.2.

During manufacturing of prestressed composites, the fibres are restrained under a constant load and this prevents fibre movement. Thus, fibre misalignment or waviness is reduced in prestressed composites. From Figure 8-11 it can be observed that prestressed composites show an absence of the microbuckling mode failure. This indicates that prestressing could have reduced fibre misalignment. It can also be observed that prestressed composites show more longitudinal splitting and fibre fractures when compared to the 0 MPa prestressed composite. This change in macroscopic failure mechanism also supports the observed improvement in the compressive strength and modulus of the prestressed composites.

8.5.2. Microscopic examination

Non-prestressed (0 MPa) composite:

Figure 8-12 illustrates a fibre "kink-band" formation observed in a non-prestressed (0 MPa) composite. This kink-band failure was observed through thickness (2 mm) of the composite specimen in the end-tab region. An arrow mark in Figure 8-12 shows the propagation direction of the kink-band failure. From Figure 8-12 it can be observed that the kink-band has initiated near the free-edge of the composite.

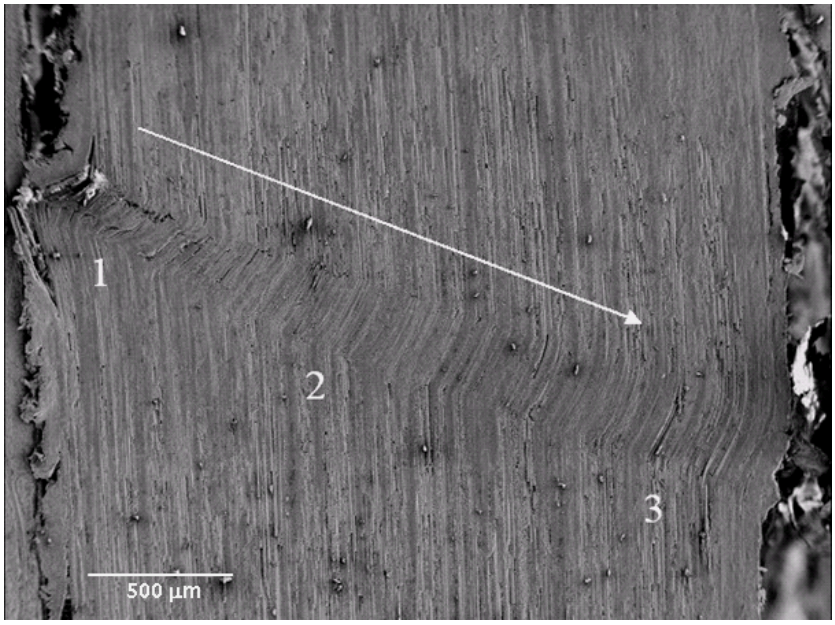

Figure 8-12: Kink-band failure mechanism observed in non-prestressed (0 MPa) composite.

Figure 8-13 and Figure 8-14 shows the positions 1 and 2 in Figure 8-12. With reference to Figure 8-13 it can be observed that initially the failure started as two bands of fibre-kinking, which then changed to one kink-band (see Figure 8-14). As the failure propagates the failure mode changed from kink-band to fibre buckling (position 3) as seen in Figure 8-12. The kink boundary orientation β was calculated to be 25° for the kink-band shown in Figure 8-14. The calculated kink-band orientation is within the typical rage (10° –30°) reported by Budiansky and Fleck.

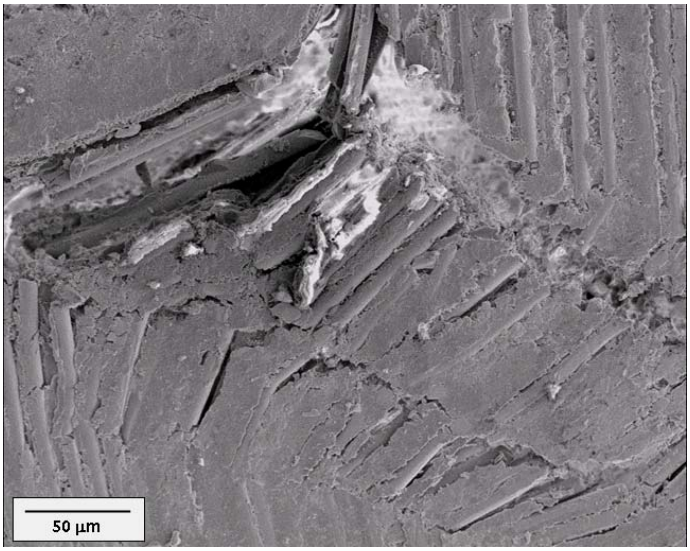

Figure 8-13: A magnified view of position 1 in Figure 8-12.

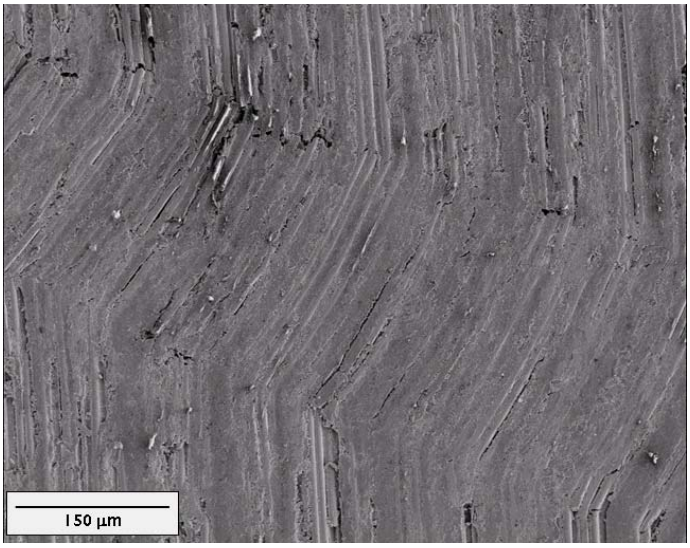

Figure 8-14: A magnified view of position 2 in Figure 8-12.

A close-in view of the Figure 8-11 (i) (compressive failure of 0 MPa prestressed composite) is presented in Figure 8-15. From Figure 8-15 it can be observed that multiple kink-band failure is apparent. From the microscopic examination it can be concluded that the 0 MPa prestressed composite fractures by a kink-band mechanism under compressive loading.

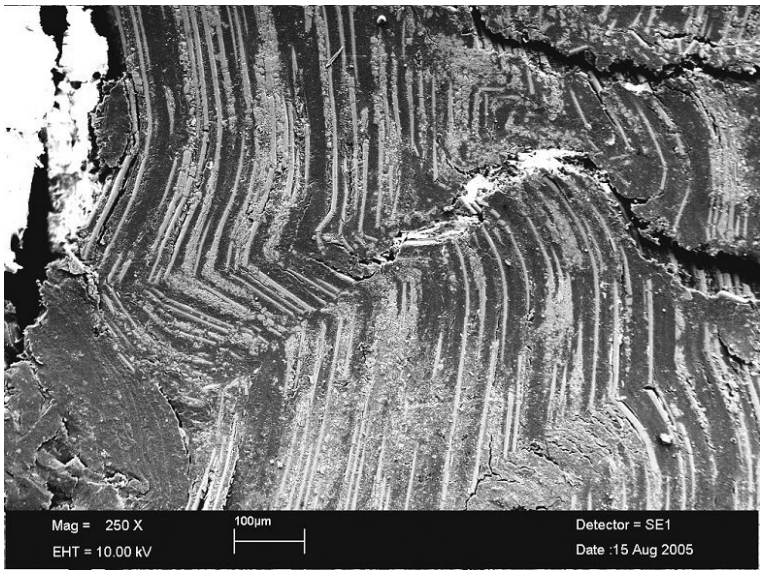

Figure 8-15: A magnified view of the Compressive failure of 0 MPa prestressed composite presented in Figure 8-11 exhibiting multiple kink-band formation.

Prestressed composite:

Prestressed composites showed extensive longitudinal splitting and fibre fracture as a result of compressive loading. Typical micrographs of prestressed composite compressive fractures are shown in Figure 8-16 and Figure 8-17.

From microscopic examination, it can be observed that prestressed composites exhibited fibre-matrix debonding (A), matrix deformation (B), hackle formation (C), fibre fracture (D) and fibre imprint (E) as shown in Figure 8-16 and Figure 8-17. In contrast to the non-prestressed composite, no fibre kink-band failure was observed.

In prestressed composite manufacture, as the fibres are prestressed, there is no possibility for the fibre to move and this reduces the fibre misalignment. When a compressive load is experienced by the prestressed composite, the brittle glass fibres fracture by crushing or collapsing damage, resulting in an imploded failure mode as represented in Figure 8-18.

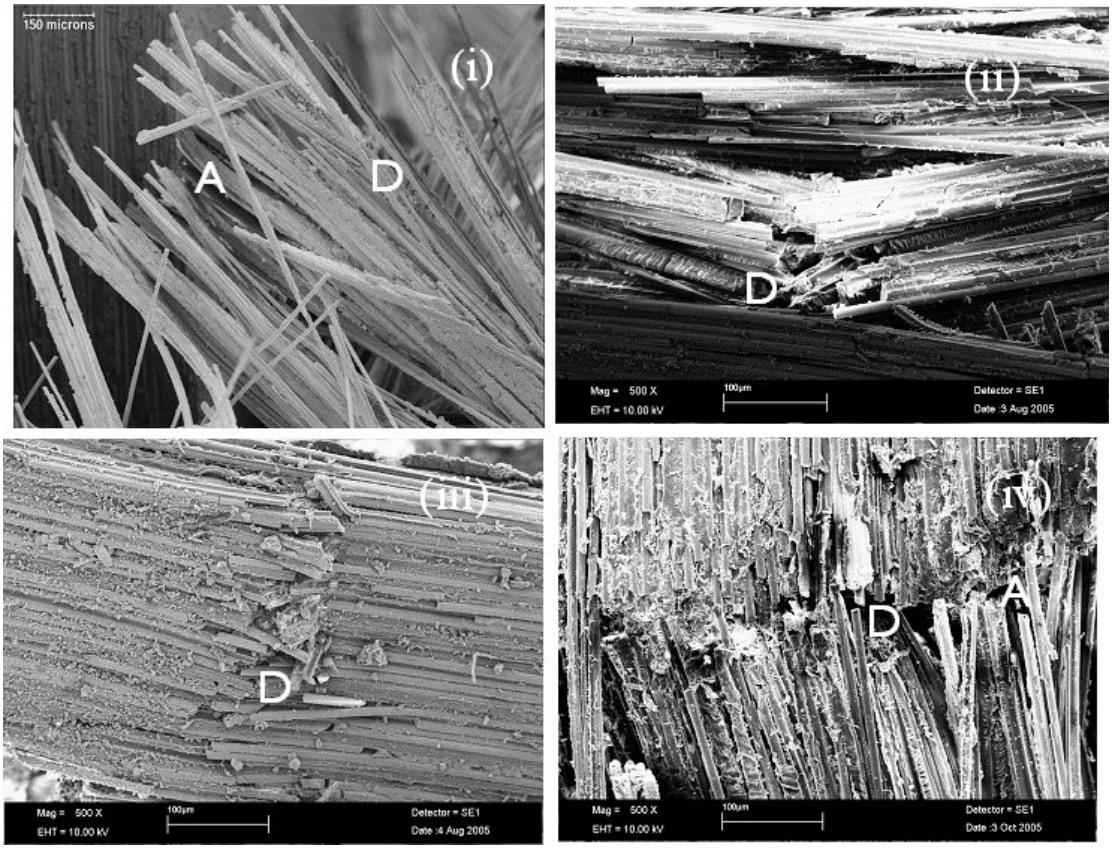

Figure 8-16: The typical fibre failure of prestressed composite in compressive loading. (i) 51 MPa, (ii) 80 MPa, (iii) 108 MPa and (iv) 150 MPa prestressed composite.

The fibre crushing mode of failure is apparent from the micrograph presented in Figure 8-16. In all prestressed composites more matrix hackle formation can be observed (see Figure 8-17), whereas in the 0 MPa prestressed sample no matrix hackle formation was observed. The possible reason for the observation of matrix hackle formation in prestressed composites is an improvement in fibre alignment and a change in the residual stresses in the matrix and interface.

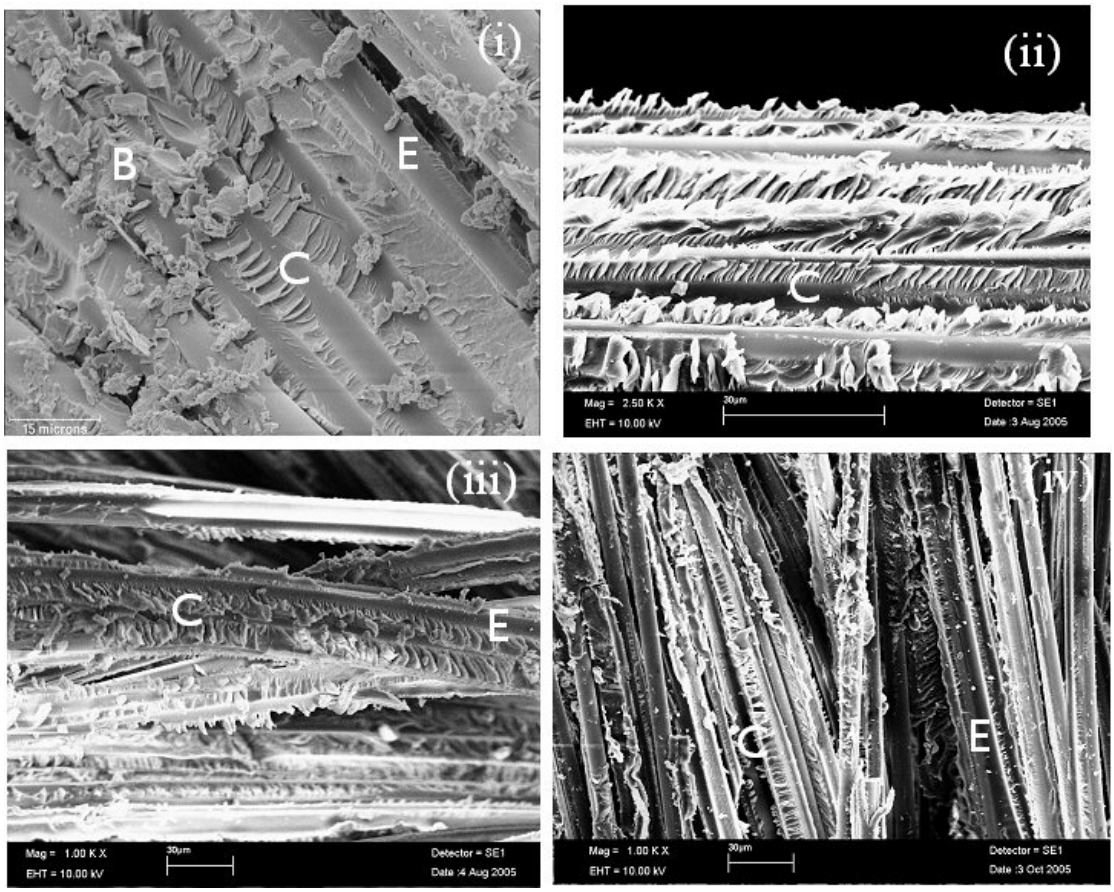

Figure 8-17: The typical matrix failure of prestressed composite in compressive loading. (i) 51 MPa, (ii) 80 MPa, (iii) 108 MPa and (iv) 150 MPa prestressed composite.

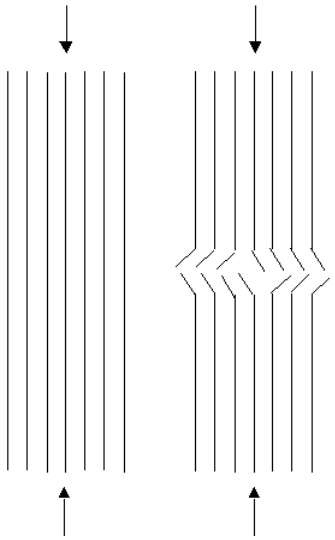

Figure 8-18: Schematic representation of imploded failure mechanism in prestressed composite during compressive loading.

Figure 8-19 shows a matrix "*curling*" fracture in a prestressed composite tested in compression. This type of matrix fracture in compressive loading of a unidirectional composite was not reported in the literature. In prestressed composites, by applying compressive stresses, matrix tensile residual stresses are reduced. With increasing prestress the compressive residual stress in the matrix will increase. When prestressed composites are subjected to compression, because of the improved fibre alignment and increase in matrix compressive stresses, the matrix could fracture normal to the fibre direction. When the fibre collapses the interfacial crack will propagate leading to relaxation of the residual stress in the interface and matrix, which could lead to *curling* of the matrix.

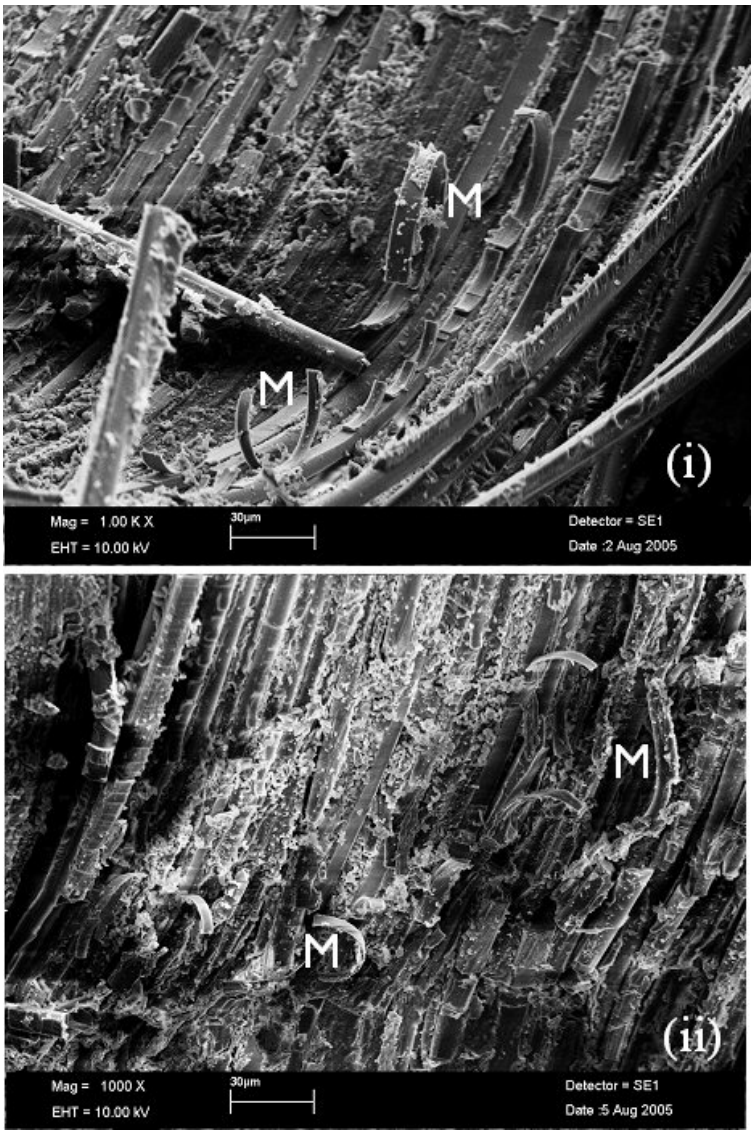

Figure 8-19: Matrix curling fracture in a prestressed composites. (i) 50 MPa and (ii) 108 MPa prestressed composite.

8.6 Concluding remarks

This chapter presented the results from static tensile and compressive properties of non-prestressed and prestressed composites. From the results presented the following conclusions can be made.

Static tensile properties

Fibre prestressed composites show an improvement in strain at deviation from linearity in their stress-strain curves. This suggests that prestressing could have increased the resistance to the onset of damage (matrix cracking, fibre-matrix debonding and weak fibre failure). This improvement in ε_{SDL} was observed up to 108 MPa prestress, above which it indicates a reduction. This suggests that an optimum prestress limit for the improvement in strain at deviation from linearity exists.

A theoretical prediction for the effect of prestress on the failure strain of composites was presented. This theory predicts that the fracture strain of the composite decreases with an increase in prestress. This is because the residual tensile stress in the fibre increases with prestress. This reduces the tensile fracture strain of the composite. However, from the experimental results no significant change in the tensile fracture strain was observed. This could be due to greater scatter in the measurements. It was also shown that the tensile strength and modulus of composites are independent of fibre prestressing.

From the macroscopic examination it can be concluded that there is no change in the composite failure mechanism with fibre prestress. However, from the microscopic examination it was found that at higher prestress levels more fibre fragmentation was observed. This could be due to (i) breaking of the weak fibres under the prestressing load leaving predominantly strong fibres in the composite and (ii) an increase in the tensile residual stress in the fibre with prestress. This results in an increased strain energy stored in the fibres.

Static compressive properties

Fibre prestressing gives an improvement in the average compressive strength and modulus by 9%. However, above an optimum prestress limit (108 MPa for compressive strength and 80 MPa for compressive modulus) the property reduces. This could be because of the increase in micro-residual stresses at the interface with fibre prestress, above the optimum limit the fibre-matrix interface is prone to debonding, which could lead to a reduction in compressive properties.

Fibre prestressing gives a change in compression damage mechanism. The non-prestressed (0 MPa) composites fractured by fibre kink-band formation, whereas prestressed composites fractured by extensive longitudinal splitting and matrix deformation. This

change in damage mechanism suggests that prestressing could have caused a reduction in the fibre waviness in composites.

From microscopic examinations, a curling mode of matrix failure was found in prestressed composites. This type of fracture mode has not been reported in the literature previously. The possible mechanisms for matrix curling could be due to the relaxation of the residual stress in the interface and matrix during fibre-matrix debonding.

CHAPTER 9

Fatigue behaviour

OVERVIEW

This chapter discusses the results from tension-tension (T-T) and tension-compression (T-C) fatigue behaviour of non-prestressed and prestressed unidirectional composites investigated in this study. Fatigue performance in both T-T and T-C modes are separately presented in four stages:

- The fatigue behaviour of non-prestressed composites is presented and compared with the published literature for the same material.
- The fatigue properties of prestressed composites are discussed by comparing the fatigue life in terms of *S-N* curves, normalisation techniques and Weibull statistics.
- The stiffness degradation and surface temperature rise during fatigue was studied to enable an understanding of the influence of prestress on damage development.
- Macroscopic and microscopic post-fatigue failure analysis was studied in order to assess the relation between the failure mode and prestress.

9.1 Tension-tension fatigue

9.1.1. Fatigue of non-prestressed composites

Figure 9-1 shows the normalised *S-N* curve for the non-prestressed unidirectional composite from the current work along with two similar systems published in the literature (Fernando and Al-Khodairi (GFAK), Broughton and Lodeiro (GBL)). The vertical axis in Figure 9-1 represents the peak stress normalised to the respective ultimate tensile strength

(UTS) for each of the composite systems. A summary of the lay-up sequence, ultimate tensile strength (UTS), fibre volume fraction and fatigue test parameters for the composites are presented in Table 9-1.

From Figure 9-1 and Table 9-1, it can be observed that firstly the relative slopes for the current work, GFAK and GBL data sets are very similar. Secondly, the scatter in the fatigue results for the current work, compared with GFAK and GBL data is less. Finally, a variation in fibre volume fraction of 51% to 62% does not seem to have an effect on fatigue properties.

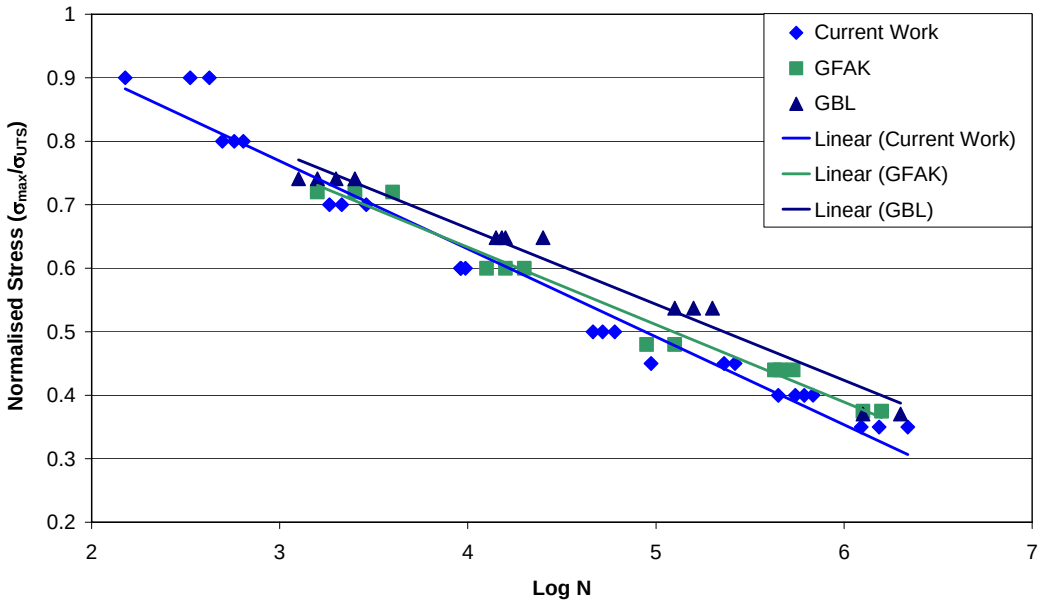

Figure 9-1: Comparison of normalised fatigue data of non-prestressed composite (current work) with similar systems reported in the literature.

Table 9-1: Summary of composite lay-up sequences and fatigue test parameters used in the current work and those reported by previous researchers.

Material (E-glass/913 epoxy)	Lay-up	Stress ratio (R)	UTS (GPa)	V_f (%)	Rate of stress application (kN s^{-1})
Current work	$[0]_{16}$	+0.1	1.31	58.2	250
GFAK	$[0]_{16}$	+0.1	1.16	62.2	500
GBL Error! Bookmark not defined.	$[0]_8$	+0.1	1.21	51.0	Fixed frequency 5 Hz

9.1.2. Fatigue of prestressed composites

Figure 9-2 represents the *S-N* curves for non-prestressed and prestressed composites with the UTS included in a linear-regression fit. The quasi-static UTS measured at 0.6 kN s^{-1} was included at 0.5 cycles (log 0.5 = -0.3) in the *S-N* curves. Table 9-2 shows the individual fatigue life results of non-prestressed and prestressed composites plotted in Figure 9-2. In the *S-N* curves, the issue of including the UTS at 0.5 cycles is questionable, because the UTS used at 0.5 cycles is measured from quasi-static test and not fatigue. Also the quasi-static test rate is different to the fatigue test rate. Therefore, *S-N* curves were also plotted without including the UTS at 0.5 cycles as shown in Figure 9-3.

Comparing Figure 9-2 and Figure 9-3 it can be observed that the *S-N* curves without including UTS show a linear behaviour in both low and high cycle fatigue regions. On the other hand, the *S-N* curves including the UTS show that the fatigue data at the low cycle region did not fit well to the linear behaviour observed at high cycle region. Both Figure 9-2 and Figure 9-3 shows a linear behaviour in the high cycle region *S-N* curves, this was previously observed by Mandell. Mandell conducted a series of experiments on different types of glass-fibre reinforced plastics (GFRP). He showed that when the number of cycles to failure lay between 10^2 and 10^6, the *S-N* curve can be approximated by a straight line of the form:

$$\sigma_{\max} = \sigma_{UTS} + b \log N \tag{9.1}$$

where σ_{max} is the maximum applied stress, σ_{UTS} is the ultimate tensile strength, N is the number of cycles to failure and b is a constant. The ratio of b/σ_{UTS} was defined by Mandell as the fractional loss in tensile strength per decade of cycles. The values of the slope (*b*) from linear-regression data analysis and the tensile strength decay per decade of cycle (b/σ_{UTS}) are summarised in Table 9-3.

From Table 9-3, it can be observed that fibre prestressing has minimised the tensile strength degradation per decade (b/σ_{UTS}) in composites when compared to non-prestressed composites. There is a reduction of 1% in the tensile strength degradation per decade with 51 MPa prestress.

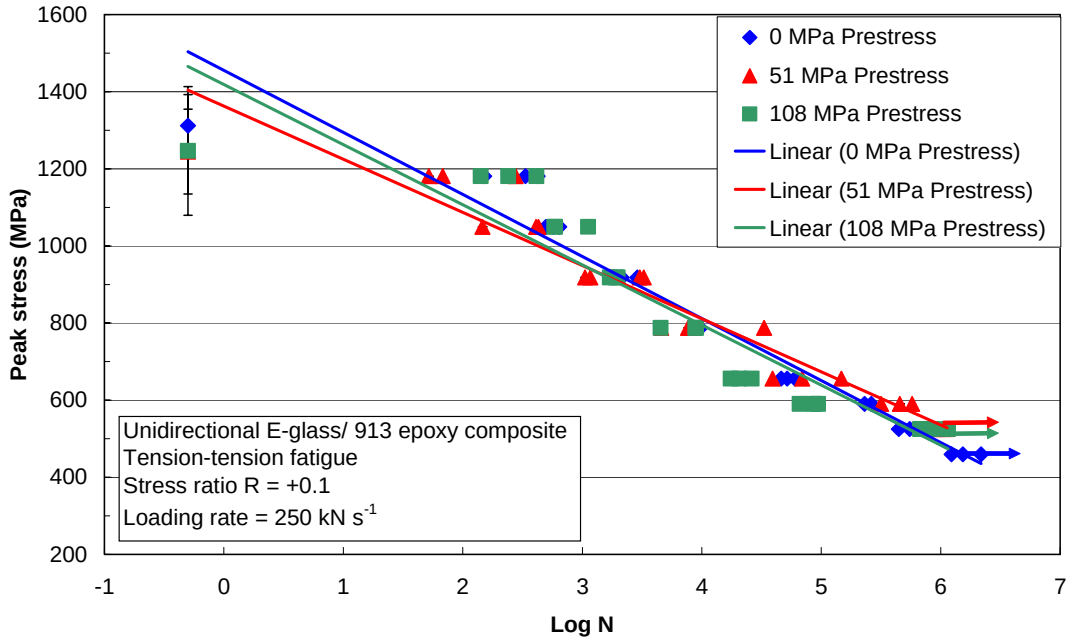

Figure 9-2: Comparison of the tension-tension fatigue results of the non-prestressed and prestressed composites. The linear regression fit was calculated including the UTS at 0.5 cycles. The arrow mark represents the sample run-out.

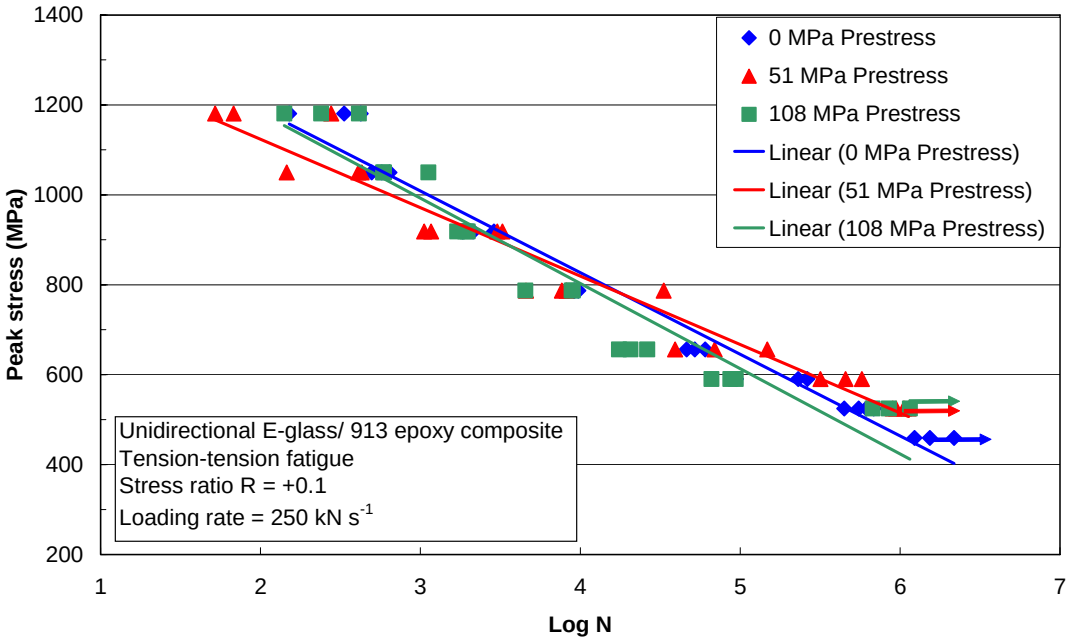

Figure 9-3: Comparison of the tension-tension fatigue results of the non-prestressed and prestressed composites. The linear regression fit was calculated without including the UTS at 0.5 cycles. The arrow mark represents the sample run-out.

Table 9-2: The individual fatigue life results of non-prestressed and prestressed composites plotted in Figure 9-2. The arrow mark (⇨) represents that the specimen ran-out.

Peak stress MPa	0 MPa		51 MPa		108 MPa	
	Number of cycles	Log N	Number of cycles	Log N	Number of cycles	Log N
1180.76	151	2.178	52	1.176	141	2.149
1180.76	334	2.523	68	1.832	240	2.380
1180.76	423	2.626	277	2.442	413	2.615
1049.56	641	2.806	146	2.164	1,122	3.049
1049.56	496	2.695	410	2.612	593	2.773
1049.56	574	2.758	430	2.633	585	2.767
918.36	1,841	3.265	3,026	3.480	1,702	3.230
918.36	2,138	3.330	3,262	3.513	1,910	3.281
918.36	2,887	3.460	1,167	3.067	1,977	3.296
918.36	-	-	1,057	3.024	-	-
787.17	9,206	3.964	33,229	4.521	4,537	3.656
787.17	9,702	3.986	8,195	3.913	8,978	3.953
787.17	9,140	3.960	7,670	3.884	8,834	3.946
655.97	46,302	4.665	39,175	4.593	20,586	4.313
655.97	52,027	4.716	69,275	4.840	17,479	4.242
655.97	60,321	4.780	147,790	5.169	26,249	4.419
590.38	94,131	4.973	577,556	5.761	86,772	4.938
590.38	262,964	5.419	455,483	5.658	66,216	4.820
590.38	230,227	5.362	317,964	5.502	94,015	4.973
524.78	446,633	5.649	900,042	5.954	851,335	5.930
524.78	550,935	5.741	942,689	5.974	673,667	5.828
524.78	614,721	5.788	1,130,147 ⇨	6.053	1,152,913 ⇨	6.061
524.78	-	-	1,058,439 ⇨	6.024	-	-
459.184	2,180,001⇨	6.338				
459.184	1,231,979 ⇨	6.090				
459.184	1,535,627 ⇨	6.186				

Table 9-3: Summary of slope (b) and degradation of tensile strength per decade (b/σ_{UTS}) of non-prestressed and prestressed composites.

Prestress (MPa)	Slope (*b*)	b/σ_{UTS} %
0	-161.0	11.1
51	-137.8	10.1
108	-156.0	10.9

However, from Figure 9-3, it can be seen that the 108 MPa prestressed composite fatigue data does not show a linear behaviour. Figure 9-4 presents a second order polynomial fit to the fatigue results without including the UTS. The polynomial fit was previously used by other researchers[85,87] to fit the fatigue data of unidirectional glass fibre/913 epoxy and cross-ply carbon/epoxy composites. From Figure 9-4, it can be seen that the low and high cycle fatigue regions of all the prestressed composites fit the polynomial curve. The polynomial curve fit could be used to estimate the number of cycles to failure at any given stress level between the UTS and the fatigue limit of the matrix (that is the run-out sample peak stress level).

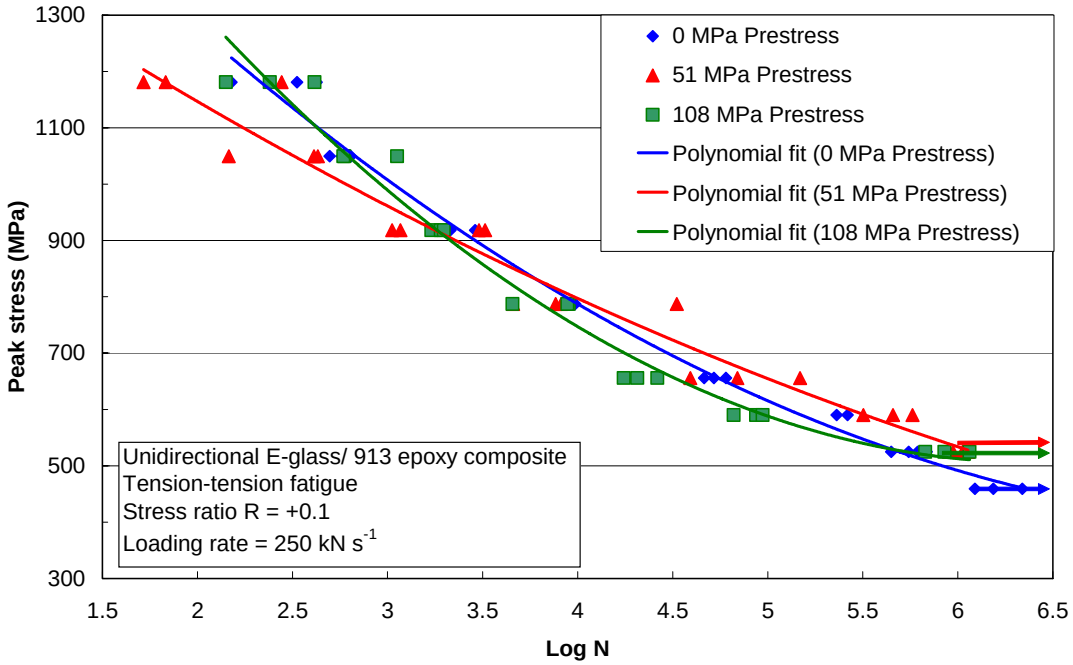

Figure 9-4: Comparison of the tension-tension fatigue results of the non-prestressed and prestressed composites. A second order fit was calculated without including the UTS.

9.1.3. Statistical analysis of fatigue data

Fatigue data from each set of non-prestressed and prestressed composites were subjected to statistical analysis to determine the effect of prestress on the fatigue life. Three types of statistical analysis were carried-out a) normalisation, b) Student *t*-test and c) a two-parameter Weibull distribution.

In order to compare the fatigue life of non-prestressed and prestressed composites, the fatigue peak stress (σ_{max}) was normalised with respect to the UTS as shown in Figure 9-5. The standard deviation presented in Figure 9-5 was calculated for the 95% confidence level. Harris *et al.*[126] have shown that by normalising the peak stress with respect to the UTS, the effect of different fibre strengths, fibre volume fractions and lay-up sequences can be eliminated.

From Figure 9-5, it can be observed that prestressing E-glass/913 composite resulted in an improvement in fatigue life in the low stress fatigue region. At a normalised stress of 0.4 (524 MPa peak stress), the improvement achieved in the average fatigue life for the 51 and 108 MPa prestressed composites were 1.75 and 1.55 times greater than that of the 0 MPa (non-prestressed) composite. However, at a normalised stress above 0.6, no significant variation in fatigue life was observed with prestress.

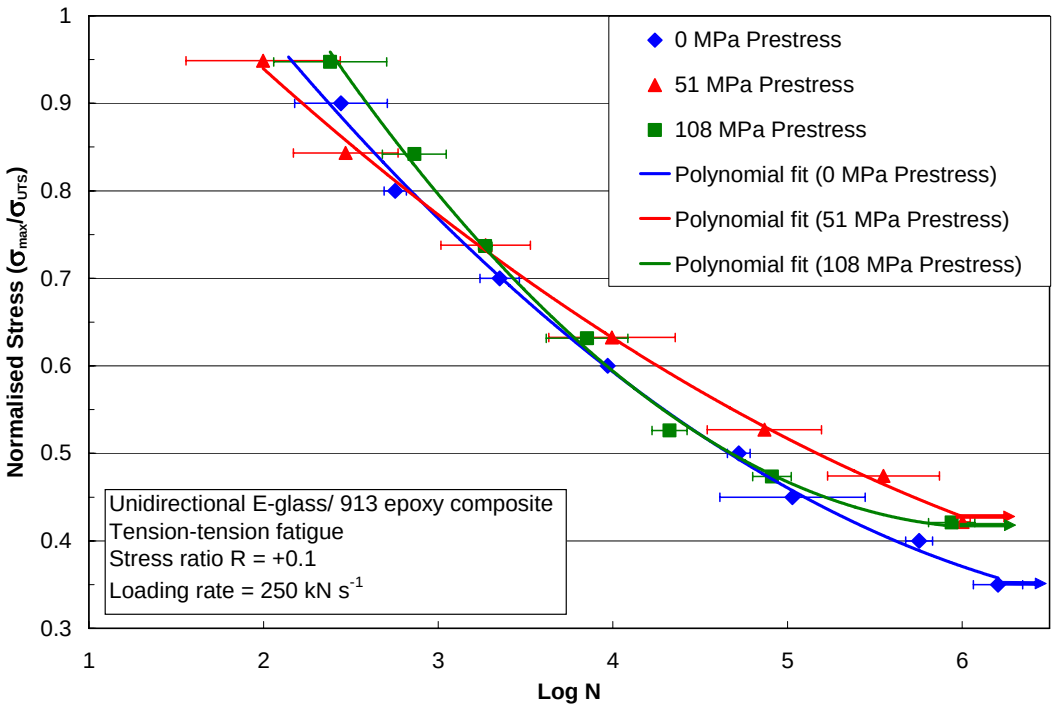

Figure 9-5: Comparison of normalised tension-tension fatigue of non-prestressed and prestressed composites. The error bars were calculated for 95% confidence level.

Figure 9-6 and Figure 9-7 show the fatigue life as a function of applied prestress in the low stress fatigue region (590 MPa and 524 MPa peak stress). At 590 MPa peak stress level three specimens with 80 MPa prestress were also tested to identify the optimum limit for the fatigue life improvement. With reference to Figure 9-6, it can be observed that the maximum fatigue life for the E-glass/913 epoxy composite system is at 51 MPa prestress. Above this prestress level, there is an indication of a reduction in fatigue life. This indicates that there is an optimum prestress limit to achieve maximum fatigue life. A student *t*-test was used to test the significance of the observed difference between the results of non-prestressed and prestressed composites at 524 MPa peak stress. The test showed that the non-prestressed and 51 MPa prestressed composites are significantly different at a 99% confidence level. From Figure 9-8, it can be observed that the fatigue life of non-prestressed and prestressed composites are all the same and shows that there is no influence of prestress in the high stress fatigue region.

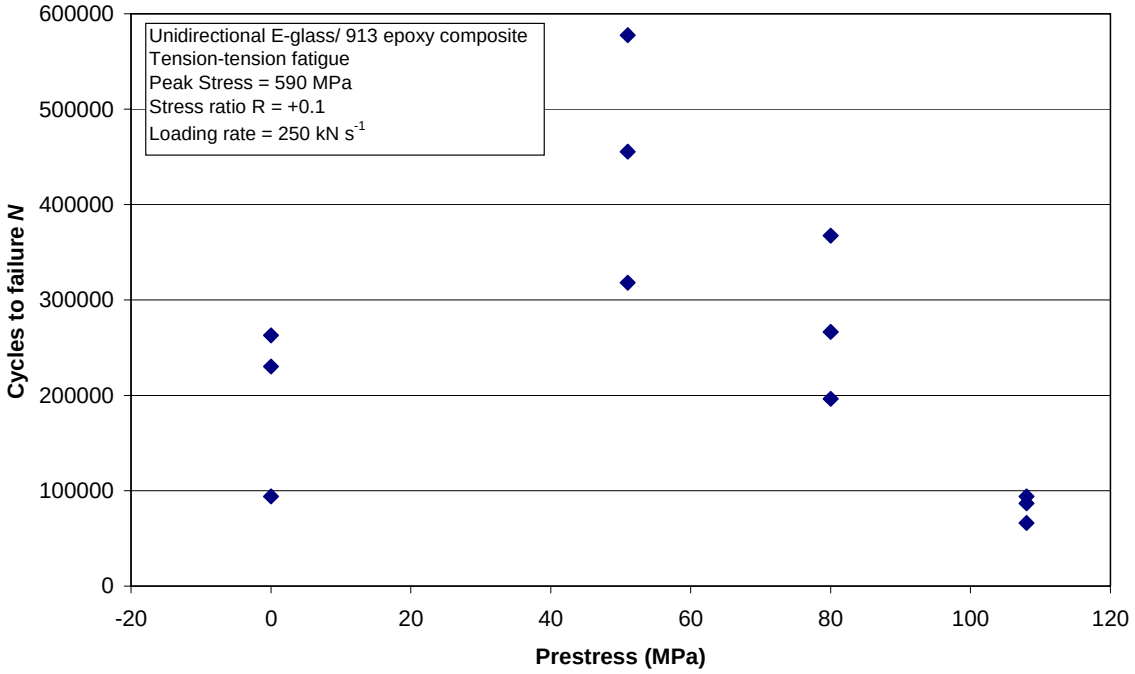

Figure 9-6: Fatigue life as a function of applied prestress in the low stress region (peak stress of 590 MPa).

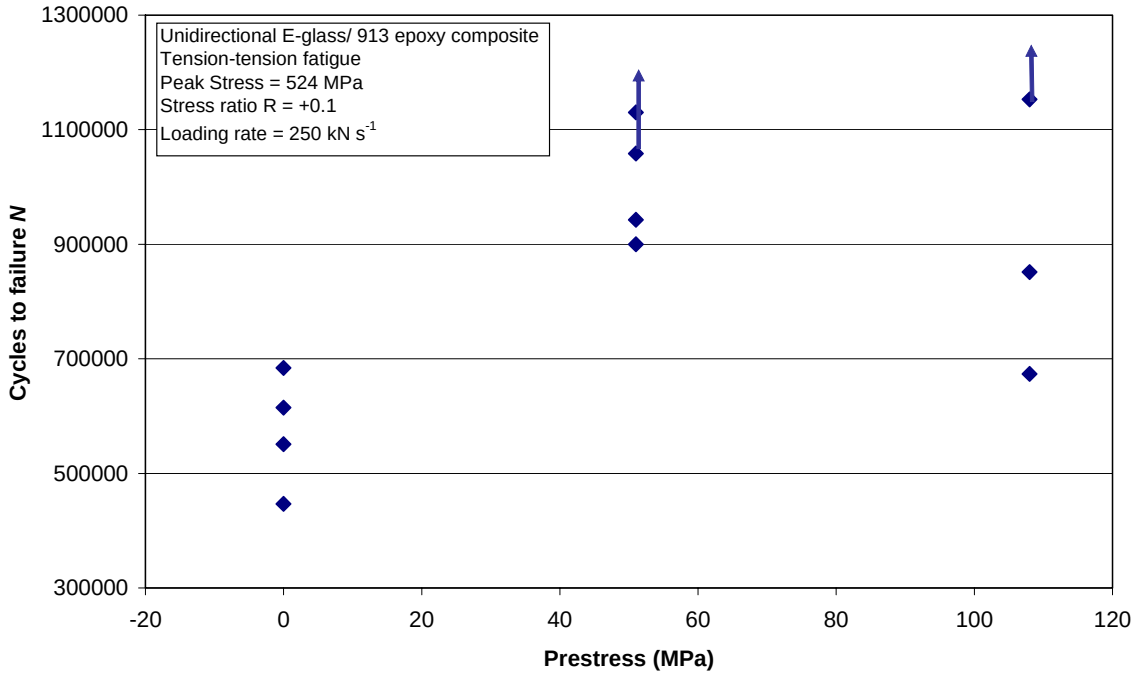

Figure 9-7: Fatigue life as a function of applied prestress in the low stress region (peak stress of 524 MPa). The arrow mark represents the specimen run-out.

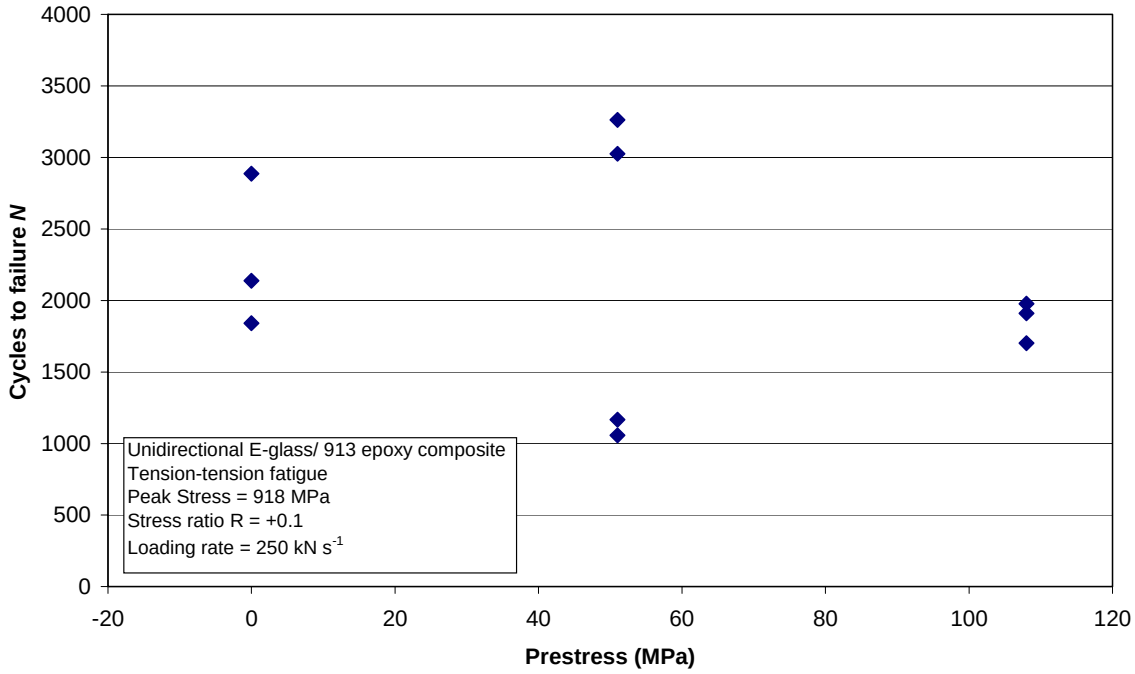

Figure 9-8: Fatigue life as a function of applied prestress in the high stress region (peak stress of 918 MPa).

Researchers[127,128] have shown that a two-parameter Weibull distribution function can be used to determine the degree of varibility of the fatigue life of the composite. A two-parameter Weibull distribution was calculated for the non-prestressed and prestressed composite fatigue life data. The two-parameter Weibull cumulative distribution function (Cdf) is given in Table 9-4.

Table 9-4: Plotting formulae for Weibull two-parameter distribution.

Distribution	Cdf *F(x)*	Horizontal axis	Vertical axis
Weibull two-parameter	$1-\exp\left(-\left(\frac{x}{\theta}\right)\right)^{m}$	$\ln(x_i)$	$\ln(-\ln(1-p_i))$

Here x_i is the cycles to failure; p_i is the probability plotting position given by the formula $(i-0.5)/n$; n is the total number of samples; θ is the characteristic value or scale parameter; m is the shape parameter usually called the Weibull modulus and reflects the degree of variability in the fatigue life. For example, the higher is the Weibull modulus, the less variable is the fatigue life.

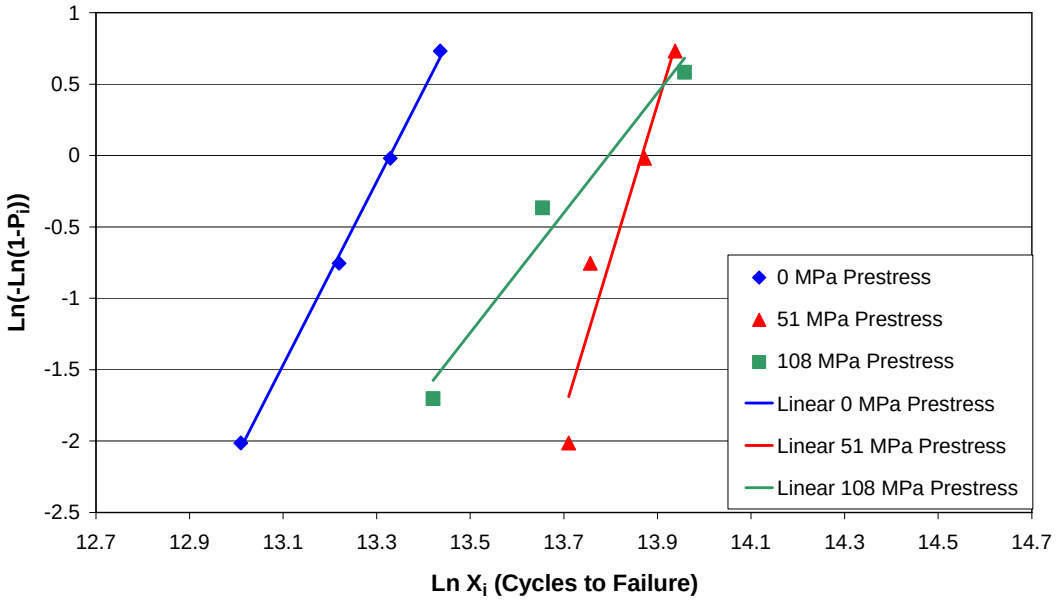

Figure 9-9: Weibull distribution for fatigue life at 524 MPa peak stress level (low stress level).

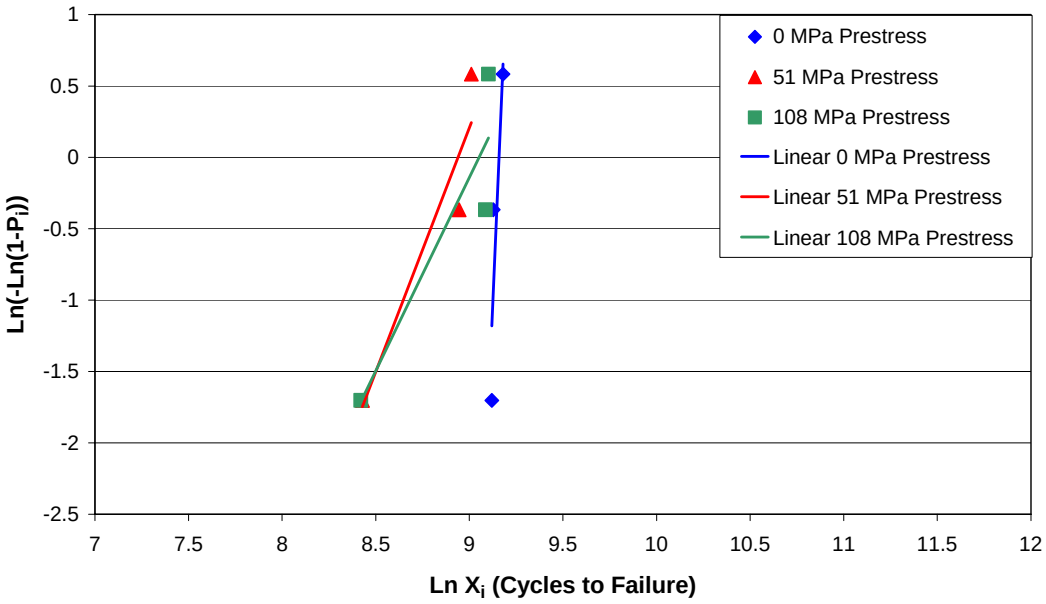

Figure 9-10: Weibull Distribution for fatigue life at peak stress level 788 MPa (middle stress level).

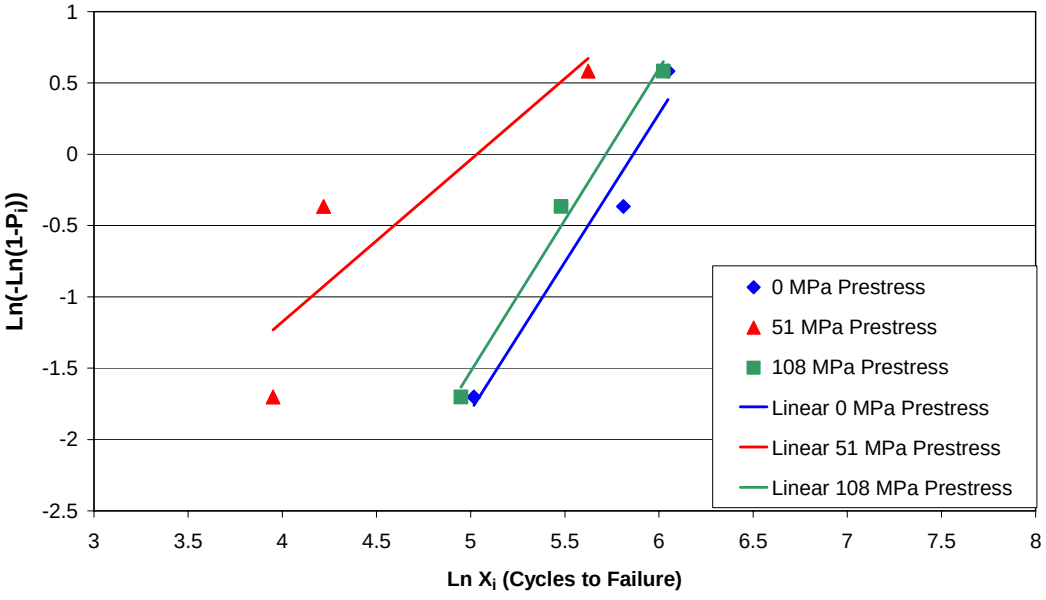

Figure 9-11: Weibull distribution for fatigue life at 1180 MPa peak stress level (high stress level).

Table 9-5 presents the Weibull modulus for the prestressed composites presented in Figure 9-9 to Figure 9-11. It can be seen that the Weibull modulus of 51 MPa prestressed composites is higher than the non-prestressed composite for low stress fatigue (524 MPa). This shows that the degree of variability in fatigue life of 51 MPa prestressed composites is

smaller than for the non-prestressed composite. This also supports the concept that the improvement in fatigue life observed at 51 MPa prestressed composites is statistically significant. However, from Table 9-5 it can be observed that the Weibull modulus is small in all the composites at high stress fatigue (1180 MPa).

Table 9-5: Summarises the Weibull modulus of non-prestressed and prestressed composites presented in Figure 9-9 to Figure 9-11.

Prestress MPa	Weibull modulus (*m*)		
	Peak stress 524 MPa	Peak stress 788 MPa	Peak stress 1180 MPa
0	6.4197	30.757	2.0826
51	10.781	3.4143	1.1388
108	4.199	2.7084	2.1251

Low stress level fatigue

From the normalisation (see Figure 9-5), student *t*-test (see Figure 9-6 to Figure 9-8) and Weibull distribution (see Figure 9-9 to Figure 9-11 and Table 9-5), it can be seen that in the low stress fatigue region there is an improvement in fatigue life with prestress. Talreja showed that in the low stress region, matrix cracking and fibre/matrix interfacial debonding are the predominant damage mechanisms. Therefore, low stress level fatigue performance of composite materials depends on the matrix and interfacial properties or in other words matrix and interface resistance to crack initiation and crack growth.

During composite processing, tensile residual stresses are developed in the matrix and corresponding compressive residual stresses are developed in the fibres due to anisotropic thermal expansion of the composite constituents (fibre and matrix). In extreme cases the tensile stress component in the matrix can be as high as the matrix yield strength[1,129]. When the composite is subjected to an external mechanical load, the first damage can prematurely occur in the matrix due to these tensile residual stresses. On the other hand in a prestressed composite, the matrix is subjected to a compressive stress due to the release of fibre prestress. This in turn reduces the process-induced tensile residual stresses in the matrix. This reduction in residual tensile stresses in the matrix would increase the strain to crack initiation and/or crack propagation in the matrix. This could have resulted in the improvement in fatigue life of the composite and suggests that prestressed composites have improved resistance to matrix damage.

From Figure 9-6, it can also be observed that there is a reduction in fatigue life above the optimum limit (51 MPa prestress). Mottahari and Cameron have also shown that there is an optimum prestress limit above which the residual stresses at the fibre/matrix interface

increase. This may reduce the resistance to interfacial crack initiation and/or crack growth. This suggests that the observed reduction in fatigue life above the optimum prestress level may be attributed to the weak interfacial crack resistance.

Middle and high stress level fatigue

From Figure 9-5, Figure 9-8, Figure 9-10 and Figure 9-11, it can be observed that above 0.55 normalised peak stress, regardless of prestressing, the fatigue life of composites are the same. This may be because the strain induced in the composite during fatigue is well above the matrix cracking strain. Also other researchers[92,107,133] have shown that in high stress fatigue, the fatigue damage is a combination of matrix cracking, interfacial debonding, delamination and fibre fracture. Above 0.8 normalised peak stress the 51 MPa prestressed composite indicated a reduction in the fatigue life. However, a statistical analysis of the data using the student *t*-test showed that there is no significant difference between the 0 MPa and 51 MPa prestressed composites.

9.1.4. Fatigue damage monitoring

In this study, the damage induced during fatigue loading was studied in non-prestressed and prestressed composites using two methods (1) real-time monitoring of stiffness degradation[88,130] and (2) surface temperature rise[131,132]. Visual inspection of specimens was also carried out. Reifsnider and other researchers[107,85] have shown that with a cyclic load, the reduction in stiffness happens continuously over a period of time and this is an excellent indicator of the damage development in composite materials. It has also been shown[131,132] that the surface temperature rise can be used as an indicator of damage development since much of the energy released during fatigue is converted into heat. The temperature rise is generally measured using an infrared thermographic technique. However, it was not possible to use this technique as it was not available and an alternative technique using a surface-bonded thermocouple was used. In this study all the fatigue test specimens were instrumented with a surface-mounted extensometer (to measure the strain) and a surface-bonded thermocouple (to measure the change in surface temperature of the specimen). The strain and corresponding load measurements were used to calculate the change in stiffness.

Non-prestressed composite

Figure 9-12 shows the normalised stiffness and surface temperature change as a function of fatigue life for a non-prestressed composite during fatigue testing at 655 MPa peak stress.

In general, the stiffness degradation during fatigue exhibited a three-stage behaviour. This was also reported by other researchers[88, 107,85]. Stage I is characterised by an initial decrease in stiffness and usually corresponds to 10% of the fatigue life. Stage II is an intermediate

but long period of approximately 85 – 90% of the fatigue life. During this period, stiffness reduction was observed to be small. Stage III is very short-lived and is characterised by a rapid decrease in stiffness as a result of catastrophic failure of the specimen. This catastrophic "sudden-death" behaviour of glass /epoxy composites was also reported by Dharan[133] and Curtis. The rapid decrease in stiffness values in stage III correlates with extensive splitting parallel to the fibres and delamination of the specimen, leading to a brush-like failure.

Steif[134] showed that fibre breakage, combined with interfacial debonding of the fibre/matrix interface, would lead to stiffness reductions. Furthermore, Fernando and Al-Khodairi have shown that the extent of the interfacial debonding was higher for samples tested at higher cyclic stress. Curtis[135] has shown that in unidirectional glass/epoxy composites, matrix cracking and interfacial debonding causes longitudinal splitting of fibres. He further showed that the rate of degradation processes in the matrix and at the interface is a function of the bulk strain in the resin as well as the nature of the matrix.

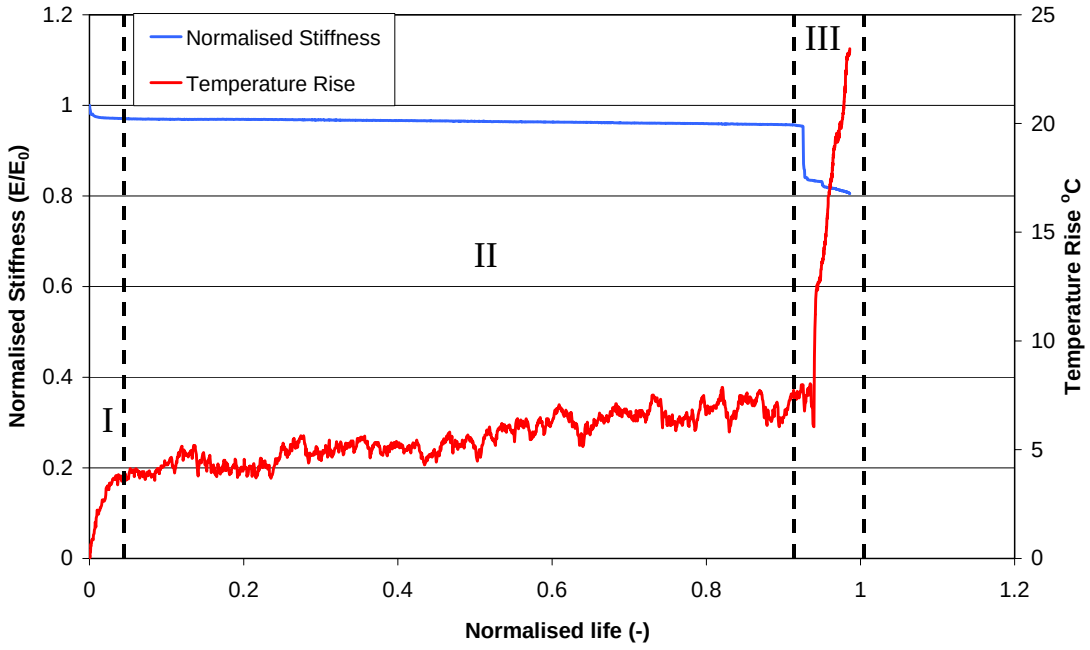

Figure 9-12: The normalised stiffness and surface temperature change as a function of fatigue life.

From Figure 9-12, it can also be observed that the surface temperature change showed a three-stage behaviour similar to the stiffness decay. Stage I shows a rapid increase in temperature. Stage II shows a small increase in the temperature rise. Stage III shows a rapid increase in temperature when approaching failure. One of the limitations of the surface-bonded thermocouple technique is the location of the thermocouple with respect to the fracture zone, which can greatly influence the measured surface temperature. In other

words, if a thermocouple were located in the vicinity of a longitudinal split or internal delamination, then a high surface temperature would be recorded. Also delamination of the surface plies in some experiments resulted in the thermocouple becoming ineffective.

During fatigue testing damage development in the composite was also monitored by visual examination of the specimens. Figure 9-13 shows the macroscopic damage development in a unidirectional composite during fatigue testing at 787 MPa peak stress. In stage I of the fatigue life, no macroscopic damage was observed. However, acoustic emissions were noticed. Bhat and Murthy[136] have shown that during fatigue of unidirectional glass fibre/epoxy composites, acoustic emissions during stage I correspond to the occurrence of a number of matrix cracks initiated and distributed over the specimen length. This could explain the possible reason for the initial reduction in stiffness and increase in surface temperature.

In stage II, at 0.2 normalised life, initiation of longitudinal splits in the surface ply of the specimen was observed (see Figure 9-13 (b)). The longitudinal splits were seen to propagate along the whole gauge length of the specimen. These longitudinal splits initiate and grow through the width (see Figure 9-13 (c and d)) and thickness (see Figure 9-13 (e)) of the composite resulting in the delamination of the inner plies. This makes the specimen act as several samples gripped together at the end-tab regions. Therefore, the load transfer between these longitudinal splits becomes limited.

When nearing the end of life (stage III), extensive longitudinal splitting resulting in catastrophic fracture was observed. This leads to the classic brush-like failure of the specimen (see Figure 9-13 (f)). In stage III it was also observed that the width of the longitudinal split reduces. In addition, the catastrophic fracture of fibres at the very end of the life emits tiny particles of fibres and matrix (see Figure 9-13 (f)).

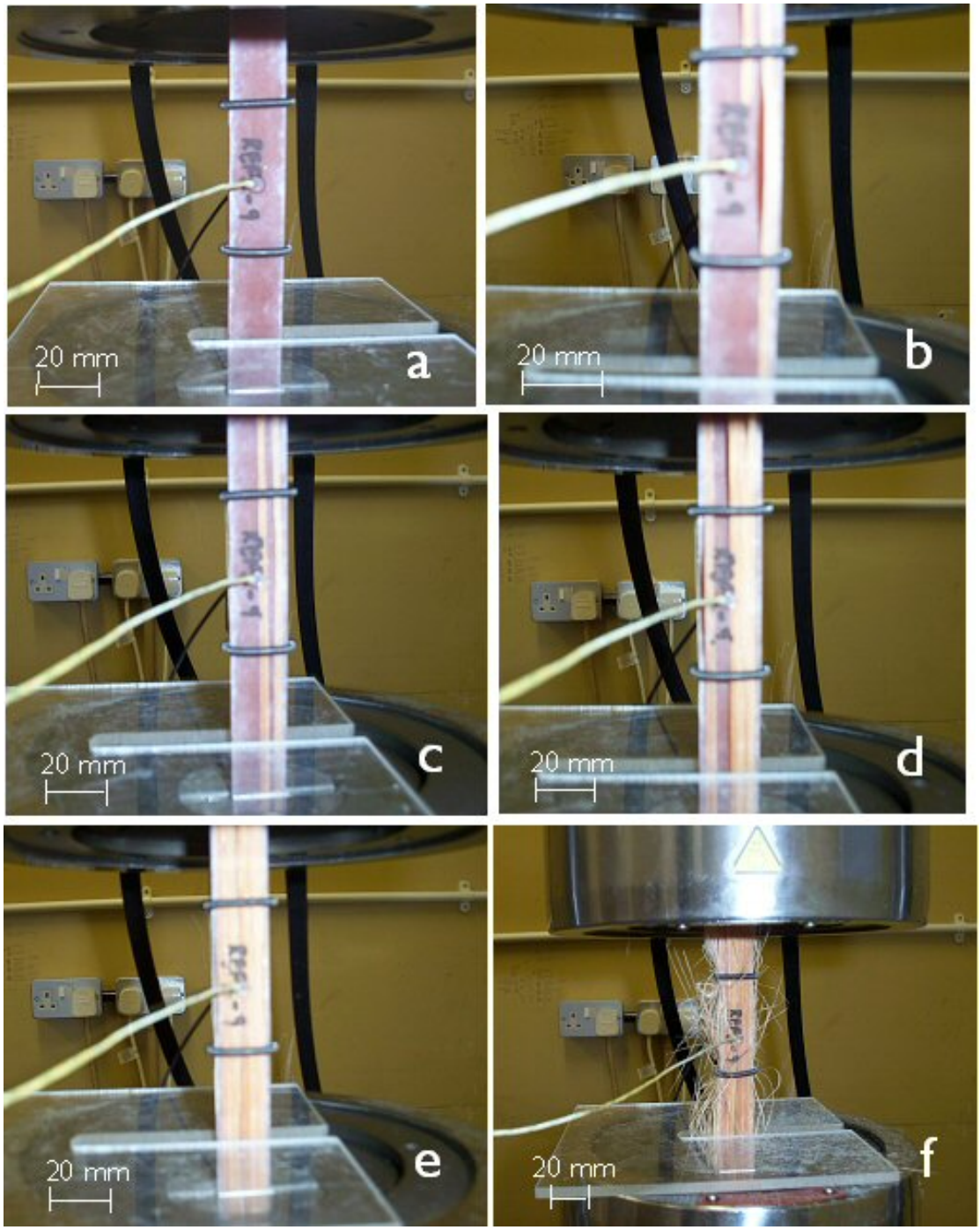

Figure 9-13: The macroscopic damage mechanisms observed visually during the tension-tension fatigue test of a unidirectional composite at 787 MPa peak stress. a) Normalised life 0, b) Normalised life 0.2, c) Normalised life 0.4, d) Normalised life 0.55, e) Normalised life 0.8 and f) Normalised life 1.

Prestressed composite

Figure 9-14 and Figure 9-15 show the stiffness reduction of non-prestressed (0 MPa) and prestressed composites during fatigue testing at peak stresses of 655 MPa and 1050 MPa, respectively. Table 9-6 and Table 9-7 summarise the stiffness degradation at selected normalised life of non-prestressed and prestressed composites. Appendix D presents the stiffness degradation at selected normalised life for all the individual samples tested at 655 MPa and 1050 MPa peak stress. In general, prestressed composites showed a three-stage behaviour for the stiffness reduction and surface temperature rise similar to that observed for a non-prestressed composite. With reference to Figure 9-14, it can be observed that in the low stress fatigue region (655 MPa), prestressed composites show an increase in resistance to stiffness degradation during stage II of the fatigue life. This suggests that the micro-crack initiation has been attenuated, and/or crack growth is reduced as a consequence of reduction in the tensile residual stresses in the matrix. The stiffness degradation in the low stress fatigue region correlates with the results from fatigue life.

On the other hand in high stress level fatigue (1050 MPa), prestressed composites show rapid stiffness degradation in both stage I and II (see Figure 9-15). The decrease in the resistance to stiffness degradation in prestressed composites at high stress level regions could be attributed to the increase in tensile residual stresses in fibres with prestress.

The surface temperature measurements from the thermocouple at low and high stress fatigue regions are presented in Figure 9-16 and Figure 9-17. In general, it can be seen that the surface temperature change measured in a prestressed composite shows a three-stage behaviour similar to a non-prestressed composite. It can be seen from Figure 9-16 and Table 9-7 that in a low stress region the surface temperature rise in prestressed composites during stage I of the fatigue life was slightly less when compared to non-prestressed composite. In stage II of the fatigue life a slightly higher temperature rise was recorded in prestressed composites. However, the temperature rise recorded from the prestressed composite was lower than the non-prestressed composite in stage III (see Figure 9-16).

The surface temperature rise in a high stress region (1050 MPa) shows a rapid linear increase with normalised fatigue life in non-prestressed and prestressed composites (see Figure 9-17). It can be observed that the surface temperature rise in prestressed composites is higher when compared to the non-prestressed composite. This could be due to accelerated damage because of the presence of the greater magnitude of micro-residual stresses in the interface and tensile residual stress in fibres.

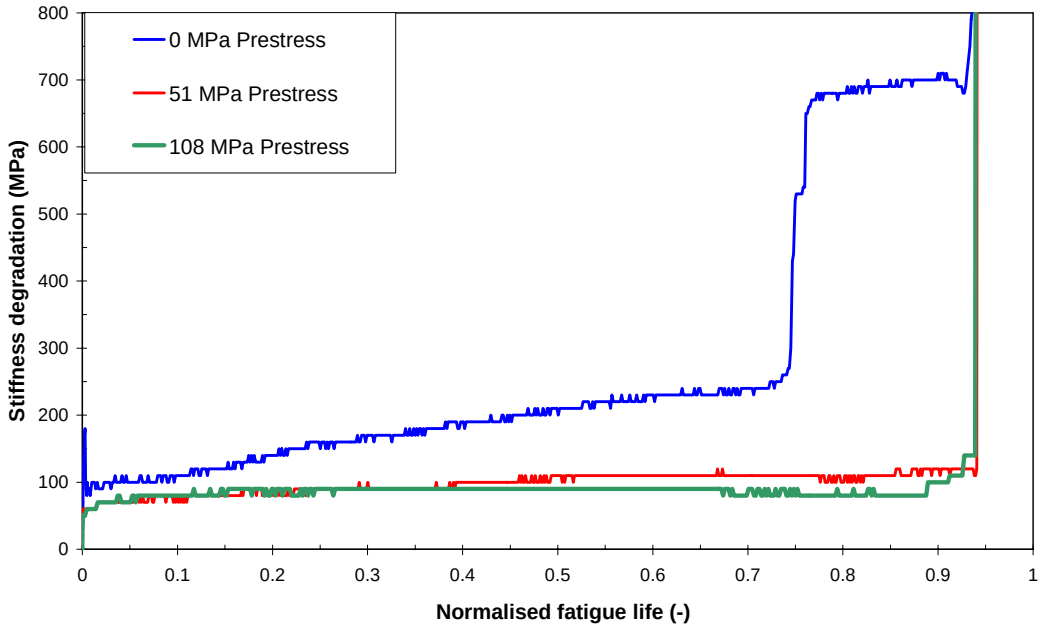

Figure 9-14: Stiffness reduction of non-prestressed and prestressed composites at 655 MPa peak stress.

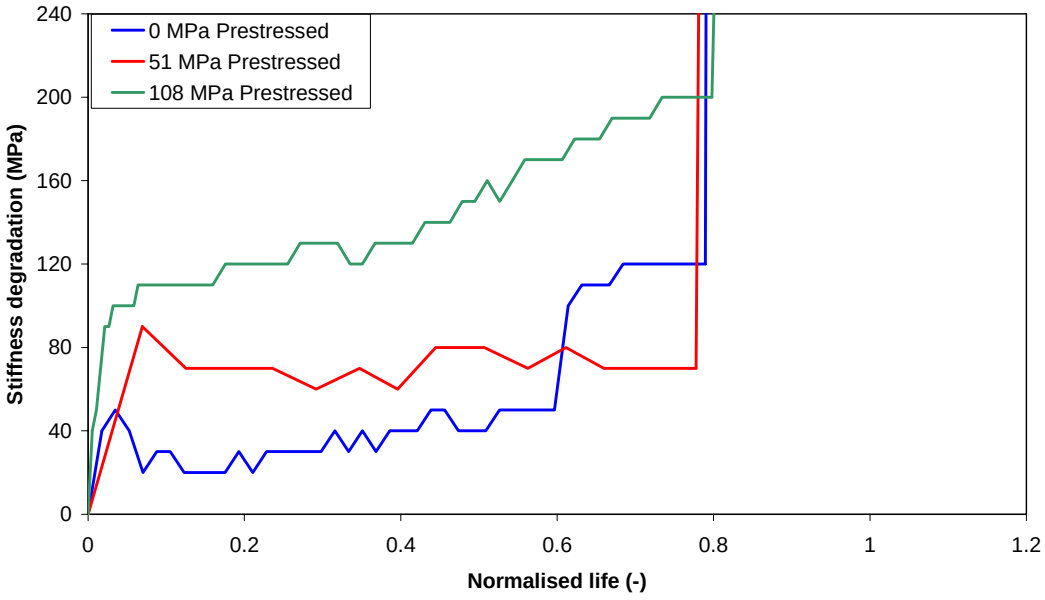

Figure 9-15: Stiffness reduction of non-prestressed and prestressed composites at 1050 MPa peak stress.

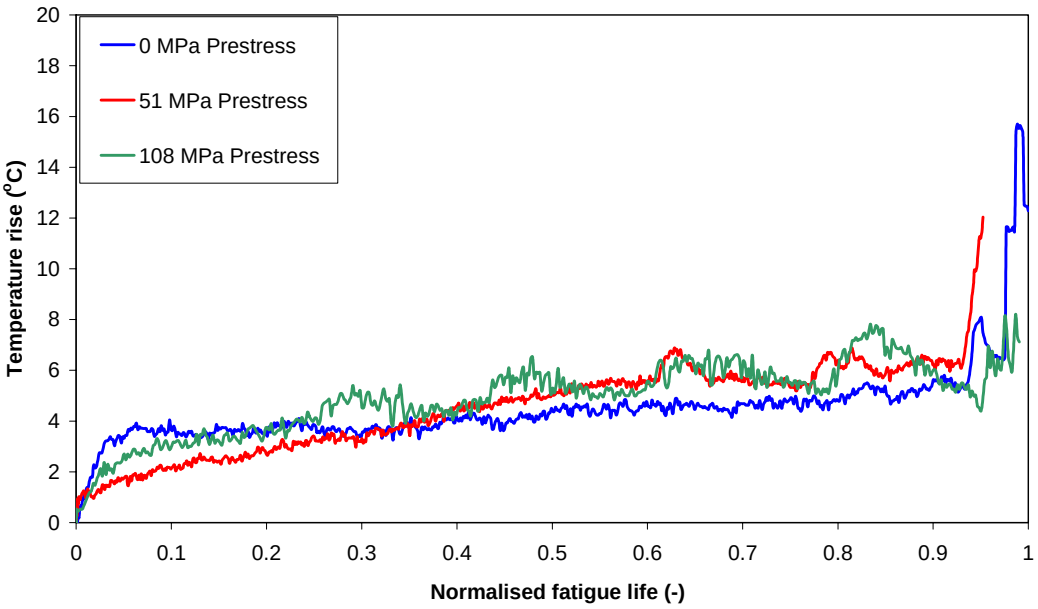

Figure 9-16: Surface temperature rise of non-prestressed and prestressed composites at 655 MPa peak stress.

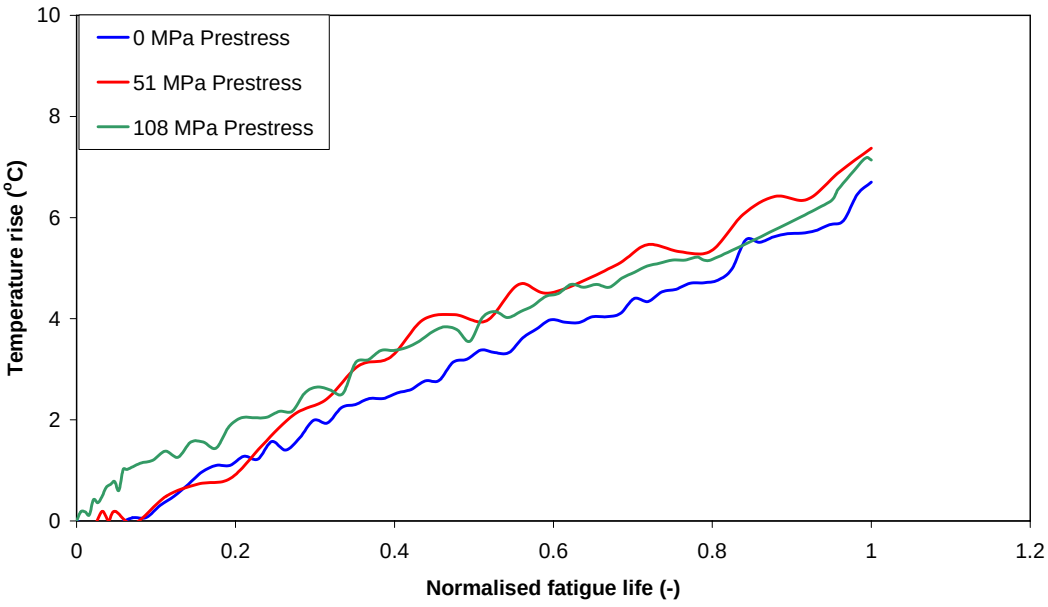

Figure 9-17: Surface temperature rise of non-prestressed and prestressed composites at 1050 MPa peak stress.

Table 9-6: Summary of the stiffness degradation and surface temperature changes for the non-prestressed and the prestressed composites at a peak stress of 655 MPa in T-T fatigue.

Normalised life	Stiffness degradation (MPa)			Temperature rise (°C)		
	Prestress (MPa)			Prestress (MPa)		
	0	51	108	0	51	108
0.1	110	80	80	3.7	2.1	2.8
0.3	170	100	90	3.6	3.3	4.5
0.5	200	110	90	4.4	5.0	5.3
0.7	680	110	90	4.7	5.7	6.2
0.9	710	120	100	5.6	6.2	6.0

Table 9-7: Summary of the stiffness degradation and surface temperature changes for the non-prestressed and the prestressed composites at a peak stress of 1050 MPa in T-T fatigue.

Normalised life	Stiffness degradation (MPa)			Temperature rise (°C)		
	Prestress (MPa)			Prestress (MPa)		
	0	51	108	0	51	108
0.1	30	30	110	0.3	0.1	1.3
0.3	30	40	130	2.0	2.4	2.6
0.5	40	70	150	3.3	3.9	3.5
0.7	120	70	190	4.4	5.5	4.9
0.8	3110	1680	18150	4.7	5.3	6.3

9.1.5. Post-failure analysis

This section will concentrate on the effect of prestress on macroscopic and microscopic damage in the composite materials investigated in this study.

Macroscopic post-fatigue (T-T) fracture

Figure 9-18 shows the macroscopic fatigue failure of non-prestressed and prestressed composites at a 1050 and 524 MPa peak stress level respectively. At high stress levels, see Figure 9-18 (a), it can be observed that both the non-prestressed and prestressed composites show a brush-like failure. This type of macroscopic fatigue failure was also observed by many researchers[89,85,122,132,133,135].

It can be observed from Figure 9-18 (b) that the samples in low stress level tests (524 MPa) show a significant reduction in the number of longitudinal splits. In general, it was

observed that the width and thickness of the longitudinal splits were greater at the low stress level. In low stress level fatigue the density of the damage in prestressed composites is less than in the non-prestressed composite (see Figure 9-18 (b)). The extent of longitudinal splitting and delamination was significantly reduced in prestressed composites. This could be attributed to the reduction in the tensile residual stresses in the matrix, which could have increased the resistance to longitudinal split initiation and split growth. It can be seen from Figure 9-18 (a) that in high stress level fatigue there is no difference between the fracture of non-prestressed and prestressed composite.

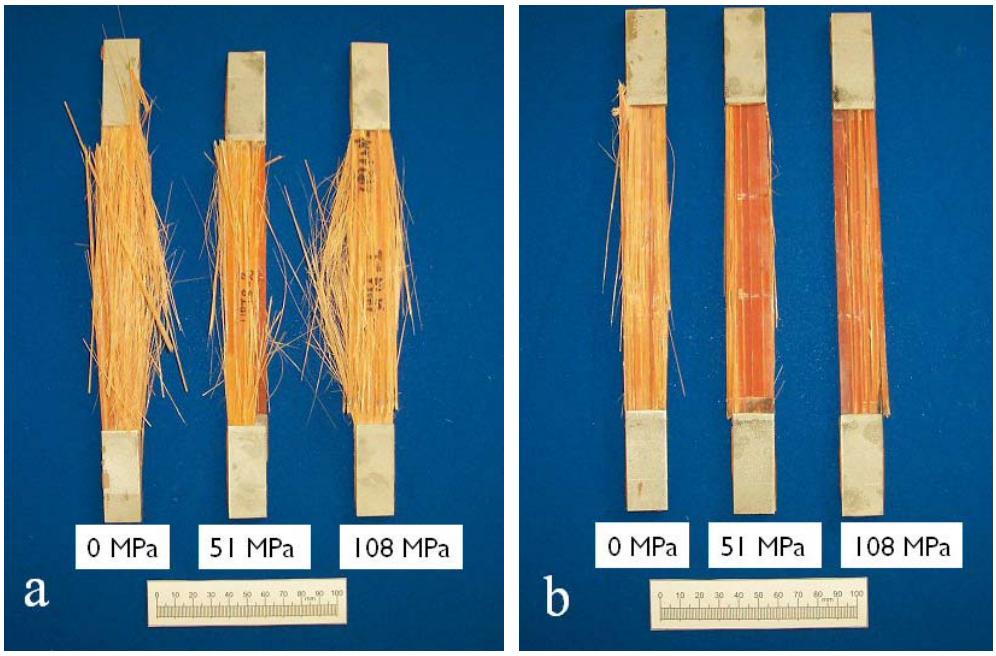

Figure 9-18: Representative macroscopic fatigue failure of non-prestressed and prestressed composites. a) 1050 MPa peak stress and b) 524 MPa peak stress.

Microscopic post-fatigue (T-T) fracture

Figure 9-19 to Figure 9-21 show the fracture surfaces of non-prestressed and prestressed composites at higher stress levels. Features such as fibre pull-out (a), matrix hackle formation (b), clean fibre surface (c), matrix plasticity (d) and fibre impression (e) can be observed.

Figure 9-22 to Figure 9-24 show the low stress fatigue damage in non-prestressed and prestressed composites. Two of the major features that characterise the fracture are hackle formation and fibre impression.

The shear failure of the matrix between two fibres or laminates resulting from the inter-fibre or inter-laminate shear stresses are referred to in the literature as hackles, serrations,

lacerations, chevrons and cusps[137, 138, 139]. A mechanism of hackle formation was proposed by Purslow and this is explained here.

When a band of epoxy matrix is subjected to a shear stress, failure will commence as a series of micro-tensile fractures in the plane of the shear band. This is generally observed to be about 45° degrees as shown in Figure 9-25. With increasing shear stress the number of tensile cracks will increase, and individually they will elongate (see Figure 9-25 (b)), and curve over as they approach the limits of the shear band (Figure 9-25 (c)). Ultimate shear failure occurs along the line of cracks when these tensile failures simultaneously coalesce, see Figure 9-25 (d). Figure 9-26 and Figure 9-27 show examples of this fractography of shear bands or hackle formation in non-prestressed composite.

From Figure 9-22 to Figure 9-24, it can be seen that the extent of hackle formation in low stress level fatigue is greater than in the high stress level fatigue (see Figure 9-19 to Figure 9-21). This indicates that the low stress level fatigue involves more interlaminar shear fracture and that the matrix dominates the damage. It was observed from the fractures in the low stress level fatigue tests that the non-prestressed and prestressed composites exhibit similar fracture features.

From the high stress level fatigue fracture (see Figure 9-19 to Figure 9-21) it was observed that there is no difference in fracture morphology between non-prestressed and prestressed composites.

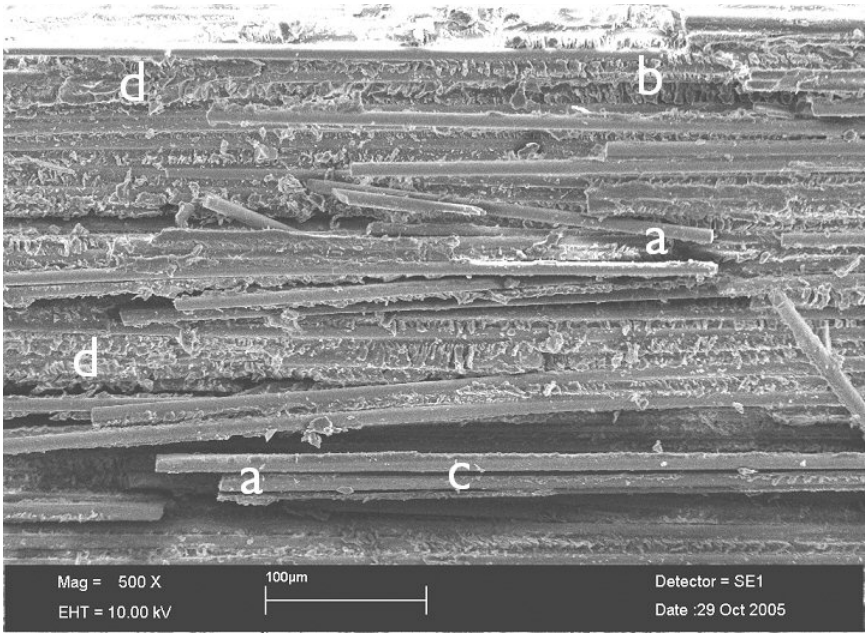

Figure 9-19: T-T fatigue fracture of non-prestressed composite (0 MPa) at a high stress level (1180 MPa). Features are marked as fibre pull-out (a), matrix hackle formation (b), clean fibre surface (c) and matrix plasticity (d).

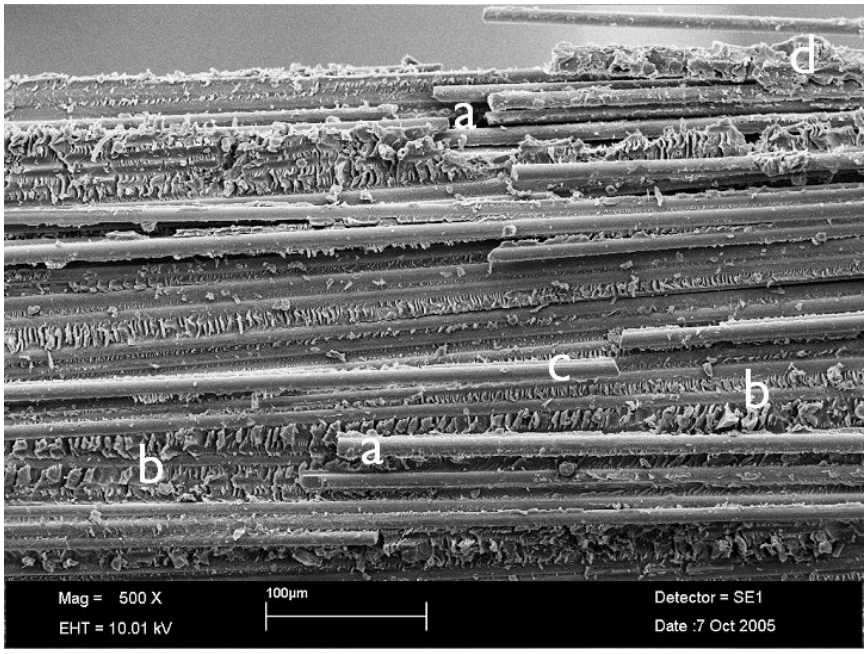

Figure 9-20: T-T fatigue fracture of 51 MPa prestressed composite at a high stress level (1180 MPa). Features are marked as fibre pull-out (a), matrix hackle formation (b), clean fibre surface (c) and matrix plasticity (d).

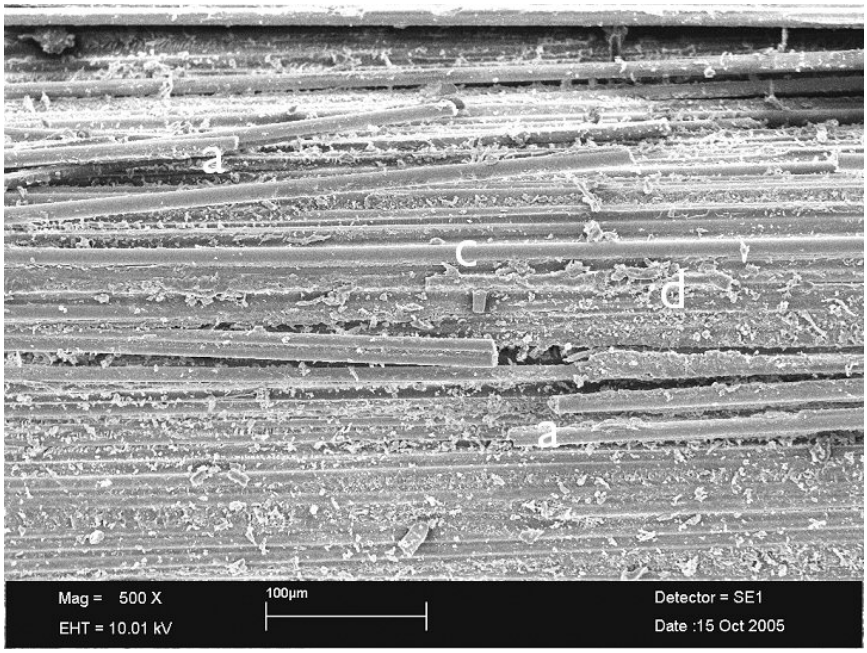

Figure 9-21: T-T fatigue fracture of 108 MPa prestressed composite at a high stress level (1180 MPa). Features are marked as fibre pull-out (a), clean fibre surface (c) and matrix plasticity (d).

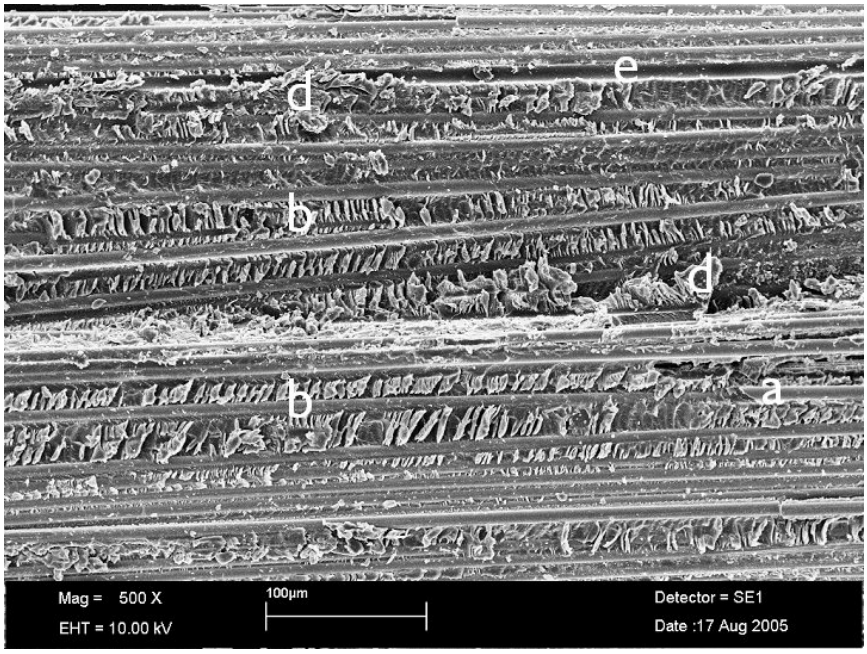

Figure 9-22: T-T fatigue fracture of non-prestressed composite (0 MPa) at a low stress level (590 MPa). Features are marked as fibre pull-out (a), matrix hackle formation (b), matrix plasticity (d) and fibre impression (e).

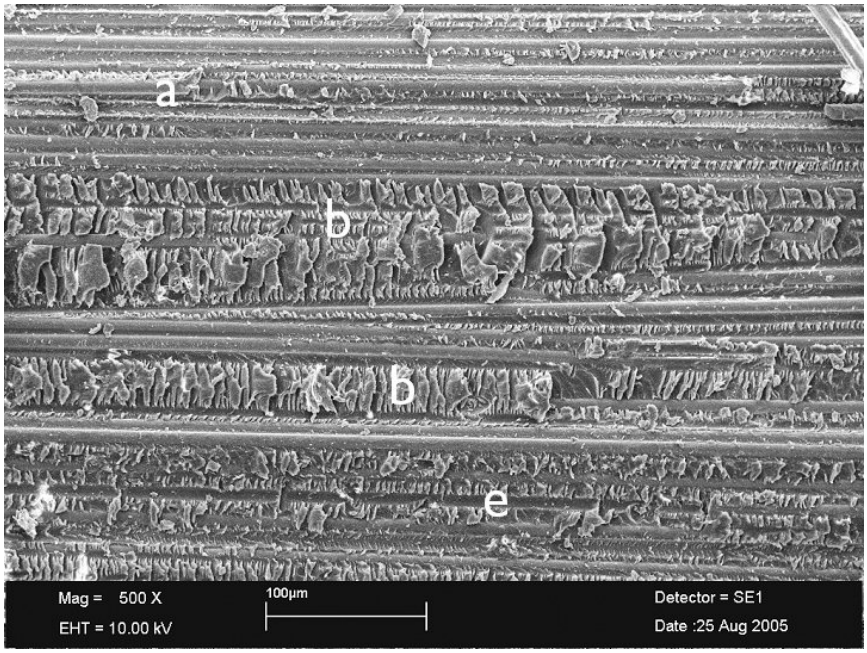

Figure 9-23: T-T fatigue fracture of 51 MPa prestressed composite at a low stress level (590 MPa). Features are marked as fibre pull-out (a), matrix hackle formation (b) and fibre impression (e).

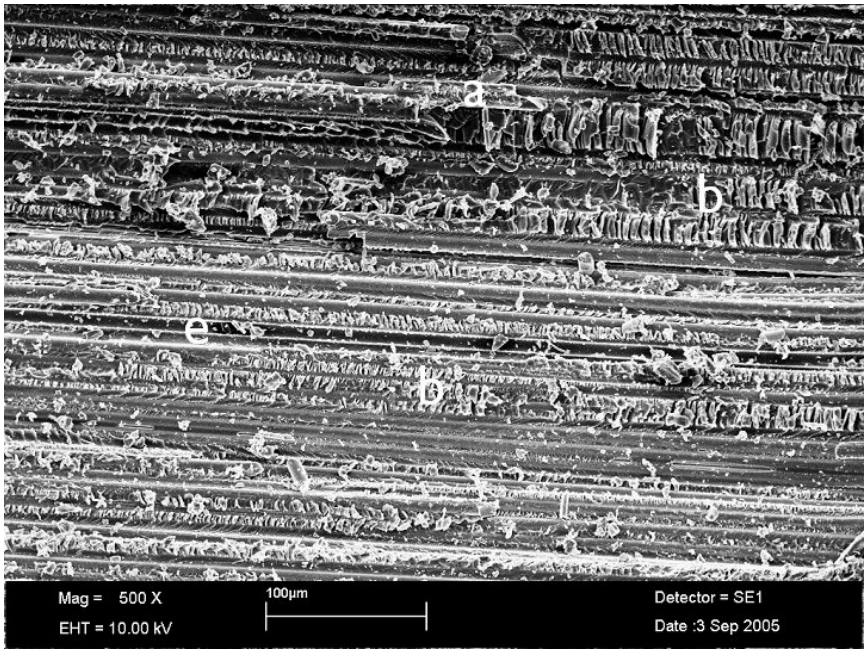

Figure 9-24: T-T fatigue fracture of 108 MPa prestressed composite at a low stress level (590 MPa). Features are marked as fibre pull-out (a), matrix hackle formation (b) and fibre impression (e).

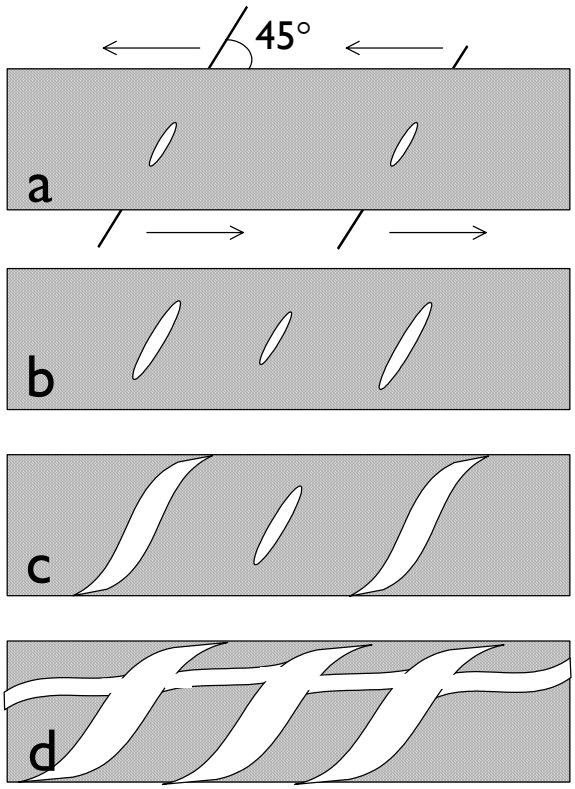

Figure 9-25: Mechanism of matrix hackle formation.

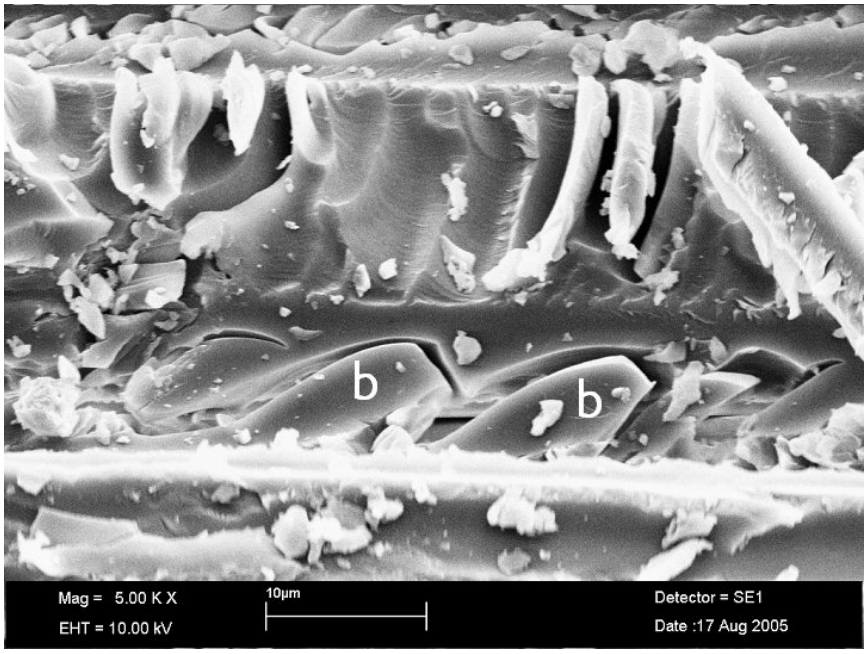

Figure 9-26: Matrix hackle formation (b) in a non-prestressed composite.

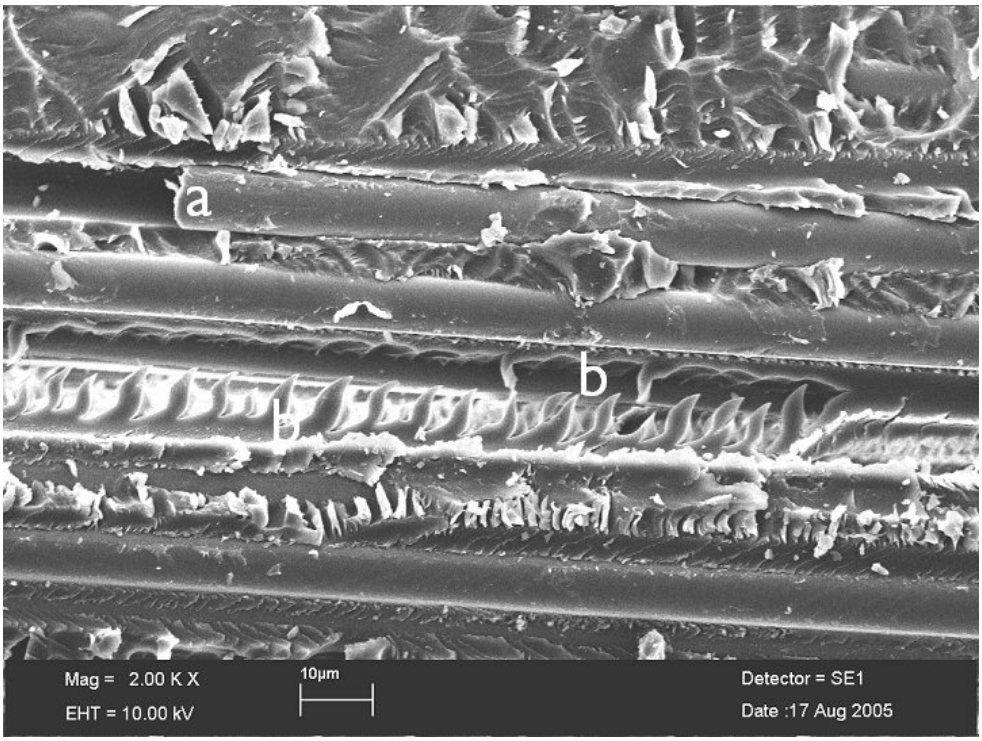

Figure 9-27: A row of matrix hackle formation (b) and fibre pull-out (a) in a non-prestressed composite.

9.2 Tension-compression fatigue

9.2.1. Fatigue of non-prestressed composite

In this study tension-compression (T-C) fatigue was conducted at a stress ratio ($\sigma_{min}/\sigma_{max}$) R= -0.3 with a loading rate of 250 kN s^{-1}. Fernando and Al-Khodari (GFAK) have investigated the T-C fatigue in the E-glass/913 epoxy composite using the same fatigue parameters used in this study. Figure 9-28 shows the normalised *S-N* curve for a non-prestressed composite (current work) along with GFAK results. With reference to Figure 9-28, it can be observed that the slopes in the current work and GFAK data set are similar. From equation 9-1 the loss in strength per decade of cycles was calculated for both the current work and GFAK results and summarised in Table 9-8. It can be seen that the calculated tensile strength losses per decade, for the current work and GFAK composites are equal.

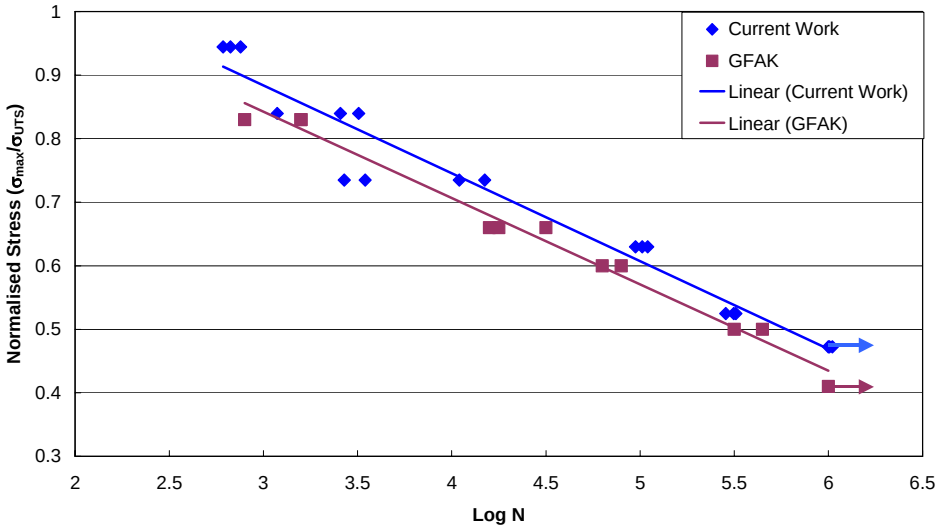

Figure 9-28: Comparison of normalised fatigue data of non-prestressed composite (current work) with a similar system reported in the literature (Fernando and Al-Khodari).

Table 9-8: Summary of slope (*b*) and tensile strength degradation per decade (b/σ_{UTS}) for current work and GFAK composites.

Material (E-glass/913 epoxy)	Slope (b)	Strength loss per decade (b/σ_{UTS}) %
Current work	0.138	10.6
GFAK	0.129	10.6

9.2.2. Fatigue of prestressed composites

Figure 9-29 presents the *S-N* curves for non-prestressed and prestressed composites along with a linear-regression fit. Table 9-9 shows the individual fatigue life results of non-prestressed and prestressed composites plotted in Figure 9-29. It can be seen that the fatigue data shows a linear *S-N* behaviour. The values of the slope (b) from linear-regression data analysis and tensile strength decay per decade of fatigue cycles (b/σ_{UTS}) are summarised in

Table 9-10. From

Table 9-10, it can be observed that prestressed composites show a 1% reduction in the strength decay during fatigue when compared to the non-prestressed composite.

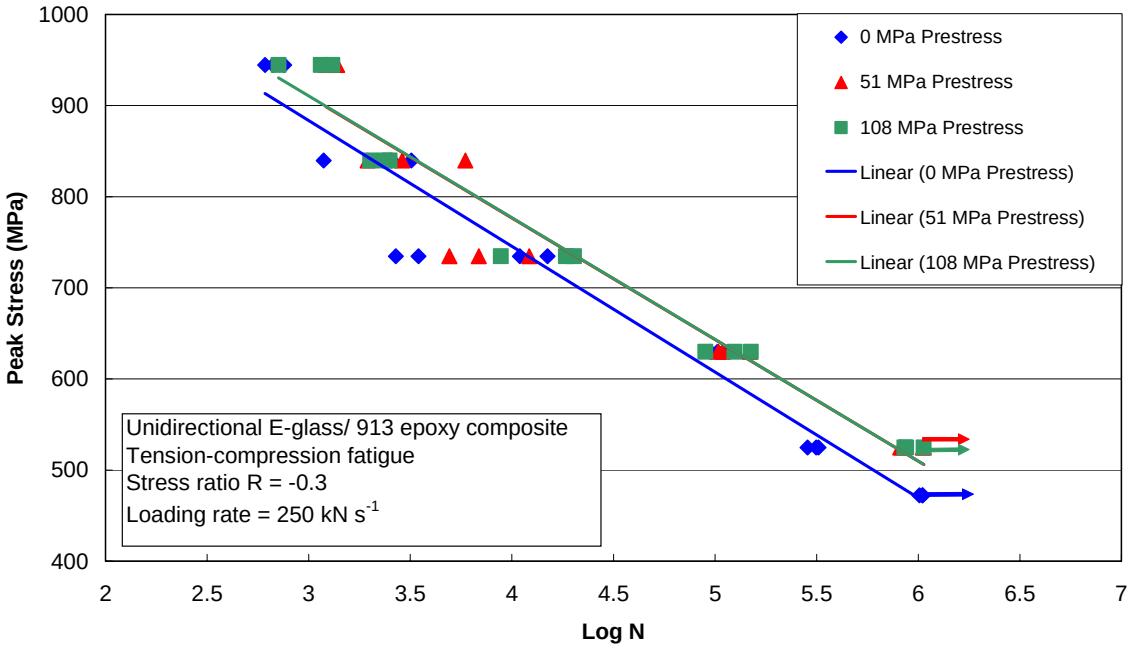

Figure 9-29: Comparison of tension-compression fatigue of the non-prestressed and prestressed composites. A linear regression fit was calculated.

Table 9-9: Summarises the individual fatigue life results of non-prestressed and prestressed composites plotted in Figure 9-29. The arrow mark (⇨) represents the sample is run-out.

Peak stress MPa	0 MPa		51 MPa		108 MPa	
	Number of cycles	Log N	Number of cycles	Log N	Number of cycles	Log N
944.60	668	2.824	1,215	3.084	1,146	3.059
944.60	610	2.785	1,380	3.139	710	2.851
944.60	756	2.878	1,357	3.132	1,307	3.116
839.65	3,201	3.505	1,951	3.290	2,011	3.303
839.65	1,184	3.073	5,906	3.771	2,505	3.398
839.65	2,564	3.408	2,885	3.460	2,370	3.374
734.69	3,467	3.539	6,865	3.836	20,220	4.305
734.69	10,957	4.039	4,930	3.692	18,440	4.265
734.69	14,975	4.175	12,173	4.085	8,825	3.945
734.69	2,685	3.428	-	-	-	-
629.73	102,690	5.011	109,200	5.038	89,590	4.952
629.73	109,811	5.040	148,440	5.171	124,759	5.096
629.73	94,640	4.976	103,920	5.016	150,000	5.176
524.78	314,556	5.497	1,053,835 ⇨	6.022	1,063,872 ⇨	6.026
524.78	285,032	5.454	815,660	5.911	856,060	5.932
524.78	322,500	5.508	1,064,911 ⇨	6.027	872,800	5.940
524.78	-	-	826,291	5.917		
472.30	1,013,352 ⇨	6.005				
472.30	1,050,184 ⇨	6.021				
472.30	1,051,543 ⇨	6.021				

Table 9-10: A summary of slope (*b*) and tensile strength decay per decade (b/σ_{UTS}) of non-prestressed and prestressed composites.

Prestress (MPa)	Slope (*b*)	(b/σ_{UTS}) %
0	-135.5	10.6
51	-121.86	9.6
108	-121.6	9.6

Figure 9-30 presents the comparison of T-T and T-C fatigue behaviour of non-prestressed composite. With reference to Figure 9-30 it can be observed that the T-C fatigue endurance of E-glass/913 epoxy composite is less when compared to the T-T fatigue endurance. The *S-N* curves of T-T and T-C fatigue data merge after 10^5 cycles. This could be because of the matrix fatigue limit. This shows that the T-C fatigue cycle of non-prestressed composites is more sensitive to damage than the T-T fatigue cycle (as expected).

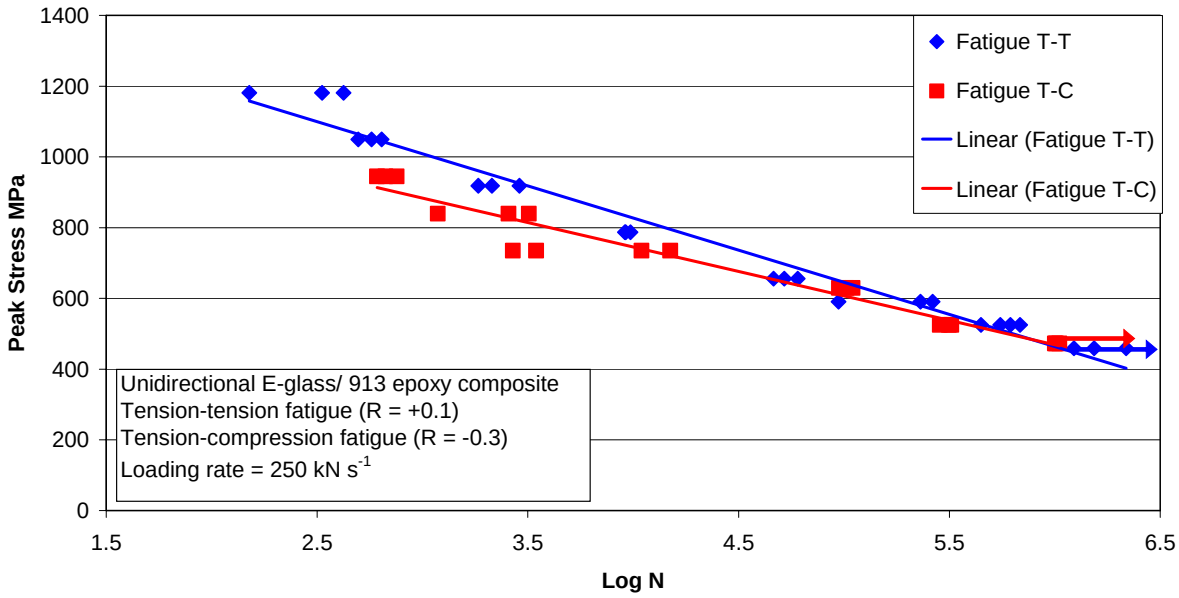

Figure 9-30: Comparison of T-T and T-C fatigue behaviour of non-prestressed composite.

The T-C fatigue data of non-prestressed and prestressed composites was also plotted with a polynomial fit (see Figure 9-31). From Figure 9-31 the calculated equivalent strength σ_{equ} is summarised along with experimentally-measured UTS and UCS as shown in Table 9-11. From the table it is interesting to observe that the calculated σ_{equ} is higher than the experimentally-measured UTS and UCS. This is because the fatigue test was conducted at 250 kN s^{-1} whereas the static tensile tests were conducted at 0.6 kN s^{-1} and the static compression test was conducted at 0.2 kN s^{-1}. It is well known that the strength properties of glass fibre/epoxy composites are loading-rate sensitive[140] and this appears to be the reason for the difference in calculated σ_{equ} and measured UTS and UCS.

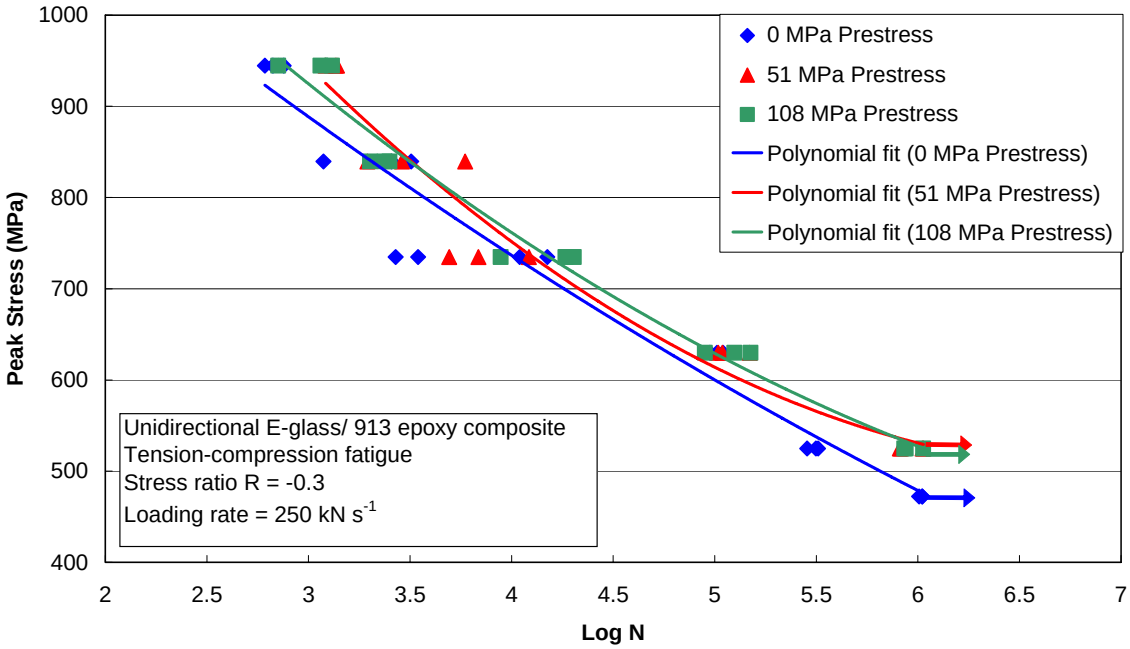

Figure 9-31: Comparison of tension-compression fatigue of the non-prestressed and prestressed composites. A second order fit was calculated excluding the static strength (UTS and UCS).

Table 9-11: Summarises the calculated equivalent σ_{equ} from second-order polynomials for the non-prestressed and prestressed composites without static strength. The number in parentheses shows the standard deviation.

Prestress (MPa)	Measured σ_{UTS}	Measured σ_{UCS}	σ_{equ}
0	1311 (80)	1177 (47)	1436
51	1244 (110)	1294 (68)	1846
108	1285 (138)	1280 (67)	1598

9.2.3. Statistical analysis of fatigue data

The effect of prestress on T-C fatigue of composites is apparent when the peak stress is normalised with respect to the UTS as shown in Figure 9-32. The standard deviation presented in Figure 9-32 was calculated for a 95% confidence level.

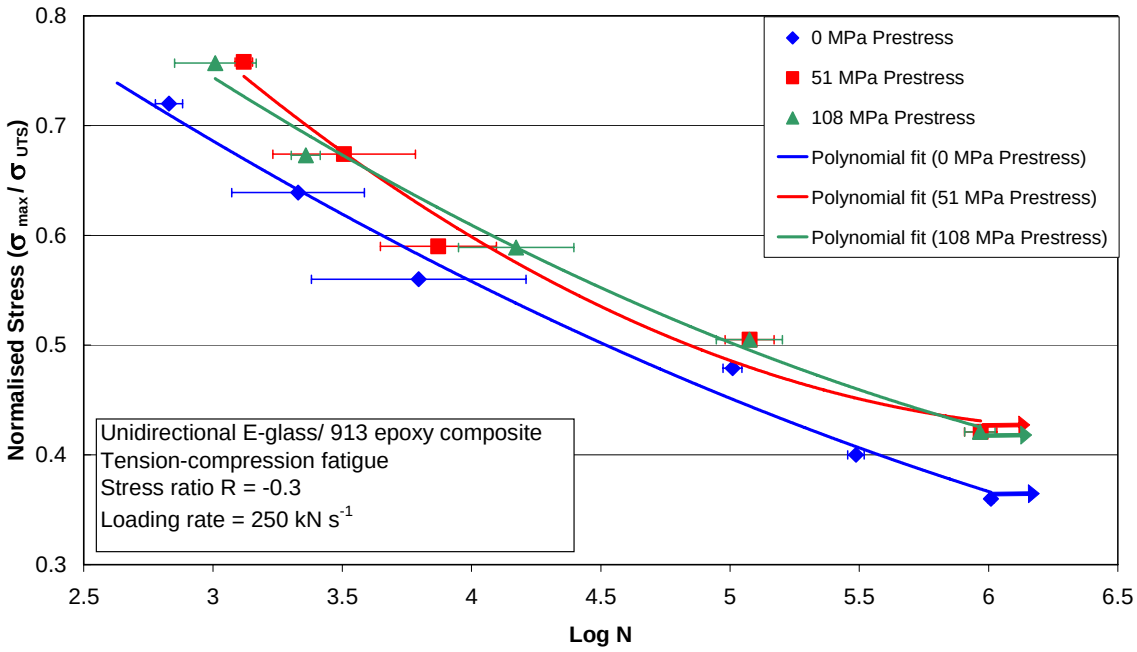

Figure 9-32: Comparison of normalised tension-compression fatigue of the non-prestressed and prestressed composites. The error bars were calculated for a 95% confidence limit.

With reference to Figure 9-32, it can be observed that the prestressed composites show an improvement in fatigue life in low and high stress fatigue regions. The individual fatigue results from non-prestressed and prestressed composites in the low stress region (524 MPa peak stress), the high stress region (944 MPa peak stress) and the middle stress regions (630 MPa peak stress) are presented in Figure 9-33, Figure 9-34 and Figure 9-35 respectively. The arrow mark in Figure 9-33 shows that the specimen run-out (the test was stopped because no macroscopic failure was observed in the specimen even after one million cycles).

From Figure 9-33 and Figure 9-34, it can be observed that with an increase in prestress the fatigue life of composites improved significantly. At 524 MPa peak stress, the improvement in the average fatigue life for the 51 and 108 MPa prestressed composite, were 3.05 and 3.02 times than that of the 0 MPa composite. Also at 944 MPa peak stress, the average fatigue life of the 51 MPa and 108 MPa prestressed composites was 1.94 and 1.50 times that of the 0 MPa composite.

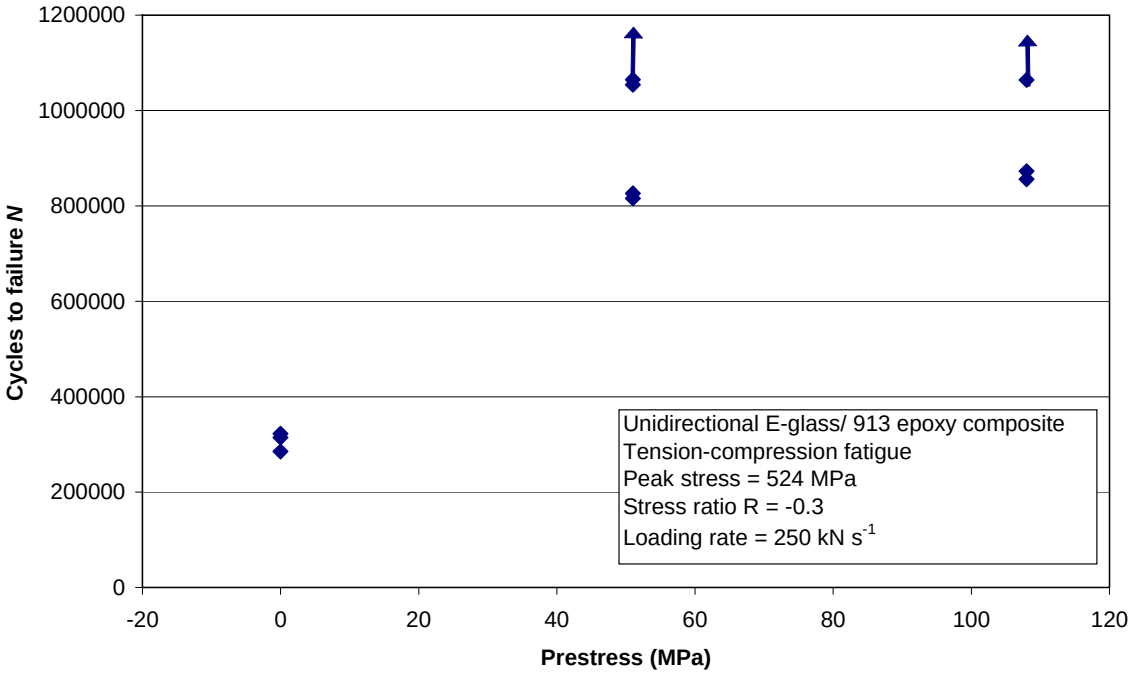

Figure 9-33: Fatigue life as a function of applied prestress in the low stress region (peak stress of 524 MPa). The arrow mark represents the specimen run-out.

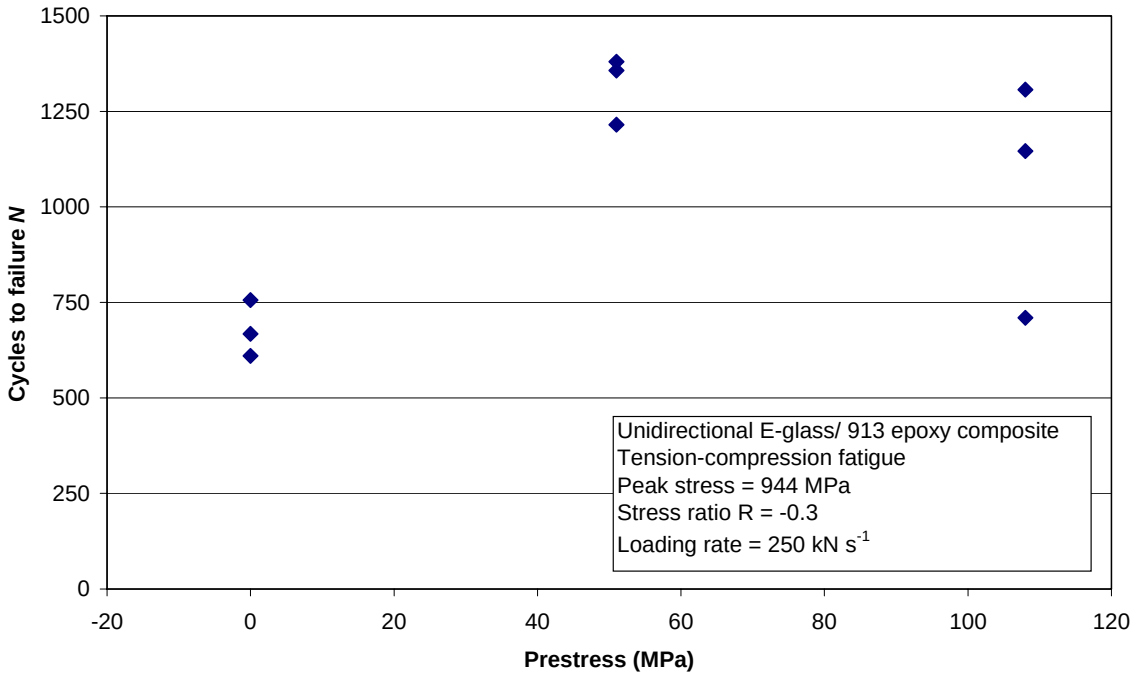

Figure 9-34: Fatigue life as a function of applied prestress in the high stress region (peak stress of 944 MPa).

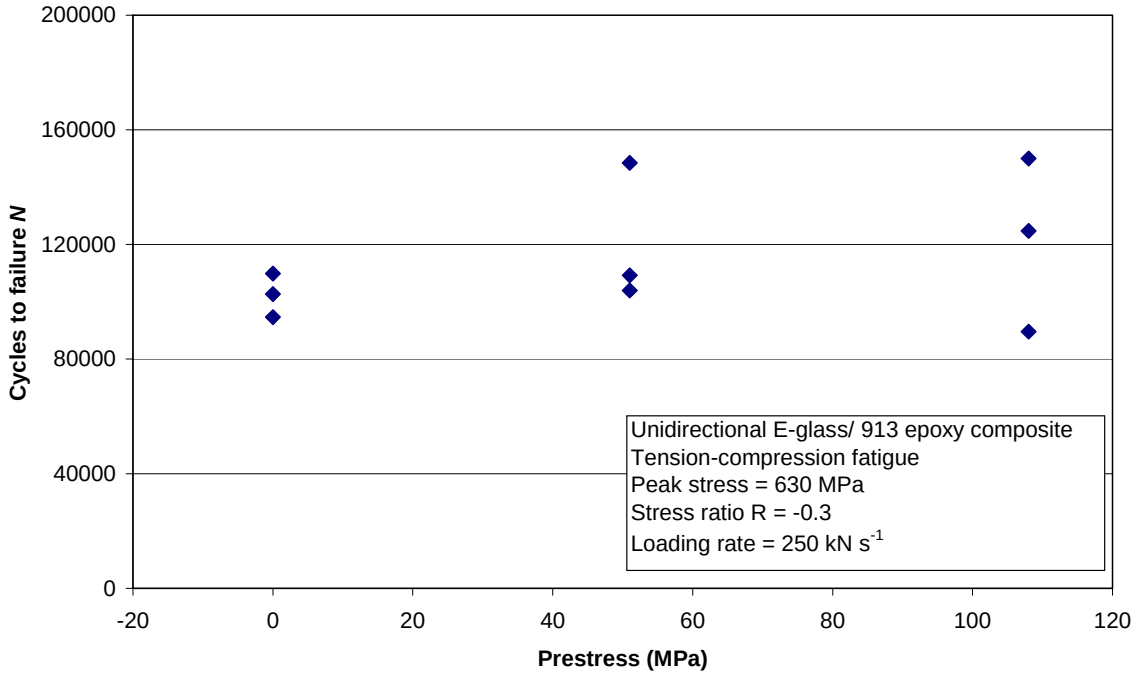

Figure 9-35: Fatigue life as a function of applied prestress in the middle stress region (peak stress of 630 MPa).

To check that the difference between the non-prestressed and prestressed composites was significant, a student *t*-test was performed. It was found that at 1% significance level for 524 MPa peak stress level fatigue, the non-prestressed and prestressed composites are from different populations. Also at a 944 MPa peak stress it was found that the 0 MPa and 51 MPa prestressed composites are from different populations with 1% significant level. However, in the middle stress region it was observed that the fatigue life of the composite was independent of prestress.

The two-parameter Weibull distribution was calculated for the fatigue results from non-prestressed and prestressed composites at 524 MPa peak stress (low stress region) (see Figure 9-36), 944 MPa peak stress (high stress region) (see Figure 9-37) and 630 MPa peak stress (middle stress region) (see Figure 9-38). Table 9-12 summarises the Weibull modulus calculated for non-prestressed and prestressed composites presented in Figure 9-36 to Figure 9-38. From these Figures and the Table, it could be observed that the improvement observed in prestressed composites at the 524 MPa peak stress level is statistically significant. Also at a 944 MPa peak stress level the fatigue life of the 51 MPa prestressed composite is greater than for the non-prestressed composite.

Table 9-12: Summarises the Weibull modulus of non-prestressed and prestressed composites presented in Figure 9-36 to Figure 9-38.

Prestress MPa	Weibull modulus (*m*)		
	Peak stress 524 MPa	Peak stress 944 MPa	Peak stress 630 MPa
0	17.099	10.475	15.405
51	6.9981	15.83	5.2383
108	8.1859	3.4881	4.3862

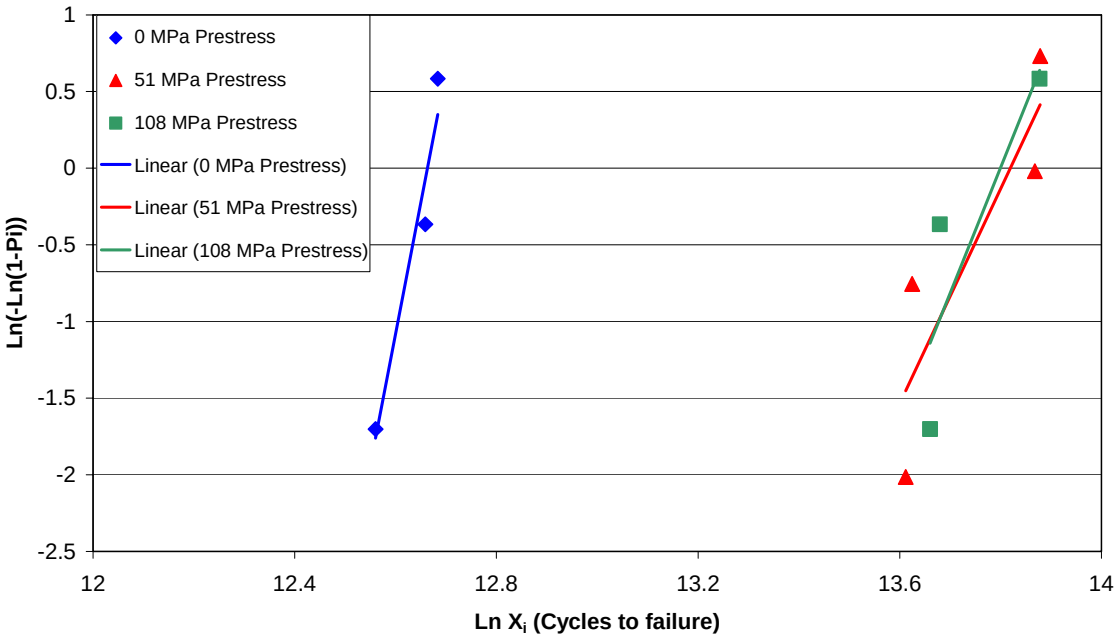

Figure 9-36: Weibull distribution for fatigue life at 524 MPa peak stress (low stress region).

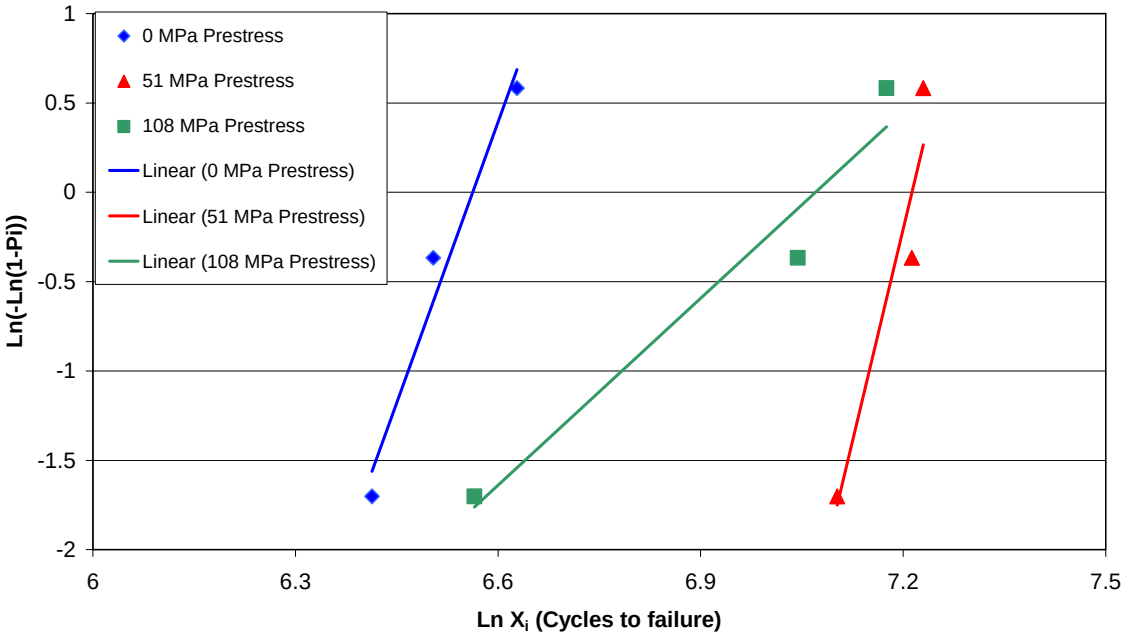

Figure 9-37: Weibull distribution for fatigue life at 944 MPa peak stress (high stress region).

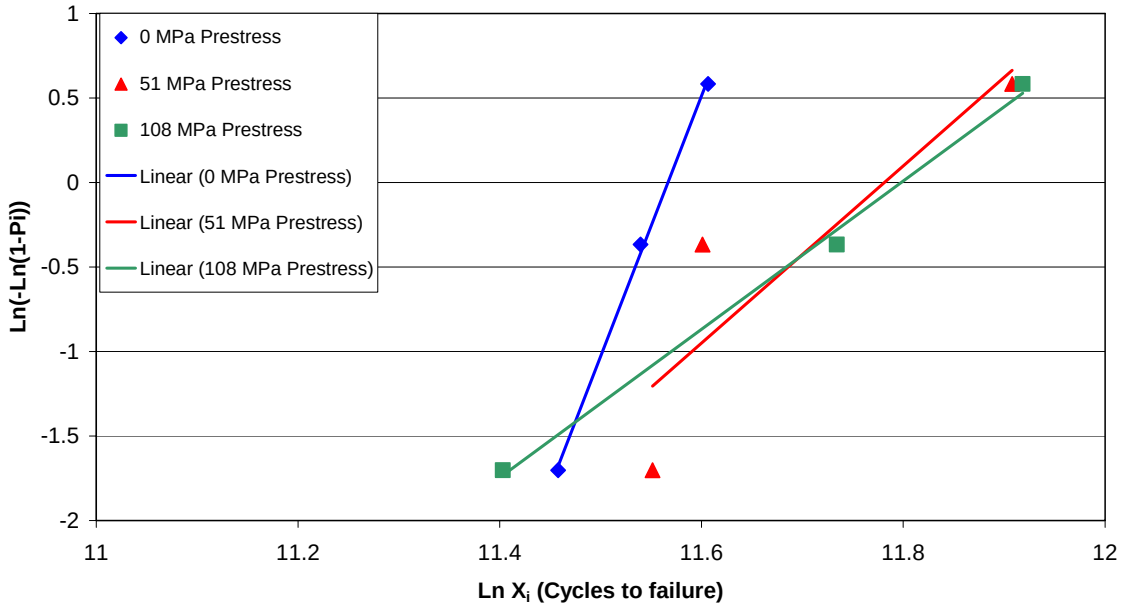

Figure 9-38: Weibull distribution for fatigue life at 630 MPa peak stress (middle stress region).

Low stress fatigue region

From the results of the statistical analysis it was shown that prestressed composites show a significant improvement in fatigue life compared to non-prestressed composites. The possible reasons for the improvement are (i) reduction in matrix residual stresses and (ii) improvement in the fibre alignment.

A reduction in process-induced residual strain in the matrix resulted in an increased strain level to matrix cracking. This could increase the critical crack length to fracture. The presence of fibre misalignment will induce a shear stress in the matrix during the fatigue cycle, which will accelerate the matrix cracking and debonding. Adams and Hyer have shown that in compression-compression fatigue, artificially-induced fibre waviness in composites reduced the fatigue life when compared to the controlled composite. It was shown in Section 6.3, Chapter 6 that fibre prestressing improved the number of fibres aligned to the 0° degree of the composite. This improvement in fibre alignment in a prestressed composite will reduced the shear stress-induced damage in the matrix and interface. This in turn would be expected to improve the fatigue life of prestressed composites.

High stress level region

At 944 MPa peak stress the 51 MPa prestressed composite showed an increase in fatigue life compared to a non-prestressed composite. The possible reasons for the increase in fatigue life are (i) an improvement in the fibre alignment and (ii) an increase in tensile residual stress in the fibres.

It is well known that the composite failure stress in compression is less than in tension. It has already been shown that fibre alignment in composites improved with fibre prestressing (see Chapter 6). This will increase the compressive failure strength of the composite (see Chapter 8). Also in Chapter 6 and 7 it was shown that the tensile residual stress in fibres increases with fibre prestress. The resulting composite has tensile residual stresses in fibres, which improves the compressive properties (as discussed in chapter 8). This may have increased the fatigue life of the composites in the 944 MPa peak stress region.

9.2.4. Fatigue damage monitoring

Figure 9-39 and Figure 9-40 present the stiffness degradation of prestressed composite and non-prestressed composites during fatigue at 524 and 840 MPa peak stress respectively. The corresponding surface temperature rises are given in Figure 9-41 and Figure 9-42. It can be seen that both the stiffness degradation and surface temperature rise show a three-stage behaviour, which was also observed in T-T fatigue. At 524 MPa peak stress it can be observed that the stiffness degradation in the non-prestressed composite is rapid during

stage II of the fatigue life when compared to the prestressed composite. This also correlates with the higher surface temperature recorded from the non-prestressed composite, whilst for the prestressed composite the recorded surface temperature was comparatively low.

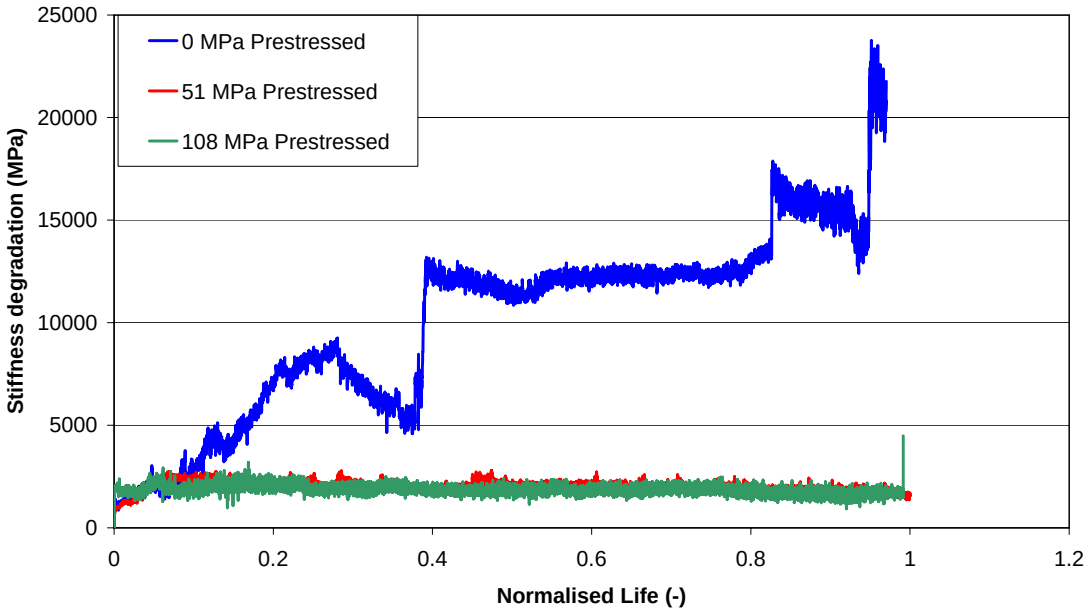

Figure 9-39: Stiffness reduction in non-prestressed and prestressed composites at 524 MPa peak stress.

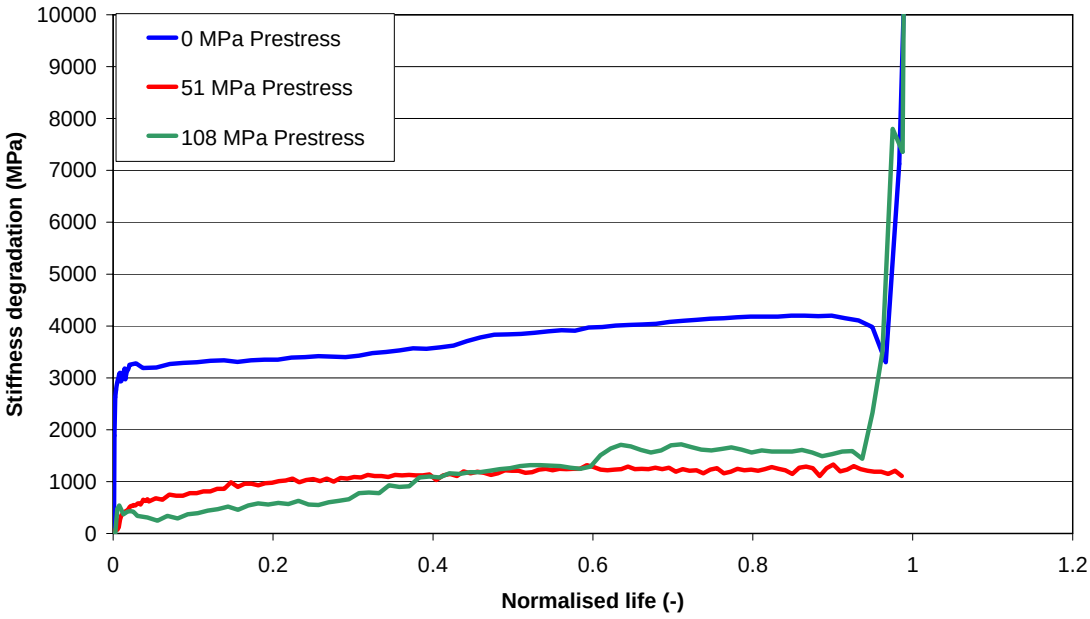

Figure 9-40: Stiffness reduction in non-prestressed and prestressed composites at 840 MPa peak stress.

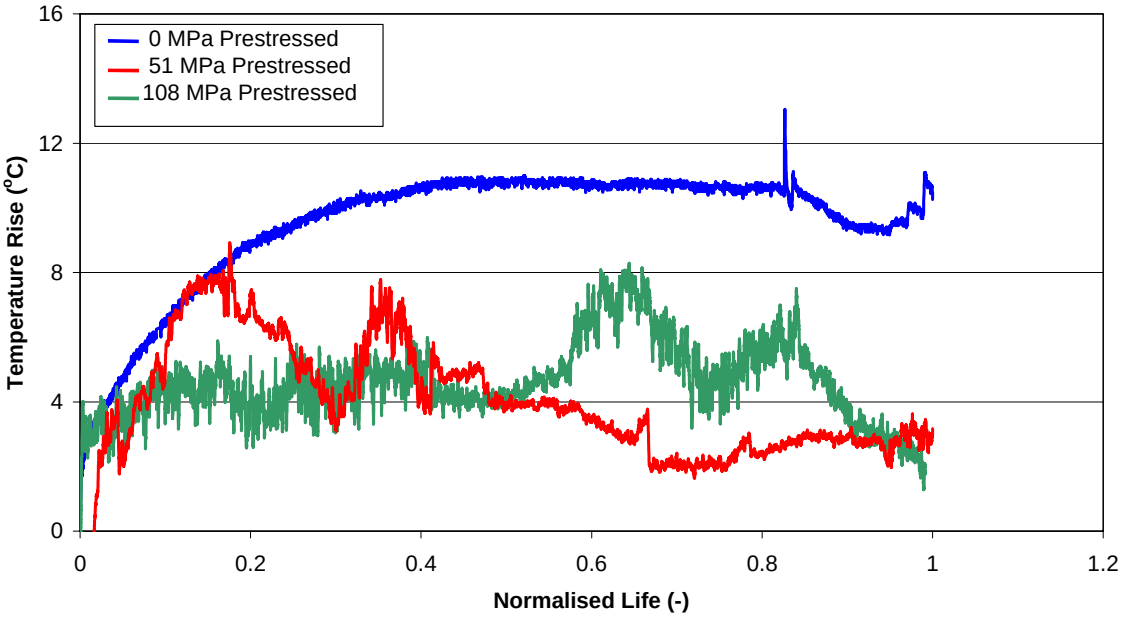

Figure 9-41: Surface temperature rise in non-prestressed and prestressed composites at 524 MPa peak stress.

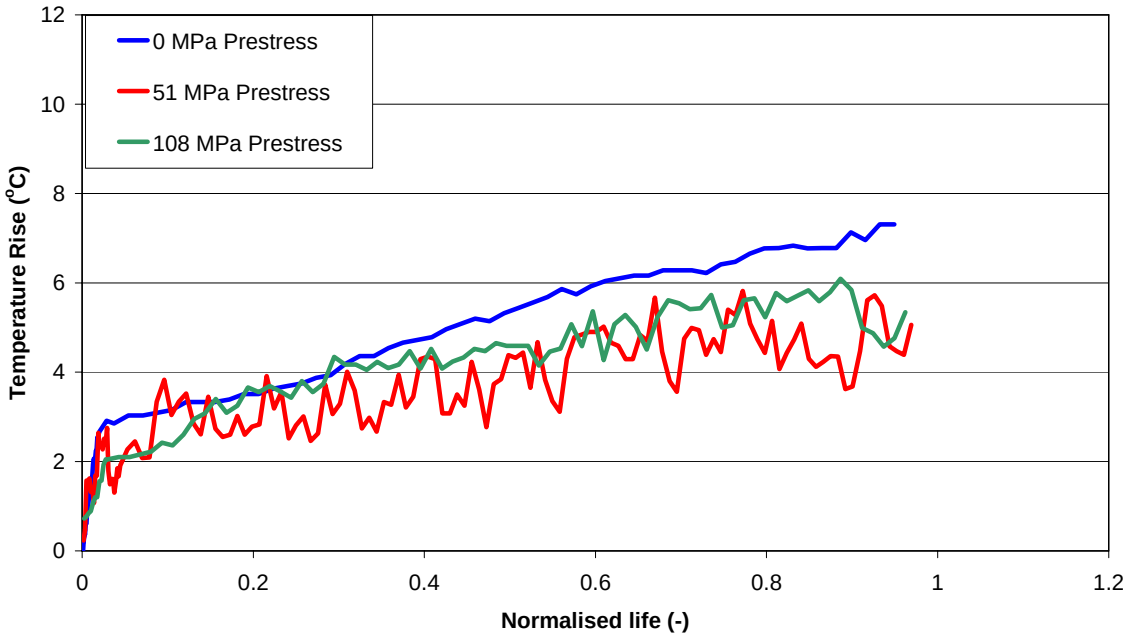

Figure 9-42: Surface temperature rise in non-prestressed and prestressed composites at 840 MPa peak stress.

Also the surface temperature recorded in prestressed composites in the low stress fatigue region shows a reduction and increase during the fatigue test (see Figure 9-41). This is because each prestressed sample endured for two and a half days. During the nighttime the

laboratory temperature slightly decreases. This is the reason for the observed decrease in temperature. On the other hand the non-prestressed specimen lasted only for 285, 032 cycles, which lasted only for 18 hours.

Table 9-13 and

Table 9-14 summarise the stiffness degradation and the corresponding surface temperature rise for non-prestressed and prestressed composites at 524 and 840 MPa peak stress fatigue. Appendix D presents the stiffness degradation and surface temperature rise at selected normalised life for all the individual samples tested at 524 MPa and 840 MPa peak stress.

At 840 MPa peak stress level the stiffness degradation during the stage I of the fatigue life shows a rapid stiffness decay in non-prestressed composites. On the other hand the stiffness decay in prestressed composites is low. In stage II of the fatigue life, the prestressed composites showed relatively lower stiffness degradation. A marginally higher surface temperature rise was recorded in non-prestressed composites compared to prestressed ones (see Figure 9-42).

At a low stress level (524 MPa peak stress) the observed rapid stiffness degradation in non-prestressed composites could be attributed to the tensile residual stresses in the matrix and fibre waviness in composites. The process-induced residual tensile stresses in the matrix lead to crack initiation and/or crack growth during the tensile phase of the fatigue cycle. The presence of fibre waviness in composites will induce shear stresses in the matrix, which could accelerate the damage in the matrix and fibre/matrix interface debonding. The combination of tensile and compressive stress excursions is likely to hasten the damage initiation and growth process. This in turn results in a rapid stiffness degradation and surface temperature rise during the fatigue cycle. On the other hand in prestressed composites, by inducing compressive stresses the matrix tensile residual stresses are reduced. As a result the prestressed composite could have a higher resistance to matrix cracking. Also by applying prestress the alignment of the fibres to the longitudinal directional (0° degree) in composites is improved. This minimises the shear stress applied to the matrix through fibre misalignment.

In high stress level (840 MPa peak stress) fatigue the prestressed composites showed a greater resistance to stiffness degradation when compared to the non-prestressed composites. In non-prestressed composites during processing, the fibres are subjected to compressive residual stresses due to the cure-induced and thermal-induced residual stresses. There is also the possibility of fibre movement due to matrix flow during the curing process; this would be expected to increase the degree of fibre misalignment in non-prestressed composites. As a result the compressive strength of non-prestressed composites could be affected. However, in prestressed composites, the movement of fibres is restricted at any stage of the curing cycle by the applied pre-load. In addition, with an increase in prestress the fibres are subjected to tensile residual stresses.

Table 9-13: Summary of the stiffness degradation and surface temperature changes for the non-prestressed and the prestressed composites at a peak stress of 524 MPa in T-C fatigue.

Normalised life	Stiffness degradation (MPa)			Temperature rise (°C)		
	Prestress (MPa)			Prestress (MPa)		
	0	51	108	0	51	108
0.1	2630	2190	1530	6.5	5.5	4.9
0.3	6980	2200	1740	9.9	3.4	2.6
0.5	11060	2200	1790	10.7	3.5	4.2
0.7	12270	2220	1960	10.7	2.2	4.7
0.9	15130	2810	1840	9.6	2.8	4.1

Table 9-14: Table 9-12: Summary of the stiffness degradation and surface temperature changes for the non-prestressed and the prestressed composites at a peak stress of 840 MPa in T-C fatigue.

Normalised life	Stiffness degradation (MPa)			Temperature rise (°C)		
	Prestress (MPa)			Prestress (MPa)		
	0	51	108	0	51	108
0.1	1410	780	390	3.1	3.0	2.4
0.3	1540	1090	780	4.2	3.3	4.1
0.5	1950	1210	1260	5.3	4.3	4.6
0.7	2190	1270	1700	6.3	3.6	5.5
0.9	2220	1330	2330	7.3	3.6	4.8

9.2.5. Post-failure analysis

This section will concentrate on the effect of prestress on macroscopic and microscopic damage of composite materials investigated in this study.

Macroscopic post-fatigue (T-C) fracture

Figure 9-43 (a) and (b) shows the macroscopic fatigue fractures of non-prestressed and prestressed composites at high (945 MPa peak stress) and low stress (524 MPa peak stress) level fatigue. The macroscopic T-C fatigue damage of composites at high stress level (945 MPa peak stress) shows a change in failure mode (see Figure 9-43) when compared to the T-T fatigue (see Figure 9-18) due to the compressive stress excursion during fatigue cycling. It is clear that the concentration of longitudinal splits and delamination are less in

T-C fatigue when compared to T-T fatigue at high stress levels. From Figure 9-43 (a) it can be seen that in high stress level fatigue no significant difference in the damage was observed between the non-prestressed and prestressed composites.

In low stress level fatigue (524 MPa peak stress), the extent of longitudinal splitting in prestressed composites is less than in non-prestressed composites (see Figure 9-43 (b)). This may be due to a reduction in matrix residual stresses and improvement in fibre alignment.

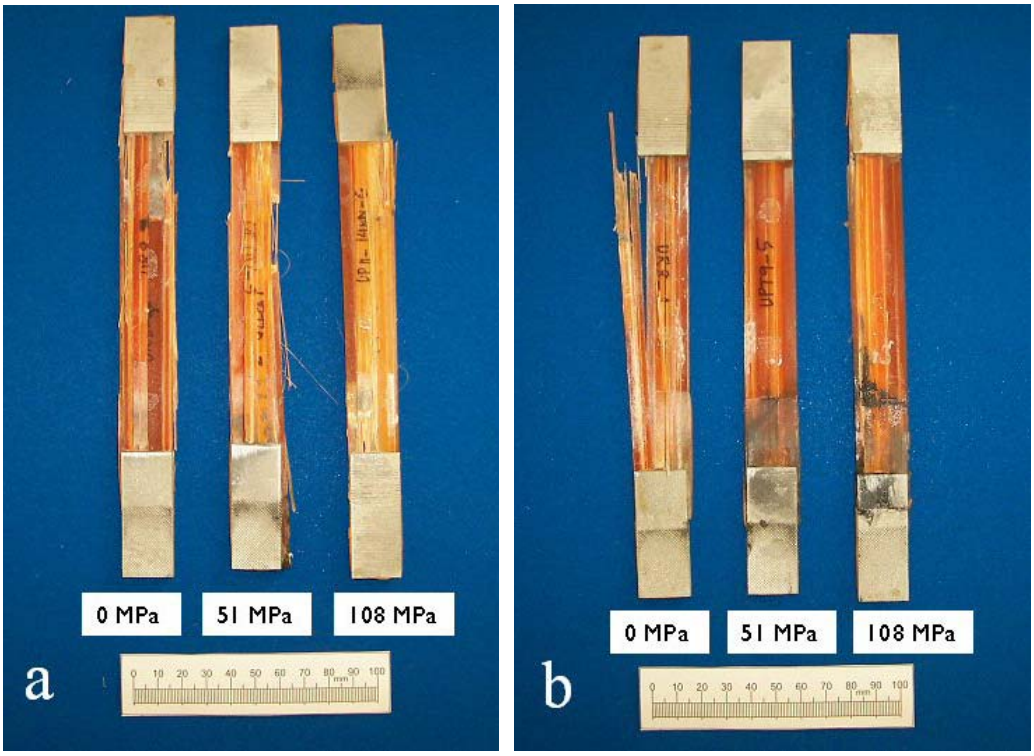

Figure 9-43: Representative macroscopic fatigue failure of non-prestressed and prestressed composites. a) 945 MPa peak stress and b) 524 MPa peak stress.

Microscopic post-fatigue (T-C) fracture

Figure 9-44 to Figure 9-50 show the microscopic failure of non-prestressed and prestressed composites tested in T-C fatigue in the high stress region (945 MPa peak stress). In these figures a number of failure mechanisms such as tensile failure (a), compressive failure (b), matrix plasticity (c), fibre fracture (d), matrix hackle formation (e), fibre pull-out (f), fibre buckling (g) and fibre imprint (h) can be seen. It was observed that the non-prestressed (see Figure 9-44) and 51 MPa (see Figure 9-46) prestressed composites show a combination of compressive and tensile fracture. However, the 108 MPa prestressed composites showed a tensile failure (see Figure 9-48). The tensile failure is associated with fibre pullout from the

matrix, whereas, compressive failure is generally attributed to the shear failure of the fibres and matrix. It can also be seen that in compression fracture, the matrix is holding the fractured fibres in place. More matrix debris was observed in the compressive failure region (see Figure 9-45). Tai *et al.*[141] has also shown that during T-C fatigue of carbon fibre/PEEK composite both tensile and compressive failures occurred.

The compressive failure in a non-prestressed composite appears very similar to the static compression failure of non-prestressed composites discussed in Chapter 8. The compressive failure of fibres is attributed to the fibre misalignment in composites. Piggott has shown a mechanism of tension-tension fatigue failure for misaligned fibres. A schematic of the mechanism is presented in Figure 9-51. When a tensile load is applied, fibres alternatively straighten and relax. Because of this process, initially the interfacial debonding occurs (see Figure 9-51 (b)) and this leads to matrix crack initiation. The cyclic loading propagates these matrix cracks and ultimate failure will occur by fibre pull-out from the matrix.

On the other hand in a tension-compression fatigue, the misaligned fibres are not only straightened in the tensile cycle but they are also subjected to a micro-buckling/bending process during the compression cycle. During the compression cycle, the matrix is subjected to a transverse tensile stress due to the Poisson's ratio difference between the matrix and fibre, and stress concentrations caused by voids can initiate fracture in the fibre/matrix interface and matrix. The presence of a misaligned fibre induces shear stresses in the matrix, which also accelerates the crack growth within the matrix. If a fibre buckles, fracture occurs at both the fibre/matrix interface and within the matrix and leads to ultimate failure.

It is conjectured that failure in compression initiated by a misaligned fibre (see Figure 9-52 (e)) during the compression cycle will initiate catastrophic failure in the next tensile cycle by fibre pull-out from the matrix (see Figure 9-52 (f)), if the load transferred to the adjacent fibres is greater than their ultimate tensile strength. This phenomenon is observed in high stress level fatigue. The difference in the failure mechanism between T-T and T-C fatigue may explain why the composites show more sensitive behaviour to T-C fatigue than in the T-T fatigue.

In Chapter 6 it was shown that prestressing improved the fibre alignment in composites and that a maximum number of fibres aligned to 0° degree (~75%) was achieved at 108 MPa prestress. It can be seen that the extent of compressive failure in 51 MPa prestressed composites is less when compared to non-prestressed composites. In 108 MPa prestressed composites, predominantly tensile failure was observed (see Figure 9-48 and Figure 9-49). In Figure 9-49, the radial fracture patterns indicate a tensile failure of the unidirectional composite. A small amount of fibre buckling was also observed in 108 MPa prestressed composites (see Figure 9-50).

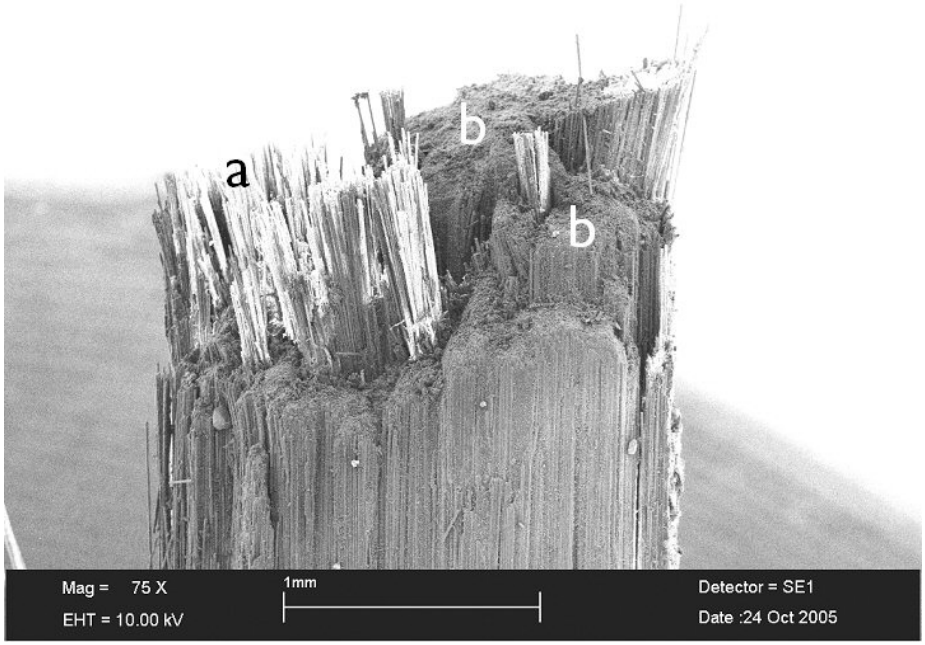

Figure 9-44: T-C fatigue fracture of a non-prestressed composite (0 MPa) at a high stress level (945 MPa peak stress). Features such as tensile fracture (a) and compression fracture (b) can be seen.

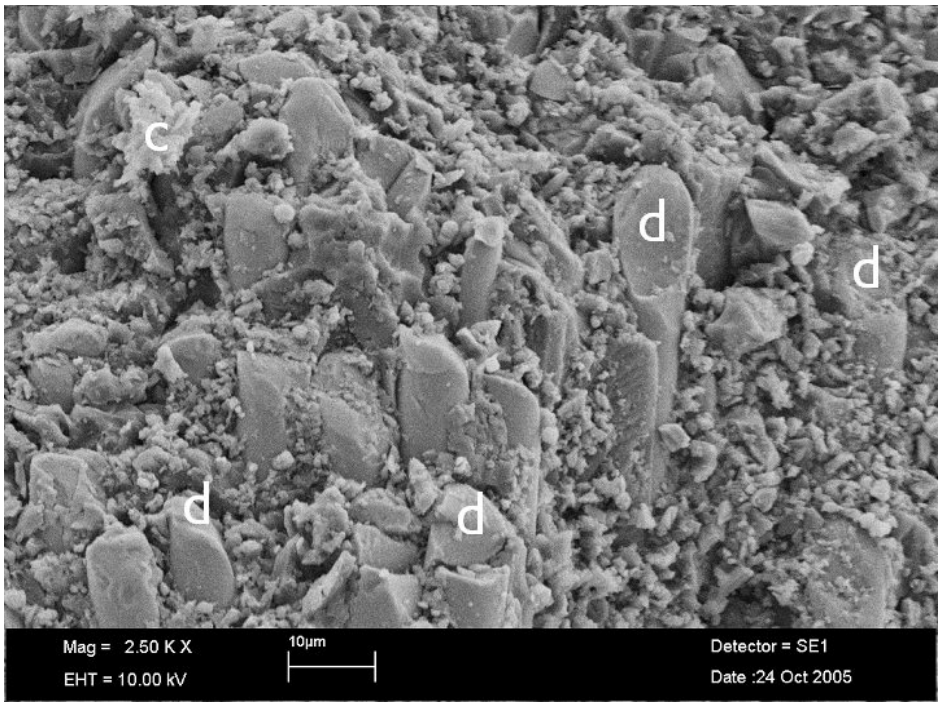

Figure 9-45: Compressive failure of a non-prestressed composite at a high stress level (945 MPa peak stress). Features such as fibre fracture (d) and matrix plasticity (c) can be seen.

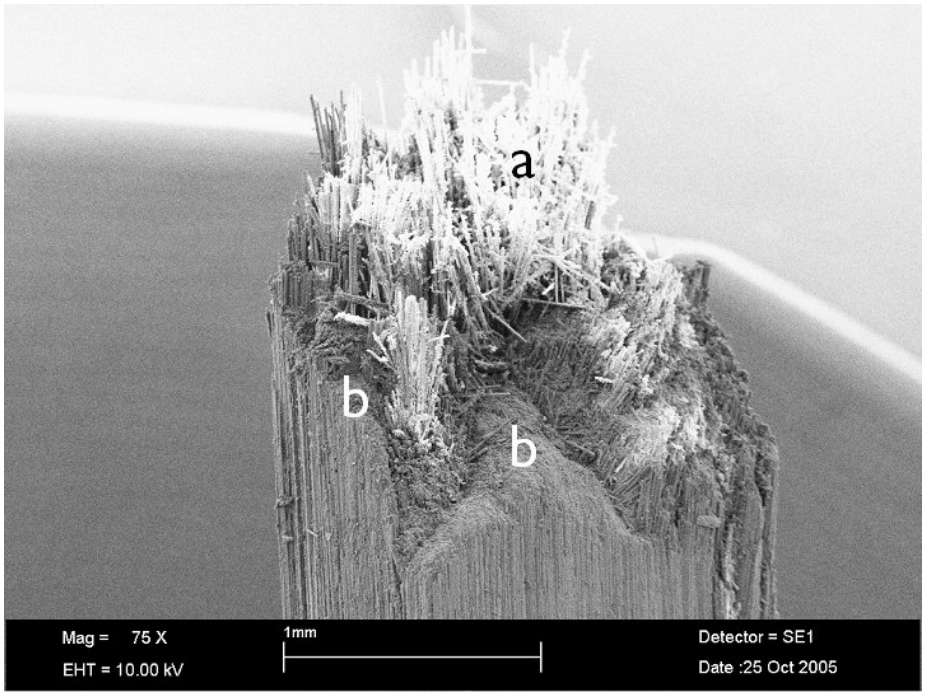

Figure 9-46: T-C fatigue fracture of a 51 MPa prestressed composite at a high stress level (945 MPa peak stress). Features such as tensile fracture (a) and compression fracture (b) can be seen.

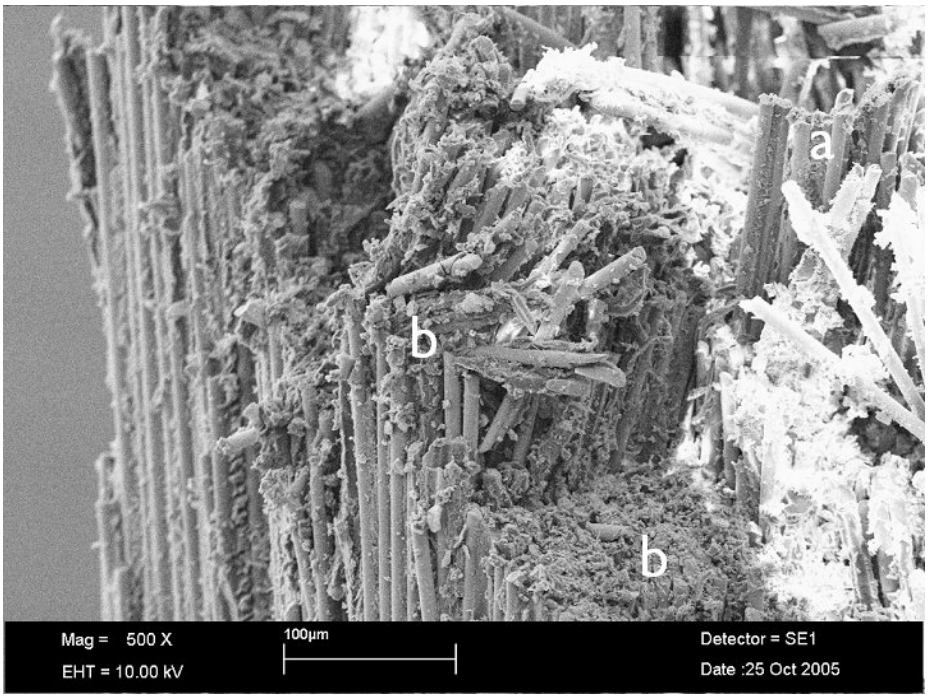

Figure 9-47: A close-up image of the failure of a 51 MPa prestressed composite shown in Figure 9-46. Features such as tensile fracture (a) and compression fracture (b) can be seen.

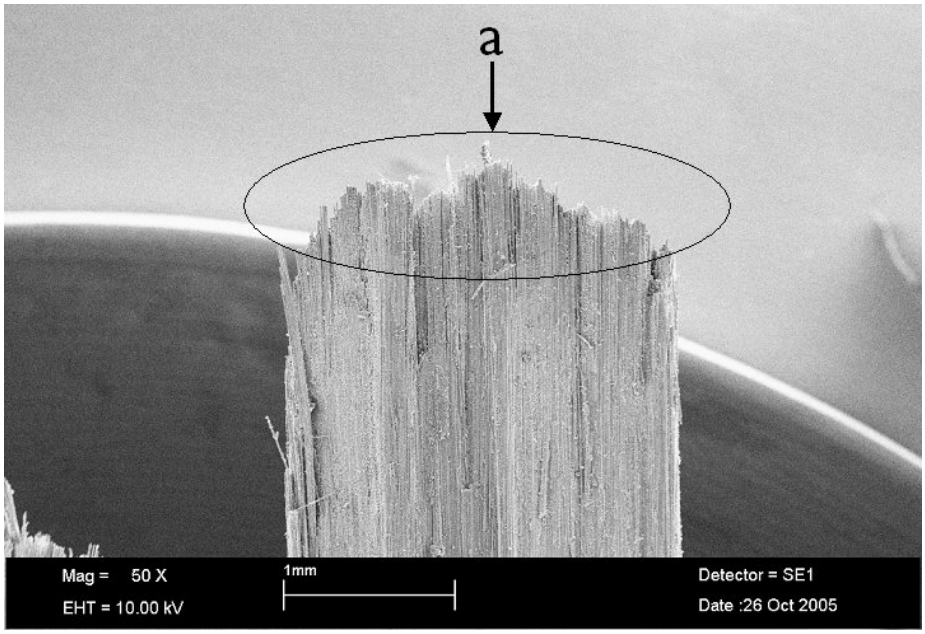

Figure 9-48: T-C fatigue fracture of a 108 MPa prestressed composite at a high stress level (945 MPa peak stress). The area marked as a, shows the tensile fracture.

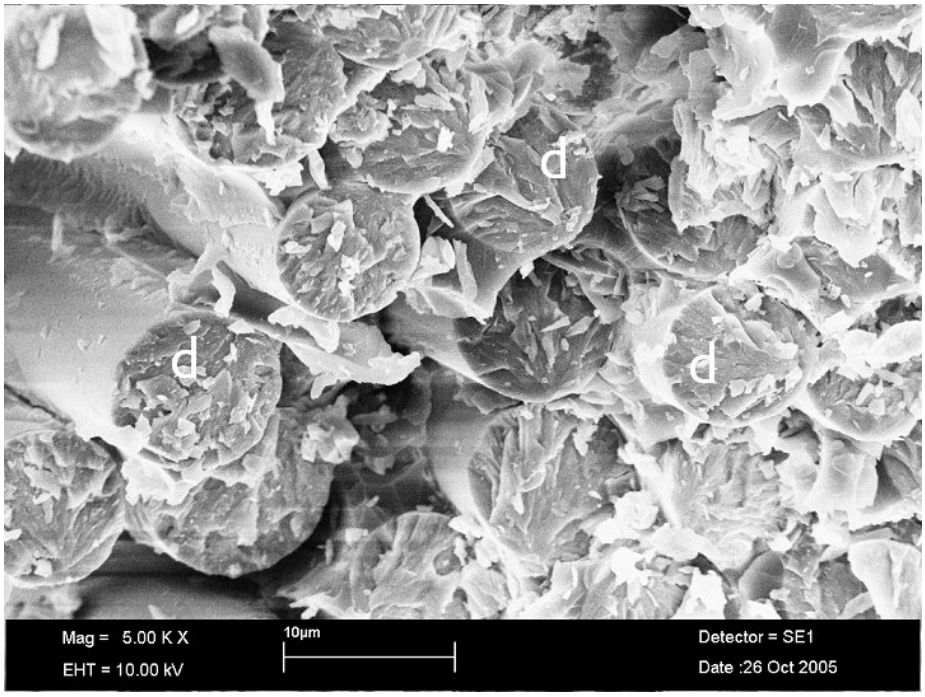

Figure 9-49: Tensile failure of a 108 MPa prestressed composites at a high stress level (945 MPa peak stress). The end face of the fractured fibre (d) represents a tensile failure.

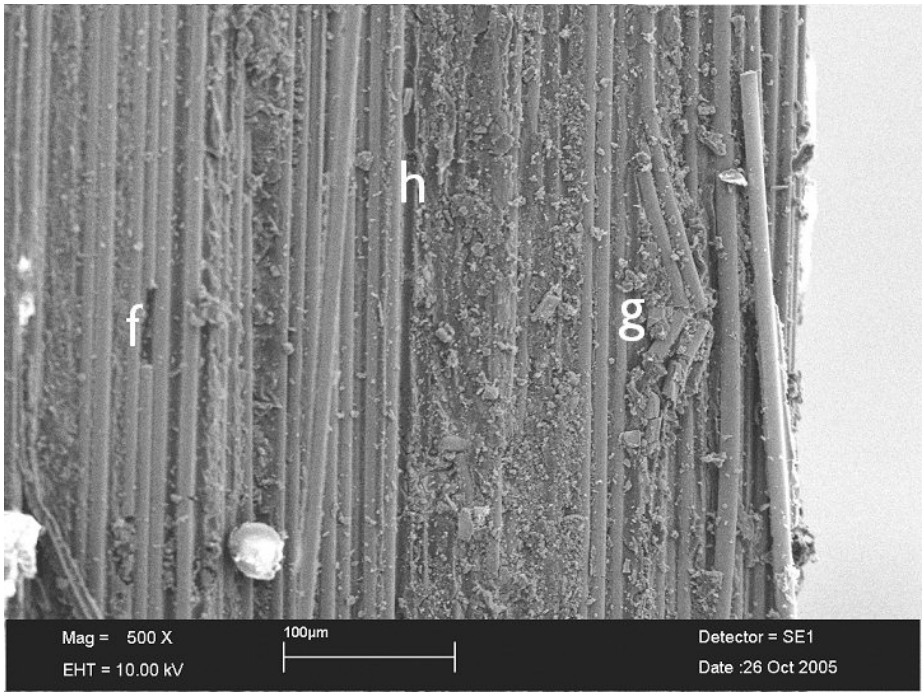

Figure 9-50: Tensile fibre pull-out (f), compressive fibre buckling (g) and fibre impression (h) observed in a 108 MPa prestressed composites at a high stress level (945 MPa peak stress).

Figure 9-53 to Figure 9-56 show the T-C fatigue fracture of non-prestressed and prestressed composites tested at a low stress level (524 MPa peak stress). Features such as matrix plasticity (c), fibre fracture (d), matrix hackle formation (e) and fibre imprints (h) can be seen on the fracture surface. It can be seen that the extent of fibre fracture in non-prestressed composites is high (see Figure 9-53 and Figure 9-56) when compared to prestressed composites. The fractures in prestressed composites are predominantly matrix and interface damage.

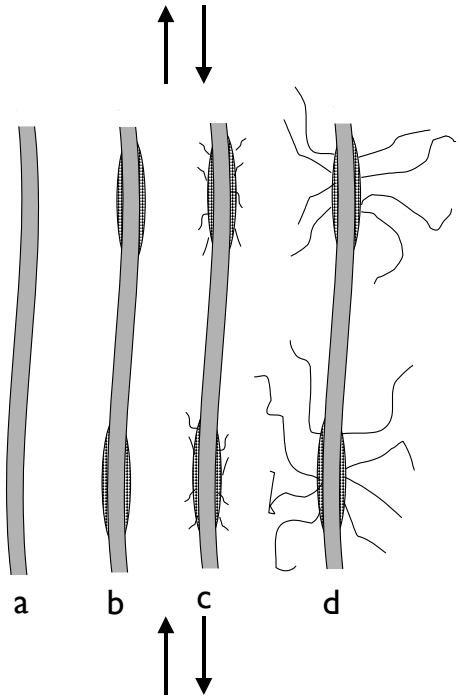

Figure 9-51: Fatigue failure involving misaligned fibres under a tension and compression cycle. a) fibre misalignment in composite, b) fibre/matrix interface debonding, c) matrix crack initiation and d) matrix crack propagation. The arrow mark shows the direction of loading.

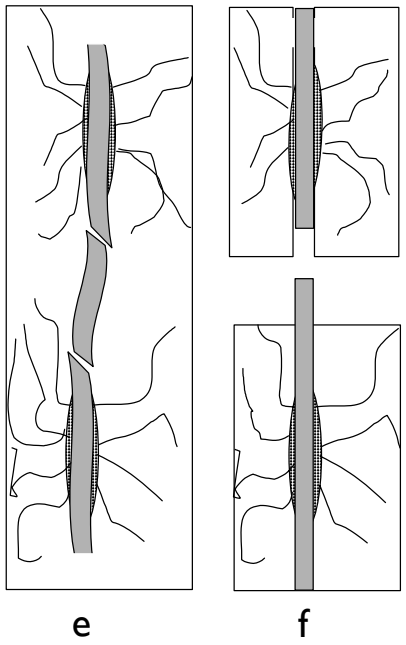

Figure 9-52: Ultimate failure of composites by e) Compression fracture and f) tensile fracture.

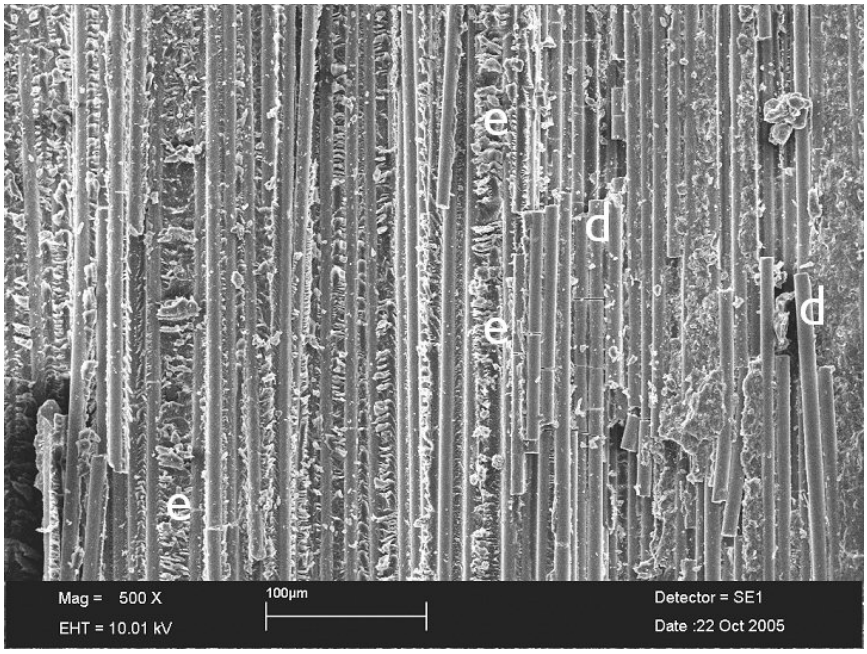

Figure 9-53: T-C fatigue fracture of a non-prestressed composite (0 MPa) at a low stress level (524 MPa peak stress). Features such as fibre fracture (d) and matrix hackle formation (e) can be observed.

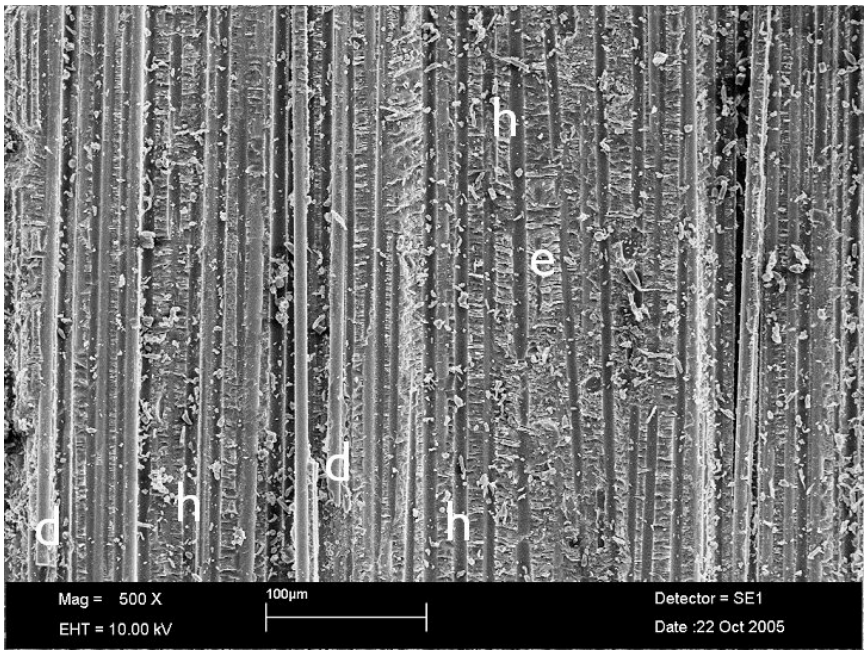

Figure 9-54: T-C fatigue fracture of a 51 MPa prestressed composite at a low stress level (524 MPa peak stress). Features such as fibre fracture (d), matrix hackle formation (e) and fibre impression (h) can be observed.

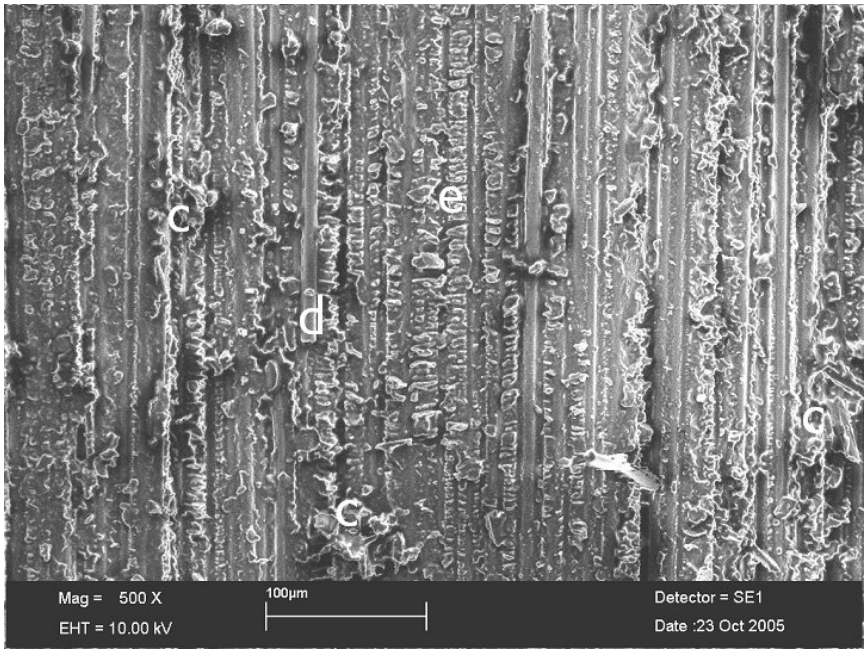

Figure 9-55: T-C fatigue fracture of a 108 MPa prestressed composite at a low stress level (524 MPa peak stress). Features such as matrix plasticity (c), fibre fracture (d) and matrix hackle formation (e) can be observed.

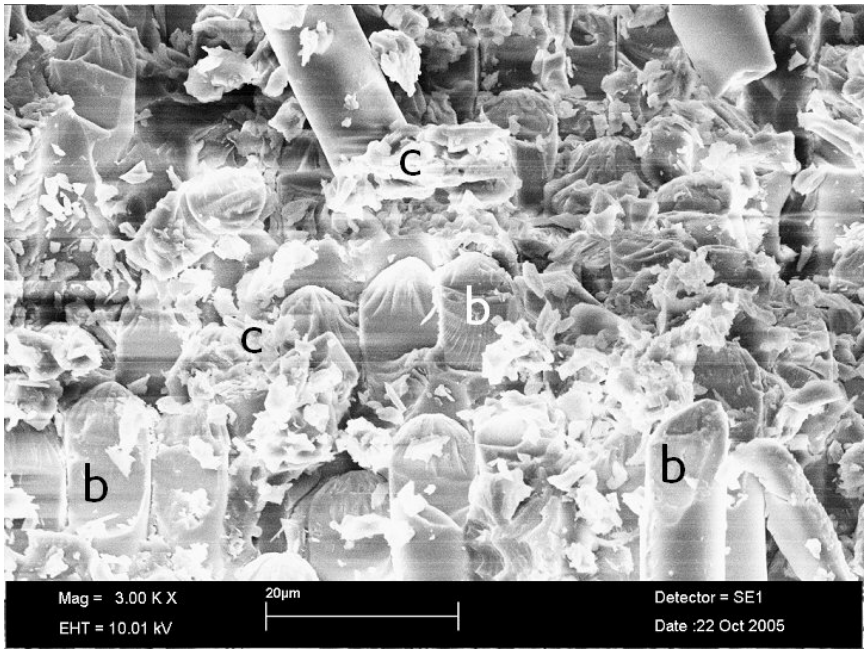

Figure 9-56: Compressive failure in a non-prestressed composite at a low stress level (524 MPa peak stress). Features such as compressive fibre fracture (b) and matrix plasticity (c) can be seen.

9.3 Concluding remarks

This chapter presented the results from tension-tension and tension-compression fatigue tests of non-prestressed and prestressed composites. From the results presented the following conclusions can be made.

9.3.1. Tension-tension fatigue

Normalised tension-tension fatigue data showed that the fatigue life of E-glass/913 composites at low stress levels was improved by prestressing. The fatigue life improvement achieved at a 524 MPa peak stress level for the 51 MPa and 108 MPa prestressed composites were 75% and 55% greater than that of the non-prestressed composites. In low stress level fatigue the damage is concentrated in the matrix leading to matrix cracking and interfacial debonding failure. The reduction in tensile residual stress in the matrix by prestressing will delay the matrix damage, which will increase the fatigue endurance limit of the composite. However, in the high stress level region no significant difference was observed between the non-prestressed and prestressed composites. This is because in high stress level fatigue the damage is dominated by the fibre properties of the composite. As the fibres are subjected to tensile residual stresses by prestressing, the applied fatigue load would be higher and this would reduce the fatigue life of the composites.

The stiffness degradation and surface temperature rise in non-prestressed and prestressed composites showed a three-stage behaviour. It was found that the prestressed composites were more effective in delaying the stiffness degradation in low stress level fatigue. The surface temperature rise in non-prestressed composites was slightly higher than the prestressed composites in stage I. This also suggests that the micro-damage in prestressed composites could be delayed. The enhanced resistance to stiffness degradation could be due to the reduction in residual stress in the matrix, which in turn reduces the micro-damage in the matrix. Whereas, in high stress level fatigue the stiffness degradation in prestressed composites was rapid and this could be due to the increase in tensile residual stresses in fibres and micro-residual stresses at the interface. This in turn reduces the resistance to interfacial crack initiation and crack growth of the composite. Also the surface temperature measurements recorded a slightly higher surface temperature in prestressed composites compared to non-prestressed composites.

From the macroscopic failure examination it is concluded that for low stress level fatigue the extent of longitudinal splitting was significantly reduced in prestressed composites. However, for high stress level fatigue both the non-prestressed and prestressed composite showed a similar brush-like failure. From the microscopic failure analysis it was found that in both low and high stress levels there is no difference in failure between non-prestressed and prestressed composites.

9.3.2. Tension-compression fatigue

A significant improvement in the fatigue life of prestressed composites was observed in the low stress level region of normalised fatigue data. The fatigue life improvements achieved at a 524 MPa peak stress for the 51 MPa and 108 MPa prestressed composites were over 200% greater than that of the non-prestressed (0 MPa) composite. The reduction in tensile residual stress in the matrix would delay the damage initiation and crack growth in the matrix, which would have increased the fatigue life of composites at low stress levels. Also for high stress level fatigue, the 51 MPa and 108 MPa prestressed composites showed an improvement in fatigue life of 94% and 50% respectively when compared with the non-prestressed composite. The improvement in fatigue life could be due to increased tensile residual stresses in fibres, which would have reduced the compressive damage in composites. However, at intermediate stress levels there appeared to be no influence of prestress on fatigue life. This could be due to the dominance of fibre, matrix and interfacial properties acting together.

The stiffness degradation in prestressed composites was significantly less when compared to non-prestressed composites in both low and high stress level fatigue cycles. The reason for the delay in stiffness degradation in low stress level fatigue could be due to the minimisation of tensile residual stresses in the matrix and improvement in the fibre alignment. This will increase the resistance to matrix and interfacial fatigue damage. Also in high stress level fatigue, the increase in the tensile residual stress in the fibre will increase the resistance to compressive damage of composites, which in turn would have reduced the stiffness degradation. The measured surface temperature rise in non-prestressed composites was greater than that in prestressed composites for low stress level fatigue. This also correlates with the stiffness degradation results and also supports the concept that the damage in prestressed composites is delayed when compared to non-prestressed composites.

From the macroscopic failures it was found that, for low stress level fatigue the degree of longitudinal splitting for prestressed composites was less than in non-prestressed composites. This could be due to the reduction in residual tensile stresses in the matrix. However, for high stress level fatigue, the degree of damage in non-prestressed and prestressed composite was similar. The microscopic analysis of composites tested from high stress level fatigue showed both compressive and tensile failures. However, the extent of compressive failure in composites reduces with prestress. This could be attributed to the improvement in fibre alignment. In low stress level fatigue region, the extent of fibre damage in prestressed composites is less when compared to non-prestressed composites. In prestressed composites the damage is predominantly in the matrix. The reason for less fibre fracture in prestressed composites could be due to the improvement in fibre alignment and an increase in tensile residual stress in the fibres.

CHAPTER 10

Conclusions and directions for future research

OVERVIEW
- Conclusions
- Future work

THE PRESENT STUDY DEMONSTRATED a flat-bed prestressing methodology to prepare prestressed composites in an autoclave and to monitor the applied load and residual strain development online during the manufacturing process. The residual stress development, quasi-static tensile and compression, and fatigue properties (both tension-tension and tension-compression) of non-prestressed and prestressed unidirectional E-glass/913 epoxy composites were investigated in this research. This chapter presents the overall conclusions and contributions from the investigation.

10.1 Fibre prestress methodology

A new approach to fibre prestressing was presented using a flat-bed prestress methodology for manufacturing prestressed composites. The FBPM was designed to apply a unidirectional prestress to the fibres. From the design calculations, it was shown that the rig is capable of applying 100 MPa prestress to the fibres. The FBPM was designed to monitor and measure the applied load to the fibres via the load cell. The salient advantages of flat-bed prestress methodology are 1) one parameter to control the applied load (load

screw), 2) ability to monitor the applied load online, 3) enables conventional vacuum bagging and 4) allows processing prepreg-based composites in an autoclave.

10.2 Evaluation of prestress methodology and sensors

Prestress rig evaluation:

From the static tensile prestress rig evaluation test, it can be concluded that the strain distribution in the steel plate is uniform. A variation of 4% strain through the width of the panel was observed. This could be due to (i) the Poisson's effect, (ii) small misalignment in the ERSG sensors and (iii) measurement errors.

A linear relationship was found between the strain measured from the steel plate and the applied load using the load screw in the prestress rig. This is because the load applied is within the elastic region of the steel plate.

Prepreg end-tab jig design and evaluation:

A flat-bed end-tab jig was designed to circumvent the fibre misalignment near the end-tab region. Using this end-tab jig it was shown that fibre misalignment near the end-tab region was eliminated.

Results from the surface profile of the composite shows that the prestressed composite manufactured with the aid of an end-tab jig eliminated the bending of the composite panel.

Sensor evaluation:

A linear relationship was observed in the load cell with an increase in temperature. A change in load of about 0.8 kN was measured for a temperature rise of 94°C. This small change in load observed is negligible and shows that the load cell is temperature compensated.

The measured thermal expansions in the unidirectional composite (in the fibre direction) from embedded optical fibre sensors are in good agreement with the theoretically-predicted thermal expansion from the micro-mechanical model.

The temperature measured from the embedded FBG temperature sensors was in good agreement with the temperature measured from the thermocouple in the autoclave.

The temperature and pressure gave no significant change in the measured strain from the reference optical fibre sensors. This shows that the recorded residual strain development from optical fibre sensors in composites was not influenced by the autoclave parameters (temperature and pressure).

Preliminary studies show that the embedded optical fibre sensor in the prepreg recorded a compressive strain of about 80 με for -830 milibars (-0.084 MPa) vacuum. However, when the vacuum is released not all the compressive strain in the optical fibre was removed. This is because prior to the solidification of the resin it is difficult to control the relative orientation of the FBG sensor.

10.3 Residual strain development

Results from the residual strain measurement using the EFPI sensors in non-prestressed and prestressed unidirectional $[0^{\circ}_{16}]$ composites show that fibre prestressing methodology can be used to reduce and control the residual strain development in composites. Also it was shown that by applying 108 MPa prestress, a composite with approximately zero final residual strain can be prepared.

Experimental residual strain results measured using EFPI and FBG strain sensors are greater than those predicted from Tsai and Hahn, and Wagner models. This is because the models predict only the thermal stresses and on a micro-mechanical scale. On the other hand the experimental results are measured in macroscopic laminates which would include the cure-induced and thermally-induced residual stresses, and the interaction of neighbouring fibres on the magnitude of residual stress in the host fibre.

Experimentally, it was also shown that the measured strain release from EFPI, FBG and ERSG sensors were in good agreement with each other. The difference in strain measured through the width of the composite is conjectured that to be due to Poisson's ratio and edge effects.

10.4 Theoretical analysis of prestressed composites

A theoretical model was developed to predict the strain released to the composite for a given applied fibre prestress. The theoretical prediction is in good agreement with the experimental results measured from EFPI, FBG and ERSG sensors.

This model was further developed to predict the Poisson's effect on the strain variation through the width of a unidirectional panel during the strain release. A small variation in strain distribution of about 1% across the width of the composite was predicted.

10.5 Fibre alignment

Fibre prestressing improves the alignment of fibres in composites. This improvement in fibre alignment resulted in an increase from 20% of fibres oriented in the 0° direction in non-prestressed composites to 75% of fibres oriented in the 0° direction for a 108 MPa

prestressed composite. Above this prestress level no further improvement in alignment of the fibre was observed.

10.6 Static mechanical properties

Tensile properties:

Fibre prestressed composites show an improvement in strain at deviation from linearity in stress-strain curve. This suggests that prestressing could have increased the resistance to the onset of damage (matrix cracking, fibre-matrix debonding and weak fibre failure). This improvement in SDL was observed up to 108 MPa prestress, above which it reduces. This suggests that an optimum prestress limit for the improvement in strain at deviation from linearity exists.

A theoretical prediction for the effect of prestress on failure strain of composites was presented. The theory predicts that the fracture strain of a composite decreases with an increase in prestress. This is because the residual tensile stress in the fibre increases with prestress. This reduces the fracture strain of the composite. However, from the experimental results no significant change in the tensile fracture strain was observed. This could be due to greater scatter in the measurements. It was also shown that the tensile strength and modulus of composites are independent of fibre prestressing.

From the macroscopic examination it can be concluded that there is no change in the composite failure mechanism with fibre prestress. However, from the microscopic examination it was found that at higher prestress levels more fibre fragmentation was observed. This could be due to (i) breaking the weak fibres during prestressing results in predominantly strong fibres in the composite and (ii) an increase in tensile residual stress in the fibre with prestress. This results in increased strain energy stored in the fibres.

Compressive properties:

Fibre prestressing shows an improvement in the average compressive strength and modulus by 9%. However, above an optimum prestress limit (108 MPa for compressive strength and 80 MPa for compressive modulus) there is an indication of reductions in compression properties. This could be because of the increase in residual stresses at the interface with fibre prestress, above the optimum limit the fibre-matrix interface is prone to debonding, which could lead to a reduction in compressive properties.

Fibre prestressing shows a change in the compression damage mechanism. The non-prestressed (0 MPa) composites fractured by fibre kink-band formation, whereas prestressed composites fractured by extensive longitudinal splitting and matrix deformation. This change in damage mechanism suggests that the improvement in fibre

alignment as a result of prestressing has changed the fibre kink-band failure mode to a longitudinal splitting and crushing mode.

An unknown matrix failure mode was observed in prestressed composites in the form of curling. This type of fracture mode has not been reported in the literature previously. The possible mechanisms for matrix curling could be due to the relaxation of the residual stress in the interface and matrix during fibre-matrix debonding.

10.7 Fatigue behaviour

Tension-tension fatigue:

Normalised tension-tension fatigue data showed that the fatigue life of E-glass/913 composites at low stress levels was improved by prestressing. The fatigue life improvement achieved at a 524 MPa peak stress level for the 51 MPa and 108 MPa prestressed composites were 75% and 55% greater than that of the non-prestressed composites. In low stress level fatigue the damage is concentrated in the matrix leading to matrix cracking and interfacial debonding failure. The reduction in tensile residual stress in the matrix by prestressing could delay the matrix damage, which would have increased the fatigue endurance limit of the composite.

In the high stress level region no significant difference was observed between the non-prestressed and prestressed composites. This is because in high stress level fatigue the damage is dominated by the fibre properties of the composite. As the fibres are subjected to tensile residual stresses by prestressing, the applied fatigue load would be higher and this would reduce the fatigue life of the composites. The stiffness degradation and surface temperature rise in non-prestressed and prestressed composites showed a three-stage behaviour. It was found that the prestressed composites were more effective in delaying the stiffness degradation for low stress level fatigue. The surface temperature rise in non-prestressed composites was slightly higher than that of prestressed composites in stage I. This also suggests that the micro-damage in prestressed composites could be delayed. The enhanced resistance to stiffness degradation could be due to the reduction in residual stress in the matrix, which in turn reduces the micro-damage in the matrix.

In high stress level fatigue the stiffness degradation in prestressed composites was rapid and this could be due to the increase in tensile residual stresses in fibres and micro-residual stresses at the interface. This in turn reduces the resistance to interfacial crack initiation and crack growth of the composite. Also the surface temperature measurements recorded a slightly higher surface temperature in prestressed composites compared to non-prestressed composites.

From the macroscopic failure examination it is concluded that for low stress level fatigue the extent of longitudinal splitting was significantly reduced in prestressed composites.

However, at high stress level fatigue both the non-prestressed and prestressed composite showed a similar brush-like failure. From the microscopic failure analysis it was found that at both low and high stress levels there is no difference in failure between non-prestressed and prestressed composites.

Tension-compression fatigue:

A significant improvement in the fatigue life of prestressed composites was observed in the low stress level region of normalised fatigue data. This fatigue life improvements achieved at a 524 MPa peak stress for the 51 MPa and 108 MPa prestressed composites were over 200% greater than that of the non-prestressed (0 MPa) composite. The reduction in tensile residual stress in the matrix would delay the damage initiation and crack growth in the matrix, which would have increased the fatigue life of composites at low stress levels.

Also at high stress level fatigue, the 51 MPa and 108 MPa prestressed composites showed an improvement in fatigue life of 94% and 50% respectively when compared with the non-prestressed composite. This improvement in fatigue life could be due to increased tensile residual stresses in the fibres, which would have reduced the compressive damage in composites. However, at the intermediate stress levels there appeared to be no influence of prestress on fatigue life. This could be due to the dominance of fibre, matrix and interfacial properties acting together.

The stiffness degradation in prestressed composites was significantly less when compared to non-prestressed composites for both low and high stress level fatigue cycles. The reason for the delay in stiffness degradation for low stress level fatigue could be due to the minimisation of tensile residual stresses in the matrix and improvement in the fibre alignment. This will increase the resistance to matrix and interfacial fatigue damage.

For high stress level fatigue, the increase in tensile residual stress in the fibre will increase the resistance to compressive damage of composites, which in turn would have reduced the stiffness degradation. The measured surface temperature rise in non-prestressed composites was greater than that in prestressed composites for low stress level fatigue. This also correlates with the stiffness degradation results and also supports the concept that the damage in prestressed composites is delayed when compared to non-prestressed composites.

From the macroscopic failures it was found that, for low stress level fatigue the degree of longitudinal splitting for prestressed composites was less than in non-prestressed composites. This could be due to the reduction in residual tensile stresses in the matrix. However, for high stress level fatigue, the degree of damage in non-prestressed and prestressed composite was similar. The microscopic analysis of composites tested from high stress level fatigue showed both compression and tensile failure. However, the extent of compressive failure in composites reduces with prestress. This could be attributed to the improvement in fibre alignment. In low stress level fatigue region, the extent of fibre

damage in prestressed composites is less when compared to non-prestressed composites. In prestressed composites the damage is predominantly in the matrix. The reason for less fibre fracture in prestressed composites could be due to the improvement in fibre alignment and an increase in tensile residual stress in fibres.

10.8 Directions for future research

This research investigated the effect of fibre prestress on residual stress, fibre waviness, static mechanical and fatigue properties in unidirectional composites. From the investigations it was found that fibre prestressing enhances the static and fatigue performance by reducing the residual stress and improving the fibre alignment in the composites. The following are the suggestions for continuing the research.

- One of the important criteria for aerospace structures is that the structure should have high fatigue resistance. This research demonstrated that fibre prestressing improves the tension-tension and tension-compression fatigue performance of unidirectional composites. Further research could investigate the effect of prestress on fatigue performance of cross-ply and quasi-isotropic laminates with glass/epoxy, carbon/epoxy and aramid /epoxy and also hybrid fibre composites.
- Prestress methodology could be designed to enable prestressing all the ply directions of cross-ply and quasi-isotropic laminates.
- Theoretical study of cure-induced residual stresses and the interaction of neighbouring fibres on the host fibre residual stress could be made. In addition, the theoretical analysis presented for the unidirectional composites in this research can be extended to a cross-ply and quasi-isotropic laminates to predict the effect of prestress on residual stresses and mechanical properties.
- The reduction in matrix residual stresses in prestressed composites may improve the fracture toughness properties. Therefore studies on the Mode I, II and III, fatigue crack propagation (delamination, transverse cracking) of prestressed multi-directional laminates could be investigated.

CHAPTER 11

References

1 D Hull, TW Clyne, "An introduction to composite materials" Cambridge solid state science series, Second edition, ISBN 0-521-38855-4, 1996.

2 ME Tuttle, "A mechanical/thermal analysis of prestressed composite laminates", Journal of Composite Materials, **22**, 1998, 780-792.

3 K Shulte, R Marissen, "Influence of artificial prestressing during curing of CFRP laminates on interfibre transverse cracking", Comoposite Science and Technology, **44**, 1992, 361-367.

4 LT Drzal, MJ Rich, PF Lloyd, "Adhesion of graphite fibers to epoxy matrices: 1. The role of fiber surface-treatment", Journal of Adhesion, **16** (1), 1982, 1-30.

5 J Kalantar, LT Drzal, "The bonding mechanism of aramid fibres to epoxy matrices: Part1 A review of the literature", Journal of Materials Science, **25**, 1990, 4186-4193.

6 FC Campbell, "Manufacturing processes for advanced composites", Elsevier Ltd., ISBN 1-85617-415-8, 2004.

7 S-Y Lee, GS Springer, "Effects of cure on the mechanical properties of composites", Journal of Composite Materials, **22**, 1988, 15-29.

8 D Kugler, TJ Moon, "Identification of the most significant processing parameters on the development of fibre waviness in thin laminates", Journal of Composite Materials", **36** (12), 2002, 1451-1479.

9 G Twigg, A Poursartip, G Fernlund, "Tool-part interaction in composites processing. Part I: experimental investigation and analytical model", Composites Part A, **35**, 2004, 121-133.

10 HT Hahn, "Effects of residual stresses in polymer matrix composites", Journal of Astronautical Science **32** (3), 1984, 253-267.

11 MR Piggott, "The effect of fibre waviness on the mechanical properties of unidirectional fibre composites: A Review", Composite Science and Technology, **53**, 1995, 201-205.

12 MS Madhukar, MS Genidy, JD Russell, "A new method to reduce cure-induced stresses in thermoset polymer composites, Part I: Test Method", Journal of Composite materials, **34** (22), 2000, 1882-1904.

13 JD Russell, "Cure shrinkage of thermoset composites", SAMPE quarterly, January 1993, 28-33.

14 SR White, HT Hahn, "Mechanical property and residual stress development during cure of a Gr/BMI composite", Polymer Engineering Science, **30** (22), 1990, 1465-73.

15 FR Jones, "Laminates – residual thermal and related strains", in Handbook of Polymer-Fibre Composites, Editor: F R Jones, ISBN 0-582-06554-2, 1994, 254 - 260.

16 NJ Rendler, I Vigness, "Hole-drilling strain-gauge method of measuring residual stresses", Experimental Mechanics, 1966, 577-586.

17 RY Kim, HT Hahn, "Effect of curing stress on the first ply failure in composite laminates" Journal of Composite Materials, **13**, 1979, 2-16.

18 PG Ifju, X Niu, BC Kilday, SC Liu, SM Ettinger, "Residual stress measurement in composites using the cure-referencing method", Experimental Mechanics, **40**, 2000, 22-30.

19 B Benedikt, M Kumosa, PK Predecki, L Kumosa, MG Castelli and JK Sutter, "An analysis of residual thermal stresses in a unidirectional graphite/PMR-15 composite based on X-ray diffraction measurements", Composites Science and Technology, **61**(14), 2001, 1977-1994.

20 X Yan, T Ohsawa, "Measurement of the internal local stress-distribution of composite-materials by means of laser imaging methods", Composites, **25** (6), 1994, 443-450.

21 Q Ma and DR Clarke, "Measurement of residual stresses in sapphire fiber composites using optical fluorescence", Acta Metallurgica et Materialia, **41**(6), 1993, 1817-1823.

22 RJ Young, RJ Day, M Zakikhani, IM Robinson, "Fibre deformation and residual thermal stresses in carbon fibre reinforced PEEK", Composites Science and Technology, **34**, 1989, 243-258.

23 IM Daniel, T Liber, "Effect of laminate construction on residual stresses in graphite/polyimide composites", Experimental Mechanics, **17**, 1977, 21-25.

24 Liu T, Wu M, Rao Y, Jackson DA, Fernando GF, "A multiplexed optical fibre-based extrinsic Fabry-Perot sensor system for in-situ strain monitoring in composites", Smart Materials and Structures, **7** (4), 1998, 550-556.

25 CM Lawrence, DV Nelson, JR Spingarn, TE Bennett, "Measurement of process-induced strains in composite materials using embedded fibre optic sensors", SPIE, **2718**, 1997, 60-68.

26 CM Lawrence, DV Nelson, TE Bennett, JR Spingarn, "An embedded fibre optic-sensor method for determining residual stresses in fibre-reinforced composite materials", Journal of Intelligent Material Systems and Structures, **9**, 1998, 788-799.

27 RM Measures, "Fibre optic sensing for composite smart structures", Composites Engineering,; **3** (7-8), 1993, 715-750.

28 V Bhatia, KA Murphy, RO Claus, TA Tran, JA Greene, "Recent developments in optical-fibre-based extrinsic Fabry-Perot interferometric strain sensing technology", Smart Materials and Structures, **4**, 1995, 246-251.

29 GF Fernando, DJ Webb, P Ferdinand, Guest Editors, "Optical-fibre sensors", MRS Bulletin, May 2002, 359-364.

30 B Degamber, GF Fernando, "Process monitoring of fibre-reinforced polymer composites", MRS Bulletin, **27** (5), 2002, 370-380.

31 C Doyle, A Martin, T Liu, M Wu, S Hayes, PA Crosby, GR Powell, D Brooks, GF Fernando, "In-situ process and condition monitoring of advanced fibre-reinforced composite materials using optical fibre sensors", Smart Structures and Materials, **7**, 1998, 145-158.

32 R Badcock, S Krishnamurthy, G.F Fernando, T Butler, R Chen and J Tetlow, "Health monitoring of composite structures using a novel fibre optic acoustic emission sensors", The 11th European Conference on Composite Materials, 31 May - 3 June 2004 Rhodes , Greece.

33 JS Sirkis, "Optical fibre strain sensing in engineering mechanics", Topics in applied Physics, **77**, 2000, 233-272.

34 A Othonos, K Kalli, "Fibre Bragg Gratings", Artech House, Boston, London, ISBN: 0-89006-344-3, 1999.

35 FM Haran, JK Rew, PD Foote, "A strain-isolated fibre Bragg grating sensor for temperature compensation of fibre Bragg grating strain sensors ", Measurement Science and Technology, **9** (8), 1998, 1163-1166.

36 M Jinno, S Sakai, K Osaka, T Fukuda, "Smart autoclave processing of thermoset resin matrix composites based on temperature and internal strain monitoring", Advanced Composite Materials, **12** (1), 2003, 57-72.

37 H Kang, D Kang, C Hong, C Kim, "Simultaneous monitoring of strain and temperature during and after cure of unsymmetric composite laminate using fibre-optic sensors", Smart Materials and Structures, **12**, 2003, 29-35.

38 SW.Tsai, H.T.Hahn, "Introduction to Composite Materials", Technomic Publications Co., Inc. Westport, CT, ISBN 0-87762-288-4, 1980, 402-407.

39 HD Wagner, "Residual stresses in microcomposites and macrocomposite", Journal of Adhesion, **52**, 1995, 131-148.

40 JA Nairn, "Thermoelastic analsyis of residual stresses in unidirectional high-performance composites", Polymer Composites, **6** (2), 1985, 123-130.

41 Y Chen, Z Xia, F Ellyin, "Evolution of residual stresses induced during curing processing using a viscoelastic micromechanical model", Journal of Composite Materials, **35** (6), 2001, 522-542.

42 Y Zhang, Z Xia, F Ellyin, "Evolution and influence of residual stresses/strains of fibre reinforced laminates", Composites Science and Technology, **64**, 2004, 1613-1621.

43 PJ Joyce, D Kugler, TJ Moon, "A technique for characterising Process-Induced fibre waviness in unidirectional composite laminates-using optical microscopy", Journal of Composite Materials, **31** (17), 1997, 1694-1727.

44 RH Knibbs, JB Morris, "The effect of fibre orientation on the physical properties of composites", Composites, **5**, 1974, 209-218.

45 AM Mrse, MR Piggott, "Compressive properties of unidirectional carbon fibre laminates: II. The effects of unintentional and intentional fibre misalignment", Composites Science and Technology, **46**, 1993, 219-227.

46 HM Hsiao, IM Daniel, "Effect of fibre waviness on stiffness and strength reduction of unidirectional composites under compressive loading" Composites Science and Technology, **56**, 1996, 581-593.

47 DO Adams, MW Hyer, "Effect of layer waviness on the compression fatigue performance of thermoplastic composite laminates", Fatigue, **16**, 1994, 385-391.

48 HJ Chun, JY Shin, IM Daniel, "Effect of material and geometric nonlinearities on the tensile and compressive behaviour of composite materials with fibre waviness", Composites Science and Technology, **61**, 2001, 125-134.

49 SW Yurgartis, "Techniques for the quantification of composite mesostructure", Composites Science and Technology, **53**, 1995, 145-154.

50 AR Clarke, G Archenhold, NC Davidson, "A novel technique for determining the 3D spatial distribution of glass fibres in polymer composites", Composite Science and Technology, **55**, 1995, 75-91.

51 SR White, HT Hahn, "Cure cycle optimisation for the reduction of processing-induced residual stresses in composite materials", Journal of Composite Materials, **27** (14), 1993, 1352-1378.

52 MS Geindy, MS Madhukar, JD Russell, "A new method to reduce cure-induced stresses in thermoset polymer composites, Part II: Closed loop feedback control system", Journal of Composite Materials, **34**, (22), 2000, 1905-1925.

53 JD Russell, MS Madhukar, MS Genidy, AY Lee, "A new method to reduce cure-induced stresses in thermoset polymer composites, Part III: Correlating stress history to viscosity, degree of cure and cure shrinkage" Journal of Composite Materials, **34** (22) 2000, 1926-1947.

54 AK Gopal, S Adali, VE Verijenko, "Optimal temperature profiles for minimum residual stress in the cure process of polymer composites", Composite Structures, **48**, 2000, 99 – 106.

55 SP systems Ltd, SE 84LV product data sheet, 2005.

56 A Singh, "Radiation processing of carbon fibre-reinforced advanced composites", Nuclear Instruments and Methods in Physics Research B, **185**, 2001, 50-54.

57 S Korenev, "Electron beam curing of composites" Vacuum **62**, 2001, 233-236.

58 DL Goodman, GR Palmese, "Curing and bonding of composites using electron beam processing", Handbook of Polymer Blends and Composites, Volume 1, A Kulshreshtha and C Vasile, eds., Published by Rapra Technology Ltd, ISBN 1-85957-249-9, 2003, UK.

59 FR Jones, "Interphase formation and control in fibre composite materials", Key Engineering Materials, **116-117**, 1996, 41-60.

60 LE Asp, LA Berglund, R Talreja, "Effects of fibre and interphase on matrix-initiated transverse failure in polymer composites", Composites Science and Technology, **56**, 1996, 657-665.

61 DL Hiemstra, NR Sottos, "Thermally induced interfacial microcracking in polymer matrix composites", Journal of Composite Materials, **27**(10), 1993, 1030-1051.

62 NR Sottos, DL Hiemstra, WR Scott, "Correlating interphase glass transition and interfacial microcracking in polymer composites", Fracture Mechanics, **25**, ASTM STP 1220, F Erdogan and RJ Hartranft, Eds., 1994.

63 AL Roytburd, J Slutsker, M Wuttig, "Smart composites with shape memory alloys", Comprehensive Composite Materials, Volume **5**, Published by Elsevier Science Ltd., ISBN 0-08-042993-9, 2000, 507-522.

64 GC Psarras, J Parthenios, C Galiotis, "Adaptive composites incorporating shape memory alloy wires, Part I: Probing the internal stress and temperature distributions with laser Raman sensor", Journal of Materials Science, **36**, 2001, 535-546.

65 J Parthenious, GC Psarras, C Galiotis, "Adaptive composites incorporating shape memory alloy wires, Part II: development of internal recovery stresses as a function of activation temperature", Composites Part A, **32**, 2001, 1735-1747.

66 LS Penn, RCT Chou, ASD Wang, WK Binienda, "The effect of matrix shrinkage on damage accumulation in composites", Journal of Composite Materials, **23**, 1989, 570-586.

67 M Shimbo, MOchi, T Inamura, M Inoue, "Internal stress of epoxide resin modified with spiro ortho-ester type resin", Journal of Materials Science, **20**, 1985, 2965-2972.

68 J Orso, AJ Vizzini, "The effects of an expanding monomer on the tensile properties of graphite / epoxy", Journal of Composites Technology and Research, **16** (3), 1994, 270-274.

69 GJ Dvorak, AP Suvorov, "The effect of fibre pre-stress on residual stresses and the onset of damage in symmetric laminates", Composites Science and Technology, **60**, 2000, 1129-1139.

70 The Oxford English dictionary, Second Edition, prepared by JA Simpson and ESC Weiner, Volume XII, Clarendon Press, Oxford, 1989.

71 LDA Jorge, AT Marques, PMST De Castro, "The influence of prestressing on the mechanical behaviour of uni-directional composites", Developments in the science and Technology of the composite materials, Elsevier Applied Science, London and New York, 1990, 897 – 902.

72 DH Rose, JM Whitney, "Effect of prestressed fibres upon the response of composite materials", Proceedings of American Society of Composites, 8th Technical conference on composites, Lancaster, PA, 1993, 489-498.

73 GX Sui, G Yao, BL Zhao, "Influence of artificial pre-stressing during the curing of VIRALL on its mechanical properties", Composite Science and Technology, **53**, 1995, 361-364.

74 ME Tuttle, RT Koehler and D Keren, "Controlled thermal stresses in composites by means of fibre prestress", Journal of Composite Materials, **30**(4), 1996, 486-502.

75 S Motahhari, J Cameron, "Measurement of micro-residual stresses in fibre pre-stressed composites", Journal of Reinforced Plastics and Composites, **16** (12), 1997, 1129-1137.

76 S Motahhari, J Cameron, "Impact strength of fibre pre-stressed composites", Journal of Reinforced Plastics and Composites, **17** (2), 1998, 123-130.

77 J Zhao, J Cameron, "Polypropylene matrix composites reinforced with pre-stressed glass fibres", Polymer Composites, **19** (3), 1998, 218-224.

78 AS Hadi and JN Ashton, "On the influence of pre-stress on the mechanical properties of a unidirectional GRE composite", Composite Structures, **40**(3-4), 1998, 305-311.

79 S Motahhari, J Cameron, "Fibre prestressed composites: improvement of flexural properties through fibre prestressing", Journal of Reinforced Plastics and Composites, **18** (3), 1999, 279-288.

80 MP Jevons, GF Fernando, and GS Kalsi, "Effect of pre-tensioning on the low velocity impact performance of glass fibre composites", Tenth European conference on composite materials (ECCM-10), June 3-7, 2002, Brugge, Belgium.

81 DAL Lee, "The effects of residual stresses in unidirectional Kevlar 49/epoxy composite upon their mechanical properties", MSc Dissertation, University of Manchester and Institute of Science and Technology, 1992.

82 N Ali, "The effects of residual stresses in unidirectional Twaron/epoxy composite upon their mechanical properties", MSc Dissertation, University of Manchester and Institute of Science and Technology, 1993.

83 YK Huang, PH Frings, E Hennes, "Mechanical properties of Zylon/epoxy composite", Composite: Part B, **33,** 2002, 109-115.

84 KS Fancey, "Prestressed polymeric composites produced by viscoelastically strained nylon 6,6 fibre reinforcement", Journal of Reinforced Plastics and Composites, **19** (15), 2000, 1251-1266.

85 GF Fernando, FAA Al-Khodairi, "The fatigue of hybrid composites", Chapter 7 in Fatigue in Composites, Edited by Bryan Harris, Published by Woodhead Publishing Limited, 2003, 189-241, ISBN 1 85573608 X.

86 JF Mandell, "Fatigue behaviour of fibre-resin composites", Developments in reinforced plastics-2, edited by G Pritchard, Applied Science Publishers, 1982, 67-107.

87 IM Daniel and A Charewicz, "Fatigue damage mechanisms and residual properties of graphite/epoxy laminates", Engineering Fracture Mechanics, **25** (5-6), 1986, 793-808.

88 KL Reifsnider, " Damage and damage mechanics", in Fatigue of composites materials, Composite Materials Series, Vol. **4**, Edited by KL Reifsnider, Elsevier Science publications, 1991.

89 PT Curtis, "A review of the fatigue of composite materials", Technical Report No. **87031**, May 1987.

90 JW Dally, LJ Broutman, " Frequency effects on the fatigue of glass reinforced plastics", Journal of Composite Materials, **1**, 1967, 424-442.

91 FR Jones, " Moisture absorption – anomalous effects", in Handbook of Polymer-Fibre Composites, Editor: FR Jones, ISBN 0-582-06554-2, 1994, 254 - 260.

92 B Harris, "Fatigue – glass fibre reinforced plastics", in Handbook of polymer-Fibre Composites, Editor: FR Jones, ISBN 0-582-06554-2, 1994, 309 - 316.

93 B Harris, "Fatigue and accumulation of damage in reinforced plastics", Composites, **8** (4), 1977, 214-220.

94 GX Sui, G Yao, BL Zhou "Effects of prestrain on the fatigue properties of VIRALL laminate", Composite science and technology, **56** (8), 1996, 929-932.

95 CT Lin, PW Kao, FS Yang, "Fatigue behaviour of carbon fibre-reinforced aluminium laminates", Composites, **22** (2), 1991, 135 – 141.

96 BW Rosen, "Tensile failure of fibrous composites", AIAA Journal, **2** (11), 1964, 1985-1991.

97 M Fuwa, AR Bunsell, B Harris, "Tensile failure mechanisms in carbon fibre reinforced plastics", Journal of Materials Science, **10**, 1975, 2062-2070.

98 HT Hahn, JG Williams, " Compression failure mechanisms in unidirectional composites" Composite Materials: Testing and Design, ASTM STP **893**, edited by JM Whitney, American Society for Testing and Materials, Philadelphia, 1986, 115-139.

99 B Budiansky, NA Fleck, "Compressive failure of fibre composites", Journal of Mechanics and Physics of Solids, **41** (1), 1993, 183-211.

100 PM Jelf, NA Fleck, "Compression failure mechanisms in unidirectional composites", Journal of Composite Materials, **26** (18), 1992, 2706-2726.

101 MR Piggot, B Harris, "Compression strength of carbon, glass and Kevlar-49 fibre reinforced polyester resins" Journal of Material Science, **15**, 1980, 2523-2538.

102 SH Lee, AM Wass, "Compressive response and failure of fibre reinforced unidirectional composites", International Journal of Fracture, **100**, 1999, 275-306.

103 P Berbinau, C Soutis, IA Guz, "Compressive failure of 0° unidirectional carbon-fibre-reinforced plastic (CFRP) laminates by fibre microbuckling", Composite Science and Technology, **59**, 1999, 1451-1455.

104 CR Schultheisz, AM Waas, "Compressive failure of composites, Part I: Testing and micromechanical theories", Progress in Aerospace Science, **32**, 1996, 1-42.

105 HM Jensen, "Residual stress effects on the compressive strength of unidirectional fibre composites", Acta Materialia, **50**, 2002, 2895-2904.

106 MS Madhukar, LT Drzal, "Fibre-matrix adhesion and its effect on composite mechanical properties. III Longitudinal compressive properties of graphite/epoxy composites", Journal of Composite Materials, **26**, 1992, 310-333.

107 R Talreja, "Fatigue of composite materials", Technomic Publishing Company, Inc, ISBN 87762-516-6, 1987.

108 FP Beer, ER Johnston, "Mechanics of Materials" McGraw-Hill, ISBN 0-07-004284-5, 1981.

109 JE Shigley, "Mechanical Engineering Design" McGraw-Hill, 1986.

110 PC Powell, "Engineering with fibre-polymer laminates", Chapman & Hall, ISBN 0-412-49620-8, 1994.

111 Hexcel prepreg selector guide, Publication number FTU064d, Published by Hexcel Ltd, Cambridge, UK, 2004.

112 Hexcel composites product data sheet, Publication FTA054b, Oct 2002.

113 MH Geier, "Quality handbook for composite materials", Published by Chapman and Hall, London, UK, First edition, ISBN 0412431203, 1994, 169-171.

114 PT Curtis, "CRAG test methods for the measurement of the engineering properties of fibre reinforced plastics", Technical Report No.**88012**, Published by Royal Aerospace Establishment, 1988.

115 JG Häberle, EW Godwin, "The Imperial college method for testing composite materials in compression" The centre for composite materials, Technical Report No. **99/03**, Imperial College, London, 1999.

116 ISO 13003, Fibre-reinforced plastics – Determination of fatigue properties under cyclic loading conditions, 2003.

117 SW Yurgartis, "Measurement of small angle fibre misalignments in continuous fibre composites", Composite Science and Technology, **30**, 1987, 279-293.

118 J Lange, S Toll, J.-AE Manson and A Hult, "Residual stress build-up in thermoset films cured below their ultimate glass transition temperature", Polymer, **38** (4), 1997, 809-815.

119 S Goutianos, T Peijs, C Galiotis, "Comparative assessment of stress transfer efficiency in tension and compression", Composites Part A, **33** (10), 2002, 1303-1309.

120 I Partridge, P Virlouvet, J Chubb,and P Curtis, "Effect of fibre volume on tensile fatigue behaviour of unidirectional glass/epoxy composite" Third European Conference on Composite Materials (ECCM 3), AR Bunsell ed., France, 1989, 451.

121 RF Dickson, G Fernando, T Adam, H Reiter, B Harris, "Fatigue behaviour of hybrid composites Part 2: Carbon-glass hybrids", Journal of Materials Science **24**, 1989, 227-233.

122 WR Broughton, MJ Lodeiro, "Cyclic fatigue of continuous unidirectional polymer matrix composites", NPL Report CMMT (A) **249**, January 2000, published by National Physical Laboratory, UK.

123 J Scherf, HD Wagner, "Interpretation of fibre fragmentation in carbon/epoxy single fibre composites: Possible fibre pre-tension effects", Polymer Engineering and Science, **32** (4), 1992, 298-304.

124 FL Matthews, "Chapter 5 – Compression" in the book Mechanical testing of advanced fibre composites, edited by Hodgkinson JM, Woodhead Publishing Ltd and CRC Press, ISBN 1-85573-312-9, 2000.

125 J Lankford, "Compressive failure of fibre-reinforced composites: buckling, kinking and the role of the interphase", Journal of Materials Science, **30**, 1995, 4343-4348.

126 B Harris, H Reiter, T Adam, RF Dickson and G Fernando, "Fatigue behaviour of carbon-fibre reinforced plastics", Composites, **21** (3), 1990, 232-242.

127 J Lee, B Harris, DP Almond and F Hammett, "Fibre composite fatigue-life determination", Composites: Part A, **28A**, 1997, 5-15.

128 NH Tai, MC Yip, CM Tseng, "Influences of thermal cycling and low-energy impact on the fatigue behaviour of carbon/PEEK laminates", Composites: Part B, **30**, 1999, 849-865.

129 T Hobbiebrunken, B Fiedler, M Hojo, S Ochiai, K Schulte, "Microscopic yielding of CF/epoxy composites and the effect on the formation of thermal residual stresses", Composites Science and Technology, **65**, 2005, 1626-1635.

130 RA Badcock, GF Fernando, "An intensity-based optical fibre sensor for fatigue damage detection in advanced fibre-reinforced composites", Smart Materials and Structures, **4**, 1995, 223–230.

131 HT Hahn and RY Kim, "Fatigue behaviour of composite laminate", Journal of Composite Materials, **10**, 1976, 156-180.

132 PT Curtis, "The fatigue behaviour of fibrous composite materials", Journal of Strain Analysis, **24**, (4), 1989, 235-244.

133 CKH Dharan, "Fatigue failure in graphite fibre and glass fibre-polymer composites", Journal of Materials Science, **10**, 1975, 1665–1670.

134 PS Steif, "Stiffness reduction due to fibre breakage", Journal of Composite Materials, **17**, 1984, 153-172.

135 PT Curtis, "Tensile fatigue mechanisms in unidirectional polymer matrix composite materials", International Journal of Fatigue, **13**, (5), 1991, 377–382.

136 MR Bhat and CRL Murthy, "Fatigue damage stages in unidirectional glass fibre/epoxy composites: identification through acoustic emission technique", International Journal of Fatigue, **15** (5), 1993, 401-405.

137 R Richards-Frandsen, Y Naerheim, "Fracture morphology of graphite/epoxy composites", Journal of Composite Materials, **17**, 1983, 105.

138 D Purslow, "Matrix fractography of fibre-reinforced epoxy composites", Composites, **17** (4) 1986, 289-303.

139 WD Bascom, DJ Boll, DL Hunston, B Fuller, PJ Phillips, "Fractographic analysis of interlaminar fracture", ASTM STP **937**, 1987, 131-149.

140 GD Sims, DG Gladman, "Effect of test conditions on the fatigue strength of a glass-fabric laminate: Part A-frequency, Plastics and Rubber, May 1978, 41-48.

141 NH Tai, CCM Ma, SH Wu, "Fatigue behaviour of carbon fibre/PEEK laminate composites", Composites, **26**, 1995, 551-559.

APPENDIX A

Bi-axial loading frame method

OVERVIEW

- Jevons *et al.*[80] method for manufacturing prestressed composites contains a frame and four clamps as shown in Figure 2.16. The pre-load is applied to the prepreg by using a tensile testing machine and locked by the bolts to the frame.
- When the rig is removed from the tensile testing machine, pre-load applied to the prepreg may change because of the frame bending.
- Calculation of the change in the pre-load applied to the prepreg using classical mechanics is presented.

A.1 Pre-load calculations

Figure A-1 shows dimensions of the prepreg and its cross-section (A-A). A ply of glass fibre/epoxy prepreg has a thickness of 125 μm. An eight-ply laminate has a thickness of 1×10^{-3} m. The volume fraction of fibres is assumed to be $V_f = 60\%$.

Cross-sectional areas (CSA) of the fibres are expressed as follows:

Prepreg CSA: $A_{Prepreg} = (250 \times 10^{-3}) \times (1 \times 10^{-3}) = 250 \times 10^{-6}\,m^2$

Fibre CSA: $A_f = (250 \times 10^{-6}) \times (0.60) = 150 \times 10^{-6}\,m^2$

To obtain 100 MPa stress in the fibres, the required force to apply is calculated as shown below:

$$\sigma = \frac{F}{A_f} \tag{A-1}$$

$$F = (150 \times 10^{-6}) \times (100 \times 10^{6}) = 15 \text{ kN}$$

This force is used in the following calculations.

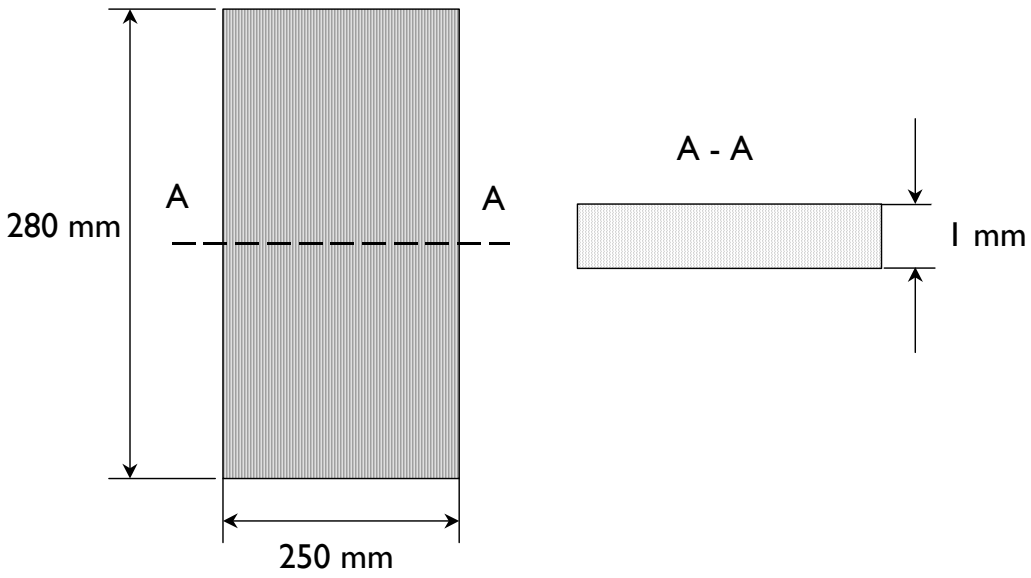

Figure A-1: A schematic diagram of prepreg and its cross-section with dimensions.

A.2 Jevons *et al.* C-Channel frame

A schematic diagram of the frame is shown in Figure A-2. The frame has holes to accommodate the bolts and clamps. However, in the following calculation, the holes are neglected for simplification.

A.2.1. Beam deflection

A uniaxial loading of the fibre prepreg clamped in the frame is considered here. In this case, the frame can be broken down into four elements: two beams, where the forces are applied, and two columns as shown in the Figure A-3. The beam can be considered as a simply supported beam. When the pre-load is locked by bolts, the force acting on the beam is a *two point load*. This is represented in Figure A-4.

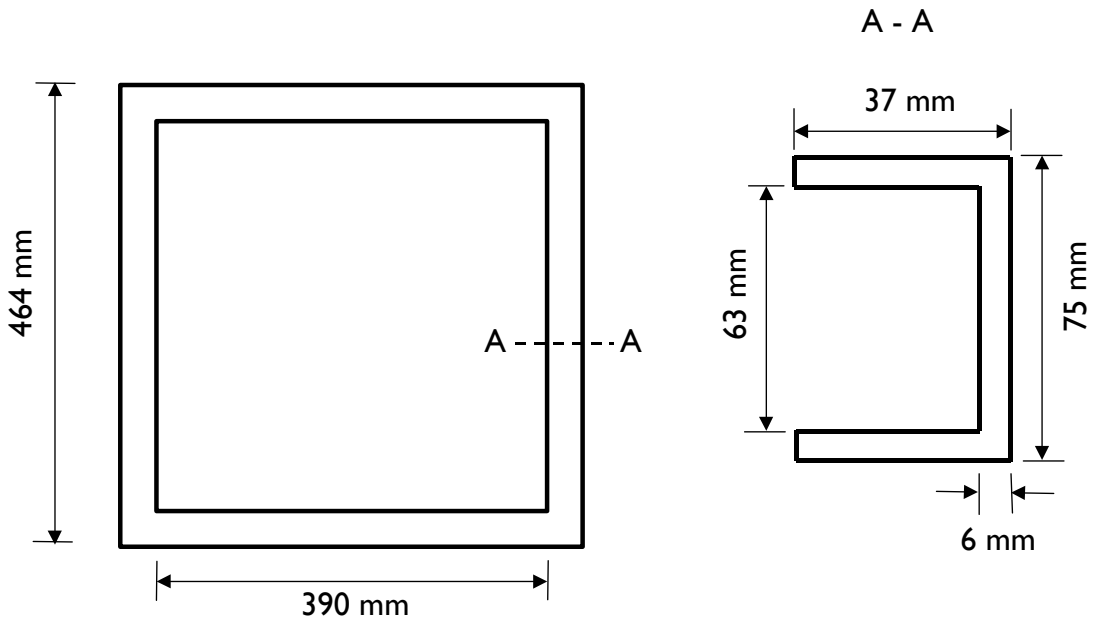

Figure A-2: A schematic representation of the frame.

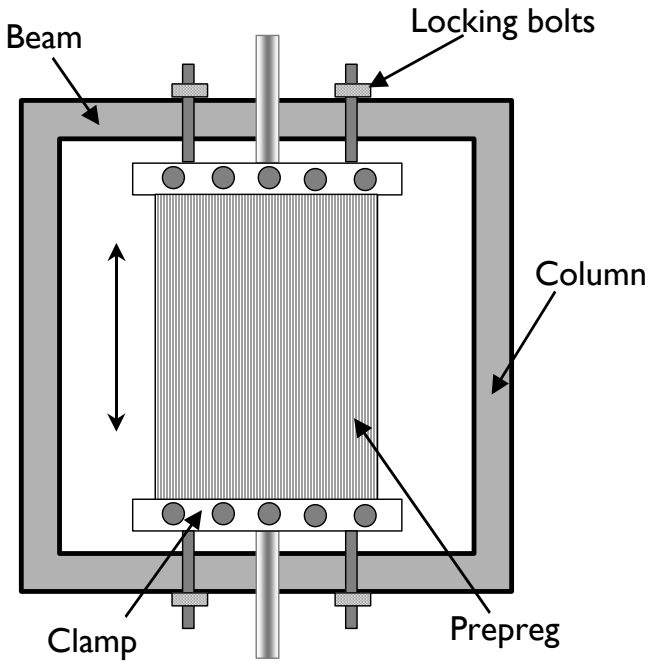

Figure A-3: Uniaxial loading in Jevons *et al.* prestress method.

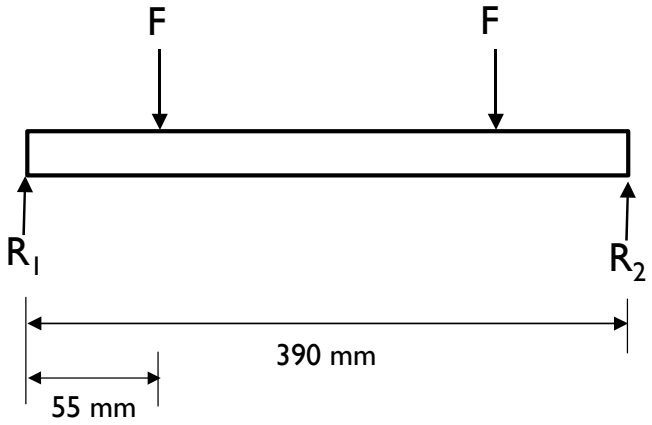

Figure A-4: Force diagrams of the beam.

Deflection of the beam can be determined by the following expression:

$$\delta = \frac{cFL^3}{EI} \qquad \text{(A-2)}$$

where c is the numerical coefficient (for a two point load c = 11/768), F is the force, L is the span length, E is the modulus of elasticity (for steel E = 200 GPa) and I is the moment of inertia of the beam.

The force F is chosen to be 15 kN because this is the load required to prestress the prepreg to 100 MPa as calculated in the previous section.

For a uniaxial loading, beam and column deflections were calculated to find the total displacement of the frame *per unit force*. The results are summarised in Table A-1.

Table A-1: Total displacement of the frame subjected to uniaxial loading.

C-Channel box section	Two point load [× 10^{-9} m/N]
Beam Deflection δ_B	38.30
Column Displacement $\Delta\delta_C$	1.08
Total Displacement $\Delta\delta$ [$\Delta\delta = \delta_B + \Delta\delta_C$]	39.38

A.2.2. Bi-axial loading of frame

In the above calculations, only one-directional *(uni-axial)* loading was considered. For prestressing cross-ply laminates, the load is applied in two directions, which deforms the frame in the respective loading directions. The deflection of the frame will be twice the deflection calculated for uni-axial loading.

APPENDIX B

Flat-bed prestress methodology

OVERVIEW

- The engineering drawings of flat-bed prestress methodology are presented.
- The photograph shows the manufactured prestress rig.
- The conventionally vacuum-bagged prepreg inside the autoclave is depicted.

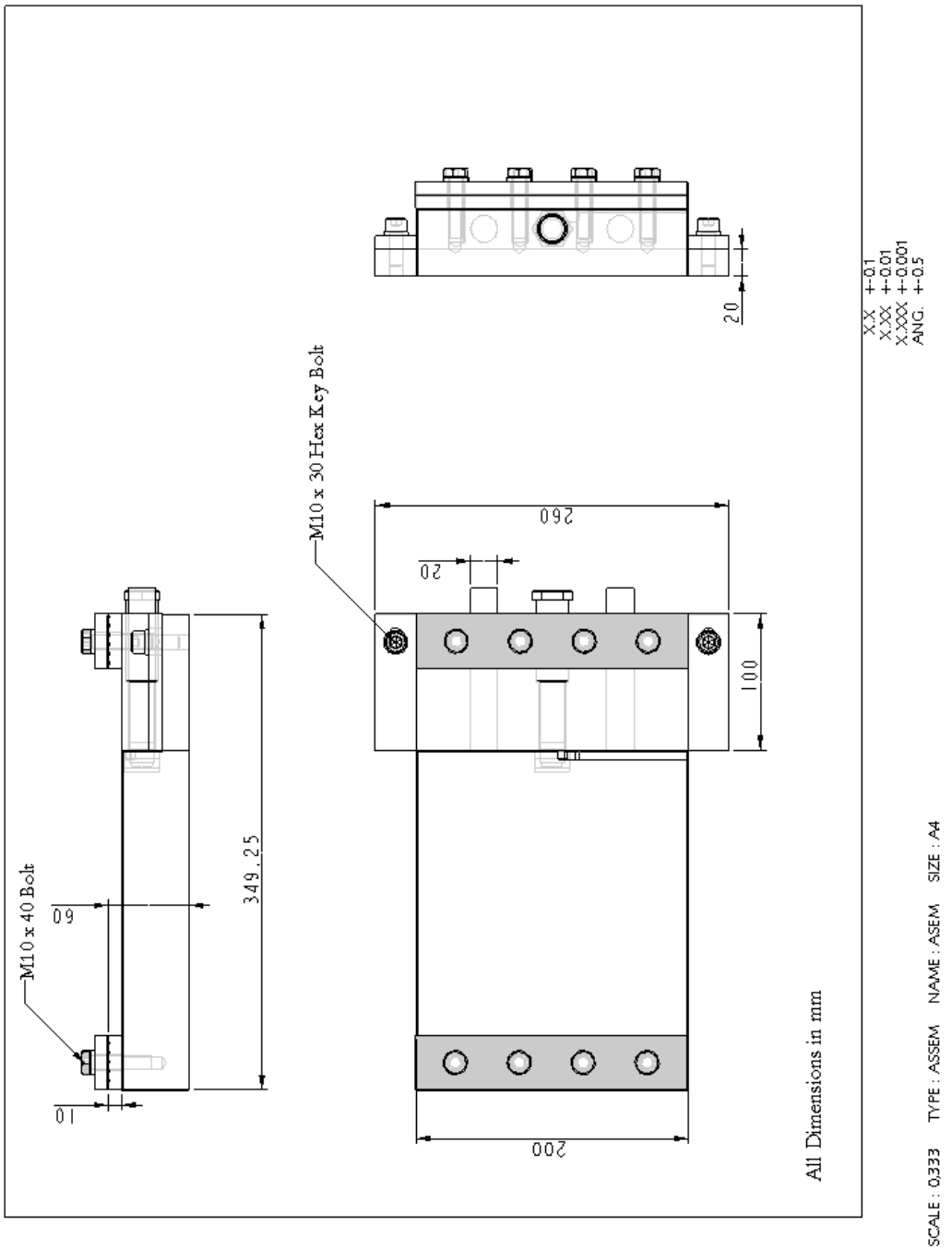

Figure B-1: Two-dimensional drawing of flat-bed prestress methodology.

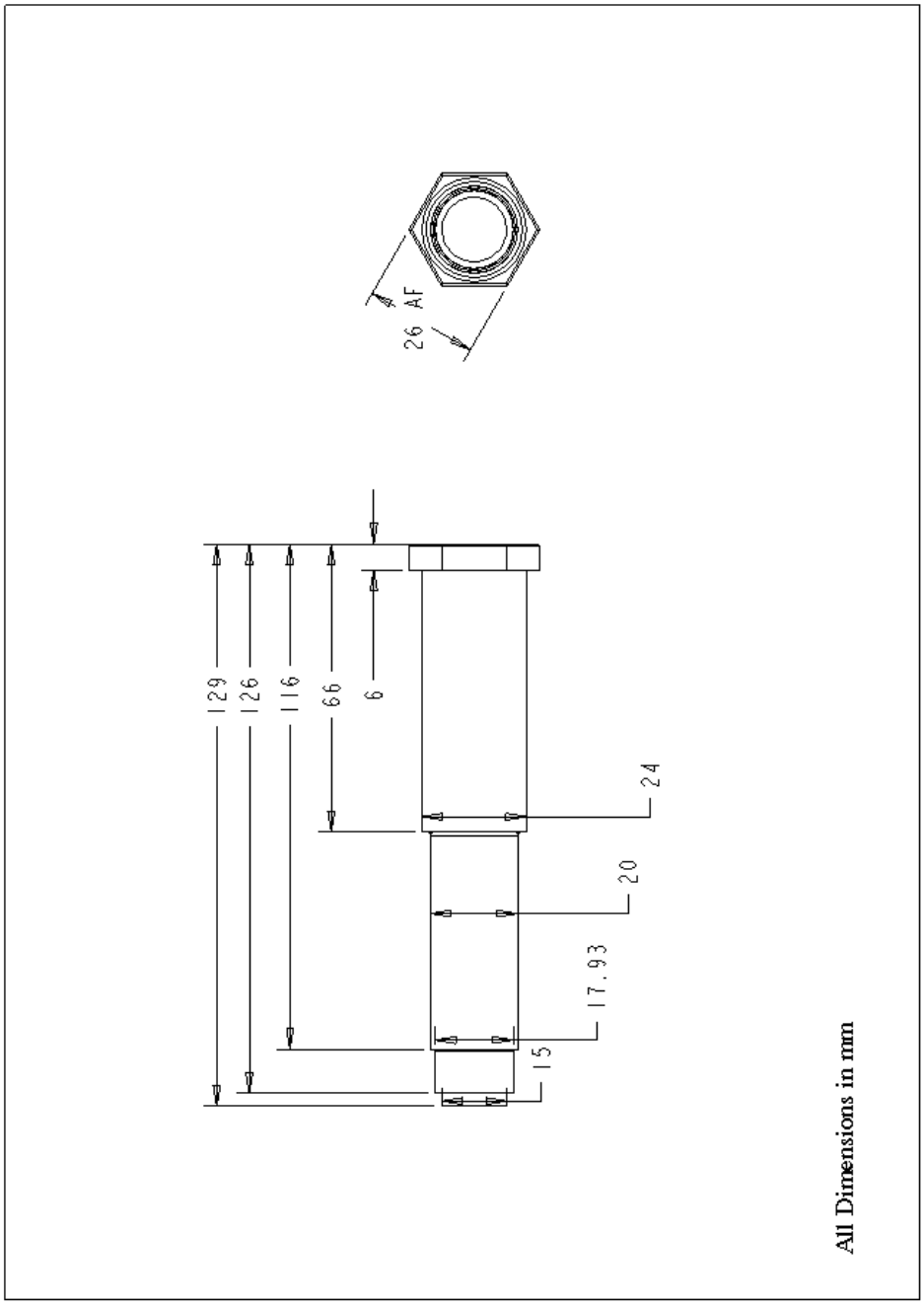

Figure B-2: Two dimensional drawing of load screw.

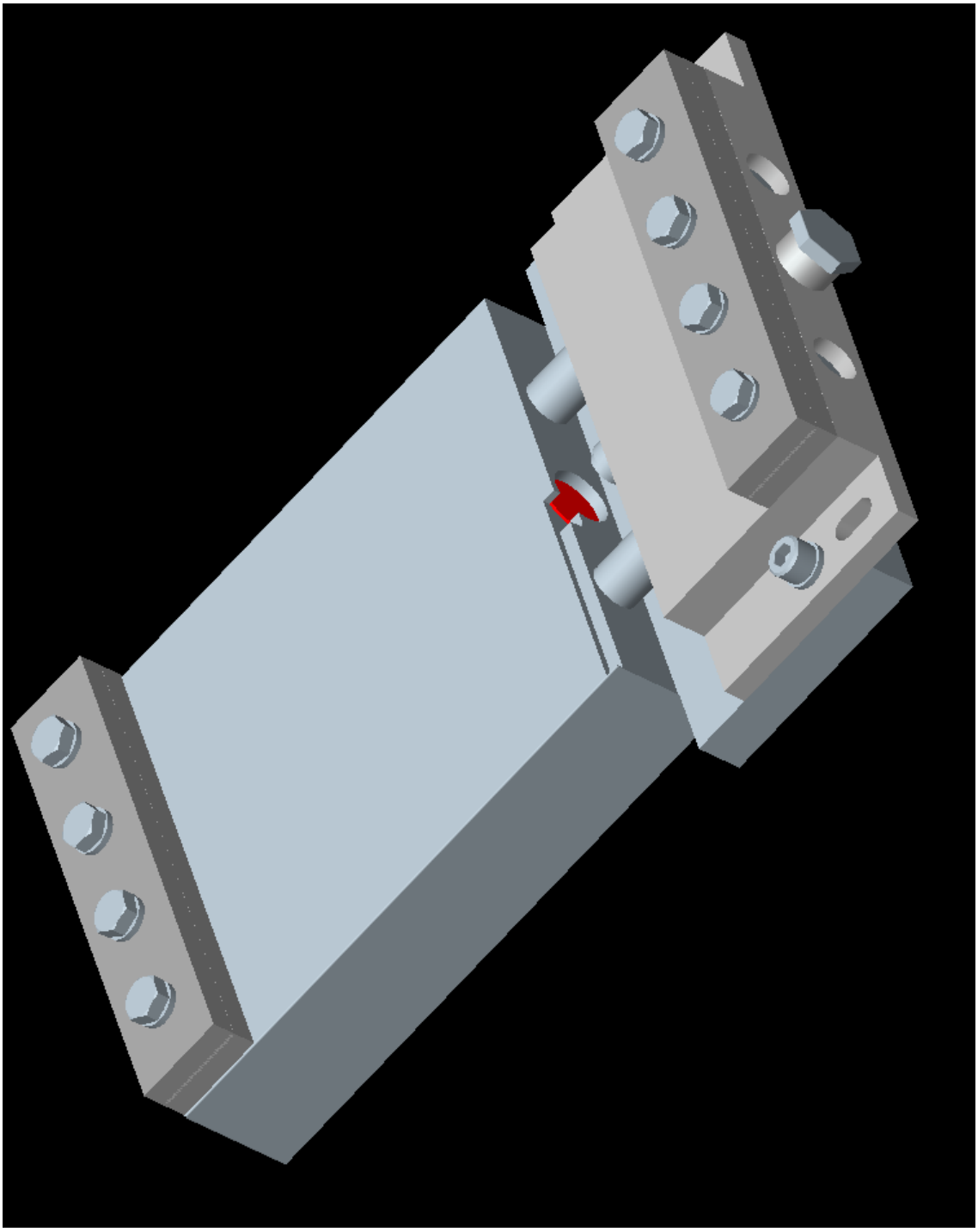

Figure B-3: Three-dimensional solid model of flat-bed prestress methodology.

Figure B-4: Photograph of manufactured flat-bed prestress rig instrumented with load cell.

Figure B-5: Photograph of conventionally vacuum-bagged prepreg laminate clamped to the FBPM inside the autoclave.

APPENDIX C

Measurements of static mechanical properties

OVERVIEW

- The static tensile and compressive test results of individual samples from all the prestress levels studied in this research are presened.

C.1 Static tensile properties

Table C-1: 0 MPa Prestressed composite

Specimen ID	Tensile strength σ (MPa)	Failure strain ε (%)	Secant modulus E (GPa)	Strain deviation from linearity (%)
Ref1b_1	1175.788	3.292	39.2	1.441
Ref1b_4	1373.597	3.092	44.6	1.531
Ref1b_10	1252.387	3.252	45.4	-
Ref2_1	1372.174	3.281	40.2	1.556
Ref3_1	1347.807	3.025	45.4	1.445
Ref3_4	1349.983	3.182	44.8	1.502
Average	**1311.956**	**3.187**	**43.3**	**1.495**
Standard deviation	**80.308**	**0.108**	**2.6**	**0.051**

Table C-2: 51 MPa prestressed composite.

Specimen ID	Tensile strength σ (MPa)	Failure strain ε (%)	Secant modulus E (GPa)	Strain deviation from linearity %
UPT2_1	1461.293	3.047	46.9	1.851
UPT1_2	1201.067	3.101	37.5	1.744
UPT2_4	1162.757	2.933	39.7	1.760
UPT2_7	1245.276	2.818	44.6	1.689
UPT3_1	1220.184	3.196	40.7	1.734
UPT3_5	1177.680	3.027	40.5	1.609
Average	**1244.710**	**3.050**	**41.6**	**1.731**
Standard deviation	**110.112**	**0.157**	**3.4**	**0.067**

Table C-3: 80 MPa prestressed composite.

Specimen ID	Tensile strength σ (MPa)	Failure strain ε (%)	Secant modulus E (GPa)	Strain deviation from linearity %
UP2_7kN_1	1381.640	3.164	44.6	1.804
UP2_7kN_2	1305.861	3.245	42.2	1.802
UP2_7kN_3	1248.431	3.159	41.3	1.780
UP2_7kN_5	1215.297	3.018	42.6	1.827
UP2_7kN_6	1327.834	3.003	47.5	1.716
Average	**1295.812**	**3.117**	**43.6**	**1.785**
Standard deviation	**65.613**	**0.103**	**2.4**	**0.042**

Table C-4:108 MPa prestressed composite

Specimen ID	Tensile strength σ (MPa)	Failure strain ε (%)	Secant modulus E (GPa)	Strain deviation from linearity %
UP1_14kN_2	1117.044	2.933	39.0	2.241
UP1_14kN_4	1187.524	3.014	41.4	1.897
UP2_14kN_4	1131.685	2.854	42.0	1.803
UP2_14kN_7	1434.793	3.305	46.6	1.887
UP4_14kN_1	1354.885	3.235	43.6	1.802
UP4_14kN_4	1337.816	3.256	43.6	2.017
UP4_14kN_6	1436.600	3.135	46.0	1.816

Average	**1285.763**	**3.104**	**43.2**	**1.923**
Standard deviation	**138.025**	**0.173**	**2.6**	**0.159**

Table C-5: 150 MPa prestressed composite.

Specimen ID	Tensile strength σ (MPa)	Failure strain ε (%)	Secant modulus E (GPa)	Strain deviation from linearity %
UP1_24kN_2	1243.290	3.188	41.4	1.750
UP1_24kN_3	1228.880	3.103	40.6	1.833
UP2_24kN_1	1228.843	2.929	42.6	1.780
UP2_24kN_2	1373.165	2.902	43.2	1.785
UP2_24kN_3	1249.423	3.096	42.1	1.855
UP2_24kN_4	1223.303	3.052	42.6	1.729
UP2_24kN_5	1365.666	3.298	45.4	1.882
Average	**1273.224**	**3.081**	**42.6**	**1.802**
Standard deviation	**66.363**	**0.138**	**1.5**	**0.056**

C.2 Static compressive properties

Table C-6: 0 MPa prestressed composite

Specimen ID	Compression strength σ (MPa)	Modulus E (MPa)
UR9_2	1171.907	41.0
UR9_3	1187.087	40.4
UR9_4	1163.510	41.3
UR9_5	1138.495	
UR9_6	1265.391	40.3
UR9_7	1135.659	
Average	**1177.008**	**40.8**
STDEV	**47.569**	**0.5**

Table C-7: 51 MPa Prestressed composite

Specimen ID	Compression strength σ (MPa)	Modulus E (MPa)
UPT7_1	1282.286	45.2
UPT7_2	1242.497	-
UPT7_3	1300.230	41.7
UPT7_4	1192.514	43.2
UPT7_5	1310.592	43.4
UPT7_6	1320.467	-
UPT7_7	1411.099	44.2
Average	**1294.241**	**43.5**
STDEV	**68.087**	**1.3**

Table C-8: 80 MPa Prestressed composite

Specimen ID	Compression strength σ (MPa)	Modulus E (MPa)
UP1_7kN_2	1313.541	44.8
UP1_7kN_4	1202.050	44.1
UP1_7kN_5	1226.011	
UP1_7kN_6	1338.159	45.7
UP1_7kN_7	1386.543	44.3
Average	**1293.261**	**44.7**
STDEV	**77.412**	**0.7**

Table C-9: 108 MPa Prestressed composite

Specimen ID	Compression strength σ (MPa)	Modulus E (MPa)
UP8_14kN_2	1231.993	44.3
UP8_14kN_3	1377.195	43.7
UP8_14kN_5	1343.674	43.8
UP8_14kN_6	1222.486	44.2
UP8_14kN_7	1283.325	45.5

UP8_14kN_8	1219.676	43.3
Average	**1279.725**	**44.1**
STDEV	**67.473**	**0.7**

Table C-10: 150 MPa Prestressed composite

Specimen ID	Compression Strength σ (MPa)	Modulus E (MPa)
UP1_24kN_1	1163.199	42.6
UP1_24kN_2	1274.530	-
UP1_24kN_3	1130.041	43.6
UP1_24kN_4	1085.053	42.6
UP1_24kN_5	1149.451	44.1
Average	**1160.455**	**43.2**
STDEV	**70.271**	**0.7**

APPENDIX D

Fatigue test results

OVERVIEW

- Individual sample results of stiffness degradation and surface temperature rise measurements during tension-tension and tension-compression fatigue test are presented.

Table D-1: Summary of the stiffness degradation for the non-prestressed and the prestressed composites at a peak stress of 655 MPa in T-T fatigue.

Normalised life	Stiffness degradation (MPa)								
	0 MPa Prestress			51 MPa Prestress			108 MPa Prestress		
	UR4_5	UR3_6	UR2_5	UPT2_3	UPT8_3	UPT3_2	UP2_14kN_6	UP1_14kN_5	UP1_14kN_6
0.1	110	100	874	80	90	30	80	70	30
0.3	170	150	1128	100	80	40	90	90	50
0.5	200	200	1149	110	80	-	90	90	60
0.7	680	310	1245	110	90	-	90	80	200
0.9	710	3990	4464	120	130	-	100	100	210

Table D-2: Summary of the surface temperature changes for the non-prestressed and the prestressed composites at a peak stress of 655 MPa in T-T fatigue.

Normalised life	Temperature rise (°C)								
	0 MPa Prestress			51 MPa Prestress			108 MPa Prestress		
	UR4_5	UR3_6	UR2_5	UPT2_3	UPT8_3	UPT3_2	UP2_14kN_6	UP1_14kN_5	UP1_14kN_6
0.1	3.7	4.3	4.2	2.1	3.81	2.66	2.8	3.64	3.63
0.3	3.6	4.49	4.4	3.3	4.59	3.85	4.5	4.09	-
0.5	4.4	5.13	4.7	5.0	4.81	-	5.3	3.53	-
0.7	4.7	6.63	5.1	5.7	4.93	-	6.2	3.55	-
0.9	5.6	7.56	6.3	6.2	6.81	-	6.0	3.04	-

Table D-3: Summary of the stiffness degradation for the non-prestressed and the prestressed composites at a peak stress of 1050 MPa in T-T fatigue.

Normalised life	Stiffness degradation (MPa)								
	0 MPa Prestress			51 MPa Prestress			108 MPa Prestress		
	UR4_2	UR1_5	UR3_2	UPT4_3	UPT2_2	UPT8_2	UP1_14kN_1	UP5_14kN_2	UP5_14kN_5
0.1	30	10	20	30	10	10	110	100	190
0.3	30	160	40	40	10	40	130	110	250
0.5	40	200	50	70	20	70	150	120	260
0.7	120	3400	60	70	30	1950	190	970	1080
0.9	3110	8300	2420	1680	2890	-	18150	2860	3890

Table D-4: Summary of the surface temperature changes for the non-prestressed and the prestressed composites at a peak stress of 1050 MPa in T-T fatigue.

Normalised life	Temperature rise (°C)								
	0 MPa Prestress			51 MPa Prestress			108 MPa Prestress		
	UR4_2	UR1_5	UR3_2	UPT4_3	UPT2_2	UPT8_2	UP1_14kN_1	UP5_14kN_2	UP5_14kN_5
0.1	0.3	0.5	1.0	0.1	0.54	0.49	1.3	1.0	-
0.3	2.0	2.0	2.0	2.4	1.2	2.41	2.6	2.0	-
0.5	3.3	4.5	2.5	3.9	2.46	3.96	3.5	3.4	-
0.7	4.4	5.5	3.5	5.5	3.06	5.46	4.9	4.6	-
0.9	4.7	6.0	4.0	5.3	4.07	6.36	6.3	5.9	-

Table D-5: Summary of the stiffness degradation for the non-prestressed and the prestressed composites at a peak stress of 524 MPa in T-C fatigue.

Normalised life	Stiffness degradation (MPa)								
	0 MPa Prestress			51 MPa Prestress			108 MPa Prestress		
	UR8_8	UR8_9	UR6_6	UPT9_4	UPT6_6	UPT10_6	UP7_14kN_6	UP6_14kN_5	UP7_14kN_7
0.1	2630	3700	8050	2190	190	220	1530	40	390
0.3	6980	20550	8560	2200	100	580	1740	30	890
0.5	11060	24250	8780	2200	130	780	1790	30	4420
0.7	12270	24580	9180	2220	230	800	1960	50	7020
0.9	15130	25090	9340	2810	110	570	2180	280	10730

Table D-6: Summary of the surface temperature changes for the non-prestressed and the prestressed composites at a peak stress of 524 MPa in T-C fatigue.

Normalised life	Temperature rise (°C)								
	0 MPa Prestress			51 MPa Prestress			108 MPa Prestress		
	UR8_8	UR8_9	UR6_6	UPT9_4	UPT6_6	UPT10_6	UP7_14kN_6	UP6_14kN_5	UP7_14kN_7
0.1	6.5	4.48	-	5.5	5.52	4.84	4.9	2.01	4.01
0.3	9.9	4.87	-	3.4	6.43	6.68	2.6	3.54	5.47
0.5	10.7	3.83	-	3.5	1.98	5.7	4.2	5.3	5.97
0.7	10.7	3.79	-	2.2	1.0	6.77	4.7	4.29	3.21
0.9	9.6	3.45	-	2.8	2.4	5.98	4.1	1.82	2.99

Table D-7: Summary of the stiffness degradation for the non-prestressed and the prestressed composites at a peak stress of 840 MPa in T-C fatigue.

Normalised life	Stiffness degradation (MPa)								
	0 MPa Prestress			51 MPa Prestress			108 MPa Prestress		
	UR7_6	UR6_2	UR10_8	UPT11_3	UPT10_4	UPT10_5	UP6_14kN_2	UP11_14kN_4	UP11_14kN_5
0.1	1410	520	2210	780	150	280	390	210	-
0.3	1540	832	3520	1090	200	420	780	310	-
0.5	1950	1345	3590	1210	250	660	1260	460	-
0.7	2190	1671	3600	1270	280	1210	1700	1760	-
0.9	2220	3785	-	1330	280	1490	2330	-	-

Table D-8: Summary of the surface temperature changes for the non-prestressed and the prestressed composites at a peak stress of 840 MPa in T-C fatigue.

Normalised life	Temperature rise (°C)								
	0 MPa Prestress			51 MPa Prestress			108 MPa Prestress		
	UR7_6	UR6_2	UR10_8	UPT11_3	UPT10_4	UPT10_5	UP6_14kN_2	UP11_14kN_4	UP11_14kN_5
0.1	3.1	-	4.43	3.0	0.72	1.83	2.4	0.5	2.2
0.3	4.2	-	6.01	3.3	1.16	4.33	4.1	1.99	4.61
0.5	5.3	-	7.09	4.3	2.82	5.82	4.6	2.87	5.41
0.7	6.3	-	8.27	3.6	2.77	5.68	5.5	3.48	6.13
0.9	7.3	-	7.53	3.6	3.66	6.03	4.8	4.38	6.55